AD-A137 997 A PHENOMENOLOGICAL MODEL OF SOIL BREAKDOWN(U) DIKEWOOD 1/2
ALBUQUERQUE NM R N CARLILE ET AL. JAN 84 AFWL-TR-83-73
F29601-81-C-0044

UNCLASSIFIED F/G 8/13 NL

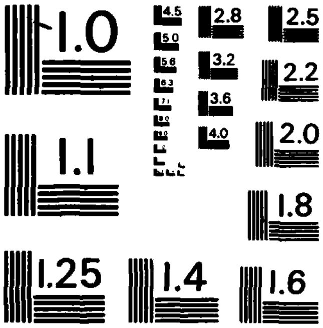
1.0
4.5
5.0
5.6
6.3
7.1
8.0
9.0
2.8
3.2
3.6
4.0
2.5
2.2
2.0
1.1
1.8
1.25
1.4
1.6

MICROCOPY RESOLUTION TEST CHART
NATIONAL BUREAU OF STANDARDS-1963-A

AFWL-TR-83-73

AFWL-TR-
83-73

AD A137997

A PHENOMENOLOGICAL MODEL OF SOIL BREAKDOWN

R. N. Carlile
M. E. Righettini

University of Arizona
Tucson, AZ 85721

January 1984

Final Report

Approved for public release; distribution unlimited.

DTIC
SELECTE
FEB 17 1984
S D
E

AIR FORCE WEAPONS LABORATORY
Air Force Systems Command
Kirtland Air Force Base, NM 87117

DTIC FILE COPY

84 02 17 033

AFWL-TR-83-73

This final report was prepared by the University of Arizona, Tucson, Arizona, under Contract F29601-81-C-0044, Job Order 672A0903, with the Air Force Weapons Laboratory, Kirtland Air Force Base, New Mexico. Lt John K. Place (NTAT) was the Laboratory Project Officer-in-Charge.

When Government drawings, specifications, or other data are used for any purpose other than in connection with a definitely Government-related procurement, the United States Government incurs no responsibility or any obligation whatsoever. The fact that the Government may have formulated or in any way supplied the said drawings, specifications, or other data, is not to be regarded by implication, or otherwise in any manner construed, as licensing the holder, or any other person or corporation; or as conveying any rights or permission to manufacture, use, or sell any patented invention that may in any way be related thereto.

This report has been authored by a contractor of the United States Government. Accordingly, the United States Government retains a nonexclusive, royalty-free license to publish or reproduce the material contained herein, or allow others to do so, for the United States Government purposes.

This report has been reviewed by the Public Affairs Office and is releasable to the National Technical Information Services (NTIS). At NTIS, it will be available to the general public, including foreign nations.

If your address has changed, if you wish to be removed from our mailing list, or if your organization no longer employs the addressee, please notify AFWL/NTAT, Kirtland AFB, NM 87117 to help us maintain a current mailing list.

This technical report has been reviewed and is approved for publication.

JOHN K. PLACE
Lt, USAF
Project Officer

FOR THE COMMANDER

JAMES A. KEE
Maj, USAF
Chief, Technology Branch

ROGER S. CASE JR
Lt Col, USAF
Chief, Aircraft & Missile Division

DO NOT RETURN COPIES OF THIS REPORT UNLESS CONTRACTUAL OBLIGATIONS OR NOTICE ON A SPECIFIC DOCUMENT REQUIRES THAT IT BE RETURNED.

REPORT DOCUMENTATION PAGE

1a. REPORT SECURITY CLASSIFICATION
Unclassified

1b. RESTRICTIVE MARKINGS

2a. SECURITY CLASSIFICATION AUTHORITY

2b. DECLASSIFICATION/DOWNGRADING SCHEDULE

3. DISTRIBUTION/AVAILABILITY OF REPORT
Approved for public release; distribution unlimited.

4. PERFORMING ORGANIZATION REPORT NUMBER(S)

5. MONITORING ORGANIZATION REPORT NUMBER(S)
AFWL-TR-83-73

6a. NAME OF PERFORMING ORGANIZATION
University of Arizona

6b. OFFICE SYMBOL *(If applicable)*

7a. NAME OF MONITORING ORGANIZATION
Air Force Weapons Laboratory (NTAT)

6c. ADDRESS *(City, State and ZIP Code)*
Tucson, AZ 85721

7b. ADDRESS *(City, State and ZIP Code)*
Kirtland Air Force Base, NM 87117

8a. NAME OF FUNDING/SPONSORING ORGANIZATION

8b. OFFICE SYMBOL *(If applicable)*

9. PROCUREMENT INSTRUMENT IDENTIFICATION NUMBER
F29601-81-C-0044 s/c Dikewood

8c. ADDRESS *(City, State and ZIP Code)*

10. SOURCE OF FUNDING NOS.

PROGRAM ELEMENT NO.	PROJECT NO.	TASK NO.	WORK UNIT NO.
64312F	672A	09	03

11. TITLE *(Include Security Classification)*
A PHENOMENOLOGICAL MODEL OF SOIL BREAKDOWN

12. PERSONAL AUTHOR(S)
R. N. Carlile, M. E. Righettini

13a. TYPE OF REPORT
Final Report

13b. TIME COVERED
FROM Feb 82 TO Jul 83

14. DATE OF REPORT *(Yr., Mo., Day)*
1984, January

15. PAGE COUNT
190

16. SUPPLEMENTARY NOTATION
The work was performed by the University of Arizona under Subcontract No. DC-SC-2030-7 for Dikewood.

17. COSATI CODES

FIELD	GROUP	SUB. GR.
08	13	

18. SUBJECT TERMS *(Continue on reverse if necessary and identify by block number)*

Corona
Streamers
Breakdown model
Source region EMP effects
Soil electrical breakdown
Soil properties

19. ABSTRACT *(Continue on reverse if necessary and identify by block number)*

This report characterizes electrical soil breakdown by models which can be incorporated into computer codes. The evolution and decay of the corona are described. Parameters which characterize these processes are defined. Where possible, their numerical values are stated. The evolution within the corona of streamers is discussed and some of their properties are described.

20. DISTRIBUTION/AVAILABILITY OF ABSTRACT
UNCLASSIFIED/UNLIMITED ☒ SAME AS RPT. ☐ DTIC USERS ☐

21. ABSTRACT SECURITY CLASSIFICATION
Unclassified

22a. NAME OF RESPONSIBLE INDIVIDUAL
Lt John K. Place

22b. TELEPHONE NUMBER *(Include Area Code)*
(505) 844-9758

22c. OFFICE SYMBOL
AFWL/NTAT

CONTENTS

Section Page

I INTRODUCTION 3

II EXPERIMENTAL SYSTEMS 4

III THE MODEL, AN OVERVIEW 7

1. CORONA 7
2. STREAMERS 12

IV THE ELECTROSTATIC MODEL OF THE CORONA 15

1. OTHER MODELS 15
2. THE CYLINDRICALLY SYMMETRIC CORONA 21
3. THE SPHERICALLY SYMMETRIC CORONA 25
4. EVOLUTION OF THE ELECTROSTATIC PHASE 28
5. CALCULATION OF MAXIMUM CURRENT 40
6. SPHERICAL CASE 49

V DYNAMIC THEORY OF THE CORONA REGION 51

1. THE DYNAMIC MODEL 51
2. RELAXATION THEORY 52
3. RESULTS 55

VI STREAMERS 61

1. CORONA ATTACHMENT 62
2. STREAMER ATTACHMENT 74

VII SUMMARY, DISCUSSION 79

1. SUMMARY 79
2. DISCUSSION OF CORONA ATTACHMENT 80

REFERENCES 82

APPENDICES

A. LINEAR ELECTRICAL CONDUCTIVITY OF SOIL 85

B. DATA BASE 98

DTIC COPY INSPECTED 2

Accession For
NTIS GRA&I ☒
DTIC TAB ☐
Unannounced ☐
Justification
By
Distribution/
Availability Codes
Dist | Avail and/or Special
A-1

I. INTRODUCTION

This report describes the development of a model of soil breakdown based on a large number of experiments which were performed under the auspices of the Air Force Weapons Laboratory (AFWL).

The purpose of this report is to make use of this experimental data to develop a phenomenological model of soil breakdown suitable for use in a computer code. The experiments performed by Mission Research Corporation (MRC) have been used because of the detail of spatial voltage variation in the presence of soil breakdown that was obtained. Nonpurturbing voltage probes were inserted into the soil samples to measure voltage versus time at a large number of discrete points.

Soil breakdown characterized by corona formation and streamer propagation has been recognized for several decades (Ref. 1). It was assumed that a corona developing about a buried electrode (subjected to a large pulse) would have streamers forming within it (Ref. 2). Corona is discussed in Reference 3 and 4. An excellent reference on both linear and nonlinear soil properties from this era is found in Reference 5. In Reference 6, B. E. Lewis has tried to model the decay of the corona as the pulser voltage relaxes. If the models of this early work are somewhat modified, they will fit the experimental data now in use. These models have been quantified in such a way that they can be uded in computer codes.

It may be useful to read Appendix A at this point before tackling the material of this report. This appendix is a description of the nature of soil from a geologist's point of view. This description defines the components of soil and then decribes through Archie's law how each component contributes to the linear ohmic conductivity of soil. It also provides a good basis on which to build an understanding of the nonlinear behavior of soil.

In Section II, the relevant feature of the experimental configurations which was used in the experiments are discussed. Section III is an overview of the model; Section IV is a development of the electrostatic model while Section V develops the dynamic model of relaxation. Section VI discusses streamers and Section VII is a summary of the important points made in this report.

II. EXPERIMENTAL SYSTEMS

Nearly all this report is based upon experiments which were performed by MRC. This work was performed in two experimental configurations both of which contained cylindrical symmetry:

a. A cylindrical wedge of angle $\pi/2$. The thickness of the wedge was either 0.1 m or 0.3 m and the radius was 0.5 or 1.0 m. When an experiment is discussed, the wedge thickness and radius will be stated. Experiments will henceforth be called Experiments A or Exp. A.

b. A full 2 π cylinder. The length was 1 m and the radius 0.5 m was 1 m. Experiments performed in this configuration will be called Exp. B.

The MRC performed the Exp. A at Physics International, San Leandro, California. The basic configuration is shown in Figure 1. The soil sample is in the shape of a $\pi/2$ wedge with a center conductor of radius a, an outer conductor (a copper sheet) of radius b, and a thickness L. In some of the experiments, the outer conductor was connected to pulser ground through a resistor of 200 Ω. The top and bottom of the soil sample as well as the sides at 0 and $\pi/2$ rad were of an insulating material. The intervening space was filled with soil. For the experiments of interest, a = 0.01 m, b = 0.5, 1 m, and L = 0.1, 0.3 m.

The center conductor was driven by a 30 to 100 kV, 0.9 μF pulser. The interesting feature about these experiments was that the voltage in the soil sample was measured at discrete points as a function of time by an array of voltage probes. A probe had a high impedance between its small spherical tip (in contact with soil) and ground. Hence, it drew little current. The probes were designed so that they would not purturb significantly the distribution of voltage in the soil sample.

The array of probe positions which were available are shown in Figure 1. There were 10 data channels available; nine of these were used for monitoring probe voltages while the tenth was used to monitor total current I through the sample. Thus, for a given discharge of the pulser (shot), nine probes could be monitored. The probes were either located in the nine radial positions in the figure or in the nine azimuthal positions.

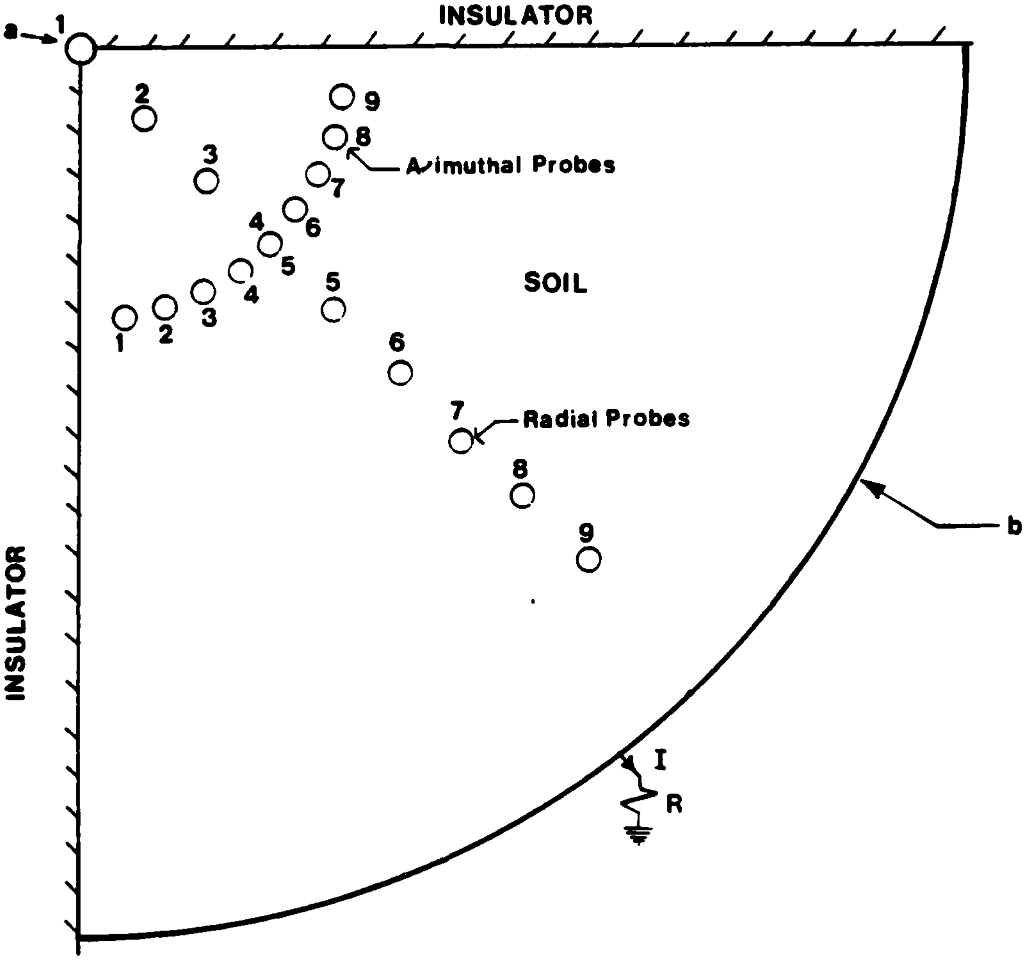
a
1
INSULATOR
INSULATOR
2
3
4
1
2
3
4
5
5
6
7
8
9
9
8
7
6
Azimuthal Probes
SOIL
Radial Probes
b
I
R

Figure 1. Radial and azimuthal probe arrays in π/2 cylindrical wedge soil sample--wedge is 0.1 or 0.3 thick; radius a of center conductor is 0.01 m; radius b of outer conducter is 0.5 or 1.0 m.

The soil types used in Exp. A which are relevant are:

a. Sand with an ohmic resistivity ρ_0 of about 150 to 2000 Ω-m;
b. a sand and gravel composite labeled SOIL-B; a typical ρ_0 is 130 Ω-m.

The MRC performed Exp. B at the McDonnell-Douglas Lightning Facility (MCAIR), St. Louis, Missouri. The sample was a full 2 π cylinder with a central conducting rod of radius a. The outer conductor was a standard steel culvert of radius b. The length of the system was L. The system had a top and bottom plate which were of an insulating material and the intervening space was filled with soil. For the experiments in this report; a = 0.01 m, b = 0.5 m and L = 1 m.

The center conductor was driven by one or two five-stage pulsers at the MCAIR facility. Each Marx pulser could be charged to 15 to 24 kV per stage with a total capacitance of 230 μF divided between the number of stages used. The same high impedance voltage probes were used in these experiments that were used in Exp. A. The probes were inserted into the soil through the top and bottom insulating plates in either a radial or azimuthal array. Of interest here is an azimuthal array described in more detail in Section VI. Twenty-six data channels were available. The soil of interest in this report is 300 Ω-m sand.

Finally, there is a set of experiments called Exp. C. Which were performed by JAYCOR. These were point-plane experiments where the soil resistivity was 50 Ω-m.

III. THE MODEL, AN OVERVIEW

The model that is adapted in the report consists of two components: the corona and streamers. Although these components are inseparable, in presenting an overview of the model, they will be discussed individually.

1. CORONA

In discussing the corona, Exp. A will be used. In Exp. A, the voltage V(r) with respect to ground was measured as a function of time by high impedance probes at the radial locations shown in the cylindrical wedge geometry illustrated in Figure 1. Also measured was the total current I flowing through the wedge as a function of time. Thus, it is possible to plot the ratio V/I (the effective resistance between the location of the probe and ground) as a function of radial position r, or more conveniently, log r. For a typical shot, this plot is shown in Figure 2.

If the cylindrical symmetry is assumed, the cylindrical wedge is electrically divided into two regions (Fig. 2). The division between the two regions occurs at a radius r_0, which for the parameters of Figure 2 would be about 0.16 m. In each region, V/I and, hence, V is nearly proportional to log r; since in this symmetrical case, $E = r\,E_r$, we are then led to E_r being proportional to r^{-1} in each region, although the proportionality constants are different. If L is the thickness of the wedge, then the current density is

$$J_r = \frac{I}{2\pi\, r\, L} = \frac{E_r}{\rho} = \frac{A}{r\rho} \tag{1}$$

where ρ is the soil resistivity and A is the proportionality constant for a region. Equation 1 states that ρ is constant in each region and the difference in proportionality constants can be accounted for by the resistivity being different in each region.

If, as in Figure 1, a is the radius of the central high voltage conductor and b is the radius of the outer grounded cylinder, then the following is assumed:

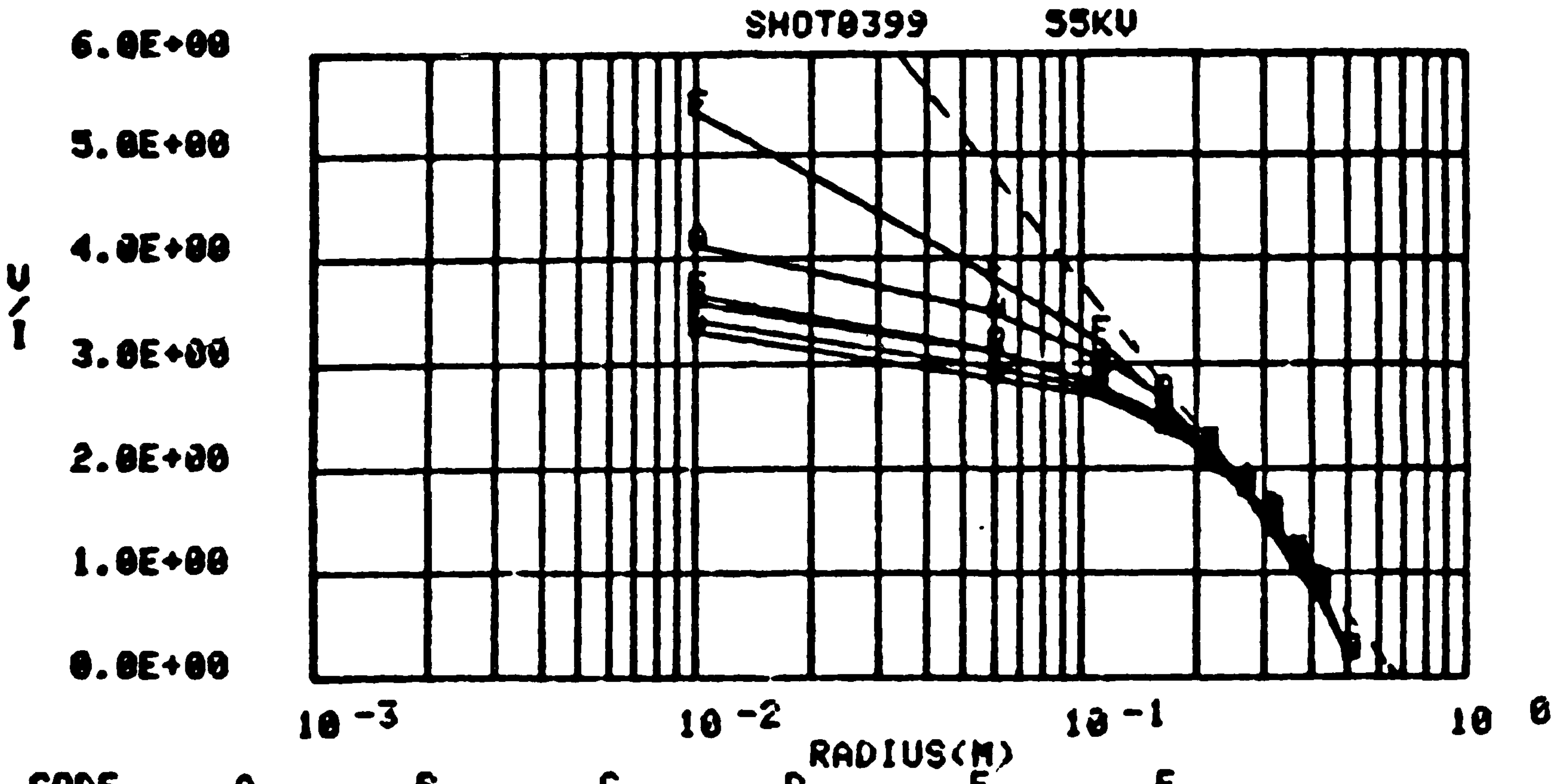

CODE	A	B	C	D	E	F
TIME	100US	200US	300US	500US	900US	1900US
CURRENT	14.00	15.25	15.00	14.00	10.75	5.00

Figure 2. Resistance (kΩ) for shot 399 at various times. Curve A, second from top; B, third; C, fifth; D, sixth; E, fourth; F, top curve. Total current through sample shown at bottom.

a. For $r_0 \leq r \leq b$, the soil is not broken and is an ohmic state such that $\rho = \rho_0$, the ohmic value; furthermore, at $r = r_0$, $E_r = E_B$, a critical electric field above which the soil will break down but below which it will not; this is called the ohmic region.

b. For $a \leq r \leq r_0$, $E_r > E_B$ and the soil is broken down in some fashion; here, $\rho = \rho_1 < \rho_0$. This is called the corona region.

This two region description of soil breakdown is referred to as the electrostatic model. A soil sample which is electrically stressed such that the electrostatic model applies is said to be in the electrostatic phase.

Although it has been assumed that the corona will adapt the symmetry of the electrode system e.g., cylindrical or spherical, assymetries in the soil or other perturbations, e.g., streamers, may cause the corona to depart from the symmetry of the electrode system. The electrostatic model may be generalized to be that in which the electrically stressed soil is still divided into two regions as illustrated in Figure 3. In the region containing the high voltage electrode or the corona region, the resistivity is $\rho_1\ (r) < \rho_0$. In the region containing the grounded electrode or the ohmic region, the soil is not broken down and the resistivity is just ρ_0. Furthermore, on the boundary between the two regions, in the ohmic region, the electric field is not necessarily normal to the boundary, but its magnitude is constant everywhere on the boundary and is E_B, the critical electric field. Finally, a critical current density can be defined at the boundary in the ohmic region,

$$\overline{J}_c = \overline{E}_B/\rho_0 \tag{2}$$

The magnitude of this current density is constant everywhere on the boundary.

It is of interest to see what precedes the electrostatic phase and how this phase decays as the voltage on the high voltage electrode decays. Call V_0 the voltage on the central high voltage electrode. As V_0 increases, the soil will remain ohmic until the electric field at the electrode $E_r(a) \equiv E_0$ approaches about 1 MV/m. Assuming a rise time of V_0 of the order of a microsecond, there will be a delay time t_i until the soil starts to break down and the soil remains ohmic. During this phase, it has been observed that the

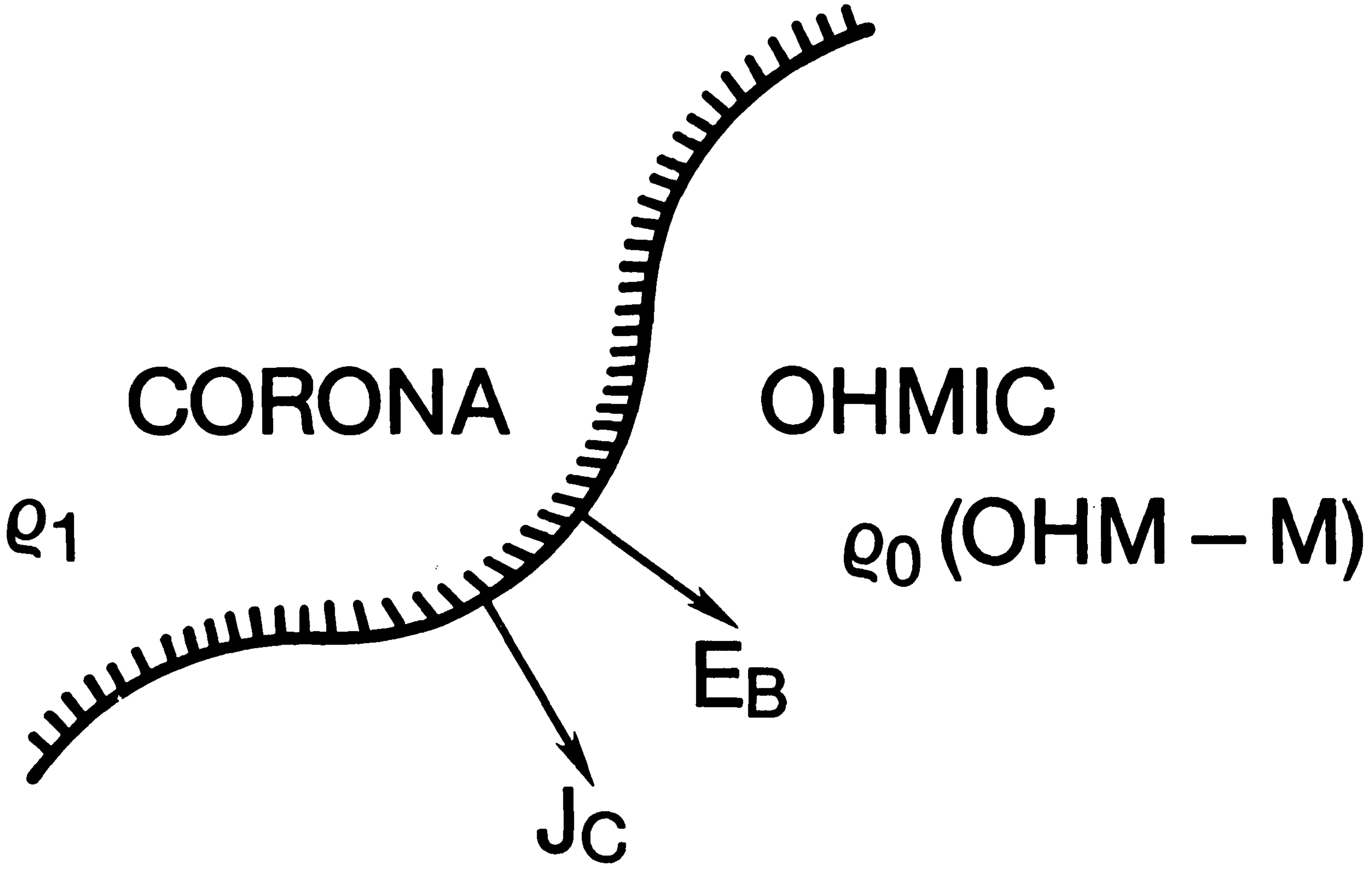
CORONA
ϱ_1
OHMIC
ϱ_0 (OHM – M)
E_B
J_C

Figure 3. Boundary between an corona region and ohmic soil region; E_B is critical electrical field and $J_c = E_B/\rho_o$.

resistivity of the soil actually is larger than ρ_0. For example, in shot 012, while the ohmic resistance of the soil is 14.7 kΩ determined by low voltage measurements, during the prebreakdown phase, the resistance was measured to be 16.1 kΩ (Exp. A).

Once breakdown begins, the resistance of the soil drops rapidly in time as the total current through the sample I rises even though the V_0 is dropping. After a few tens of μs, r_0 begins to appear as the sample begins to enter the electrostatic phase. Two cases must be distinguished at this point. The first is that V_0 can be sufficiently large to cause the corona to extend all the way to the grounded conductor at $r = b$. We call this corona attachment. Then I will increase to a large value, and will only be limited by the low resistance of the soil. Corona attachment can occur if V_0 is so large that for a symmetric corona, $r_0 = b$, or r_0 exceeds a critical radius. Breakdown to the outer conductor can also occur by streamer attachment discussed in paragraph 2. The second case is that if V_0 is not large enough for any of these events to occur, the corona remains stable, I will increase to a maximum value, and then decline to zero as the voltage V_0 falls to zero. For a symmetric, stable corona, see in Figures B.21 and B.22 (Appendix B) how the current I rises as the voltage V_0 falls after the onset of breakdown for shot 399.

For shot 399 at 30 μs, the ohmic region could be distinguished as can be seen in Section IV and there is indeed a region of corona where $\rho_1 < \rho_0$. The current reaches its maximum about 200 μs. From 30 to 200 μs, the electrostatic phase is clearly defined. Thus, it takes the order of 30 μs for the electrostatic phase to be reached, which is typical for shots of Exp. A.

If $\overline{J}_c$ is nearly normal to the boundary separating the corona from the ohmic region, and since its magnitude is constant over this surface, then

$$I = \int \overline{J}_c \cdot \overline{dS} \approx \frac{E_B}{\rho_0} \pi r_0^2 \tag{3}$$

so that for E_B being regarded as a constant, the surface of the boundary is a maximum when I is a maximum, for the symmetric corona, r_0 is a maximum when I is a maximum. Maximum I and r_0 should depend on maximum V_0, and as maximum or peak V_0 increases, so does maximum r_0.

As the current decays after reaching its maximum, then the symmetric corona enters what is called the dynamic phase. Modeling the decay of the corona after Liew, et al. (Ref. 6) a third region is postulated to exist, bounded by an inner radius r_1, where the current density if J_c, and an outer radius r_0, corresponding to r_0 at maximum I.

The three regions of the dynamic mode are defined as follows:

Region 1: $a \leq r \leq r_1$, $J \geq J_c$ with $J = J_c$ at $r = r_1$; ρ_1 = const.
Region 2: $r_1 \leq r \leq r_0$, $J \leq J_c$ with ρ_2 dependent on r.
Region 3: $r_0 \leq r \leq b$, the ohmic region with $\rho = \rho_0$.

The dynamic model is discussed in Section V.

2. STREAMERS

It is well established that a second method of soil breakdown occurs in which narrow channels of high conductivity form at the high voltage electrode and proceed to grow outward at some velocity. These channels have been called streamers. A model proposed in Reference 2 has been adapted in which a streamer is viewed as contained inside the corona as shown in Figure 4. In this model, the corona forms first, the streamer may initiate at some point on the high voltage electrode for reasons that are not understood. The streamer grows outward distorting the symmetry of the corona. In this figure a symmetric corona (dashed line) containing no streamers is contrasted with one containing one or more streamers. The streamers always stay inside the corona's boundary and the electric field remains at E_B at the boundary of the corona.

This model is reasonable if one accepts that the resistivity of the streamer is very low. Then the voltage drop along the streamer will be small, and its potential will approximate that of tne high voltage electrode. Just as this electrode will cause soil breakdown some distance out from it, so the streamer, which must have a large electric field at its surface, will cause breakdown in the nearby surrounding soil. This model of a corona surrounding a streamer has been adopted by Longmire et al.

It is also predicted by the University of Arizona that once a streamer is formed, the thermodynamics and electrical properties of the streamer tip will cause it to propagate outward with a predictable velocity. Eventually, the

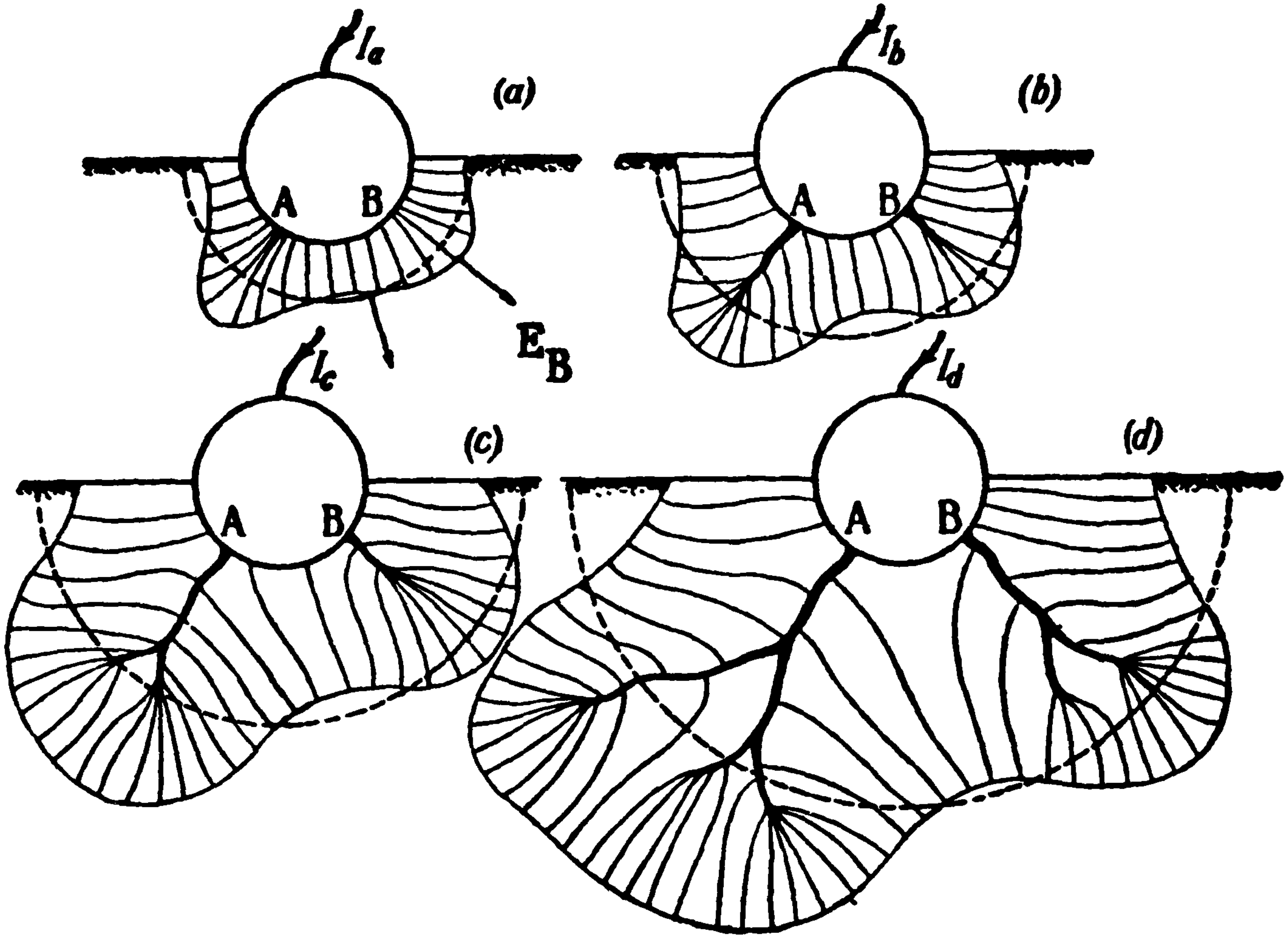

Figure 4. A buried spherical electrode with streamers propagating outward from points A and B. Streamers are embedded in corona (outer medium dark line). Dashed semicircle is corona boundary if streamers are absent. Current into electrode increases from (a) to (d) as does corona boundary surface. (Fig. 14 of Ref. 2).

streamer will push the corona surrounding its tip out to the grounded electrode at $r = b$, followed by the streamer itself attaching to this electrode. This form of breakdown to the grounded conductor is called streamer attachment.

In Section VI, we are able to make an estimate of the radius of a streamer that occurred in a nearly symmetric corona. In that case, it was found that the radius was about 1 cm.

IV. THE ELECTROSTATIC MODEL OF THE CORONA

As seen in the preceding section, the electrostatic model is the cornerstone of the corona model. In this section, some other possible corona models will be discussed and the use of the electrostatic model justified. The details of the theory of the electrostatic model will be presented first for the symmetric cylindrical case and then for the symmetrical spherical case. Next, the electrostatic phase through experimental data will be characterized. Finally, it will be shown that the peak current can be accurately predicted by the electrostatic model.

1. OTHER MODELS

In referring to Figure 2, since V(r) appears to vary in a manner proportional to log r in both the corona and ohmic regions, it is concluded that in each region E_r is proportional to r^{-1}. Thus, it is assumed that

$$V(r) = V_0 - V_1 \log (r/a) \tag{4}$$

On the other hand, Longmire el al. claim that the electric field in the corona is clamped to that required for electron avalanching to be just balanced by electron diffusion and attachment (Ref. 7). This electric field is estimated to be about 1 MV/m. In any case, E_r is assumed to be independent of r, or E_r = const.

This would lead to a linear dependence of V(r) on r,

$$V(r) = V_0 + V_2 \left(1 - \frac{r}{a}\right) \tag{5}$$

An attempt was made to distinguish between these types of voltage variation in the corona by considering in detail the data from shot 399 of Exp. A. The raw data or data base from this shot are shown in Figures B.1 through B.10 (Appendix B). Figures 5 through 8 show the plotted data from the radial probes at the locations shown in Figure 1 versus log r at two early times, 30 and 60 μs and at two times when the total current I was nearly its maximum, i.e., 100 and 300 μs.

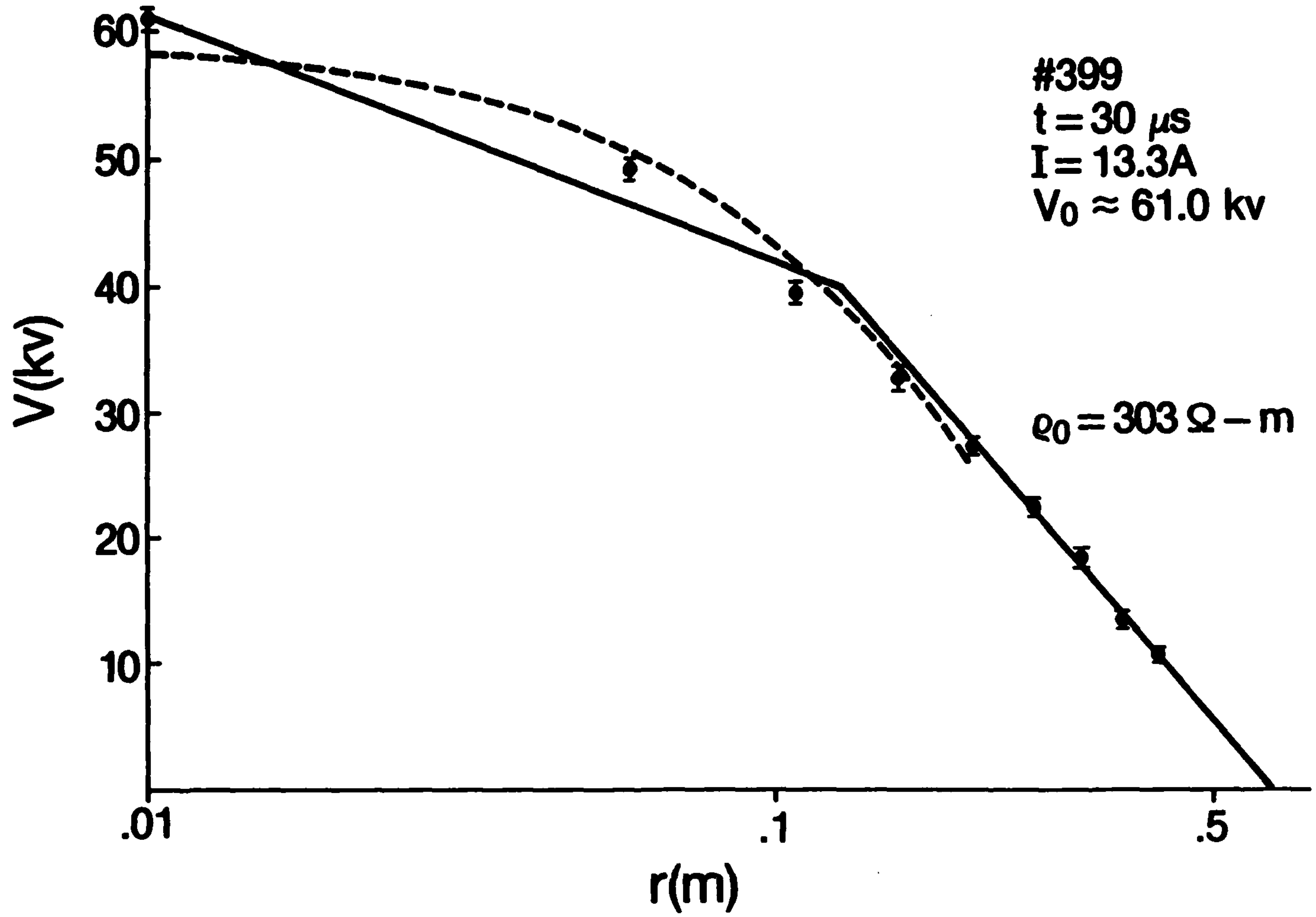

Figure 5. Log r (solid line) and linear r (dashed line) fit to radial voltage probe data for shot 399; t = 30 μs.

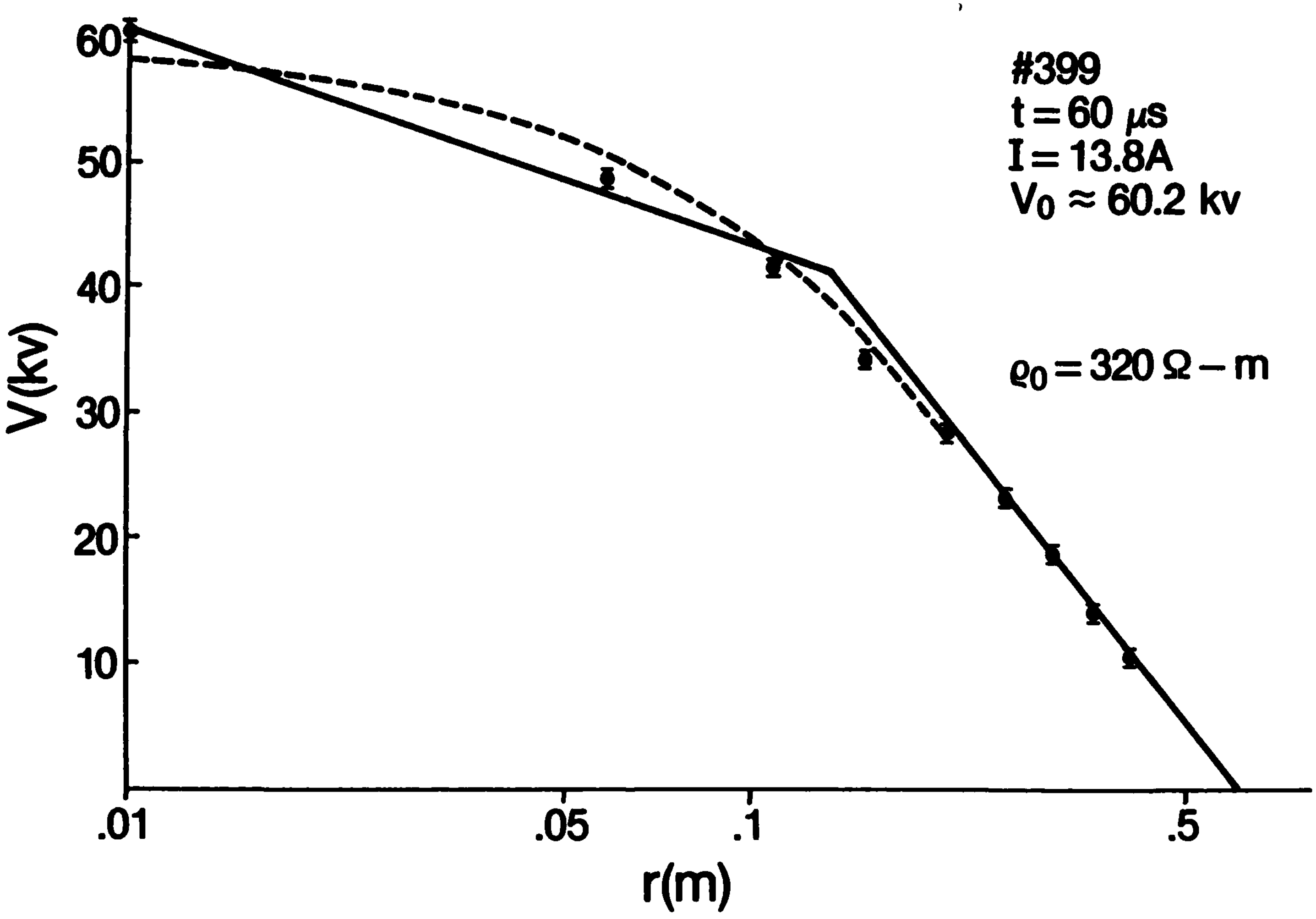

Figure 6. Log r (solid line) and linear r (dashed line) fit to radial voltage probe data for shot 399; t = 60 μs.

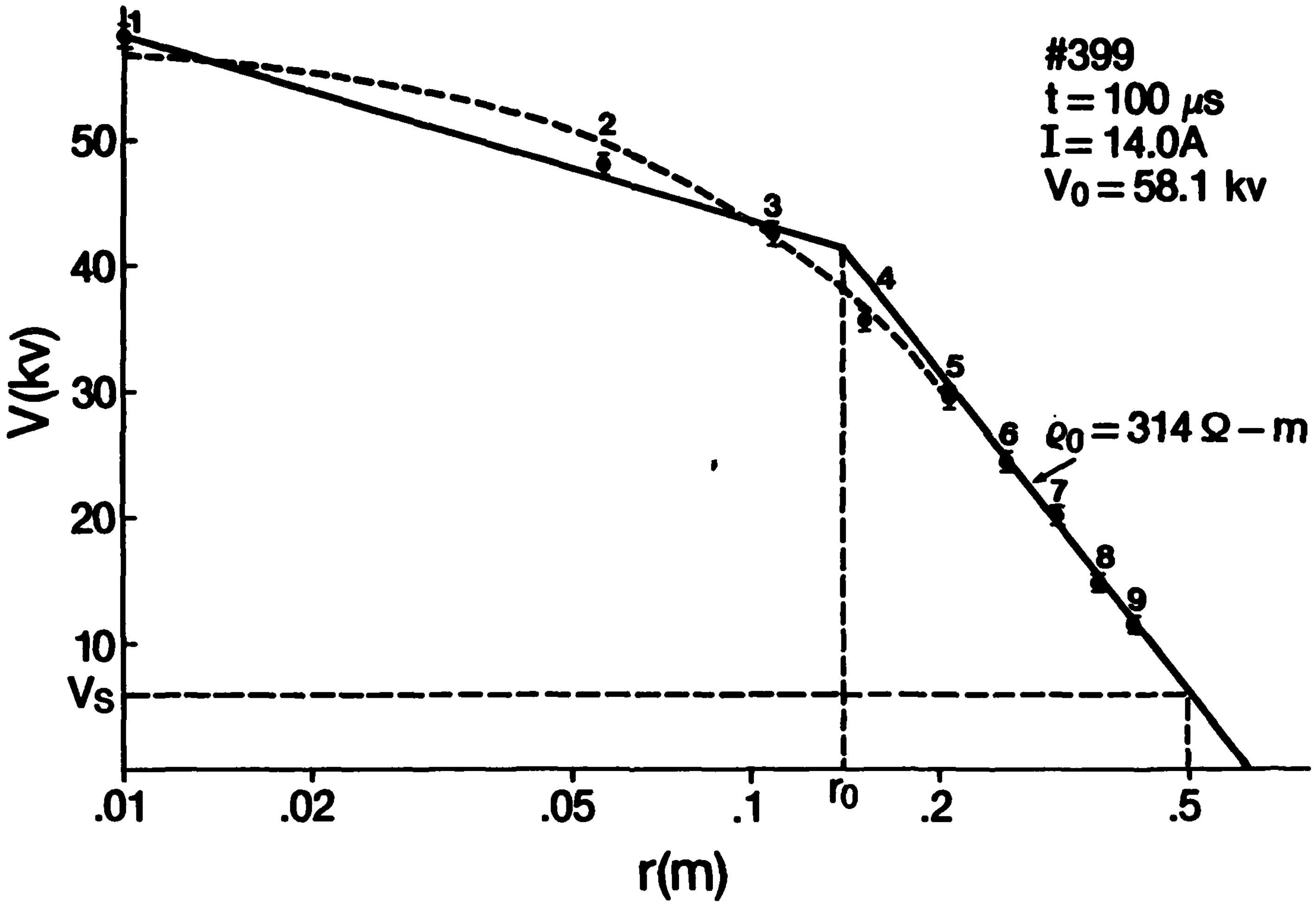

Figure 7. Log r (solid line) and linear r (dashed line) fit to radial voltage probe data for shot 399; t = 100 μs.

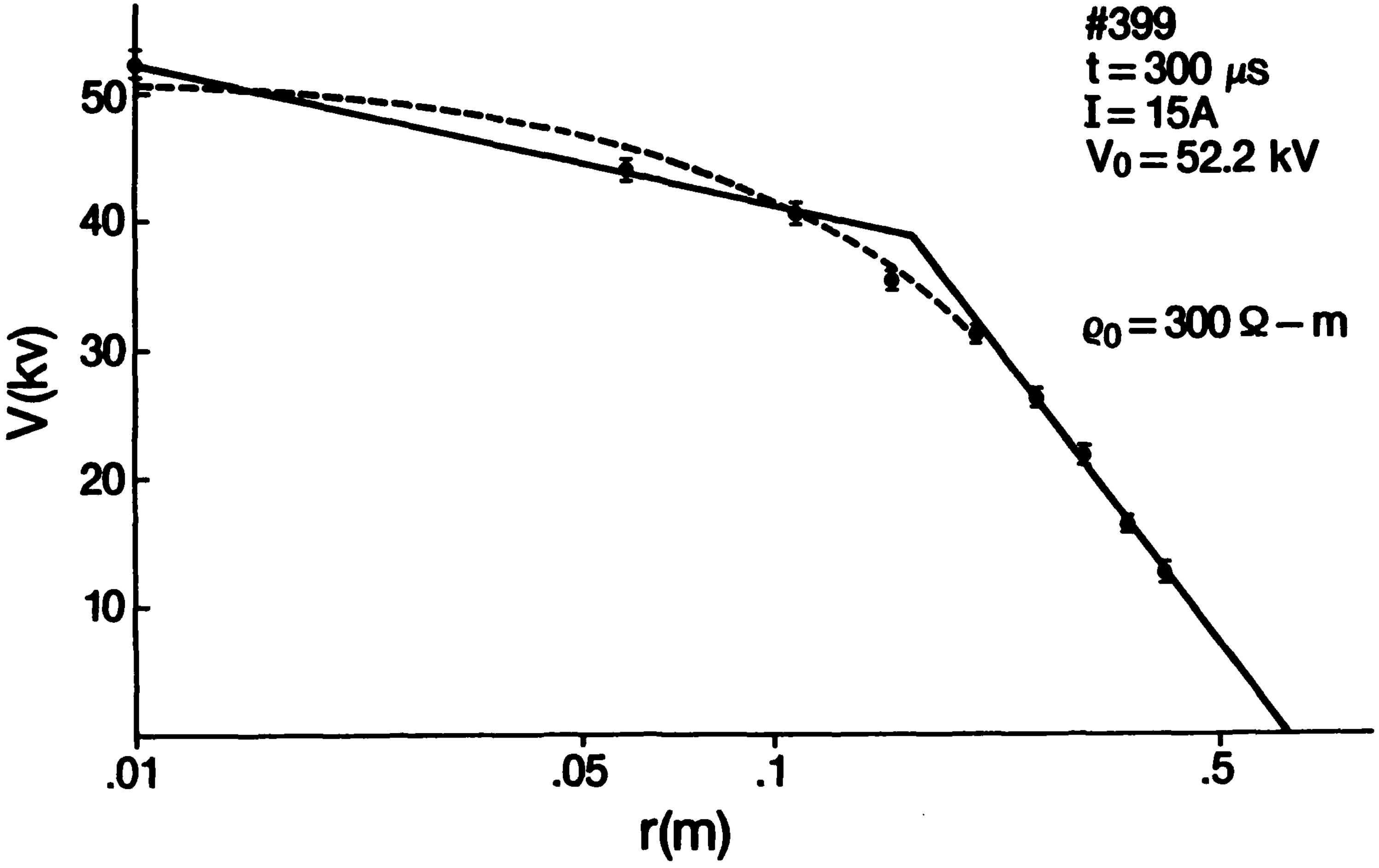

Figure 8. Log r (solid line) and linear r (dashed line) fit to radial voltage probe data for shot 399; t = 300 μs.

Consider Figure 7 for 100 μs. The probes in Figure 1 are numbered 1 through 9 and the voltage at each probe is shown by a heavy dot in Figure 7 with the number of the probe from which it was obtained shown above the point. The experimenters claim that the random error in a probe measurement had a standard deviation of 4 percent which is interpreted to mean a random error of ±2%. This error is shown by the error bars on the data points.

A least squares logrithmic regression fit has been done of Figure 5 on points 1, 2, and 3 and the resulting curve is shown at the solid curve in Figure 7. These three points were used since these were the only probes in the corona region.

A least squares linear regression fit of Figure 6 has been done on points 1, 2, 3, 4, and 5 and the resulting curve is shown as dashed in Figure 7. Although the error bars tend to support the log r dependence, this conclusion is somewhat tentative. There were only three probes in the corona region; had there been more, a more certain conclusion might have been reached. Notice that to distinguish between the two types of voltage dependence on r, very precise measurements of V are required. A ±2% error is the outside limit of what can be tolerated.

The same kind of least squares fit of Figure 5 and 6 have been made on the same groupings of points in Figures 5, 6, and 8 for 30, 60, and 300 μs, respectively. At 30 μs, neither dependence seems correct based on the error bars. At 60 μs, the log r dependence gives a better fit than the linear fit as is the case at 100 μs. At 300 μs, the log r fit is nearly exact. Thus, as time proceeds toward I reaching its maximum, the log r fit gets progressively better.

In what follows, a log r dependence will be assumed. From the point of view of trying to develop a phenomenological model of the corona which is suitable for computer codes, whether on selects Figure 5 or 6, certain important parameters would be predicted in either case. Voltage v(r) would be satisfactorily predicted since the difference between the solid and dashed curves in the figures is not large. Also, the total current I and current density as well as r_0, the boundary between the two regions, would be predicted. What would be lost would be E_r and the dependence of ρ_1 on r.

In Figures 5 through 8 a least squares logrithmic regression fit on points 5 through 9 in the ohmic region has been performed. The fit is excellent. The slope of this curve determines the ohmic resistivity. It can be seen that there is a significant apparent variation of ρ_0 among the four times. Assume that this variation is not real, but reflects errors in measuring I, which was used in the computation of ρ_0.

The intersection of the log r curve for points in the ohmic region and the log r curve for points in the corona region determines r_0, as is shown in Figure 7. Further, it is seen each time that at $r = 0.5$ m, which is the location of the grounded electrode, the voltage $V(r)$ is not zero, but has some finite value, V_s. This is because there was a 200 Ω resistor attached between this electrode and pulser ground.

2. THE CYLINDRICALLY SYMMETRIC CORONA

Figure 9 shows a diagram which will serve to illustrate both the cylindrically and spherically symmetric corona. It is assumed that the inner electrode of radius a is connected to a high voltage pulser which has negligible series inductance and resistance. The corona region, for which $a \leq r \leq r_0$, is characterized by a resistivity ρ_1 and permittivity ε_2. The ohmic region for $r_0 \leq r \leq b$ has an ohmic resistivity ρ_0 and a permittivity ε_2. The outer conductor of radius b is connected to pulser ground through a resistor R.

It is a simple matter to apply Gauss' law to this system and the details will be omitted. Note, however, the following points:

a. By assumption, the electric field $E = r\ E\ (r)$ is radial and proportional to r^{-1} in both regions. This leads to $\nabla \cdot E = 0$. Also, the resistivity is constant in each region.

b. The boundary condition at r_0 is that the normal component of the current density is continuous across the boundary. This will require a charge on the boundary determined by the permittivity and resistivity of both regions.

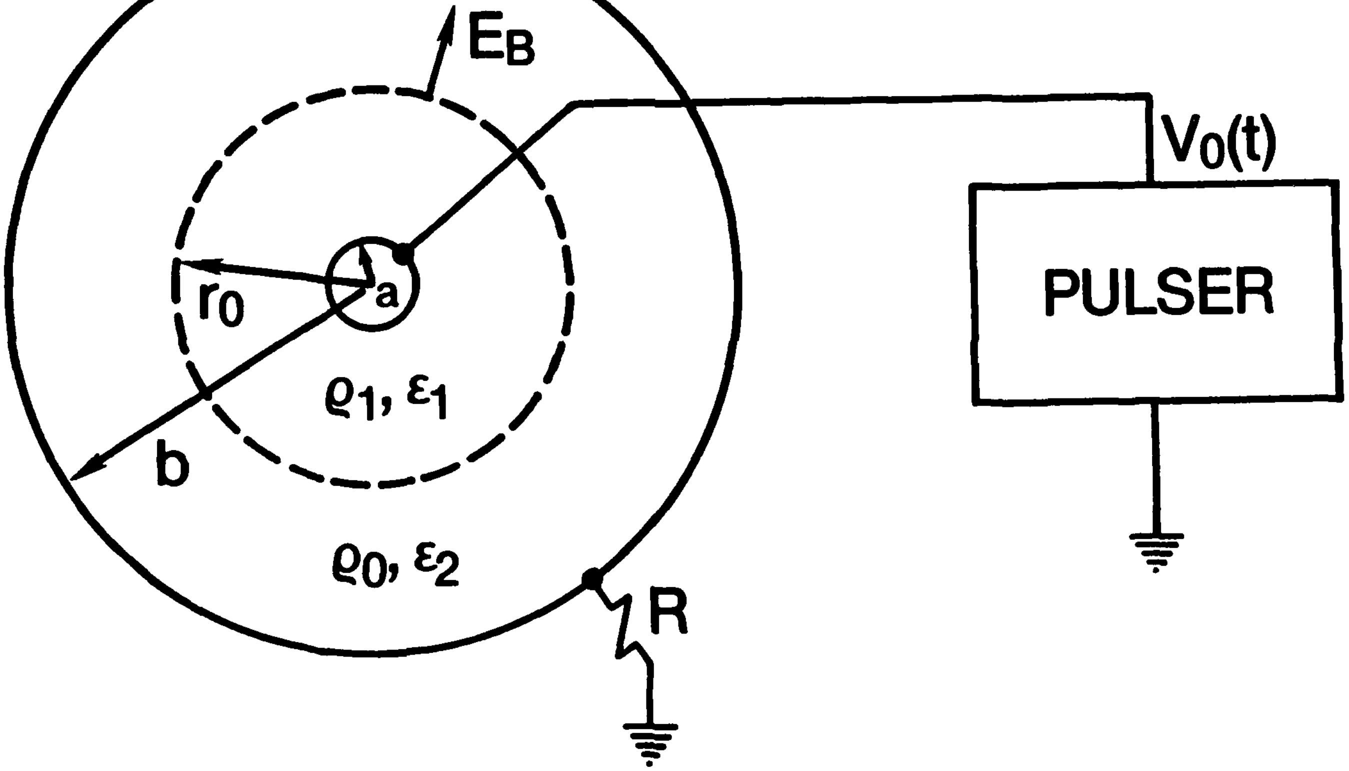
E_B
$V_0(t)$
PULSER
r_0
a
ϱ_1, ε_1
b
ϱ_0, ε_2
R

Figure 9. A cylindrical or spherical soil sample in the electrostatic phase. $a \le r \le r_o$; corona region; $r_o \le r \le b$ Ohmic region.

c. If both the electric field E(r) and the voltage V(r) are expressed as a function of the voltage on the inner conductor V_0, the permittivities ε_1 and ε_2 will not explicitly appear in the expressions for either of these quantities.

d. The potential at r = b is V_s. This could be attributed to a resistor between this electrode and ground or to a contact potential at r = b.

With these comments, the expressions for E(r) and V(r) are:

$a \leq r \leq r_0$

$$V(r) = \frac{(V_0 - V_s)}{D}\left[\ell n \frac{b}{r_0} + \frac{\rho_1}{\rho_0} \ell n \frac{r_0}{r}\right] + V_s \tag{6}$$

$$E(r) = \frac{V_0 - V_s}{D} \frac{\rho_1}{\rho_0} \frac{1}{r} \tag{7}$$

$r_0 \leq r \leq b$

$$V(r) = \frac{V_0 - V_s}{D} \ell n \frac{b}{r} + V_s \tag{8}$$

$$E(r) = \frac{V_0 - V_s}{D} \frac{1}{r} \tag{9}$$

where

$$D = \ell n \frac{b}{r_0} + \frac{\rho_1}{\rho_0} \ell n \frac{r_0}{a} \tag{10}$$

We may obtain a number of useful expressions from these equations. The critical electric field (E_B) may be obtained from Equation 9 by setting $r = r_0$:

$$E_B = \frac{V_o-V_s}{D}\,\frac{1}{r_o}$$

$$= \frac{V_o - V_s}{r_o\left[\ell n\,\dfrac{b}{r_o} \quad \dfrac{\rho_1}{\rho_o}\,\ell n\,\dfrac{r_o}{a}\right]} \tag{11}$$

If α is the angle of the cylindrical wedge and L is its depth, then the total current through the sample I is

$$I = \alpha r_o L\,\frac{E_B}{r_o} = \frac{\alpha L}{\rho_o}\,\frac{V_o-V_s}{D} \tag{12}$$

Thus, from Equation 8 and 12

$$V(r) = \frac{\rho_o}{\alpha L}\,I\,\ell n\,\frac{b}{r} + V_s \tag{13}$$

and

$$\frac{\partial V}{\partial(\log r)} = -\,2.303\;I\,\frac{\rho_o}{\alpha L} \tag{14}$$

where $\ell n\ 10 = 2.303$. Thus, if $\partial V/\partial\ (\log r)$ and I are obtained from the experimental data; use Equation 14 to calculate ρ_o.

From Equations 6 and 8

$$\frac{\partial V}{\partial\,\log\,r} = \begin{cases} K\,\dfrac{\rho_1}{\rho_o} & a \leq r \leq r_o \\[2ex] K & r_o \leq r \leq b \end{cases} \tag{15}$$

where $K = -2.303\ (V_o - V_s)/D$. Thus, the ratio of the slopes of the two solid curves in Figure 7 will give ρ_1/ρ_o.

Finally, it is of interest to define

$$x \equiv r_0/a \tag{16}$$

and

$$y \equiv (V_0 - V_s)/a\ E_B \tag{17}$$

Then rewrite Equation 11

$$y = -x \ln \frac{a}{b}x + \frac{\rho_1}{\rho_0} x \ln x \tag{18}$$

We have plotted y versus x with $b/a = 50$ and ρ_1/ρ_0 as the parameter in Figure 10. For small ρ_1/ρ_0, y exhibits a maximum at some x. For example, for $\rho_1/\rho_0 = 0$, the maximum will occur at $x = (b/a)e^{-1} = 18.4$ which corresponds to $r_0 = b/e$. As V_0 increases so that y increases with E_B assumed to be constant, r_0 will increase. If V_0 is so large than r_0 or x reaches the point corresponding to the maximum, the system will become unstable and breakdown will occur all the way to $r = b$ (Ref. 8). Thus, the corona will attach to the grounded conductor.

As ρ_1/ρ_0 *increases from zero, the maximum moves to the right in Figure* 10. At $\rho_1/\rho_0 = 0.203$, it has just arrived at $x = 50$, or $r = b$ with $y = 39.7$. The system is, therefore, unconditionally stable for $\rho_1/\rho_0 > 0.203$ for $b/a = 50$.

The external resistance R in Figure 9 will also tend to stabilize the corona. It is shown in Reference 8 that if a resistance of value

$$R_c = \rho_0/\alpha L \tag{19}$$

is inserted in series with the soil sample, the corona will be unconditionally stable. For a $\pi/2$ wedge with $L = 0.1$ m and $\rho_0 = 350\ \Omega$-m, $R_c = 2229\ \Omega$.

3. THE SPHERICALLY SYMMETRIC CORONA

Figure 9 suffices to describe this system. Assume here that $\overline{E}$ is again radial and proportional to r^{-2}. Once again, $\nabla \cdot E = 0$ and ρ_1 is a constant. Points 2, 3, and 4 in the previous section once again apply. The expressions for V(r) and E(r) are:

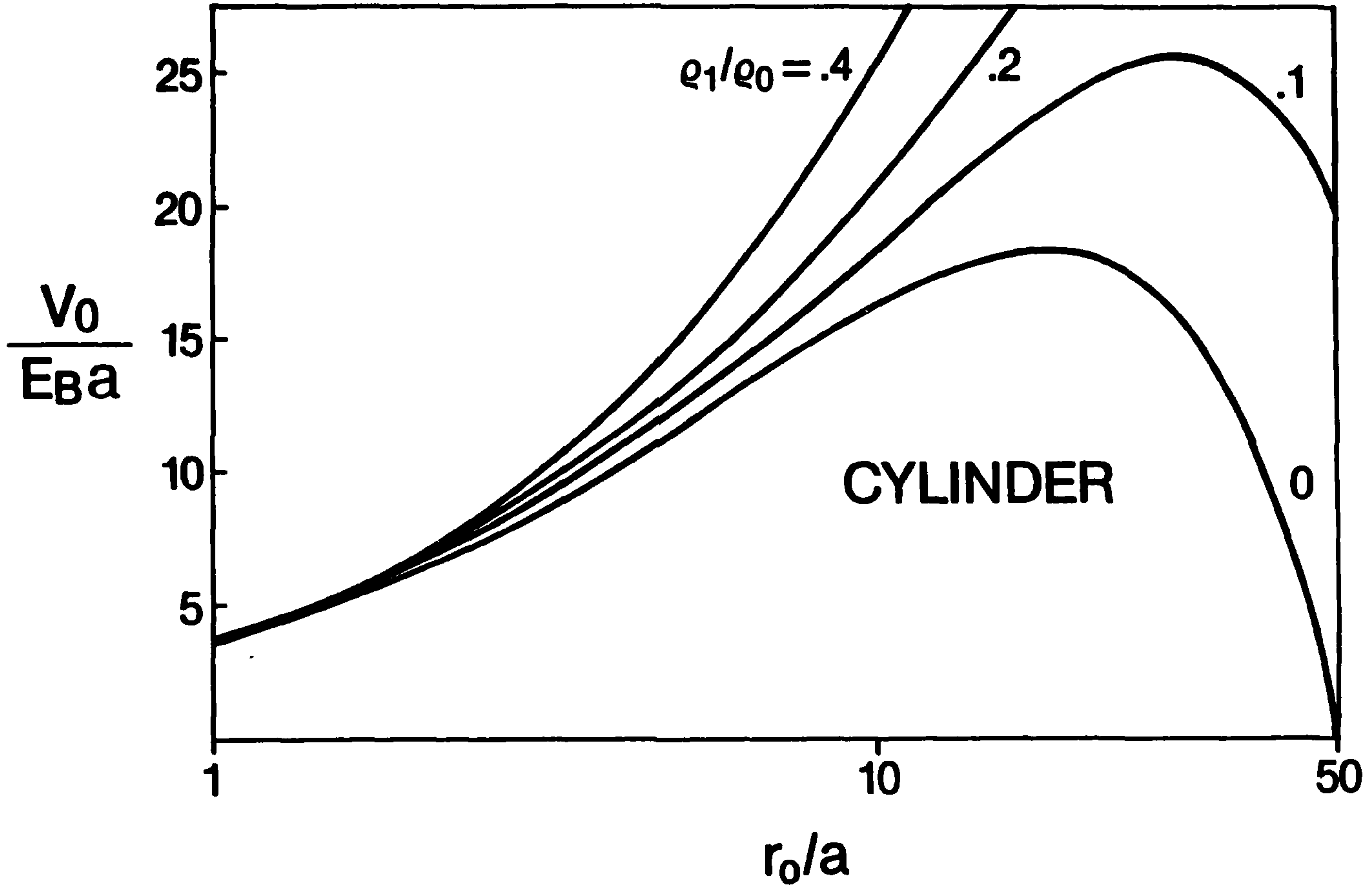

Figure 10. Stability curves for a cylindrical soil sample which is symmetrically broken down. V_o on the ordinate is, in fact, V_o-V_s if there is a resistance between the soil and pulser ground; b/a = 50.

$a \geq r \geq r_o$

$$V(r) = \frac{V_o - V_s}{D'} \left[\left(1 - \frac{\rho_1}{\rho_o} \right) \frac{1}{r_o} - \frac{1}{b} + \frac{\rho_1}{\rho_o} \frac{1}{r} \right] + V_s \tag{20}$$

$$E(r) = \frac{V_o - V_s}{D'} \frac{\rho_1}{\rho_o} \frac{1}{r^2} \tag{21}$$

$r_o \geq r \geq b$

$$V(r) = \frac{V_o - V_s}{D'} \left(\frac{1}{r} - \frac{1}{b} \right) + V_s \tag{22}$$

$$E(r) = \frac{V_o - V_s}{D'} \frac{1}{r^2} \tag{23}$$

where

$$D' = \left(1 - \frac{\rho_1}{\rho_o} \right) \frac{1}{r_o} - \frac{1}{b} + \frac{\rho_1}{\rho_o} \frac{1}{a} \tag{24}$$

From Equation 22

$$E_B = \frac{V_o - V_s}{D'} \frac{1}{r_o^2}$$

$$= \frac{V_o - V_s}{\left(1 - \frac{\rho_1}{\rho_o} \right) \frac{1}{r_o} - \frac{1}{b} + \frac{\rho_1}{\rho_o} \frac{1}{a}} \frac{1}{r_o^2} \tag{25}$$

The total current I through the sample is

$$I = 4\pi r_o^2 \frac{E_B}{\rho_o} \tag{26}$$

so that the total resistance from the high voltage electrode to r = b is:

$$R = \frac{V_0}{I} \approx \frac{\rho_0}{4\pi} D' \tag{27}$$

For the case, $b \to \infty$, $\rho_1/\rho_0 \to 0$, $D' = r_0^{-1}$, so that

$$R = \frac{\rho_0}{4\pi r_0} \tag{28}$$

If we define

$$x = r_0/a$$

and

$$y = (V_0 - V_s)/aE_B$$

Then Equation 24 becomes

$$y = x^2 \left[\left(1 - \frac{\rho_1}{\rho_0}\right)\frac{1}{x} - \frac{a}{b} + \frac{\rho_1}{\rho_0}\right] \tag{29}$$

The quantity y has been plotted versus x with $b/a = 50$ and ρ_1/ρ_0 as the parameter in Figure 11. The system has an instability for $\rho_1/\rho_0 = 0$ at $r_0 = b/2$. However, it quickly stabilizes at small values of ρ_1/ρ_0. For example, the system is stable at $\rho_1/\rho_0 = 0.01$.

For the case $b \to \infty$, Equation 28 becomes

$$y = \left(1 - \frac{\rho_1}{\rho_0}\right)x + \frac{\rho_1}{\rho_0} x^2 \tag{30}$$

and the system is unconditionally stable.

4. EVOLUTION OF THE ELECTROSTATIC PHASE

Soil will break down at a metal-soil interface when the electric field is about 1 MV/m. For example, in Figure 12 for Exp. A where the electric field was initially 1.8 MV/m (Fig. B.11, Appendix B), it can be seen that the soil remains ohmic for about 10 μs, and then breaks down characterized by the current starting to rise. Call the delay until breakdown occurs, t_i, as shown in Figure 12.

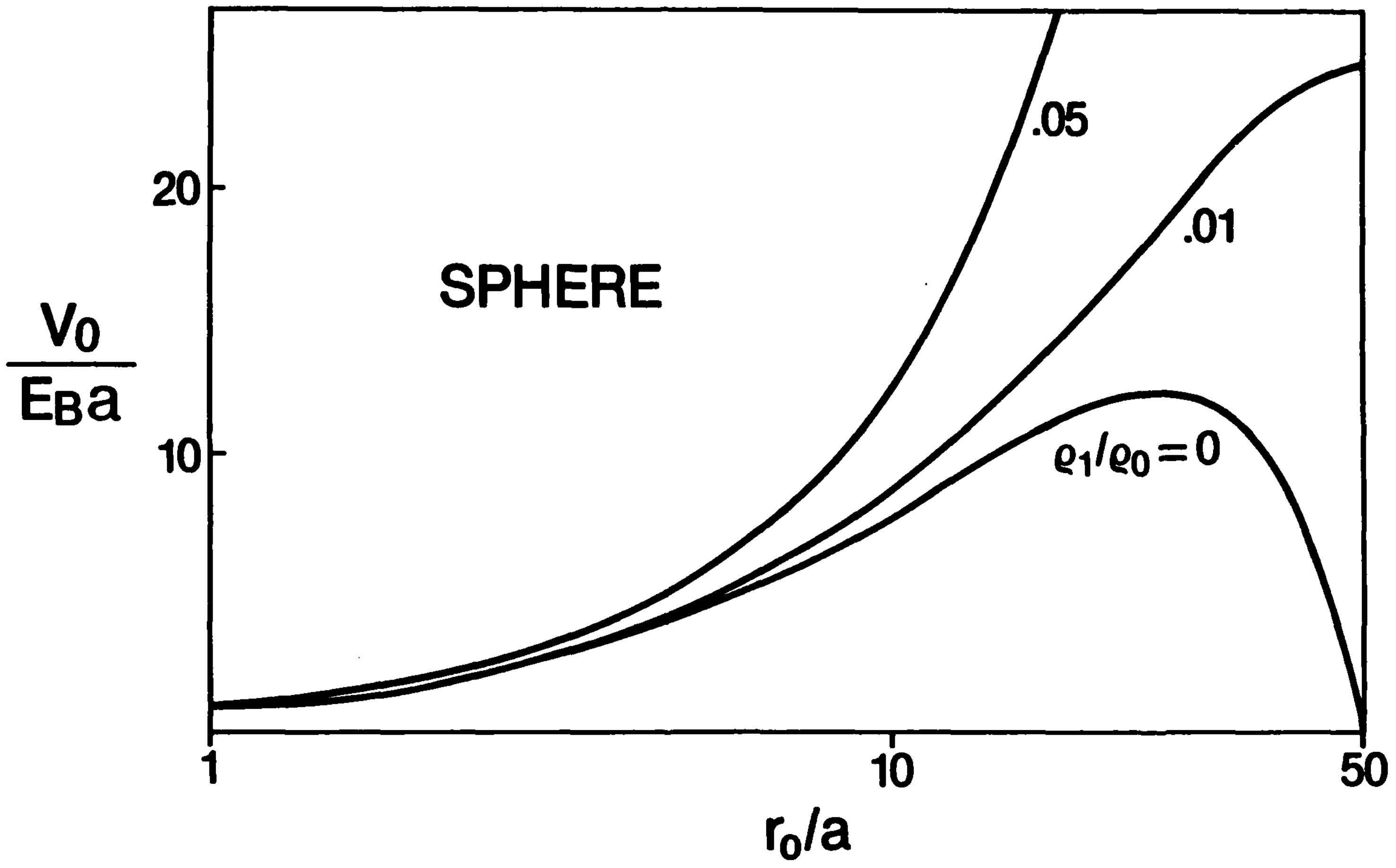

Figure 11. Stability curves for a spherical soil sample that is symmetrically broken down; b/a = 50.

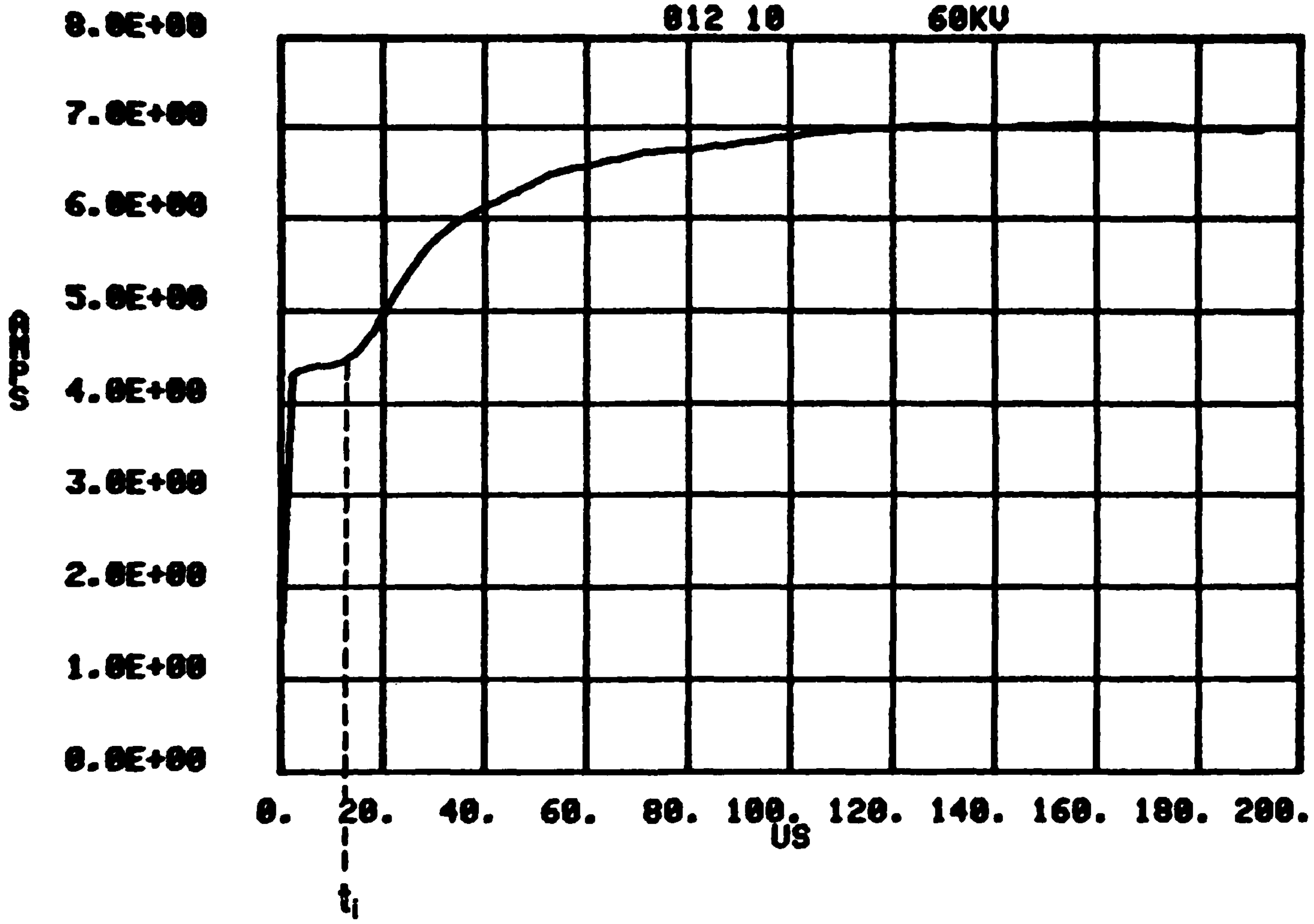

Figure 12. Current versus time for shot 012 (cylindrical wedge soil sample). The soil remains nearly ohmic until time t_i after the application of V_o.

Breakdown is characterized by the formation of the corona, a subsequent lowering of the sample impedance, and an increase in the total sample current I as shown in Figure 13 with the accompanying voltage characteristic on the center conductor being illustrated in Figure 14. If the voltage is not large enough to push r_0 either to a radius where instability will occur or to the outer conductor, the current will reach a maximum at a time t_m as shown in Figure 13 and then will decline to zero. If, on the other hand, as instability radius is reached or the corona reaches $r = b$, then breakdown to the outer conductor at $r = b$ occurs, at some time t_B, and the current I will increase suddenly at t_B as shown in Figure 15.

In Figure 12 where $\rho_0 = 1500\ \Omega\text{-m}$, for $t < t_i$, $V_0/I = 16.1\ \text{k}\Omega$ whereas the calculated ohmic resistance R_0 given by

$$R_0 = \frac{\rho_0 \ell n\ (b/a)}{\alpha L} \tag{31}$$

is 14.7 kΩ. The measured resistance is characteristically larger than the bulk low voltage resistance apparently due to "a small increase in effective resistivity with increase in current density, a small increase in impedance near the small diameter center electrode, and a small increase with time of the contact impedance" at the center electrode (Ref. 2). This subject has been treated exhaustively.* Also the relationship between the applied electric field at the center conductor E_0 and the time of initiation of breakdown, t_i has been shown experimentally. In Figure 16, the dependence of t_i with E_0 is shown where the parameter is geometry and in Figure 17, the parameter is soil type. In all cases, t_i decreases as E_0 increases. Typically, t_i has dropped to about 1 μs if E_0 is greater than 2 MV/m.

Only the stable case where breakdown does not reach $r = b$ will now be considered, and the current reaches a maximum as in Figure 13; note that in Exp. A, t_m ranges from 100 to 100 μs. There is a rough correlation between t_m and the peak applied voltage: t_m increases with increasing V_0 peak.

---

*Buried Conductor Studies, AFWL-NTA-TN-83-0308. Electrical Breakdown Characteristics in 0.8 and 1.0 Meter MX Soil Samples, JAYCOR, San Diego, Calif, 1981; and Theoretical Note-318, 1982.

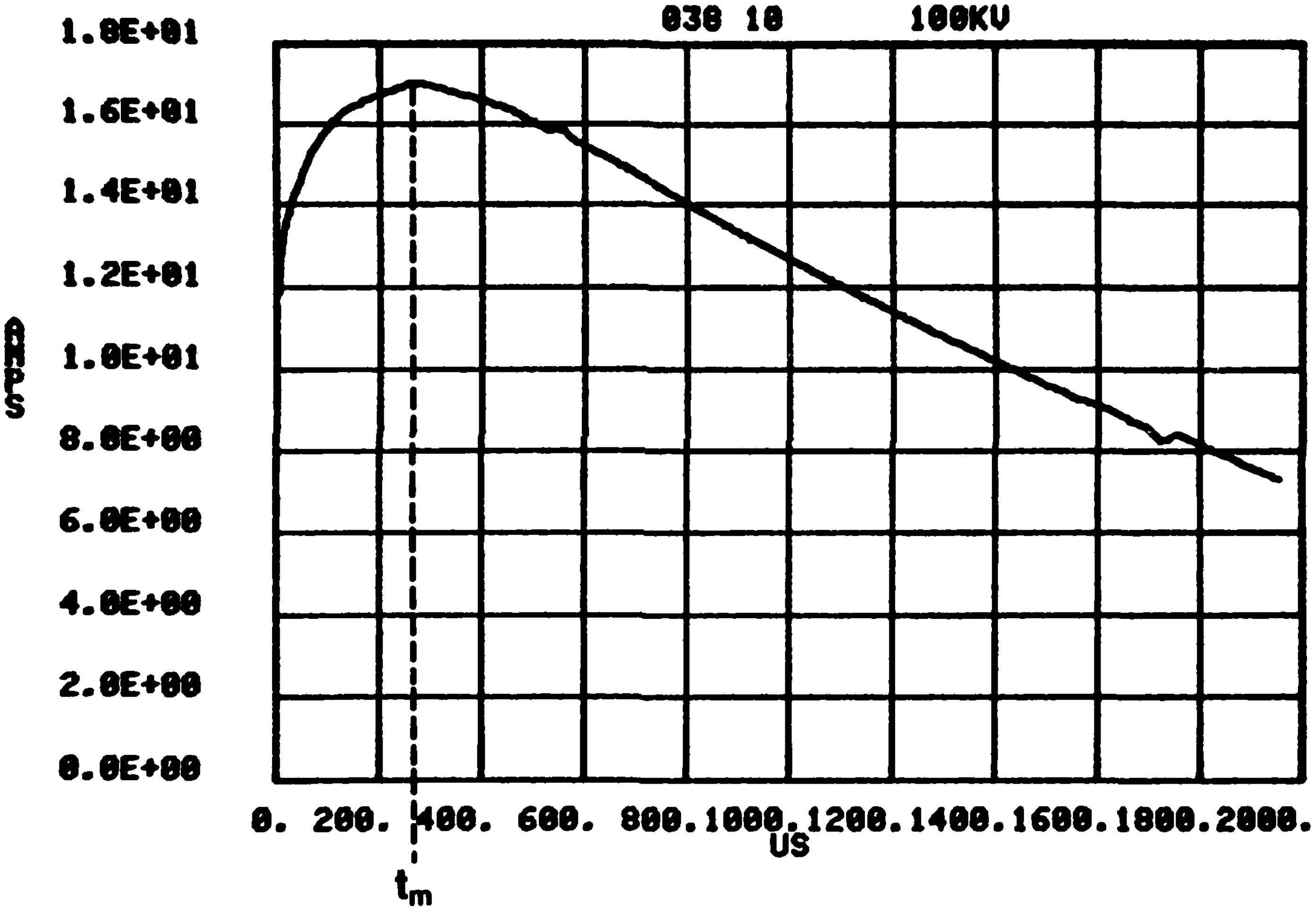

Figure 13. Current versus time in shot 038 (cylindrical wedge soil sample). The current rises to a maximum at time t_m.

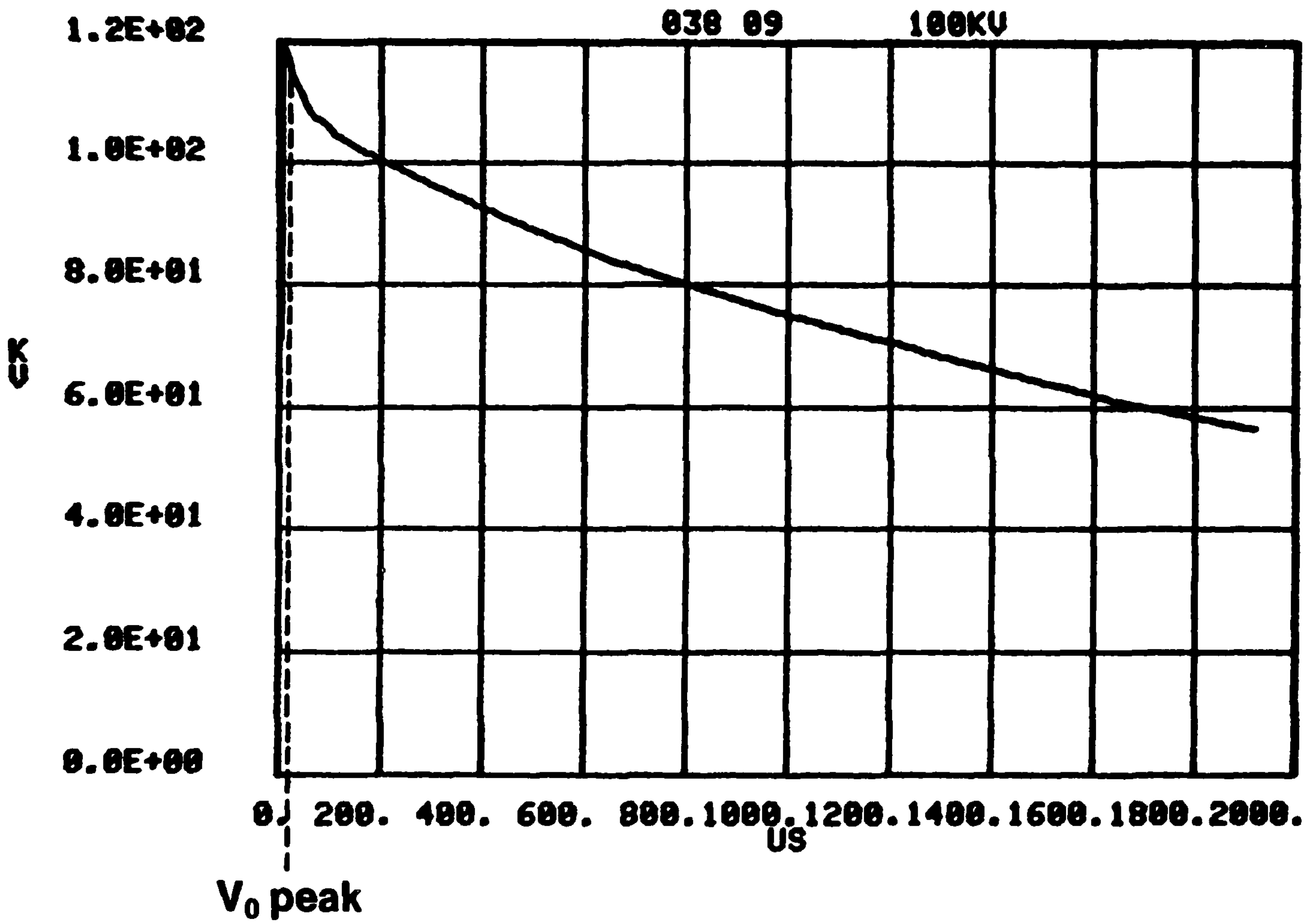

Figure 14. Voltage versus time in shot 038 (cylindrical wedge soil sample).

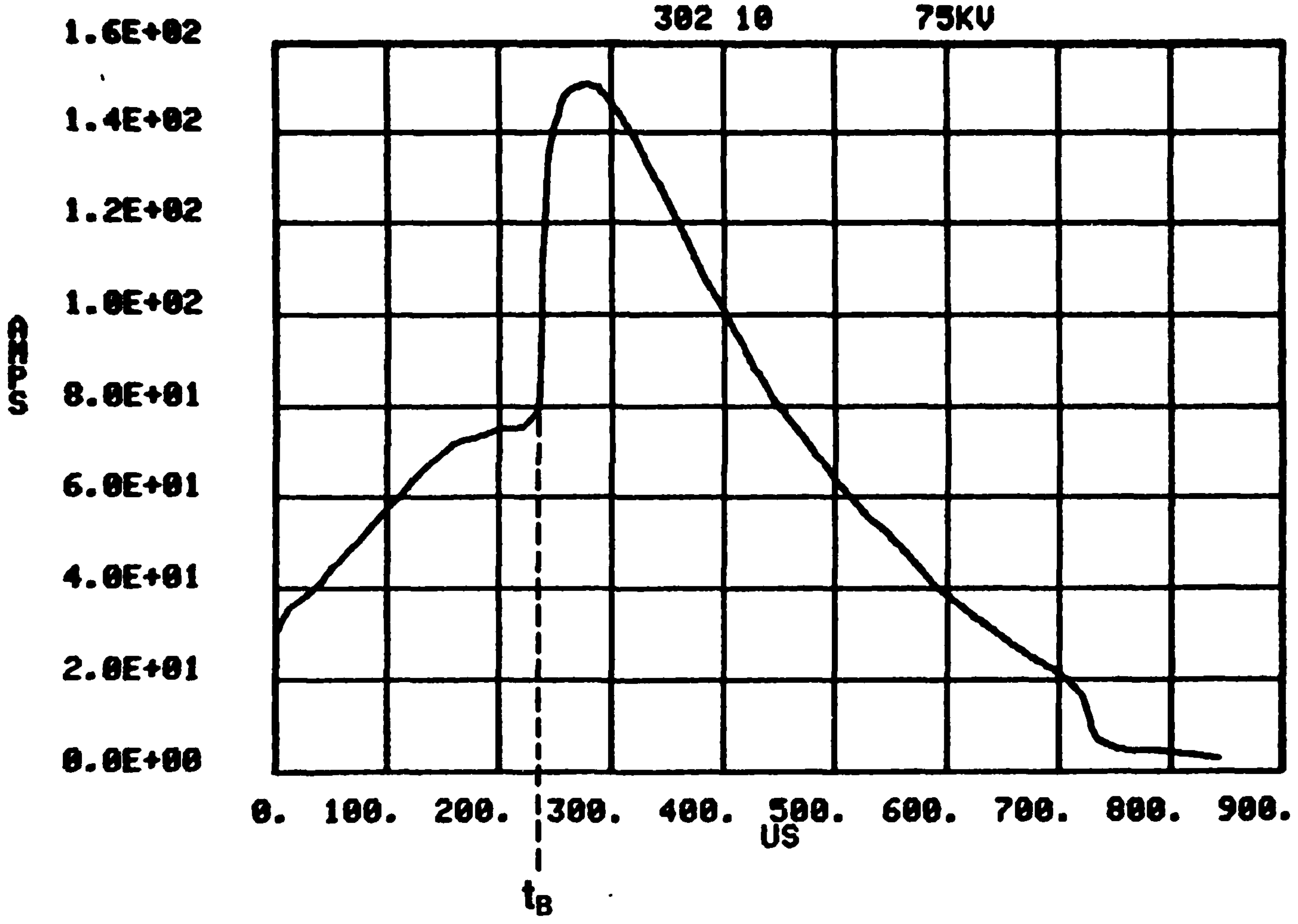

Figure 15. Current versus time in shot 302 (cylindrical wedge soil sample). The current rises with time as if to a maximum, and then at t_B the sample breaks down to the outer conductor.

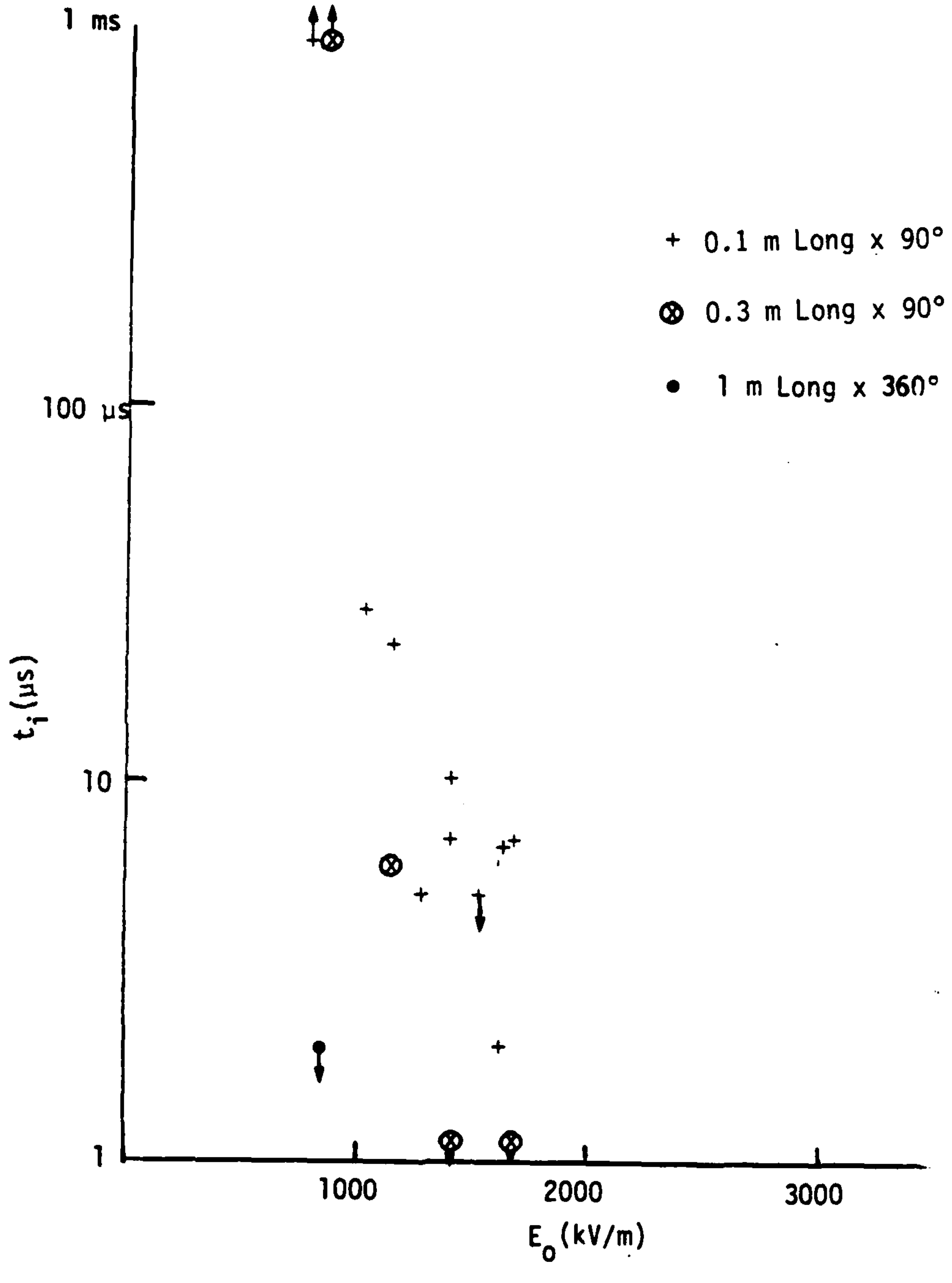

Figure 16. Time to breakdown t_i for three geometries.*

---

*Ibid

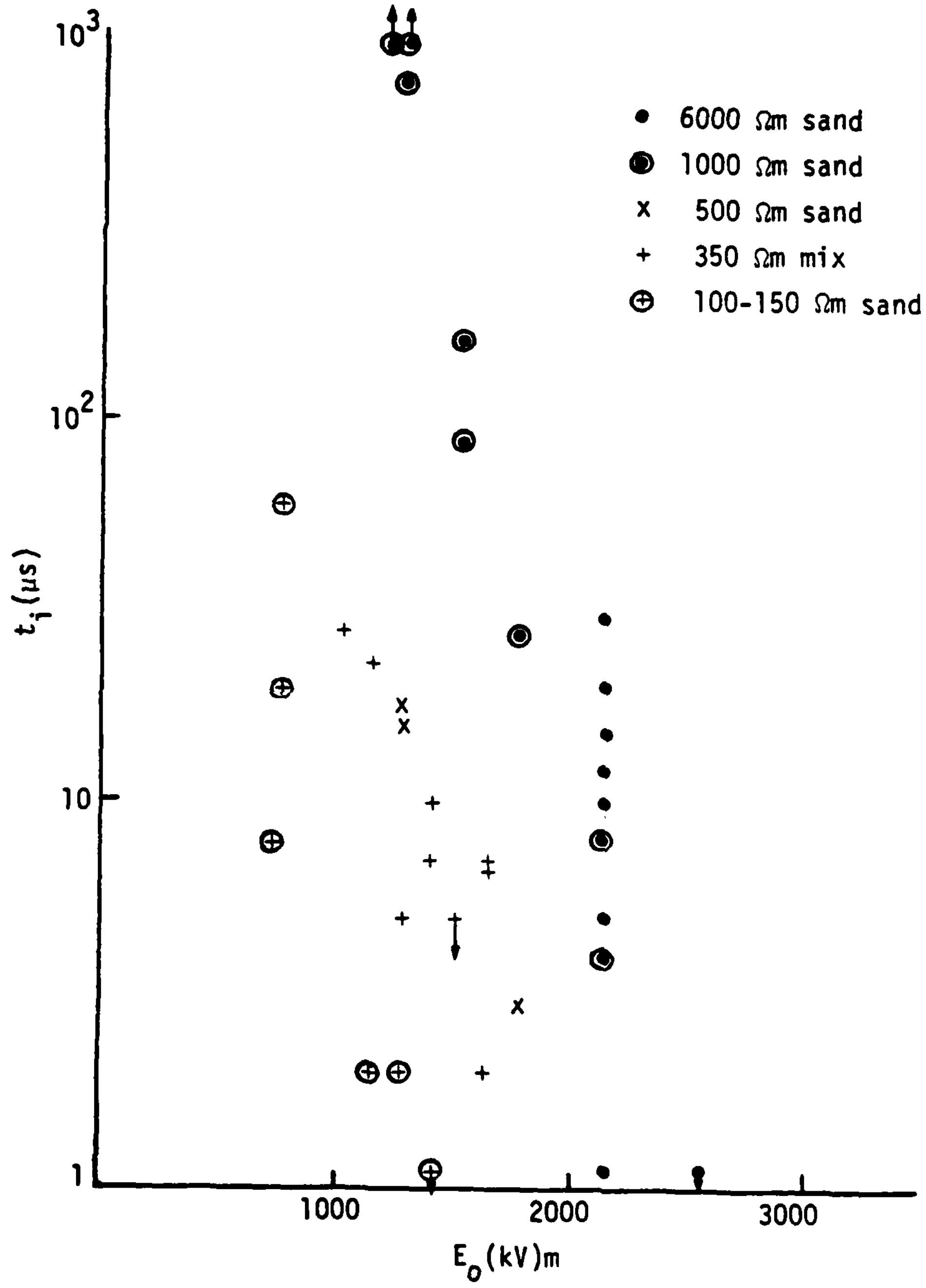

Figure 17. Time to breakdown t_i for various soil types.*

---

*Ibid

It has been pointed out in paragraph 2 that given a plot of V(r) versus log r, as shown in Figure 7, r_0 may be obtained from the intersection of the log r approximations to the ohmic region and the corona region. From the slopes of these two curves, ρ_1/ρ_0 may be found from Equation 15 and then E_B may be calculated from Equation 11. There were a large number of shots obtained in the Exp. A in a 350 Ω-m sand mix which allows these quantities to be investigated in detail.

Use shot 399 as an example. Plots of V/I versus log r for this shot are shown in Figure 2, and V versus log r in Figures 5 to 8. Maximum current for this shot is 15.25 A occurring at 200 μs. From these figures, as time increases r_0 increases and ρ_1/ρ_0 decreases. At 30 μs: $r_0 = 0.127$ m, $\rho_1/\rho_0 = 0.334$; at 60 μs: $r_0 = 0.135$ m, $\rho_1/\rho_0 = 0.28$ at 100 μs, $r_0 = 0.141$, $\rho_1/\rho_0 = 0.23$; and at 200 μs, $r_0 = 0.16$ m, $\rho_1/\rho_0 = 0.13$. For time greater than 200 μs, the dynamic region considered in Section V, is reached.

In the other shots which have been investigated, r_0, ρ_1/ρ_0, and E_B at current maximum have been found. For all these shots (12 in all, see Figures B.1 through B.10 and B.12 through B.31) E_B ranges from about 100 to 250 kV/m. It is interesting that this range coincides with that found in Reference 6. The correlation between E_B and ρ_1/ρ_0 with various parameters such as the total current I, the current density and the peak V_0 have been investigated. It was found that these quantities correlate best with V_0 peak. This may be justified by noting that the breakdown behavior of the soil may be determined by the initial value of the electric field at the center conductor. Note that this electric field E_0 is related to V_0 peak by

$$E_0 = \left(V_0 \text{ peak}\right) \Big/ \left(a \ \ln \frac{b}{a}\right) \tag{32}$$

In Figures 18 and 19, E_B and ρ_1/ρ_0 versus E_0 have been plotted. This data has been processed by the least squares linear regression method, which shows that the following linear relationships best fit the data:

$$E_B = 54.5 + 87.6 \ E_0, \ R^2 = 0.69 \tag{33}$$

$$\rho_1/\rho_0 = 0.97 - 0.48 \ E_0, \ R^2 = 0.87 \tag{34}$$

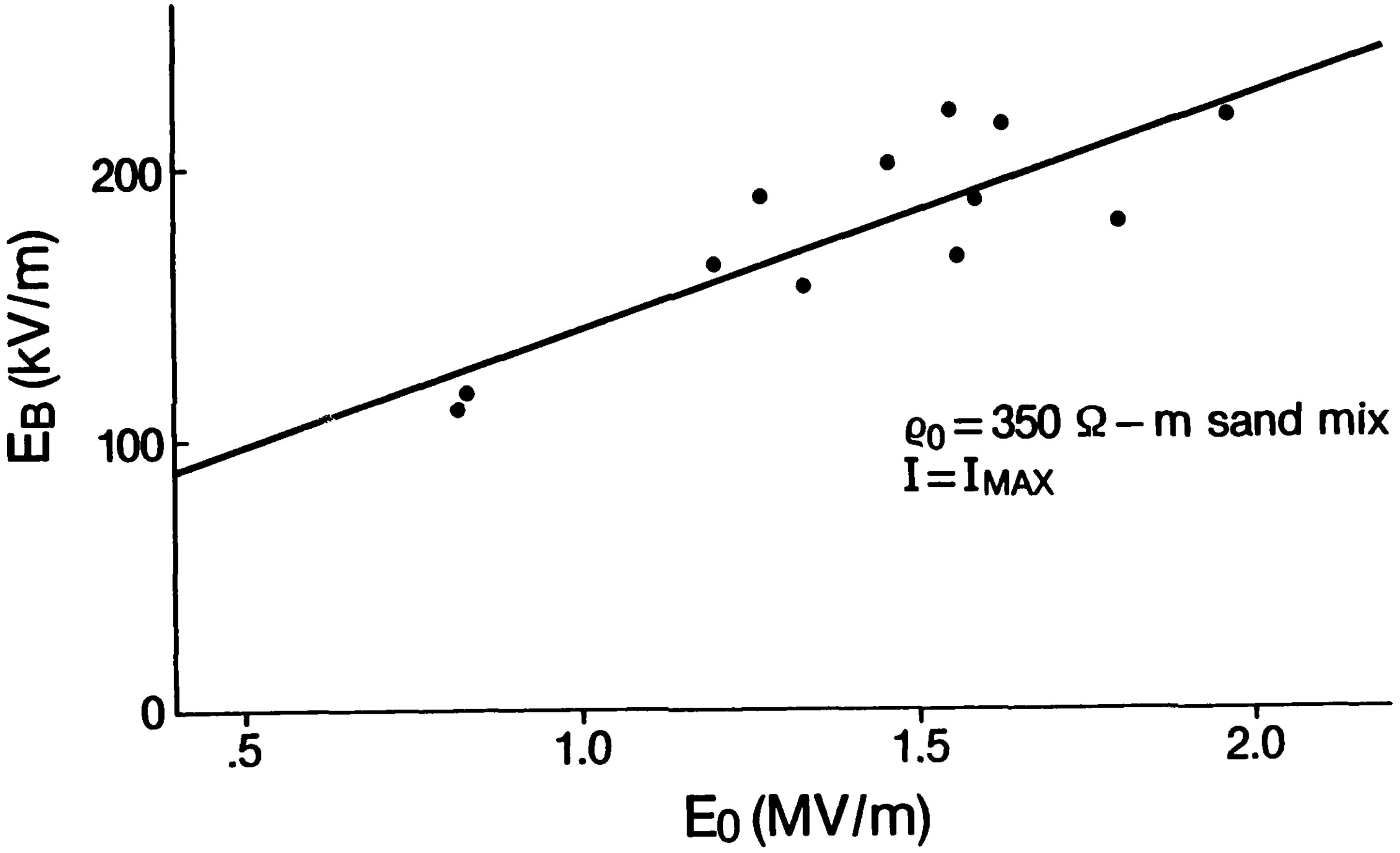

Figure 18. Linear regression of critical electric field at current maximum with peak electric field at center conductor ρ_0 = 350 Ω-m sand mix.

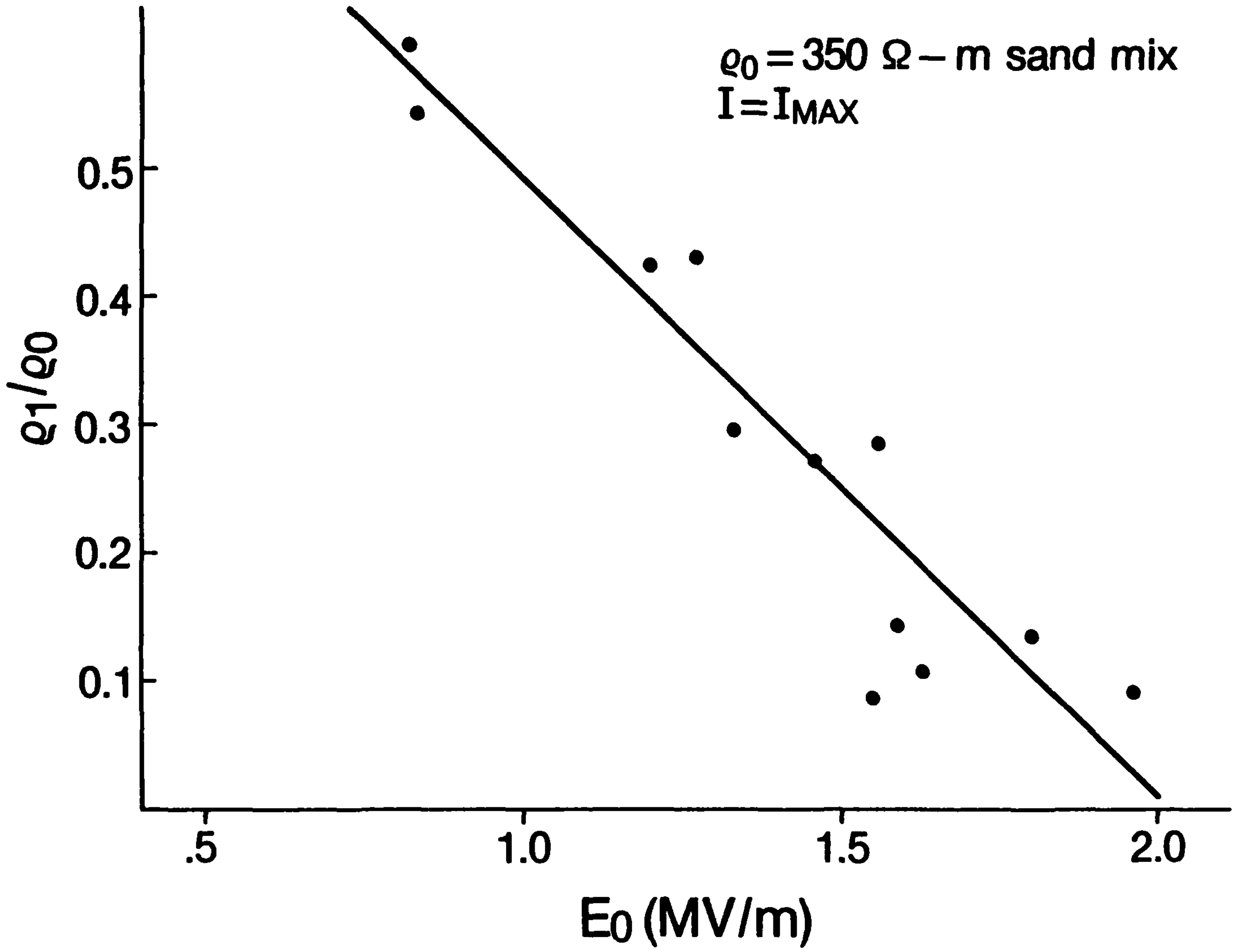

Figure 19. Linear regression of ρ_1/ρ_0 at current maximum with peak electric field at center conductor. ρ_0 = 350 Ω-m sand mix.

If E_0 is in MV/m, E_B will have the units of kV/m; similarly, E_0 should be in MV/m in Equation 34. The coefficient of determination, R^2, is shown for each least squares linear fit. The range of E_0 for which this data is valid is $0.5 \geq E_0 \geq 2$ MV/m.

In Exp. A, there were some data available from which plots of E_B and ρ_1/ρ_0 versus E_0 were obtained, for soils with other ohmic resistivities than 350 Ω-m (Figs. B.32 through B.45, Appendix B). These are shown in Figures 20 through 25 for soils with resistivities of 200, 170 and 130 Ω-m. These data should be used with caution because generally no more than four points were available to determine each curve, and some of the data points did not correspond to t_m when I as a maximum, but were obtained at an earlier time. With this qualification, these curves tend to show that E_B increases as the ohmic resistivity increases.

5. CALCULATION OF MAXIMUM CURRENT

One of the real achievements of the electrostatic model is its ability to predict the maximum value of the current through the sample. The maximum current, I_M, which is shown in Figure 13, has been measured for a number of shots for the 350 Ω-m sand mix.

The general expression for current through the sample is given by

$$I = \frac{\alpha L\ r_0}{\rho_0} E_B \tag{35}$$

If r_0 and E_B at $I = I_M$ are used, Equation 35 yields I_M. But, E_B for I_M is given in Figure 18 and r_0 was also tabulated for this current.

In Figure 26, the measured value of I_M versus V_0 has been plotted at t_m, i.e., the center conductor voltage at the time when the current is maximum. Of the 12 shots for ρ_0 = 350 Ω-m, 4 were for a sample with L = 0.1 m, while 8 were for L = 0.3 m. The experimentally measured values of I_M are shown by the solid dots in Figure 26.

Alternately, Equation 35 has been used to predict I_M where we have used the actual r_0 and E_B obtained for a shot. This prediction of I_M is shown by the open circles in Figure 26. The agreement is usually very close. The percentage differences are tabulated in Table 1.

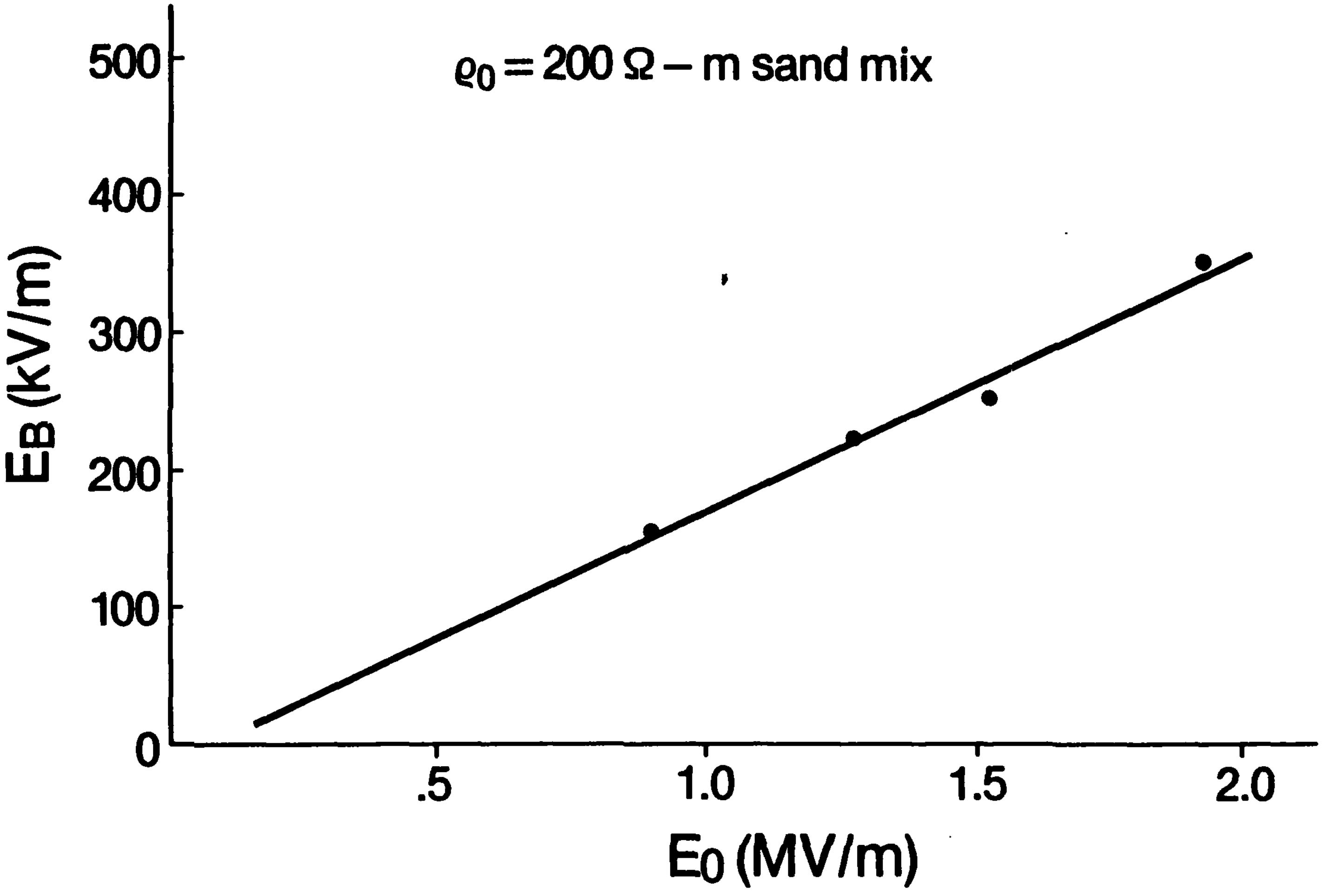

Figure 20. Linear regression of critical electric field at current maximum with peak electric field at center conductor. $\rho_0 = 200\ \Omega\text{-m}$ sand mix.

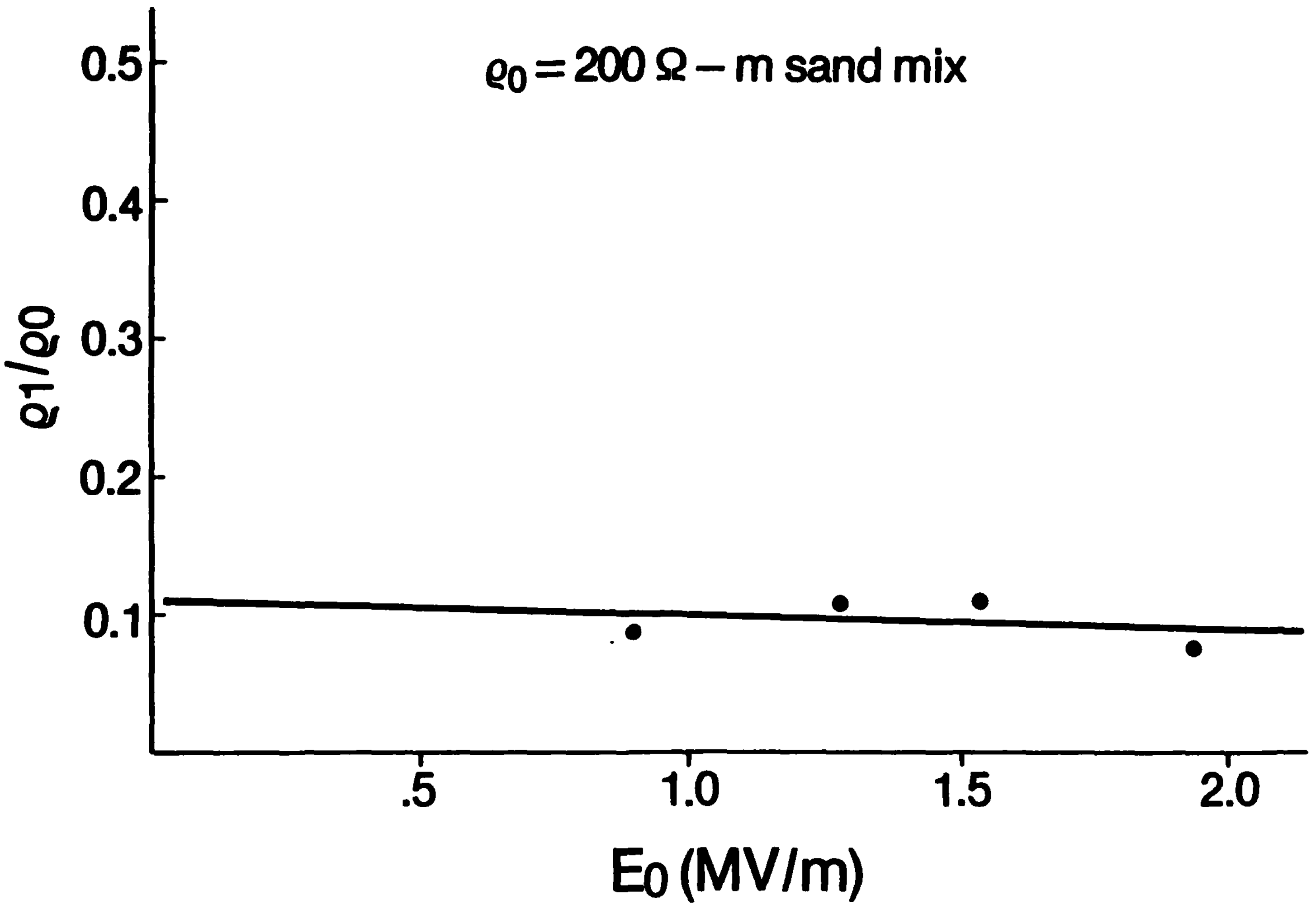

Figure 21. Linear regression of ρ_1/ρ_0 at current maximum with peak electric field at center conductor. ρ_0 = 200 Ω-m sand mix.

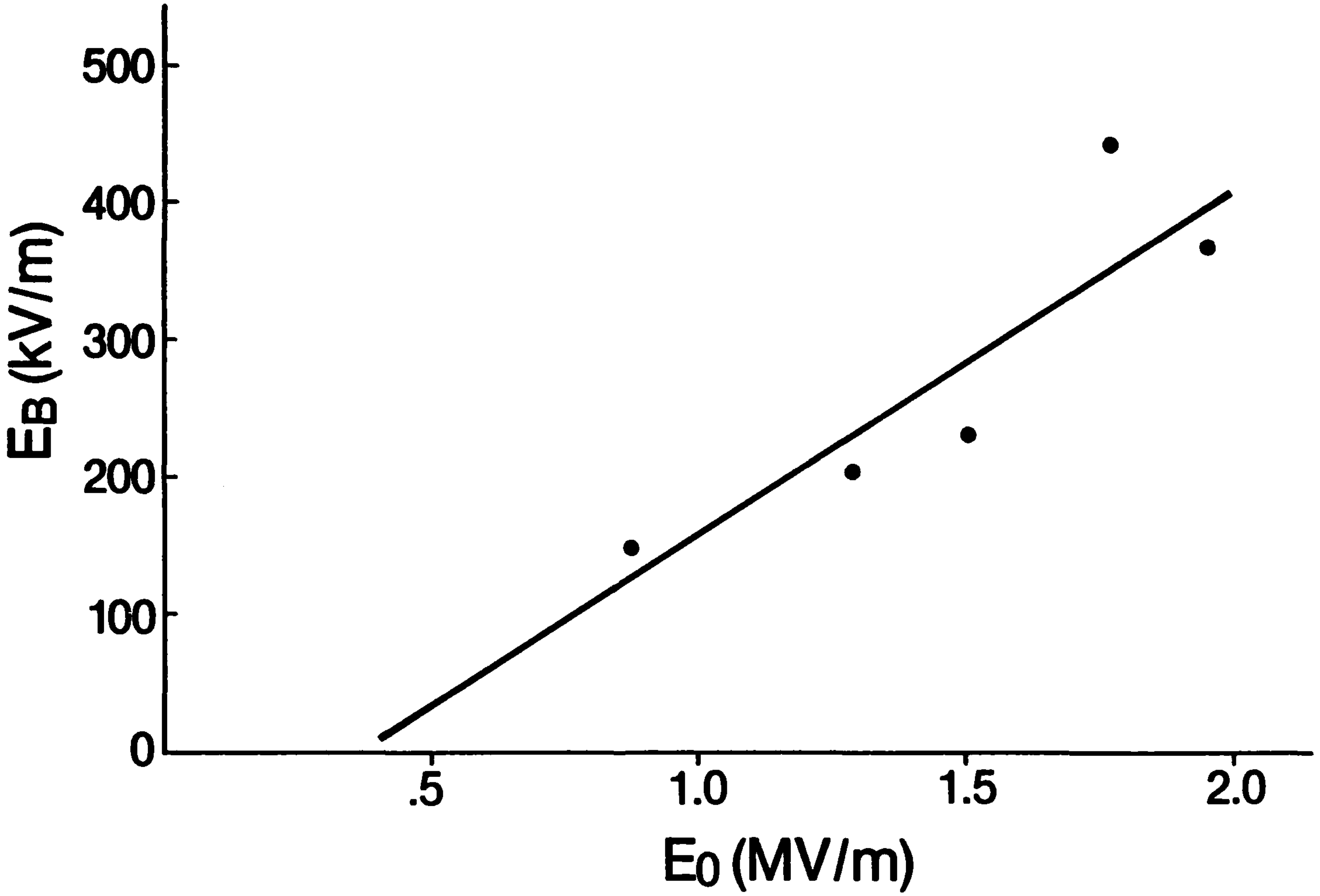

Figure 22. Linear regression of critical electric field at current maximum with peak electric field at center conductor. ρ_o = 170 Ω-m sand mix and Soil-B.

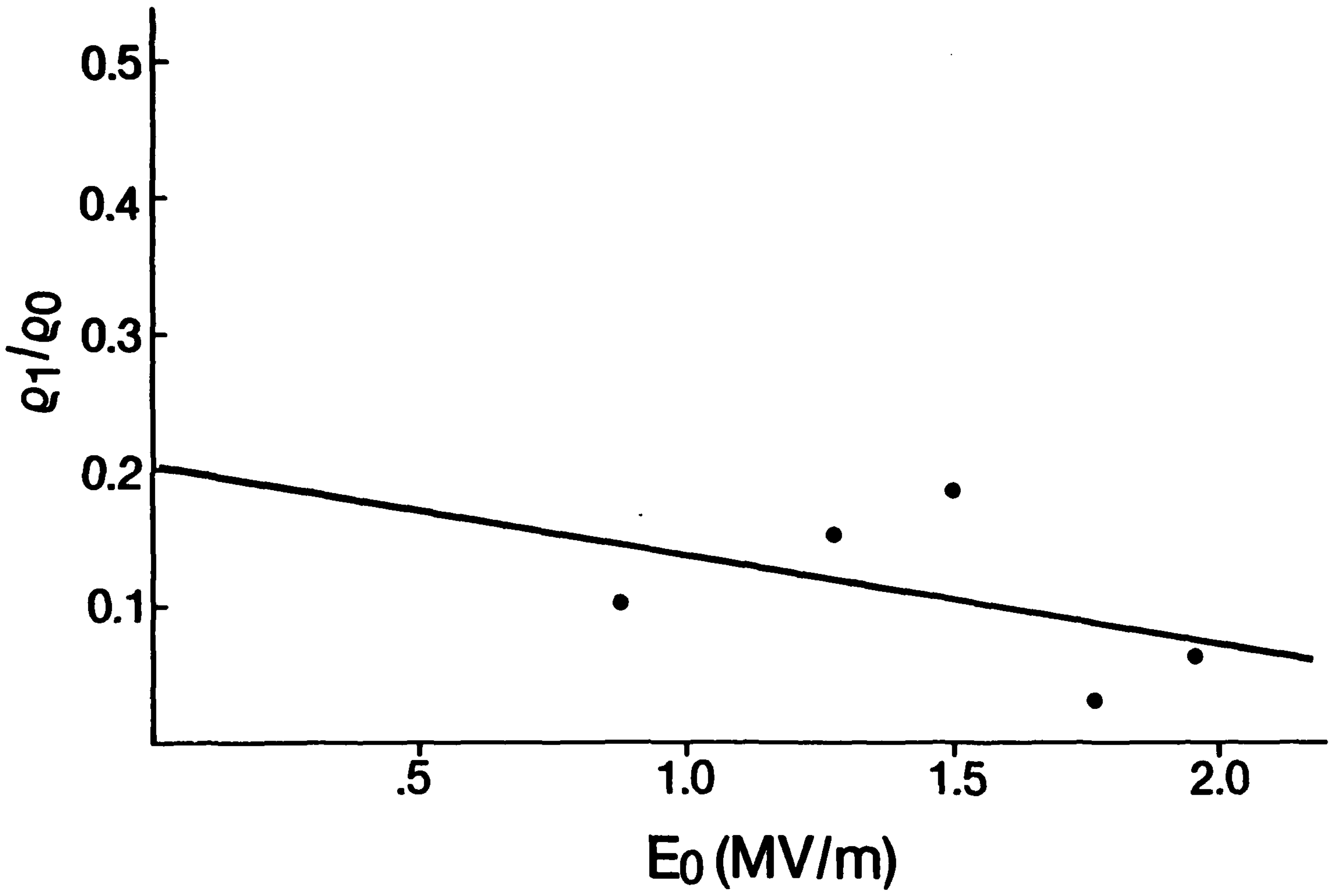

Figure 23. Linear regression of ρ_1/ρ_0 at current maximum with peak electric field at center conductor. ρ_0 = 170 Ω-m sand mix and Soil-B.

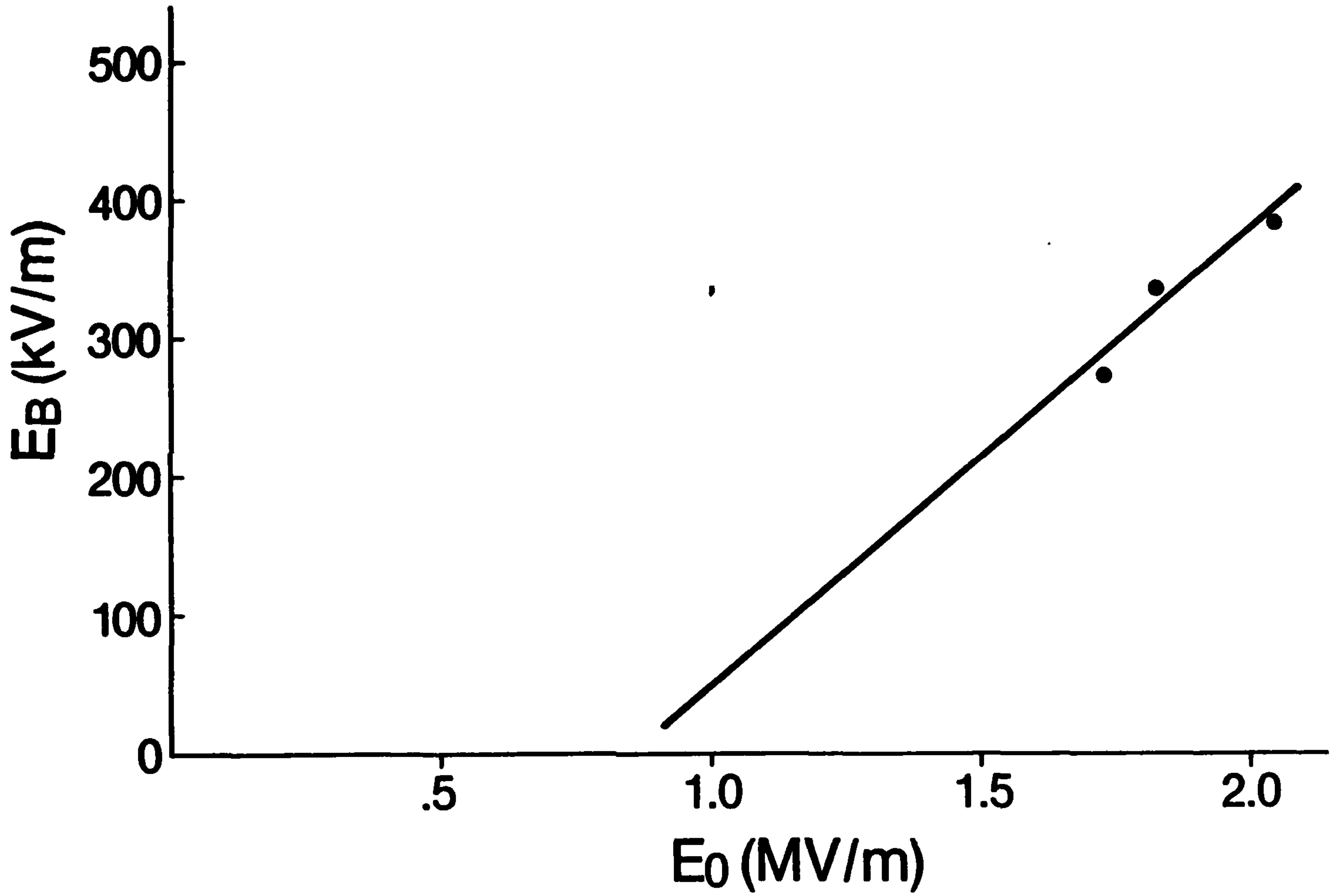

Figure 24. Linear regression of critical electric field at current maximum with peak electric field at center conductor. ρ_0 = 130 Ω-m Soil-B.

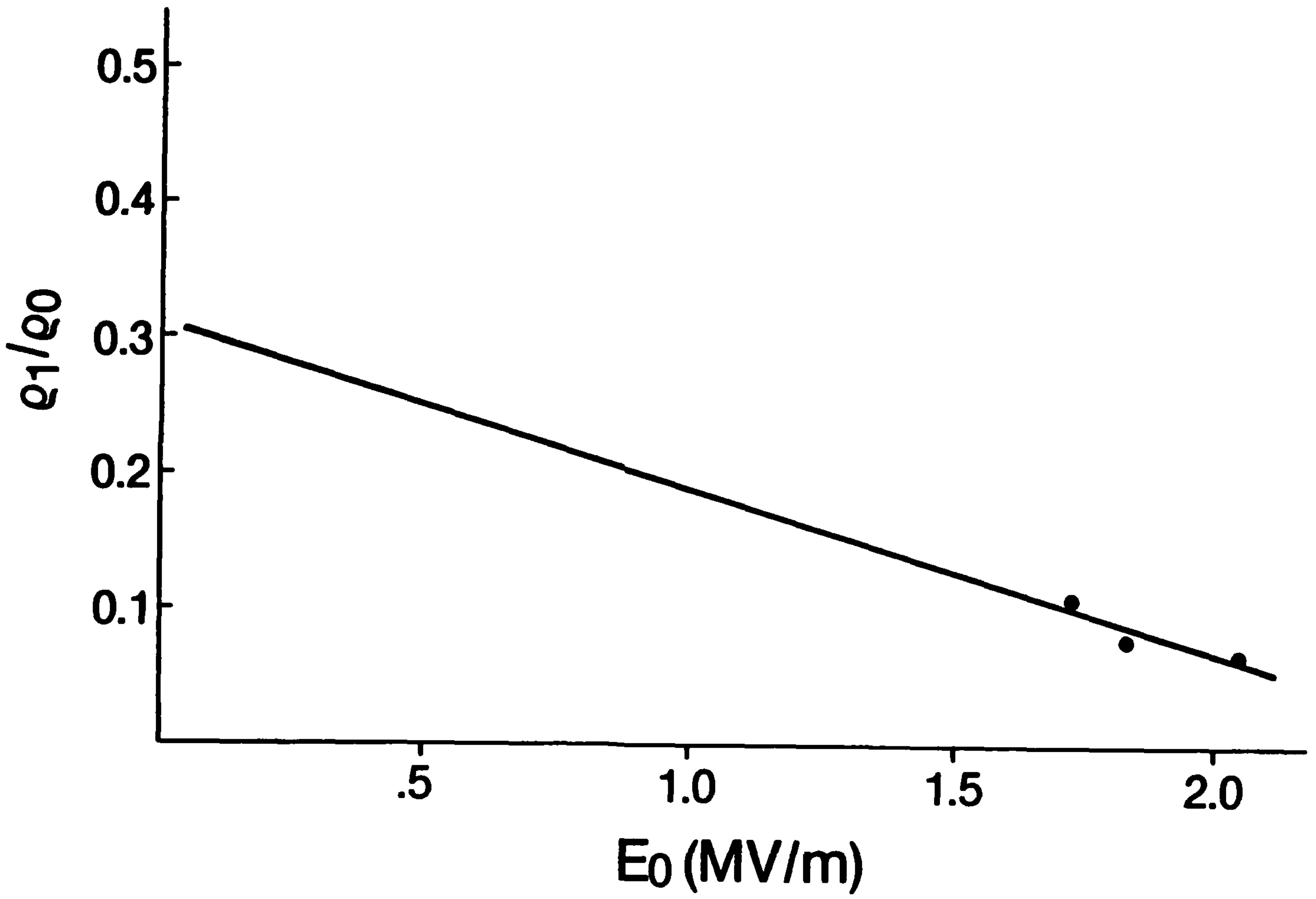

Figure 25. Linear regression of ρ_1/ρ_0 at current maximum with peak electric field at center conductor. ρ_0 = 130 Ω-m Soil-B.

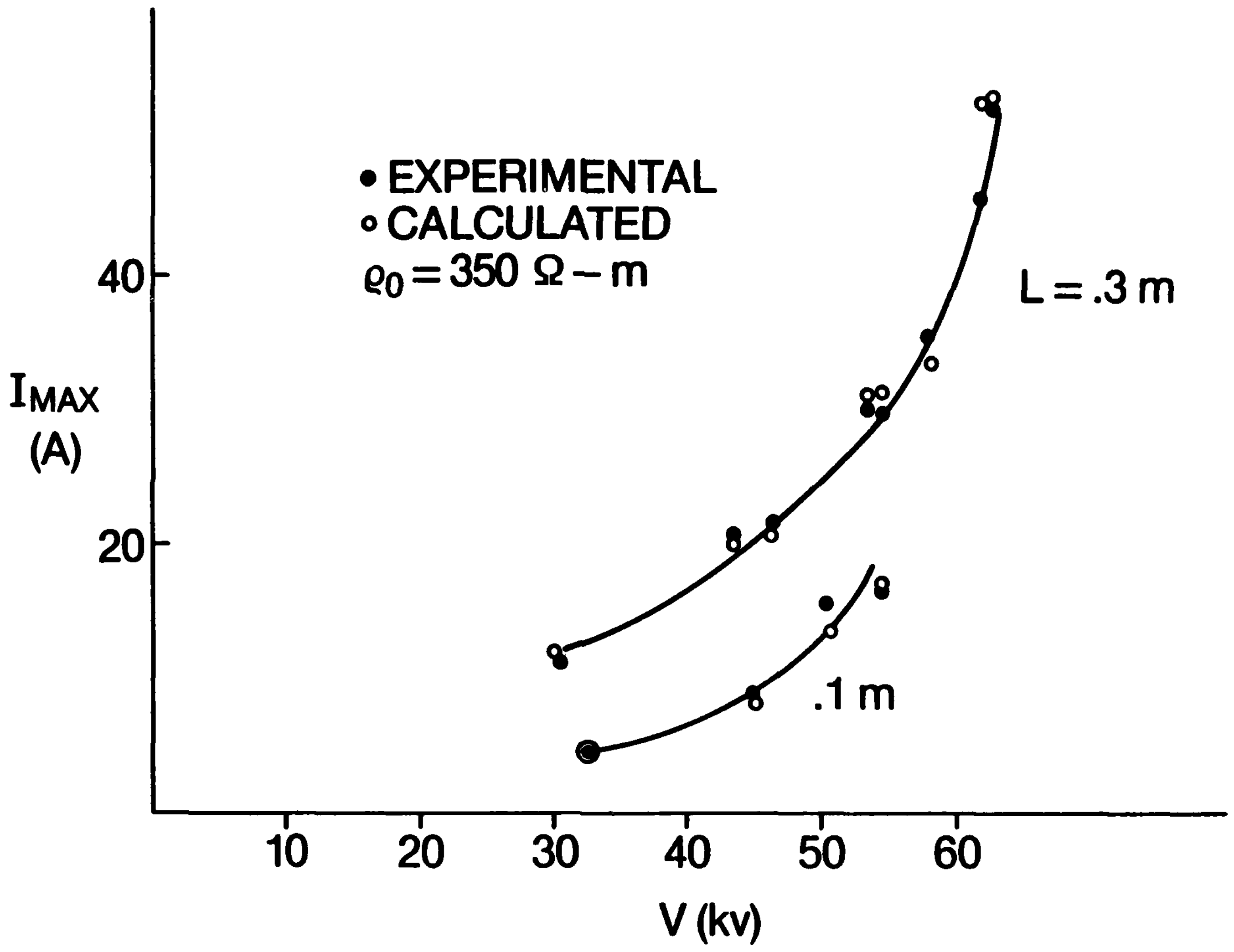

Figure 26. Max current versus voltage at center conductor. Dots: measured; open circles: calculated.

The most important conclusion to be drawn from the generally remarkable correspondence between the measured and calculated I_M is that the corona must be very azimuthally uniform. The radial probes which measure V, from which r_0 and E_B are determined, lie at an angle of 45 deg as shown in Figure 1. Thus, r_0 and E_B are really only valid for this angle. If, for example, they were quite different at some other angle, then the current density would be azimuthally asymmetric and the total current could not be predicted by Equation 35. That may explain the discrepancies (15.5 and 21.1 percent) in shots 424 and 426. The fact that there is so little percent difference leads to the conclusion that the corona is azimuthally symmetric and r_0 and E_B do not vary with angle. The fact that electrical phenomena within the 90 deg cylindrical wedge sample must have exact images in the wedges constituting the other three quadrants of the circle, as well as in the wedges stacked on top and below (to satisfy the boundary conditions at the insulating walls of the wedge), may tend to preserve azimuthal symmetry.

TABLE 1. MAXIMUM CURRENT I_M THROUGH 90 DEG WEDGE SAMPLE

Shot No.	I_M(A) (Measured)	I_M(B) from (280)	Difference %
394	4.8	4.8	0
398	8.8	8.35	5.1
399	15.6	15.3	1.9
401	16.8	17	-1.1
419	11.3	12	-6.2
420	20.5	20	2.4
421	21.3	20.5	3.8
422	29.8	31.7	-6.3
423	30	31.3	-4.3
424	45.9	53	-15.5
426	55.4	43.7	21.1
427	52.8	53.3	-0.9

6. SPHERICAL CASE

Referring to Figure 9, consider a spherical geometry in which the spherical inner electrode has a radius a and the outer spherical shell will be removed to infinity, so that $b \to \infty$. Then, Equation 25 may be written as:

$$E_B = \frac{V_0}{\left(1 - \rho_1/\rho_0\right)\frac{1}{r_0} + \left(\frac{\rho_1}{\rho_0}\right)\frac{1}{a}} \quad \frac{1}{r_0{}^2} \tag{36}$$

For the high voltages used in Exp. C (point-plane experiments), e.g., about 200 kV, the estimate of ρ_1/ρ_0 indicates that it will be less than 0.1. Therefore, if ρ_1/ρ_0 is set equal to zero in Equation 36 the simple result is:

$$r_0 = V_0/E_B \tag{37}$$

By using E_B = 200 kV, and V_0 = 200 kV, Equation 37 indicates that r_0 is about 1 m.

As an indication of the validity of these calculations, it should be noted that Exp. C* has not yielded a direct measurement of the radius of the spherical corona region. Rather, what has been observed is that while the ohmic resistance from the high voltage electrode to infinite ground is about 200 Ω, when 200 kV is applied, the resistance initially at $t = 0$ is about 30 Ω and then declines to about 4 Ω. Subsequently, it drops to 1 Ω where it is believed that a streamer is propagating. If a spherical corona region which is growing in radius is postulated, one may thus account for the decreased resistance.

The total current flowing in the soil may be calculated by reference to Figure 9. At r_0, it is:

$$I = \frac{E_B}{\rho_0} 4\pi \, r_0{}^2$$

---

*Private Communication, Charles Mallon, JAYCOR, San Diego, Calif.

Making use of Equation 37, the resistance R to infinite ground is:

$$\frac{V_0}{I} = R = \frac{\rho_0}{4\pi} \frac{E_B}{V_0} \qquad (38)$$

For V_0 having its peak value, 200 kV, and using the measured ohmic soil resistivity at the experimental site for Experiment C,

$$\rho_0 = 50 \ \Omega\text{-m}$$

we obtain:

$$R = 2.0 \times 10^{-2} \ E_B(\text{kV/m}) \ \Omega$$

A resistance of 4 Ω could be accounted for if E_B = 200 kV/m corresponding to r_0 = 1 m.

V. DYNAMIC THEORY OF THE CORONA REGION

In Section IV, the formation of the corona region about a high voltage electrode was discussed. The model is a simple one in which there are two regions: one adjacent to the high voltage electrode called the corona region and the second called the ohmic region. The corona region has radius r_0 and resistivity ρ_1, while the ohmic region exists for $r \geq r_0$, and has the ohmic resistivity ρ_0. The corona region is in some fashion broken down electrically.

1. THE DYNAMIC MODEL

If the relaxation phase of the voltage pulse is considered; i.e., the time after the current has reached its peak value and is declining to zero, then a third region can be identified with a resistivity ρ_2, which is dependent on a current density J, and is intermediate between ρ_1 and ρ_0 (Ref. 6). By introducing this third region, Liew, et. al., could phenomenologically predict their experimental results quite accurately. They referred to this model as a dynamic model of soil breakdown.

In a manner similar to that of Reference 6, the following model of corona relaxation is proposed. As the voltage rises at the high voltage electrode, assume that the soil breaks down as described in Section IV; i.e., the soil breaks down out to a maximum radius r_0 determined by E_B, the peak applied voltage, ρ_1 for $r \leq r_0$, and ρ_0 for $r \geq r_0$. It should be noted that at r_0 in the ohmic region, there is a current density

$$J_c \equiv E_B/\rho_0 \tag{39}$$

which has been called the critical current density.

As the applied voltage and current relaxes to zero, a new region forms. It is defines by $r_1 \leq r \leq r_0$, where r_0 is determined from the electrostatic phase--call this region 2. The radius r_1 is defined such that at r_1, the current density is J_c. The resistivity in region 2, ρ_2, depends on J and, therefore, on r. Since ρ_2, does not equal ρ_0 the resistivity of this region undergoes hysteresis--call this the relaxation phase.

During the relaxation phase, we can thus identify three soil regions which are shown in Figure 27. (This figure could represent either a cylindrical or spherical system.):

Region 1, corona region, $a \leq r \leq r_1$:
$\rho = \rho_1$, a constant; $J > J_c$.
Region 2, hysteresis region, $r_1 \leq r \leq r_0$:
$\rho = \rho_2(r)$; $J < J_c$ with $J = J_c$ at $r = r_1$.
Region 3, ohmic region: $r_0 \leq r \leq b$.
$\rho = \rho_0$, a constant.

2. RELAXATION THEORY

Consider a cylindrical system, the calculations shall be compared with the results of shot 399, of Exp. A.

For region 2, use

$$\rho_2 = \rho_1 + (\rho_0 - \rho_1)(1 - J(r)/J_c)^2 \qquad (40)$$

which is approximately the expression that was empirically determined to give the best agreement between theory and experiment (Ref. 6).

Note that at r_1, $\rho_2 = \rho_1$ and the resistivity is continuous across the boundary between regions 1 and 2. From Equation 1, E_r will be continuous (since J_r must be continuous), and there will be no charge on this boundary. At $r = r_0$, however, $\rho_2 \neq \rho_0$, so that the resistivity and E_r is discontinuous across the bondary between regions 2 and 3. There must be charge on this boundary.

Let $V_0(t)$ be applied voltage at the center electrode of radius a. Then a total current I(t) will flow, and

$$J(r,t) = I(t)\alpha r\ell \qquad (41)$$

where α is the wedge angle and ℓ is the length of the cylindrical sample. For Figure 27, $\alpha = 2\pi$ rad.

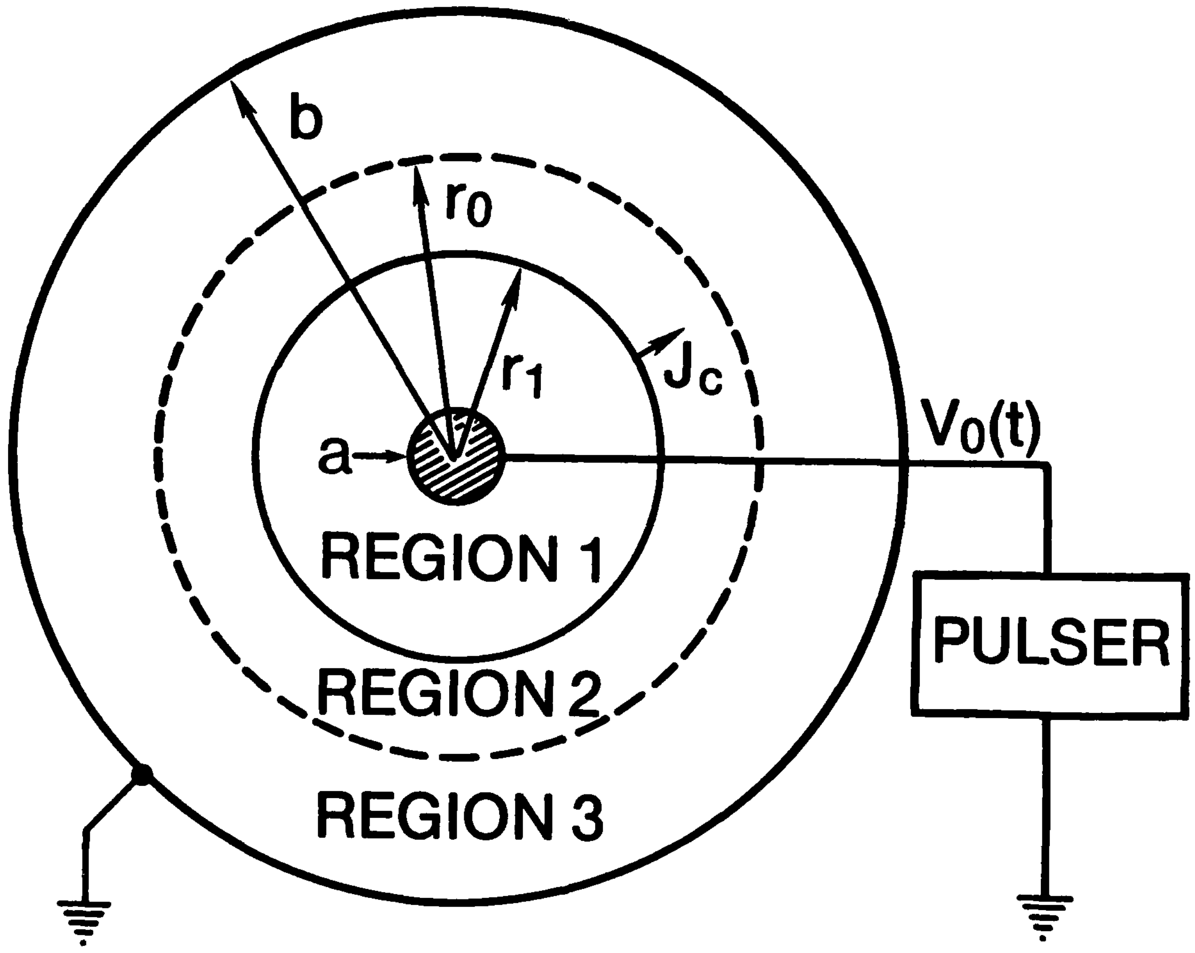
b
r_0
r_1
J_c
$V_0(t)$
a
REGION 1
REGION 2
REGION 3
PULSER

Figure 27. Cylindrical or spherical system for dynamic model. Region 1: corona; region 2: hysteresis; region 3: ohmic.

The resistance of the system $R(r)$ which is defined as the resistance between radius r and the grounded electrode at $r = b$ shall be calculated. By this definition, $R(a)$ would be a total resistance such that $I = V_0/R(a)$.

Consider two closely spaced cylindrical shells with the inner shell at radius r and the separation of the shells being dr. Then the resistance of the region between the shells is:

$$dR = \rho \frac{dr}{\alpha \ell r}$$

and

$$R(r) = \int_r^b \rho \; \frac{dr}{\alpha \ell r} \tag{42}$$

It is not difficult to obtain:

Region 3, $r_0 \leq r \leq b$

$$\left(\frac{\alpha \ell}{\rho_0}\right) R(r) = \ell n \left(\frac{b}{r}\right) \tag{43}$$

Region 2, $r_1 \leq r \leq r_0$

$$\left(\frac{\alpha \ell}{\rho_0}\right) R(r) = \ell n \left(\frac{b}{r}\right) - 2r_1 \left(1 - \frac{\rho_1}{\rho_0}\right)\left(\frac{1}{r} - \frac{1}{r_0}\right) + \frac{1}{2}\left(1 - \frac{\rho_1}{\rho_0}\right) r_1{}^2 \left(\frac{1}{r^2} - \frac{1}{r_0{}^2}\right) \tag{44}$$

Region 1, $a \leq r \leq r_1$

$$\left(\frac{\alpha \ell}{\rho_0}\right) R(r) = \ell n \, \frac{b}{r^1} + \frac{\rho_1}{\rho_0} \, \ell n \, \frac{r_1}{r} + \left(1 - \frac{\rho_1}{\rho_0}\right) \left[\frac{1}{2r_1{}^2} \left(\frac{1}{r_1{}^2} - \frac{1}{r_0{}^2} \right) - (2r_1) \left(\frac{1}{r_1} - \frac{1}{r_0} \right) \right] \tag{45}$$

where

$$r_1 = I/J_c \alpha \ell \tag{46}$$

3. RESULTS

Shot 399 is reproduced in Figure 2 where the ordinate is just $R(r)$ in kilo-ohms and the abscissa is log r. For this shot, $\rho_0 = 350$ Ω-m, $\alpha = \pi/2$ rad, $\ell = 0.1$ m, $a = 0.01$ m, and $b = 0.5$ m. Each curve shot 399 is at a different time with curve A occurring at the earliest time and curve F at the latest time. The times for each curve are shown in Figure 2; also shown is the current I that was measured at each time.

Under the assumption that J_c is a constant, maximum radius r_0 which marks the end of the electrostatic phase would occur when I is a maximum. This would correspond approximately for curve B at 200 μs. Measure r_0 directly by approximating curve B by two straight lines which are seen to intersect at $r = 0.16$ m. Take this value of r to be r_0. Using the techniques described in Section IV, para 4, obtain $\rho_1/\rho_0 = 0.129$ from which E_B may be calculated by the method described to be 231.5 kV/m. Alternately, since I was measured to be 15.25 A for curve B, at $r_0 = 0.16$ m, J_c is 607 A/m^2, and from Equation 27, $E_B = 212.3$ kV/m. This value of E_B is 8 percent lower than the value calculated using these techniques.

Now use $J_c = 607$ A/m^2 and $r_0 = 0.16$ m to predict curves C, D, E, and F. Adjust ρ_1/ρ_0 as may be necessary. The results are shown in Figures 28 through 31 where we have made use of Equations 43 through 46. The value of ρ_1/ρ_0 required are as follows:

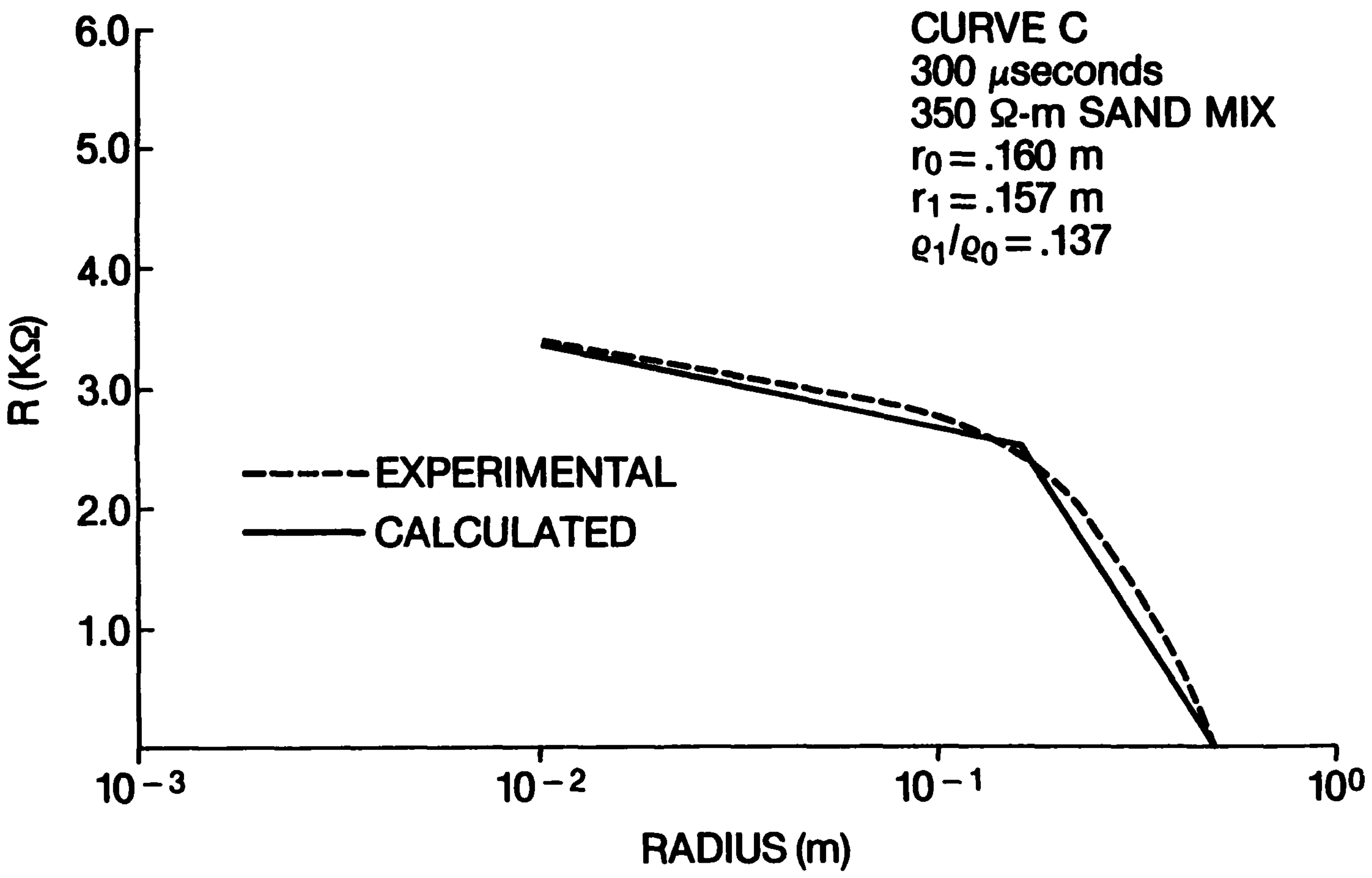

Figure 28. Dynamic model prediction (dashed line) of Curve C of Figure 2, $\rho_1/\rho_0 = 0.137$.

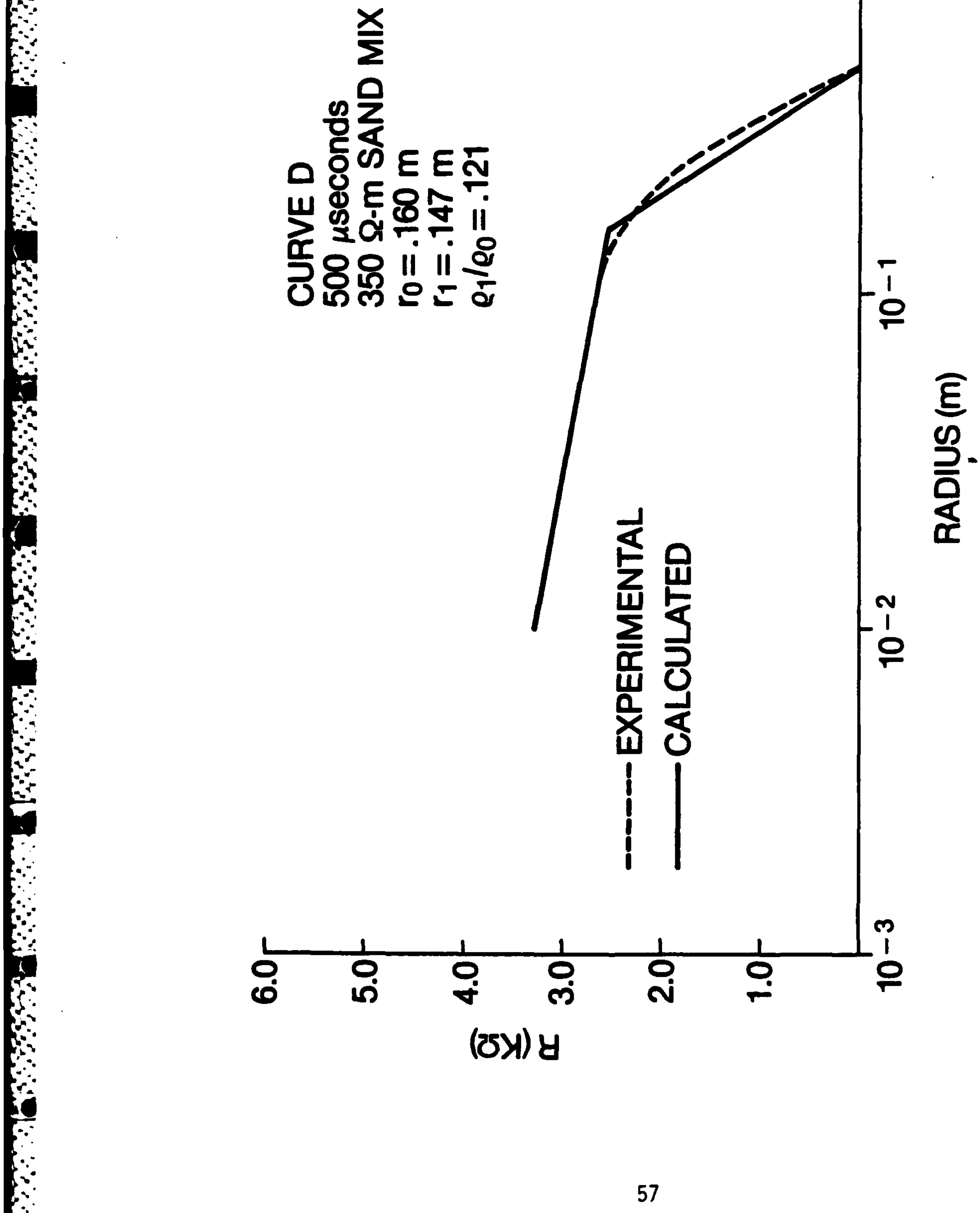

Figure 29. Dynamic model prediction (dashed line) of Curve D of Figure 2, ρ_1/ρ_0 = 0.121.

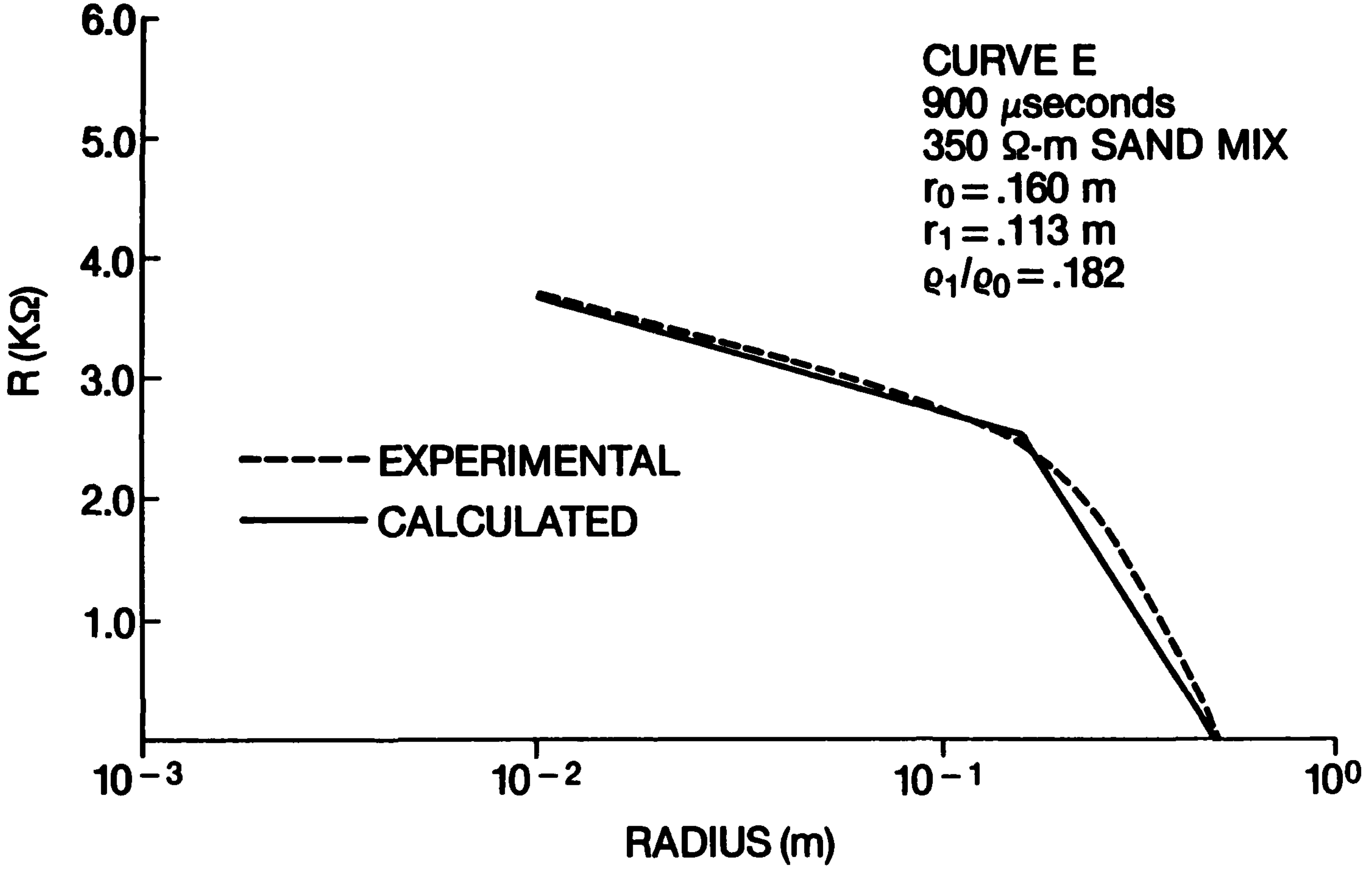

Figure 30. Dynamic model prediction (dashed line) of Curve E of Figure 2, $\rho_1/\rho_0 = 0.182$.

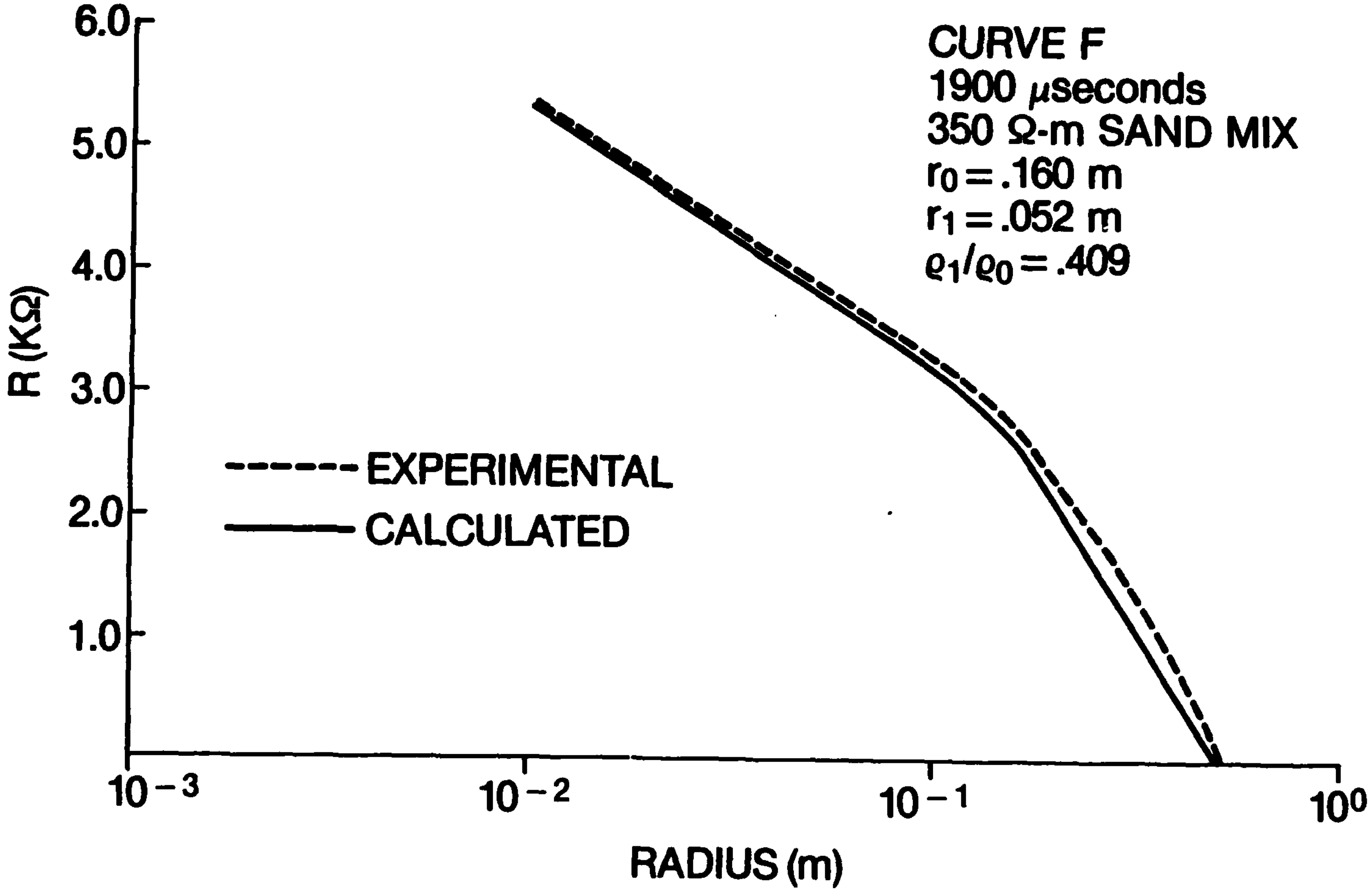

Figure 31. Dynamic model prediction (dashed line) of Curve F of Figure 2, $\rho_1/\rho_0 = 0.409$.

Curve	I/A	ρ_1/ρ_0
C	15	0.137
D	14	0.121
E	10.75	0.182
F	5	0.409

Thus, a good agreement may be obtained between the dynamic model and the experimental data, providing that ρ_1/ρ_0 is allowed to increase as the total current decreases, not an unexpected result.

VI. STREAMERS

If the voltage on the center conductor V_0 is large enough, the current through the sample will first start to rise, as if toward a maximum, but then will suddenly increase as is shown in Figure 15. This sudden increase indicates that the broken down portion of the soil sample extends all the way to the grounded conductor, or that it has attached to the grounded conductor. This state is referred to as attached breakdown.

Attached breakdown can occur for the following reasons: If the corona is symmetric at its boundary as is the case in Figure 26, the corona will attach if:

a. r_0 becomes large enough so that it equals the critical stability radius; if the system is stable, or the critical stability radius exceeds b, the corona will attach if V_0 is so large that:

b. $r_0 = b$.

The symmetric corona may contain streamers, but they apparently are not dominant enough to significantly distort the boundary, so that the boundary retains the symmetry of the electrode system. Corona attachment is discussed in paragraph 1. On the other hand, streamers may dominate the corona. Then attachment occurs if:

c. The streamer propagates as described in Reference 7 which characterizes the streamer propagating outward with a velocity. For this case, envision the streamer pushing the corona ahead of it as shown in Figure 4 so that the corona attaches first followed by streamer attachment. Streamer attachment is discussed in paragraph 2.

For cases a and b, when corona attachment occurs, presume that the current is carried more or less uniformly by the corona. For case c, when streamer attachment occurs, the current is presumed to be carried primarily by the streamer, which may benefit from attachment in the sense that its resistivity may decrease, its current increase, and its diameter increase. This, however, is speculation.

As seen in Figure 26 the corona in Exp. A is cylindrically symmetric. Therefore, corona attachment of types (a) or (b) should occur in these experiments. On the other hand, in paragraph 2, Exp. B, streamers exist after attachment has occurred. Thus, in these experiments, the attachment should be of type (c), streamer attachment.

To strengthen these conclusions, refer to Figure 32 which is a plot of attachment time t_B versus V_0 peak, the peak voltage on the center conductor. These data were obtained from both Exp. A and B. The x and open circles o are data from Exp. A. It is seen that, at least, for times t_B less than 1 ms attachment does not occur for V_0 below about 65 kV.

These data were obtained from a system in which a = 0.01 m and b = 0.5 m. If the data for E_B and ρ_1/ρ_0 for ρ_0 = 350 Ω-m in Figures 18 and 19 are used and Equation 18, it is possible to show that the system is stable up to V_0 = 65.7 kV. At that voltage, E_B = 190 kV/m and ρ_1/ρ_0 = 0.17 leading to an instability radius of 0.4 m. The system continues to be unstable for V_0 larger than 65.7 kV. This result is in accord with the observation that in Figure 32 attachment does not occur for Exp. A below 65 kV. This is further evidence that corona attachment is occurring in Exp. A.

On the other hand, data from Exp. B (represented by the solid dots) shows a correlation between V_0 and t_B such that t_B clearly decreases as V_0 increases, with attachment occurring below 40 kV. This behavior is in accord with current theories of streamer attachment. For example, Smith* predicts a phenomenological dependence of V_0 and t_B of $V_0 t_B^n$ = const where n is approximately 3/8.

1. CORONA ATTACHMENT

In shot 302 (Exp. A) the voltage on azimuthally located probes is measured (Figs. B.46 through B.54, Appendix B). The location of the probes are

---

* In a set of notes which have not been published, I. Smith predicts a phenomenological dependence among streamer closure distance d(cm) between a high voltage electrode and a ground plane, time for closure t (μs), and voltage V (kV) of the high voltage electrode, which is

$$\frac{V}{d} t^{3/8} d^{1/6} \approx 12$$

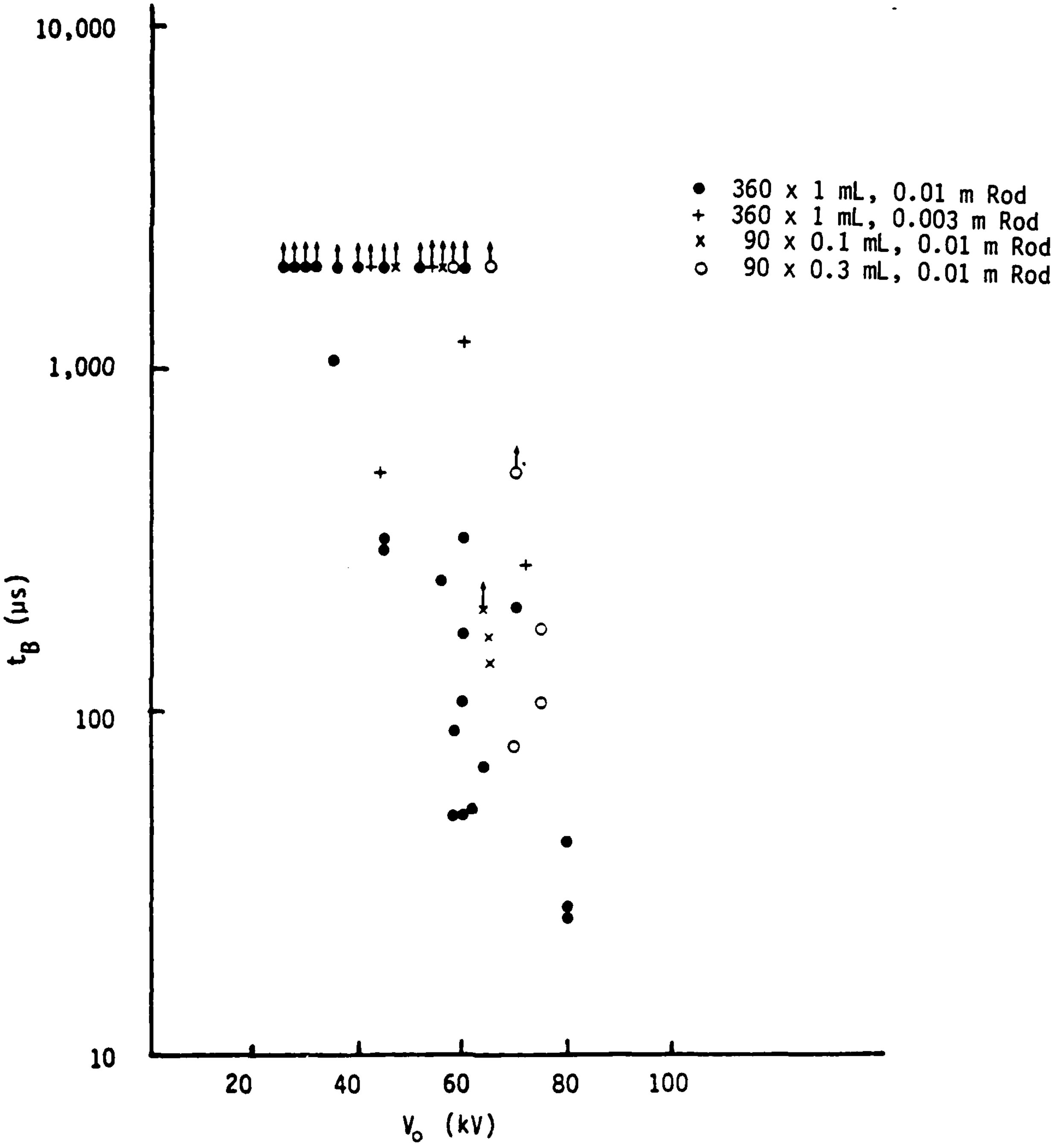

Figure 32. Time t_B for attachment to occur. x and o: corona attachment; streamer attachment.

shown in Figure 1, where the radius of the probe arc is 0.144 m. Also, b = 0.5 m and a = 0.01 m, L = 0.1 m. A flattened-out view of this arc is shown in Figure 33 where the x coordinate measures distance along the arc, and y measures distance down (Fig. 1) into the soil sample. Since L = 0.1 m, $0 \leq y \leq 0.1$ m while x ranges from zero to $\pi/2 \times 0.144 = 0.226$ m. Figure 33 shows that the nine probes are of unequal depth.

In Figure 34, data from these voltage probes are presented in the form of a resistance R_{eff} which is defined as:

$$R_{eff} = (V_0 - V_n)/I \tag{47}$$

where V_n is the voltage at the nth probe and I is the total current through the sample. Thus, R_{eff} is the effective resistance between the center conductor and probe n if all the other probes were at the same potential as V_n. The smaller is R_{eff}, the closer is V_n to V_0. The voltage V_n versus time are given in Figures B.12 through B.20, Appendix B.

The current I through the sample is shown in Figure 15. Attachment occurs at about 240 μs and that from 300 μs to about 700 μs, the current rapidly decays. At time greater than above 730 μs, the soil is nearly ohmic.

From Figure 34, during the current decay (curves for 300 μs and 700 μs) the voltages V_n are nearly equal, indicating a high degree of azimuthal symmetry of the voltage at 0.144 m. This symmetry strongly supports the idea that streamers are absent and that corona attachment has occurred.

After attachment, the resistance of the sample, $R = V_0/I$, is shown in Figure 35. At 300 μs, it is about 400 Ω, and then increases slowing with time. Assuming corona attachment, the resistivity of the broken down soil may be calculated. Assuming that it is uniform, it is found to be 16.1 Ω-m. The ohmic resistivity of the soil sample (Soil-B) is 130 Ω-m, so that the ratio of these resistivities is 0.123. From Figure 25 this ratio is typical for this type of soil.

The complete picture of how the sample resistance R varies with time is shown in Figure 36 for shot 403 (Figs. B.55, B.56, Appendix B). The corresponding V_0 and I are shown in Figures B.21 and B.22. The ohmic resistance of

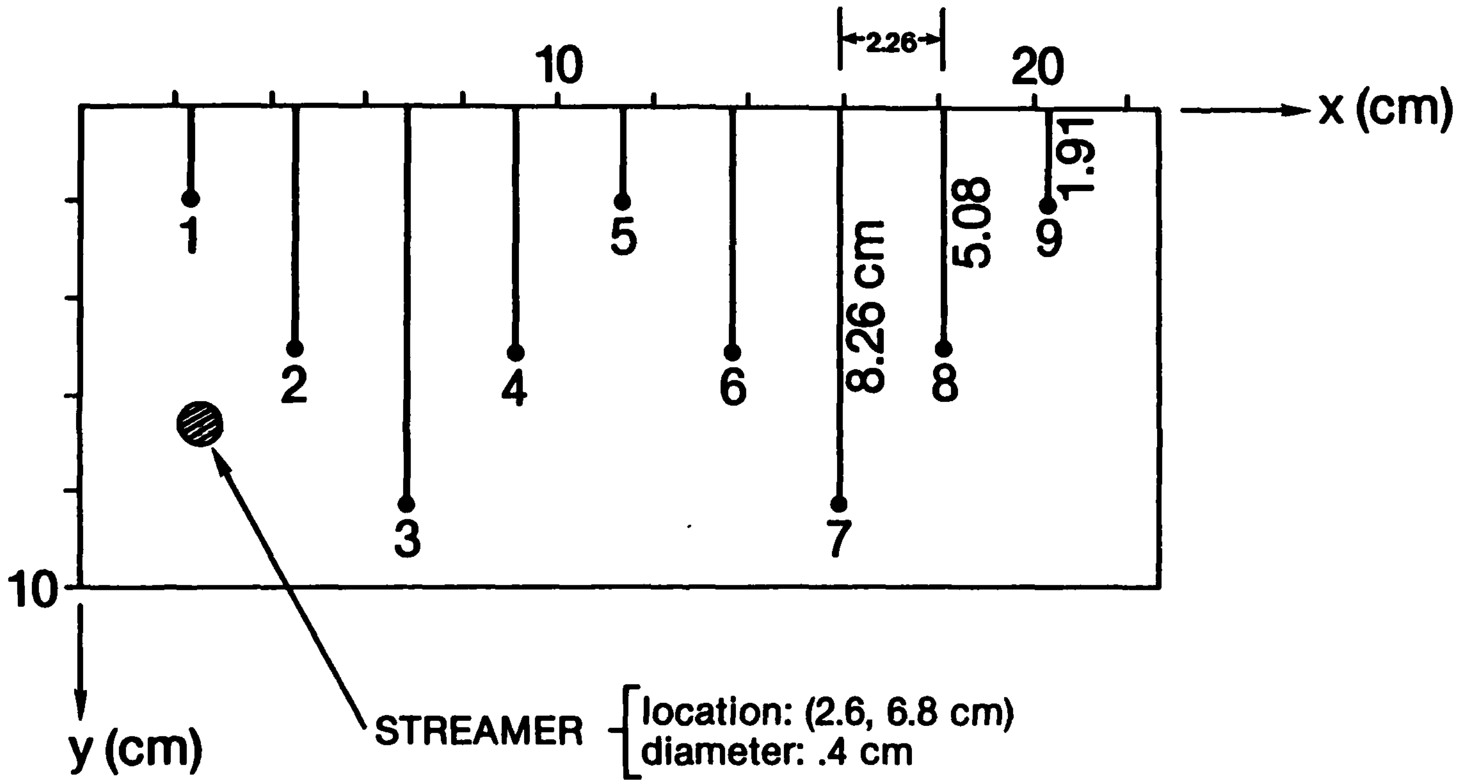
10
20
x (cm)
10
y (cm)
2.26
1
2
3
4
5
6
7
8
9
8.26 cm
5.08
1.91
STREAMER
location: (2.6, 6.8 cm)
diameter: .4 cm

Figure 33. Location of azimuthal probes on probe arc of Figure 1 radius of probe arc: 0.144 m, x measures distance along arc, y into soil sample. Streamer location also shown.

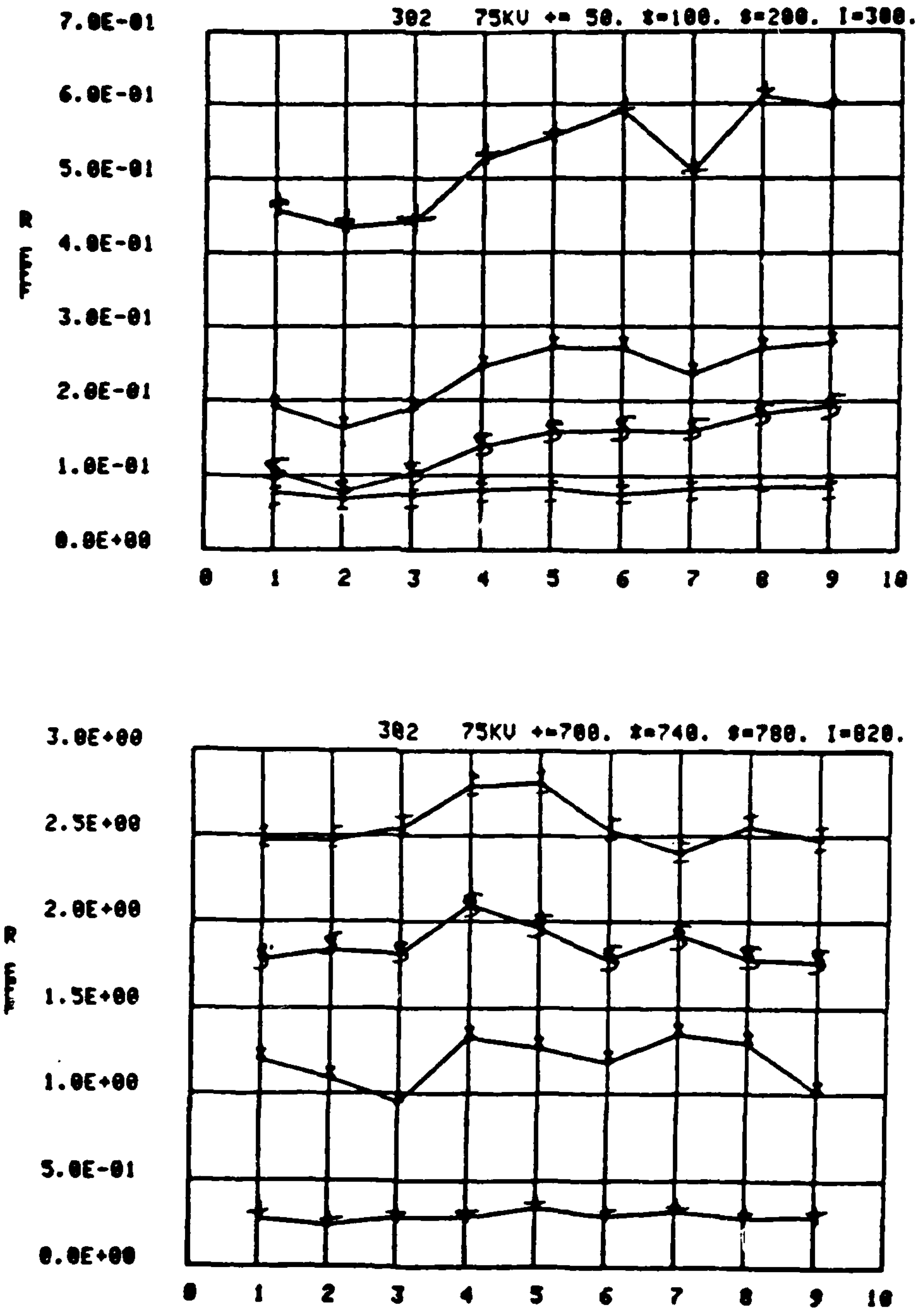

Figure 34. Resistance R_{eff} (Ω) between center conductor and probe n for azimuthal probes.

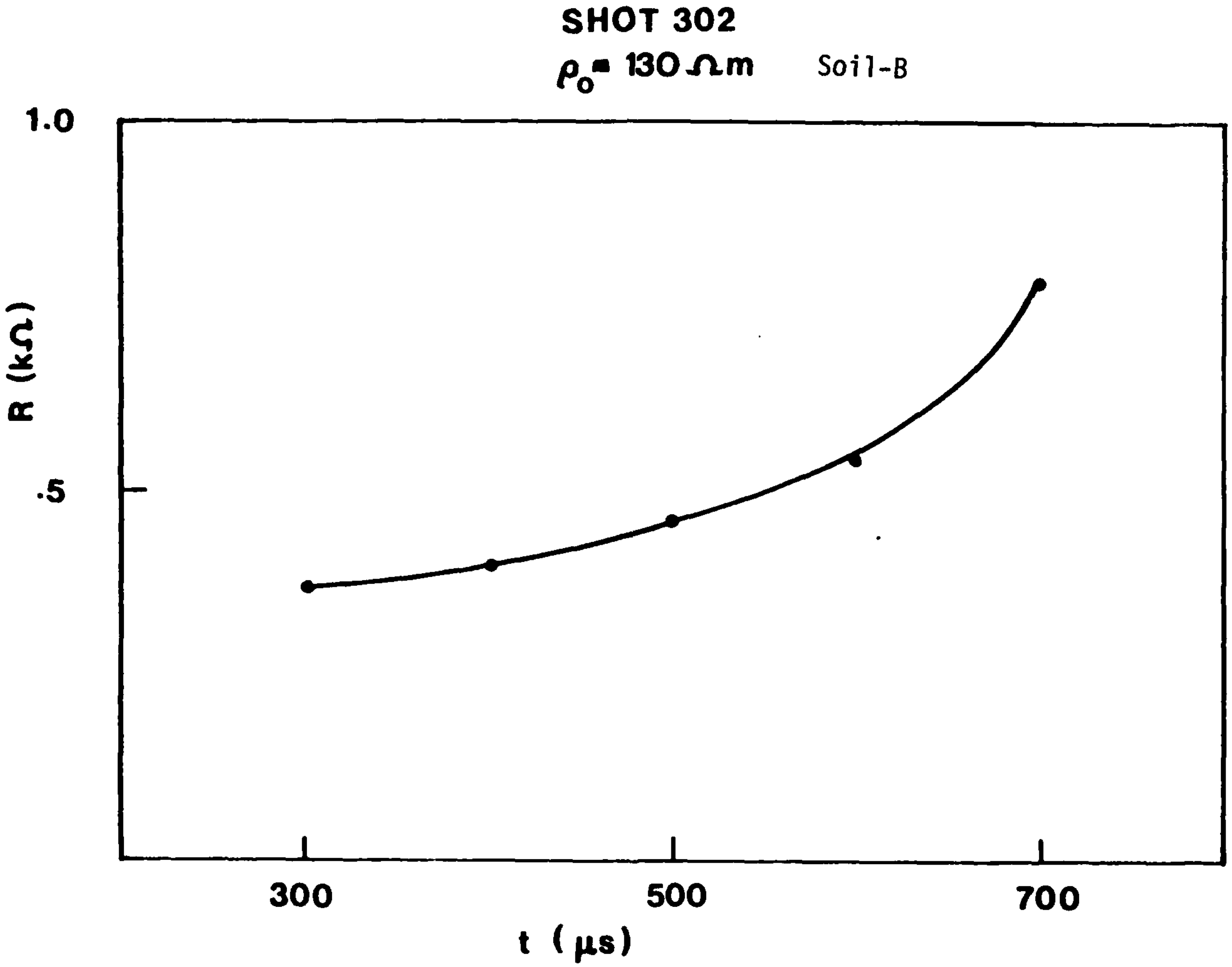

Figure 35. Resistance versus time for shot 302 after corona attachment.

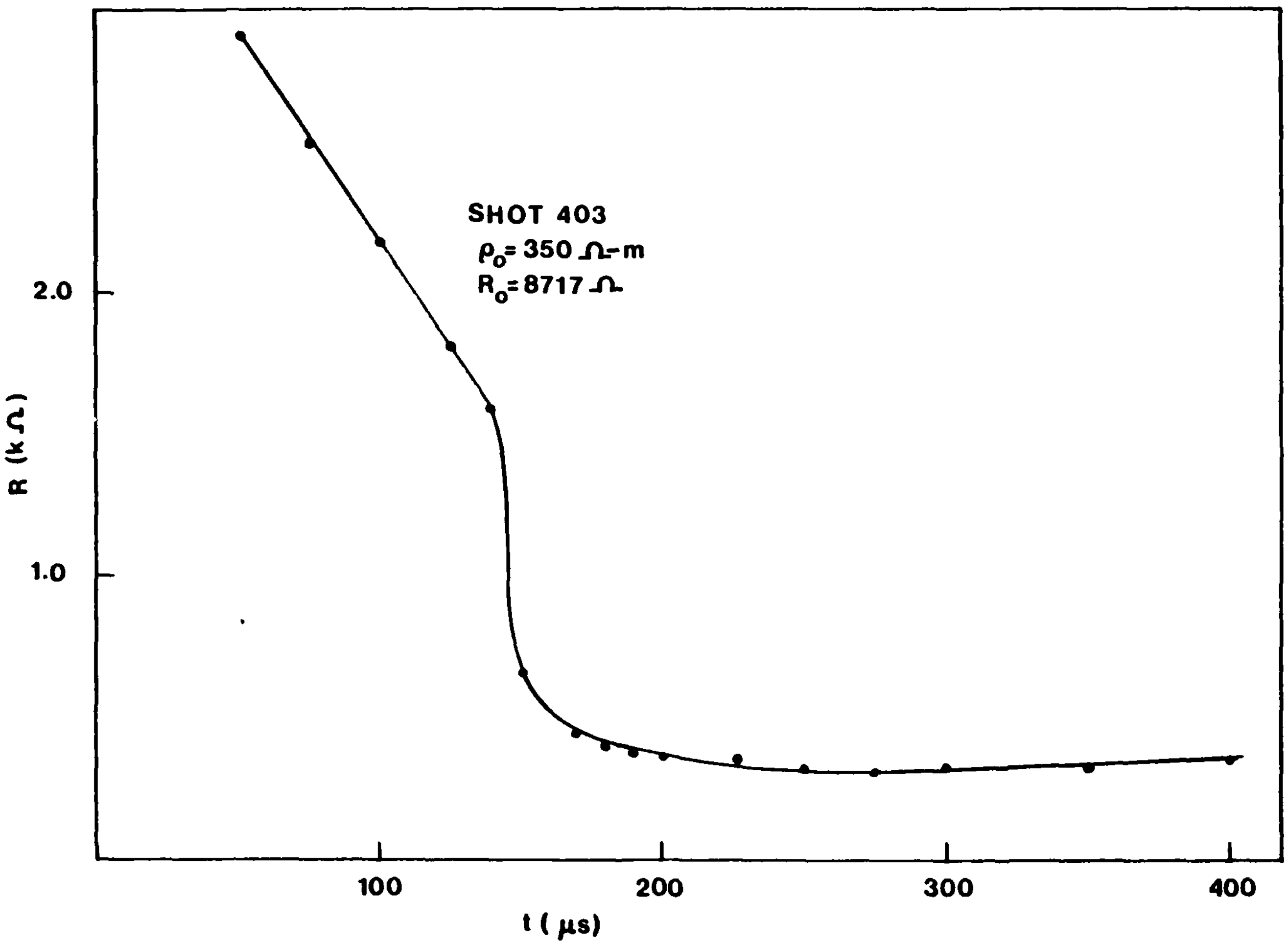

Figure 36. Resistance versus time for shot 403.

the sample is 8717 Ω. As the current starts to rise after t_i, R drops rapidly to below 2000 Ω. At about 150 μs, attachment occurs; R then drops below 400 Ω and recovers very slowly. Eventually it will revert to its ohmic value.

Returning to shot 302, it is of interest to examine the behavior of the sample before attachment. In Figure 15 the current just prior to attachment (at 240 μs) is 75 A. This current may be predicted from Equation 13 if we use as r_0 the instability radius. The peak V_0 is about 70 kV or E = 1.8 MV/m. From Figure 25 this leads to $\rho_1/\rho_0 = 0.1$. From Figure 7 it is seen that the instability radius is about 0.29 m. Thus, using E_B from Figure 24, we calculated from Equation 13 that I = 91 A compared with measured 75 A. Considering the error in E_B due to the few points available and other factors, the agreement is not bad. In this calculation, a symmetric corona was assumed. In Figure 34, just prior to attachment at 200 μs, it is seen that R_{eff} is azimuthally varying, with a minimum occurring at probe 2. The actual voltages (at 200 μs) on the nine probes are shown in Figure 37; V_0 at 200 μs is 65 kV.* This suggests that there may be a streamer near probe 2 which is causing its voltage to approach V_0.

A model for the corona and streamer is shown in Figure 38 just prior to attachment. In this figure, the corona boundary has arrived at the instability radius, 0.29 m. A streamer has formed at the center conductor and has propagated out past the array of probes and is, perhaps, deforming the boundary. Corona attachment subsequently occurs. It is interesting that within the framework of this model that the streamer clearly disappears as is shown in Figure 34 for 300 μs. It could be speculated that the resistance to the outer conductor through the corona is lower than that through the streamer. Thus, the corona drains current from the streamer and the streamer disappears.

It is possible to calculate approximately where the streamer is located and estimate its radius. An extremely simple model of a streamer is shown in Figure 39. The streamer is modeled as a cylinder of radius a_0 with a resistivity which is low compared to the surrounding corona.

---

*This number was calculated from the data in Figures 34 and 37. It is not clear how the experimenters measured this voltage.

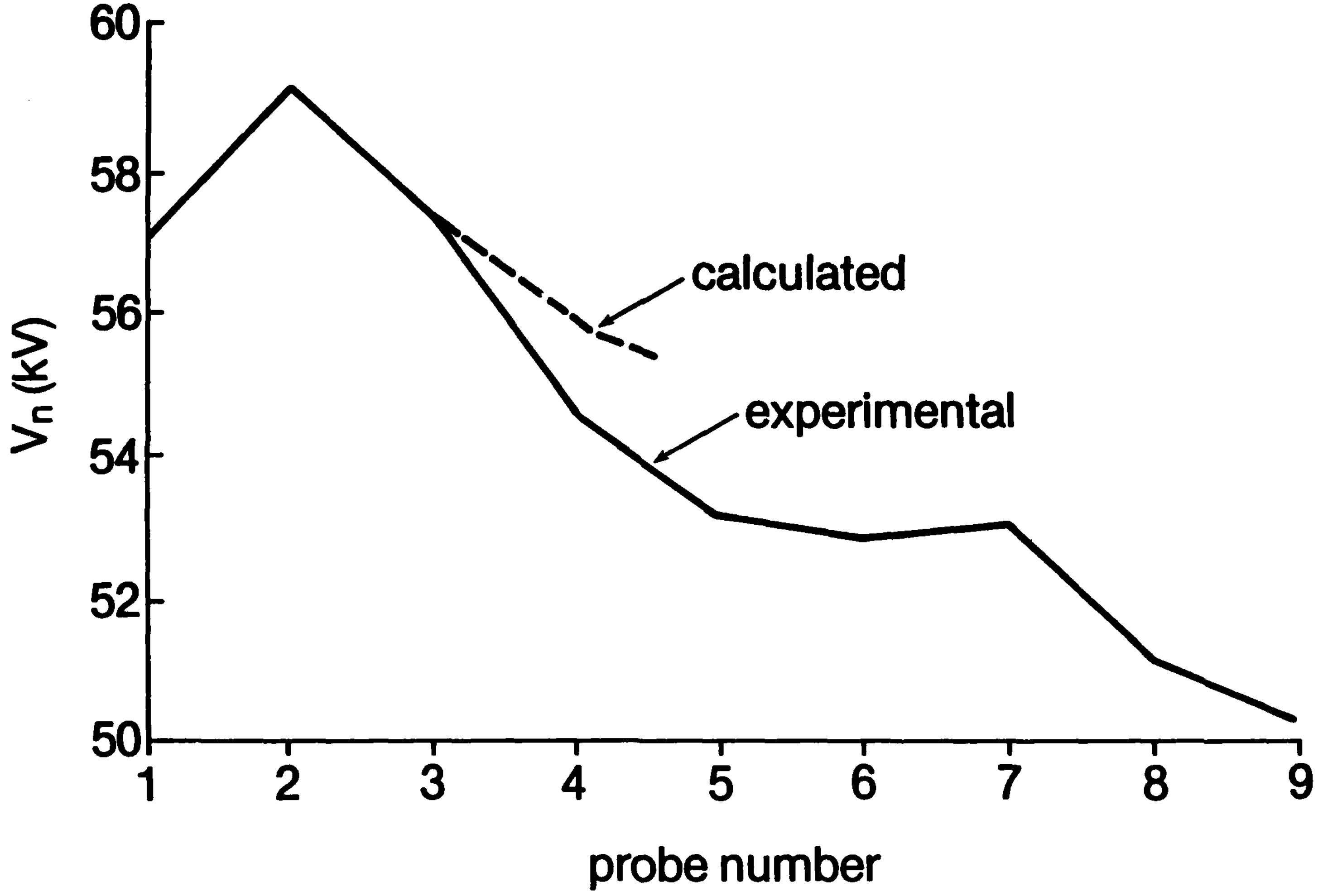

Figure 37. Voltage at azimuthal probe n for shot 302 at 200 μs.

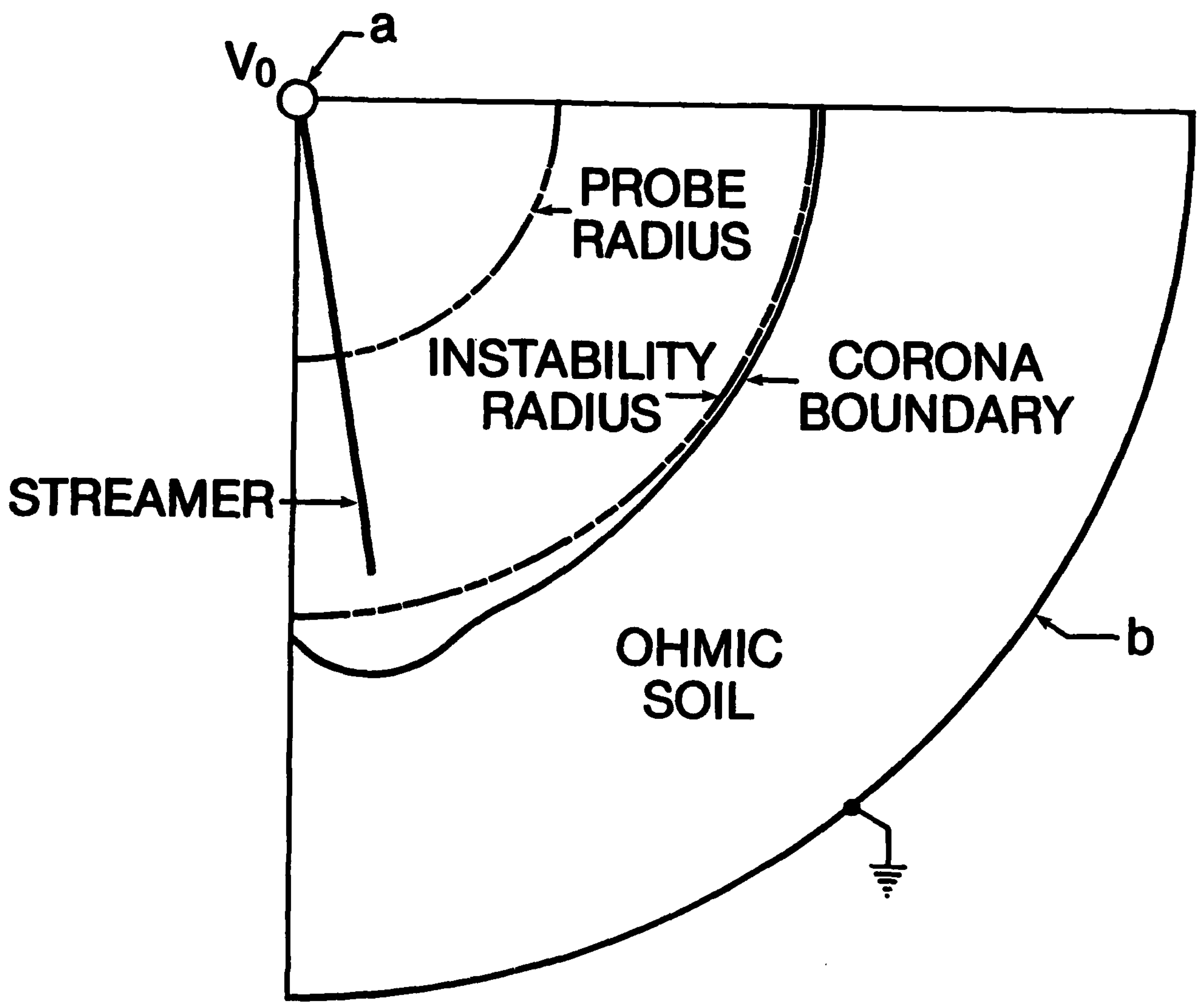
a
V_0
PROBE RADIUS
INSTABILITY RADIUS
CORONA BOUNDARY
STREAMER
OHMIC SOIL
b

Figure 38. Speculation about corona boundary and streamer location in shot 302 just prior to corona attachment.

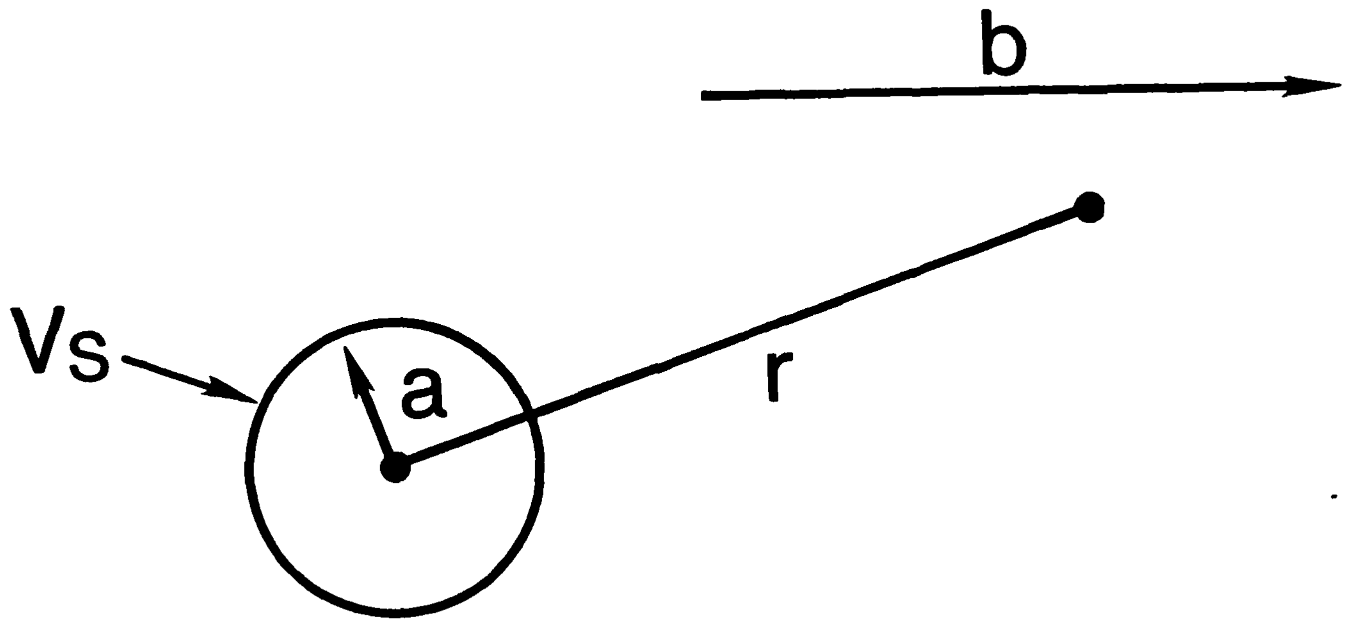

Figure 39. Streamer model.

Let V_s be the potential at the surface of the streamer, assumed to not differ appreciably from the center conductor. Then if V_0' is the corona potential in the absence of the streamer, the potential $V(r)$ in the vicinity of the streamer may be approximated as:

$$V(r) = \frac{V_s - V_0'}{\ln \frac{b_0}{a_0}} \ln \frac{b_0}{r} + V_0' \qquad (48)$$

where r is the cylindrical coordinate radial distance from the streamer to the point where $V(r)$ is being calculated, and b_0 is some reference distance where the effect of the streamer is no longer felt.

Let $V(r)$ be evaluated at probes, 1, 2, and 3, which appear to be the closest to the streamer. Let

$$A = \frac{V_s - V_0'}{\ln \frac{b_0}{a_0}} \qquad (49)$$

Then Equation 47 becomes

$$V_n = A \ln(b_0/r_n) + V_0' \qquad (50)$$

where r_n is the distance from the streamer to the nth probe, and $n = 1, 2, 3$.

Call (x,y) the location of the center of the streamer where it cuts the arc shown in Figure 33. Then $r_n = r_n(x,y)$. Dividing the equation for V_1 and V_3 by the equation for V_2 (Eq. 50), we obtain two equations which do not contain A:

$$\frac{V_1 - V_0'}{V_2 - V_0'} = \frac{\ln(b_0/r_1)}{\ln(b_0/r_2)} \qquad (51)$$

$$\frac{V_3 - V_0'}{V_2 - V_0'} = \frac{\ln(b_0/r_3)}{\ln(b_0/r_2)} \qquad (52)$$

The terms V_1, V_2, and V_3 are known from Figure 37, and we estimate V_0' and b_0. Then there are two equations and two unknowns, x and y. Recognizing that r_n really depends on x_n' shown in Figure 40 and not x_n, Equations 51 and 52 have been solved by a Newton-Raphson technique. We have used $V_0' = 50.5$ kV from Figure 37 corresponding to V at a remote location (probe 9) and for b_0 the outer radius was selected, i.e. $b_0 = 0.5 - 0.144 = 0.356$ m. We then find that x = 0.26 m, y = 0.68 m. The location of the streamer is shown in Figure 33.

These values of x and y will guarantee that V_n, n = 1, 2, 3, where V_n is given by Equation 50 will have the values shown in Figure 37. Any one of these equations may be used to find A: A = 3.2 kV. Letting $V_s \cong V_0 = 65$ kV, $\ln (b_0/a_0) = 4.53$, and for $b_0 = 0.356$ m, $a_0 = 0.0038$ m = 0.38 cm. Thus, the radius of the streamer is predicted to be 0.38 cm.

It is clear that there are many sources of error in this calculation, e.g., streamer images were neglected, and the value of b_0 is unclear. Thus, this is only an order of magnitude calculation. Note, however, that the presence of streamers can be easily detected by probes that, as in Figure 33 are about 4 cm apart.

2. STREAMER ATTACHMENT

As an example of streamer attachment, consider shot 525 from Exp. B (Figs. B.57 through B.90, Appendix B). In this shot, the parameters of the system are a = 0.01 m, b = 1 m, L = 1 m, and $\rho_0 = 300$ Ω-m sand. The total current I through the sample and V_0 are shown versus time in Figures B.57 and B.58. In Figure B.57 for I, an error occurred in recording I between 120 μs and 240 μs so that the peak current is not available. The plot in Figure B.57 is truncated during this time interval. Note that I first rises slowly until about $t_B = 80$ μs when attachment occurs. The current rises rapidly to its peak value (not recorded) and then decays as the voltage decays. The resistance R of the sample is shown in Figure 41. It drops from its ohmic value of 220 Ω to about 100 Ω at t_B, then drops rapidly during attachment to less than 10 Ω and then rises slowly as the soil recovers.

Figure 42 is a plot for shot 525 similar to that shown in Figure 34. A set of azimuthally located voltage probes were located on an arc with a 6-in radius at the top insulating plate of the system. The probes were separated

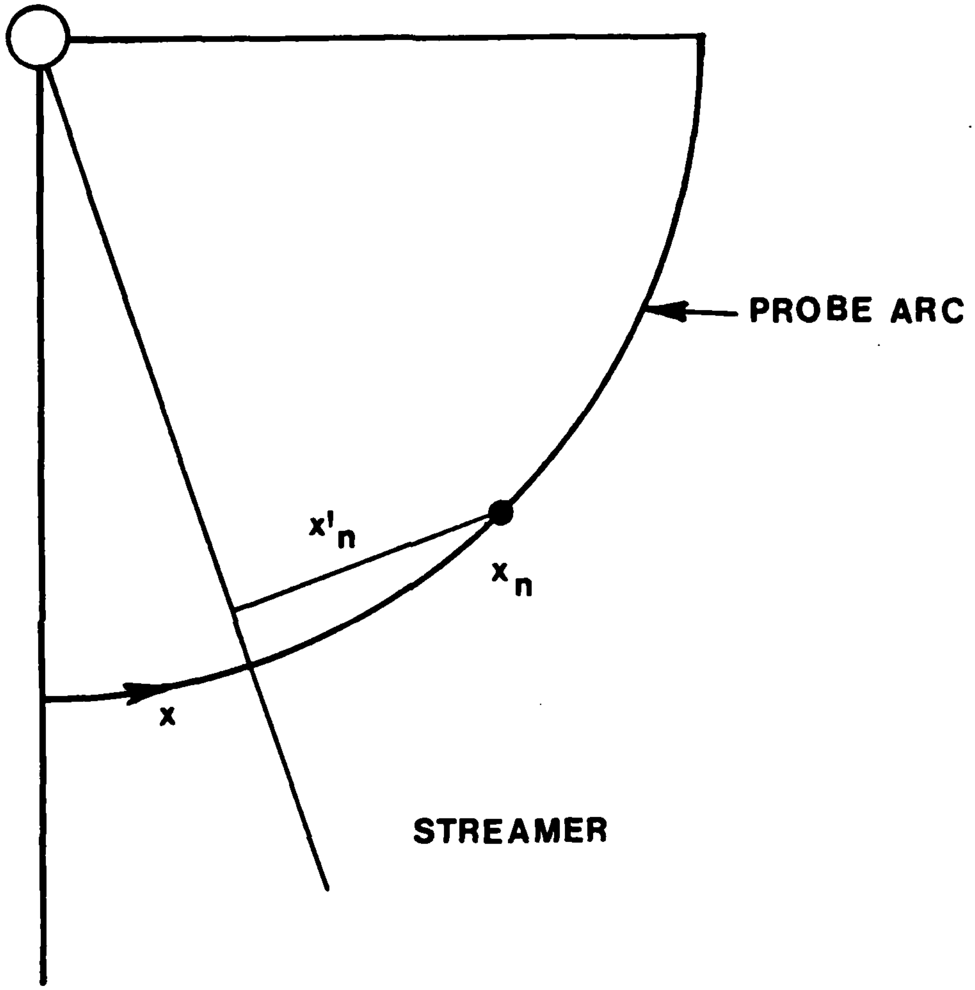
PROBE ARC
x'n
xn
x
STREAMER

Figure 40. Arc distance is x_n from streamer to probe n; x_n' is shortest distance.

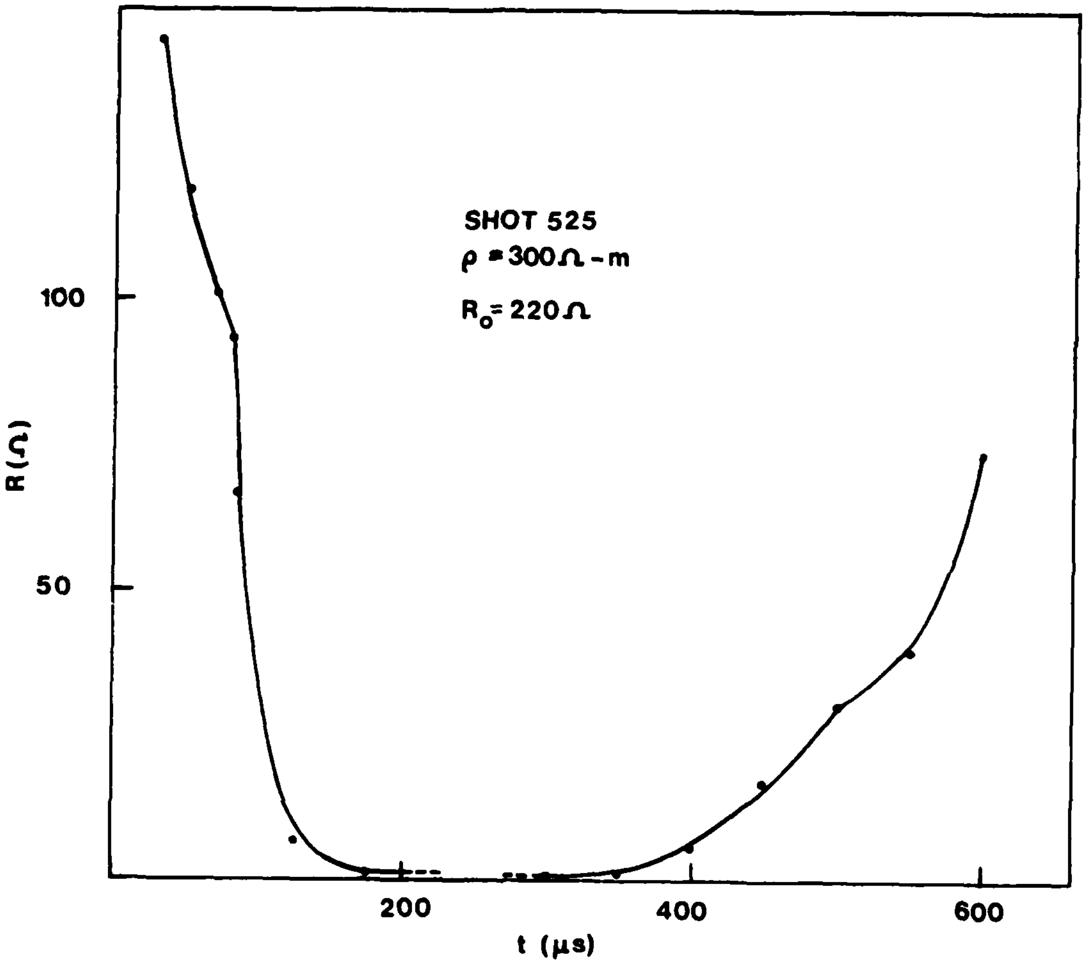

Figure 41. Resistance versus time for shot 525. R_0 is ohmic resistance.

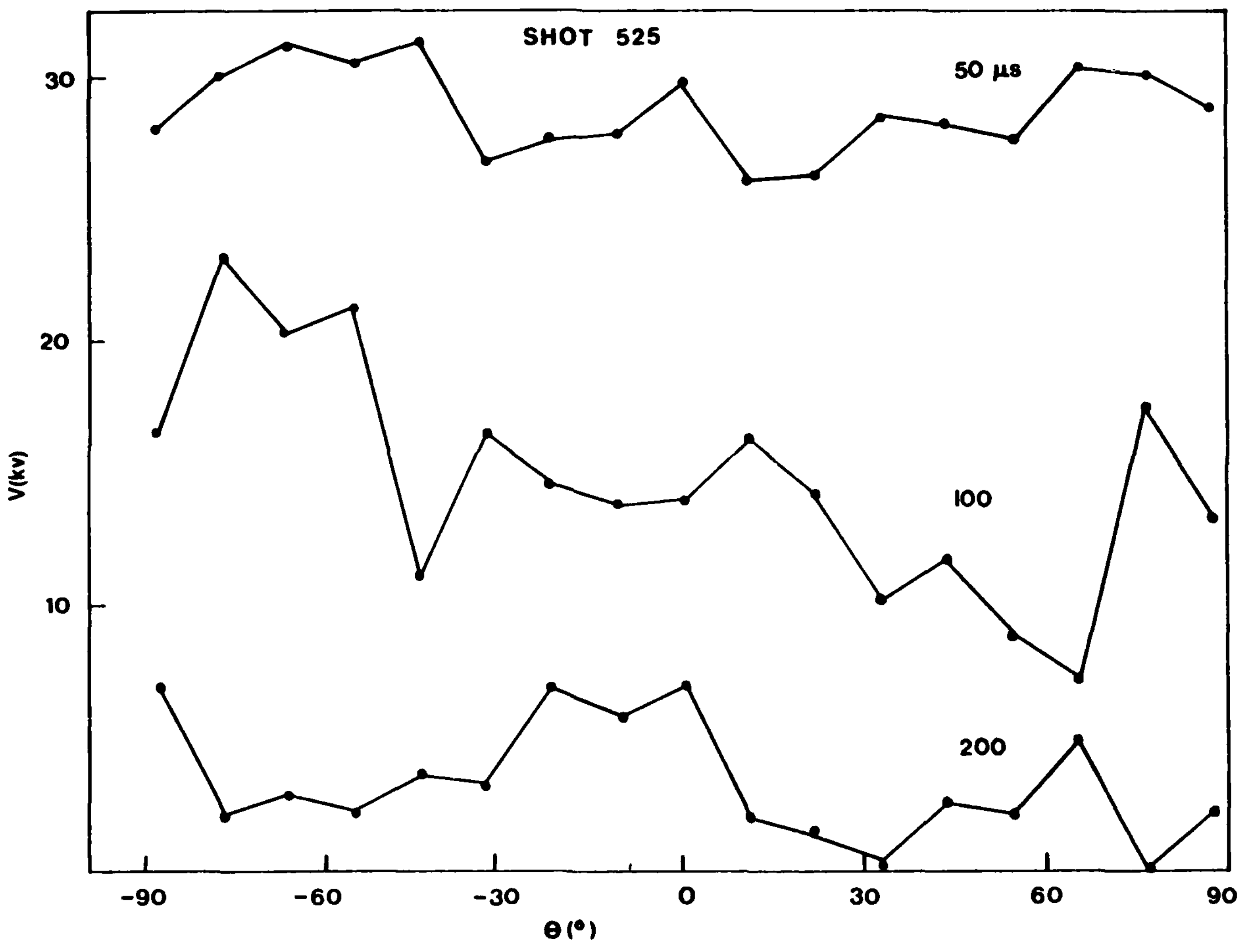

Figure 42. Voltage on 19 azimuthal probes (17 shown) located on 6-in arc in top plate.

by 11 deg; there were 19 probes covering 198 deg, approximately a semicircle. The voltage on these probes versus angle at 50 μs have been plotted, prior to t_B; at 100 μs during the build-up of current during attachment; and at 200 μs when the voltage has decayed and the current is just starting to decay. This latter time would corrrespond to the time 300 μs in Figure 34 when it was seen that the voltage was uniform with angle. For shot 525, however, it is seen that at 200 μs, the voltage is not at all uniform. The voltage at the center conductor V_0 at 200 μs is 7.2 kV. There are three angles at which the probe voltage is close to 7.2 kV: -90 deg, -15 deg and 65 deg. This is interpreted to mean that there is a streamer occurring at each of these angles. Since attachment occurs in the presence of streamers, this is streamer attachment. It is likely that the streamer carry the bulk of the current.

VII. SUMMARY

1. SUMMARY

The important points made in the report are listed as follows. The electrode configuration is cylindrical.

a. The important features of the corona, including the location of maximum r_0, are defined by about 30 μs.

b. Sample current reaches a maximum or else attachment occurs in a symmetric corona in about 100 - 200 μs.

c. The corona can be defined by two parameters, E_B and ρ_1/ρ_0. These parameters have been tabulated here at maximum current and find that both parameters correlate well with peak V_0. Note that maximum r_0 which occurs at maximum I can be calculated from E_B and ρ_1/ρ_0. It is found that E_B and ρ_1/ρ_0 depend on ρ_0. We have tabulated E_B and ρ_1/ρ_0 versus V_0 peak for four values of ρ_0.

d. For the cases examined here, $\rho_1/\rho_0 \approx 0.8 - 0.1$ and E_B was 100 - 200 kV/m at maximum I.

e. For a symmetric corona, maximum I could be accurately predicted from the model, requiring only that peak V_0 and ρ_0 be known.

f. The relaxation of the current through the sample as the voltage decayed was accurately predicted using a dynamic model in which a third region was introduced. It was required that ρ_1/ρ_0 increase slowly from its value at maximum I. No general data on this increase ρ_1/ρ_0 are presented.

g. Attachment occurs by two different methods: corona and streamer attachment.

h. Corona attachment is associated with a radius of instability in a cylindrical system. This radius can be calculated. Also, there is a voltage which can be calculated below which the system is corona stable.

i. A spherical corona is inherently stable.

j. For the geometry investigated (b = 0.5 m), the time for corona attachment ranged from 100 to more than a few milliseconds in a random manner that showed no correlation with pulser voltage, V_0.

k. Streamer attachment time correlates with V_0.

l. The location of streamers can be predicted by voltage probes that are spaced 4 cm apart. Probably larger probe spacings are possible.

m. A streamer radius is of the order of 0.4 cm.

2. DISCUSSION OF CORONA ATTACHMENT

This is a phenomenon which has not been recognized previously. Two independent pieces of evidence which support its existence have been presented in this report. The conditions under which this type of attachment exist are more restricted than for streamer attachment.

a. The corona must have a high degree of the symmetry of the initiating electrode system. This was the case in the $\pi/2$ wedge. It has been theorized that the corona and streamer images in the other three quadrants of the circle, as well as in the image wedges stacked above and below the real wedge, contributed a high degree of symmetry in the wedge. Another way to bring about enhanced symmetry is to drive the center electrode at a voltage so high that the electric field at the surface of the electrode is well above the threshold value for metal-soil interface breakdown. The idea here is that if the corona really consists of a lot of small streamers, a large electric field will cause many of these to form; i.e., they occur with a high density, thus keeping the outer surface (corona boundary) uniform. If, on the other hand, only a few little streamers form, the boundary is poorly defined, and there is no shielding of one little streamer from the next. Thus, one little streamer will start to propagate as described in Reference 7, and it may evolve into a large streamer.

b. The grounded electrode must have an area large enough so that it intercepts a significant portion of the corona boundary and current will flow through a significant portion of the corona volume.

Note, that if a symmetric corona arrives at a grounded electrode which has a small area relative to the corona boundary, it can be speculated that a streamer might form at the grounded electrode and propagate backwards toward the high voltage electrode. Also, note that in most of the experiments reported to date, attachment of any sort has not occurred over distances much larger than 1 m. Since coronas have been observed to have radii of this order of magnitude, they should not be ruled out as the main mechanism for attachment.

REFERENCES

1. Mallon, C., Denson, R., Leadon, R. E. and Flanagan, T. M., "Elecrical Breakdown Characteristics of Soil Samples," Theoretical Note-316, JAYCOR, San Diego, California, January 12, 1981.

2. Petropoulos, G. M., J. IEE, Pt. II, *95*, 59, 1948.

3. Bellaschi, P. L., *Trans. Am. Inst. Elec. Engr.*, *60*, 123, March 1941.

4. Bellaschi, P. L., Armington, R. E. and Snowden, A. E., *Trans. Am. Inst. Elec. Engr.*, *61*, 349, 1942.

5. Sunde, E. W., *Earth Conduction Effects in Transmission Systems*, D. Van Nostrand Co., 1949.

6. Liew, B. E., and Darveniza, M., *Proc. IEE (Australia)*, *121*, 123, February 1974.

7. Snowden, D. P., Erler, J. W., Gilbert, J. L. and Longmire, C. L., *Soil Breakdown Modeling Studies*, MRC/SD-R-106, Mission Research Corp., San Diego, California, November 1982.

8. Carlile, R. N., "A Geometrical Instability in a Soil Filled Coaxial Structure," EMP Theoretical Note, No. 313, April 17, 1981.

BIBLIOGRAPHY

Archie, G. E., Transactions of the AIME, 146, 54, 1942.

Blatt, H., Middleton, G. and Murray, R., Origin of Sedimentary Rocks, Prentice-Hall, Inc., Englewood Cliffs, New Jersey, 1980.

Ingram, J., Research, 14, 20, 1961.

Jackson, P. D., Taylor-Smith, D. and Stanford, P. N., Geophysics, 43, 1250, 1978.

Middleton, H. E., Slater, C. S. and Byers, H. G., "The Physical and Chemical Characteristics of the Soils from the Erosion Experiment Stations-Second Report," US Dept of Agriculture Technical Bulletin 430, p. 1, August 1934.

Richards, L. A., ed., Diagnosis and Improvement of Saline and Alkali Soils, US Department of Agriculture, Agriculture Handbook No. 60. 1954.

Tagg, G. F., Earth Resistances, G. Newnes Co., London, 1964.

Winsauer, W. D., Shearin, H. M. Jr., Masson, R. H. and Williams, M., Bull of American Assn. Of Petroleum Geologists, 36, 253, Feb, 1952.

APPENDIX A: LINEAR ELECTRICAL CONDUCTIVITY OF SOIL*

At low voltages, soil is known to exhibit electrical conductivity which is relatively independent of frequency below 10^5 Hz. The conductivity varies, however, from soil to soil and varies with time in a single soil. This suggests that the conductivity of a soil is a complex property dependent on a number of variables. The purpose of this Appendix is to discover what the variables are and to attempt to define them quantitatively. A literature search has shown that the variables of interest include the nature of the soil involved, the nature and amount of fluids held in the soil, and the temperature of the system. This Appendix will discuss these parameters and their interrelationship which determines the conductivity of a given soil.

In order to discuss soil conductivity, we must first define what is meant by 'soil'. A simplistic definition of soil is 'weathered rock', or rock that has been physically broken apart and chemically and biologically altered. The soil is a complex system which extends from the surface of the earth down to the unaltered rocks of the earth's curst, and consists of minerals, organic material, and voids between grains which may be filled with air or water. Soil has a diverse spectrum of compositions which vary both laterally and from the surface to extreme depths. In general, the soil close to the surface has a high proportion of organic material, such as decaying plant remains, organisms, and microorganisms, while the soil at large depth consists almost entirely of broken up bits of rock. The lower boundary of the soil is a point of debate among pedologists, most of whom claim that a soil must have at least some organic component in addition to mineral components to qualify as a soil, thus, excluding sand and gravel from the realm of soils. Similarly, pedologists may claim that lithified materials, that is, materials whose component grains have become cemented together by precipitation of chemicals carried in groundwater, have ceased to be soils and become rocks. From an electrical standpoint, however, these are philosophical matters, since neither organic material or cements have a pronounced effect on the electrical properties of the materials involved. For this discussion, the soil is simply a veneer on the earth's surface between the actual surface and unaltered rock at large depth.

---

* The material in this Appendix was prepared by Mr. Rik E. Lantz, a graduate student in the Department of Geosciences at the University of Arizona. It was prepared as an individual studies project under the direction of one of the authors, and was completed in December, 1982.

The formation of soil from rock is a complex process, involving the physical cracking and disintegration of the rock to smaller grains, and chemical activity of groundwater, plants, and microorganisms on these grains. Physical breakdown occurs because of temperature variations at the surface, which induce stresses between grains due to differing coefficients of thermal expansion, as well as erosion by wind and water and a myriad of other mechanical processes. Chemical breakdown occurs because most rocks were formed at pressures and temperatures profoundly different from those at the surface. As a result, the mineral phases which were stable at the time of formation are not stable at surface temperatures and pressures, and with the aid of water, oxygen, and organic activity, they break down to more stable phases, notably clays. The fact that weathering begins at the surface and works its way downward has marked effects on soil formation. As mentioned previously, the soil near the surface may have a high proportion of organic material. Rainwater which falls on this organic matter may become acidic and begin percolating down through the soil, dissolving certain solids from the zone immediately below the organic matter. As the acidic water dissolves more and more solids, its pH changes, until a point may be reached where saturation in one or more ions occurs, and these will precipitate.

This is a very oversimplified sketch of the formation of soil horizons, but has been included here to introduce an important characteristic of soil, namely that it is exceptionally heterogeneous. Not only do compositions vary from one location to another, but they will vary with depth at a single location. The development of different horizons results in horizontal stratification of soil and may juxtapose two types of soil with contrasting electrical properties in a relatively short vertical distance. This anisotropy will have a complex effect on the behavior of electric fields in the soil which is difficult to define quantitatively. The following discussion has, therefore, been limited to an electrically homogeneous, isotropic soil, and the relationships discussed will apply only to this case. A single layer within a stratified soil is a close approximation to such a case, as are relatively simple porous media, such as loose sand and gravel.

Soil is made up of three components: mineral material, organic material, and voids which may or may not be filled with fluid. The conductivities of the overwhelming majority of minerals is very low (10^{-12} mhos/m for quartz, 0.5×10^{-12} mhos/m for calcite, 10^{-6} mhos/m for muscovite), as is the conductivity of dry organic matter. As a result, conductivity in the soil is dominated by the third component, the fluids in the voids. Pores in the soil may be filled to varying degrees with fluid, usually water with some dissolved solids. The conductivity of wet soil is much greater than the conductivity of dry soil. Conductivity of a slightly damp soil is somewhere in between. Put simply, the more water available to conduct electricity, the greater the conductivity of the soil as a whole. Conductivity is dependent on the amount of space available to be filled with water as well, so a porous garden soil will have a greater conductivity than a densely compacted chunk of clay. The conductivity of the fluid itself is another factor. Finally, conductivity is dependent on the distance the current has to travel. Soil with relatively straight water filled pores will have higher conductivity than the same soil with contorted water filled pores. The conductivity of soil, or of any porous medium, is described by a formula derived by G.E. Archie in 1941, which takes all of the above factors into account. This relationship, known as Archie's Law [13], is as follows:

$$\frac{1}{\sigma_\varepsilon} = \alpha \phi^{-m} s^{-n} \frac{1}{\sigma_\omega}$$

where σ_ε = overall conductivity of soil with fluid;

σ_ω = conductivity of pore filling fluid;

α = an empirically determined constant of proportionality: $0.5 < \alpha < 2.5$;

ϕ = porosity, the ratio of the volume of the voids between grains to total volume of soil: $0 \leq \phi \leq 1$;

m = an empirically determined constant which takes into account particle shape and pore geometry: $1.3 \leq m \leq 2.5$;

s = fraction of pore spaces filled with fluid: $0 \leq s \leq 1$;

n = an empirically determined constant $n \approx 2$.

As a specific case, Archie's Law for unconsolidated sand is given by:

$$\frac{1}{\sigma_\varepsilon} = 0.65 \phi^{-1.5} s^{-2} \frac{1}{\sigma_\omega}$$

where $a = 0.65$ [14], $m = 1.5$ [15], and $n = 2$ [13].

Conduction of current through aqueous solutions is achieved by ions which carry charge. For this reason, a solution's conductivity is governed by the concentration and electrical affinity of these ions. Fig. A.1 shows the effect of concentration of various ionic solutions on resistivity. High ion concentrations have low resistance and high conductivity, and low concentrations have high resistance and low conductivity. In the southwest, the ion content of groundwater tends to be very high, so fluids in the soil here should have high conductivity. Solution conductivity is also governed by temperature. Low temperatures hinder the movement of ions in solution and, thus, the solution's capacity to carry current. A rough rule of thumb is that resistivity changes 2% per degree Centigrade [16].

The factor ϕ is the porosity of the soil, or the ratio of the volume of voids (pore spaces) to the total volume. Porosity ranges from 0 to about 0.75, and depends on a number of factors including grain size, range of grain sizes, grain shape, and packing. Coarse grained soils tend to have higher porosities than fine grained soils. A wide range of grain sizes will allow very small grains to occupy pore spaces and, thus, reduce porosity. Platy grains, such as clays, can be packed together more closely than nearly spherical grains, such as rounded quartz sand grains, implying that pure clay will have lower porosity than sand. Finally, it is obvious that a compacted soil will have lower porosity than an uncompacted soil. As an example, Blatt et al. [17] quote a porosity of 45% for freshly deposited River Sand. Middleton, et al. [18] give other examples of porosity values for various soil types which are shown in Table A1.

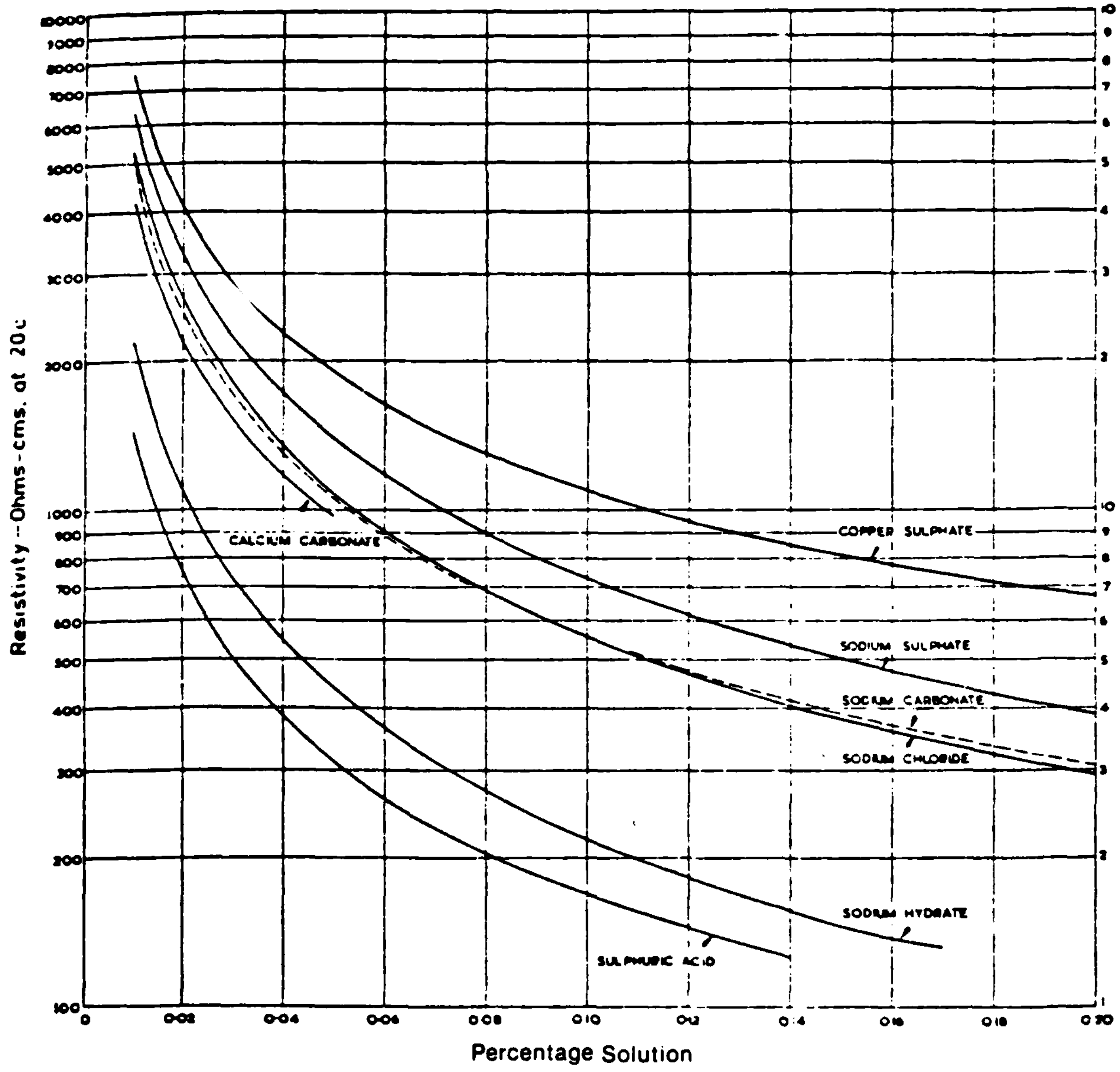

Fig. A.1 - Diagram showing relationship of concentration to resistivity for ionic solutions with different electrical affinities. (Fig. 1.2 from Tagg [19]).

TABLE A1

Type of Soil	depth	porposity (%)	depth (cm)	porosity (%)
Kirvin fine sandy loam Taylor, TX.	surface	29.7	76	53.4
Cecil sandy clay loam Statesville, NC	surface	44.0	69	52.0
Shelby silt loam Bethany, MO	surface	46.2	91	34.9
Houston black clay Temple, TX	surface	61.0	89	40.2

The factor m is an empirically determined constant related to the route the current travels through the rock, which is quantitatively defined as tortuosity. Tortuosity is the ratio of the actual length of a path through a medium to the linear distance between the starting point and ending point. The more tortuous or contorted a path, the greater the value of tortuosity. Due to the complex geometries of soil pores and the nature of electric fields in conductors, current can flow through a number of paths, as shown in Fig. A.2. The tortuosity in this case is simply the average path length the current flows through, divided by the shortest possible path (see Fig. A.2). Winsauer et al. [14] have devised a simple experimental method to determine tortuosity, τ, directly,[*] and have found that

---

[*] Winsauer et al. assume complete saturation, $S = 1$ and, in this case, Archie's Law reduces to $\phi^{-m} = \frac{\sigma_\omega}{\sigma_\varepsilon}$. They state in equation (9) that $\frac{\tau^{1.67}}{\phi} = \frac{\sigma_\omega}{\sigma_\varepsilon}$. Substituting ϕ^{-m} for $\frac{\sigma_\omega}{\sigma_\varepsilon}$, the equation $\tau^{1.67} = \phi^{1-m}$ is obtained.

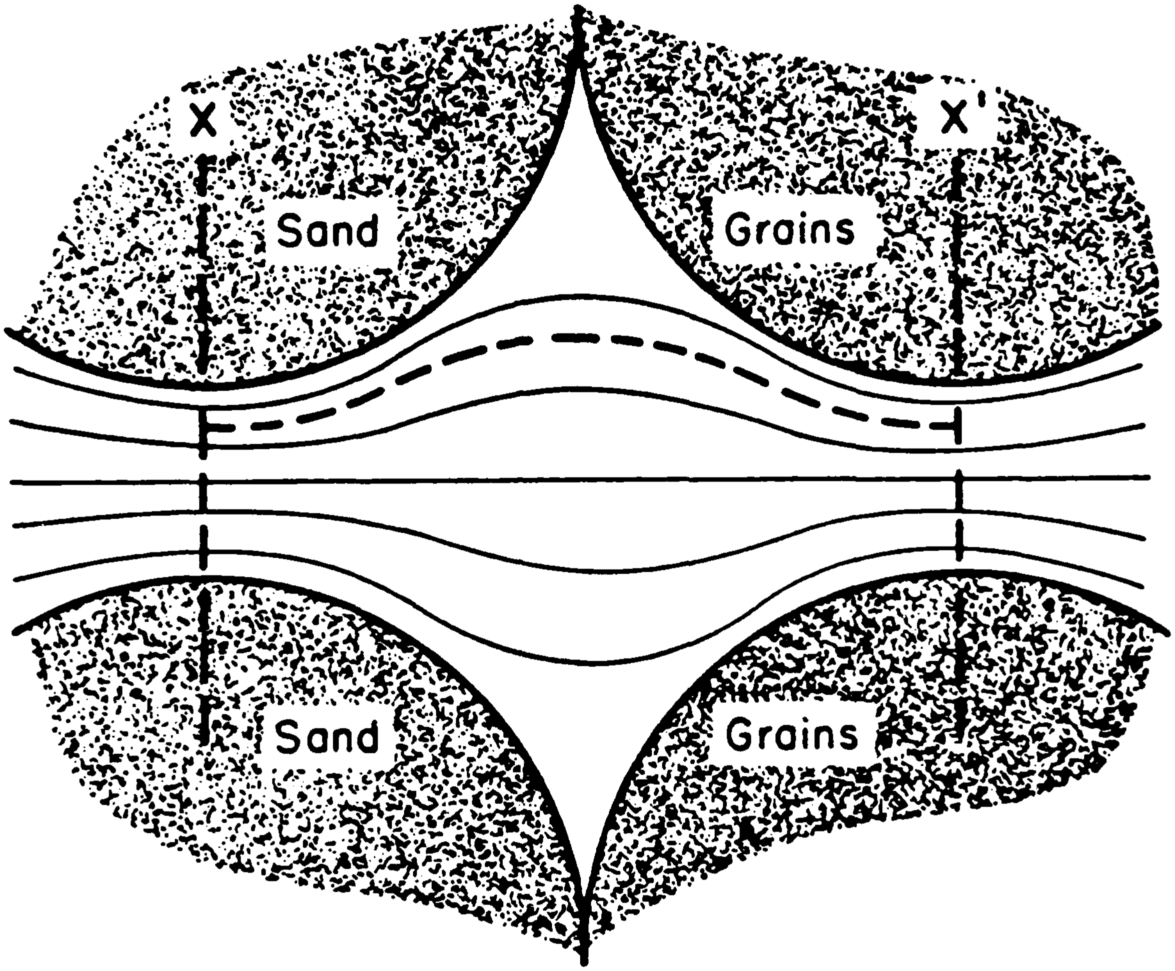
X
X'
Sand
Grains
Sand
Grains

Fig. A.2 - Diagram illustrating the flow of current in pores. A relatively small amount of current flows through the straight path from A to A'. The average of all of the current paths is B to B', and the tortuosity is BB'/AA'. (Fig. 1 from Winsauer et al. [14]).

$$\tau^{1.67} = \phi^{1-m} \quad .$$

Measuring tortuosity and porosity allows empiric determination of m.

Tortuosity is, in part, a result of particle shape, and Jackson et al. [15] have attempted to evaluate the effect of particle shape on m. Their work has shown that particle shape and m are directly related, and that the more angular the particles, the greater the value of m. The result of their research is illustrated in Fig. A.3. The figure shows m = 1.2 for commercially produced glass spheres, m = 1.85 for extremely angular shell fragments of the same size, and intermediate values of m for intermediate grain shapes. Their experimental approach to empirical determination of m was to completely saturate their sands with fluids, decrease the porosity by successively compressing the samples, and determine m as the slope of the line when ϕ was plotted against $\frac{\sigma_\omega}{\sigma_\varepsilon}$. This method is probably more accurate than the method derived from Jackson's work because it is a more direct measurement.

The parameters take into account the amount of fluid actually held in the pore spaces. The parameter is a saturation factor ranging between 0 and 1, which is simply a ratio of the amount of pore space filled with fluid to the total pore space. The parameter is yet another empirically determined constant, which can be evaluated by determining all other constants and varying s. There are some physical constraints which in very dry conditions limit the values of s. One of these is the phenomenon of adsorption, which results from an electrical imbalance of minerals in the soil. Due to the nature of crystal growth, the surfaces of minerals often have unneutralized charges, which can attract one or more layers of dipolar water molecules (see Fig. A.4). Even when the mineral

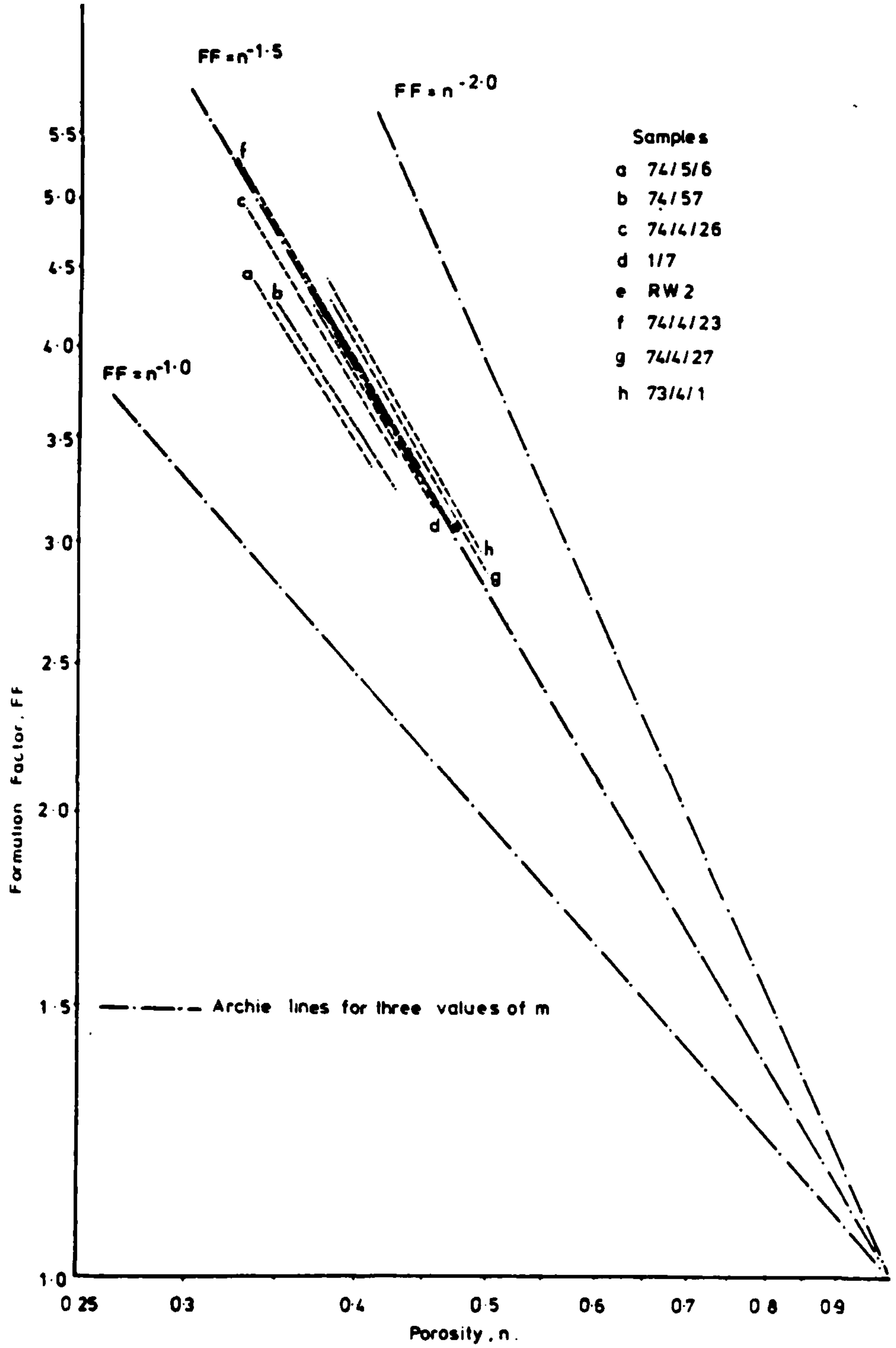

Fig. A.3 - Diagram showing the effect of particle shape on m. The particles are increasingly angular from A to E. The linear groups of points reflect successive decreases in porosity for each sample. Their notation has $\sigma_{\omega}/\sigma_{\epsilon}$ = FF, and ϕ = n. (Fig. 6 from Jackson et al. [15].)

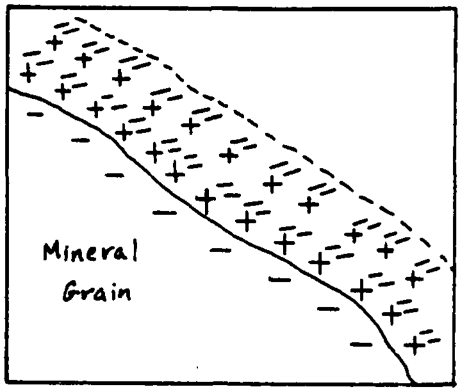

Fig. A.4 - Diagram showing charge distribution at the surface of a mineral crystal and two adsorped layers of water molecules. The symbol = + represents a dipolar water molecule.

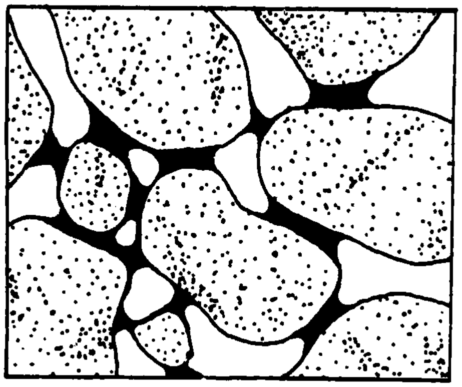

Fig. A.5 - Schematic illustration of meniscus contacts. Water is in black, grains are shaded, and air filled pore space is white. When the radius of curvature of the meniscus gets very small, surface tension forces are high, and the water will not evaporate.

AD-A137 997 A PHENOMENOLOGICAL MODEL OF SOIL BREAKDOWN(U) DIKEWOOD 2/2
ALBUQUERQUE NM R N CARLILE ET AL. JAN 84 AFWL-TR-83-73
F29601-81-C-0044

UNCLASSIFIED F/G 8/13 NL

END
FILMED
4-84
DTIC

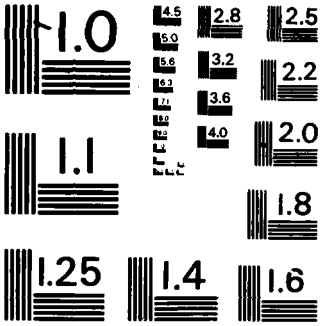
1.0
4.5
5.0
5.6
6.3
7.1
8.0
9.0
2.8
3.2
3.6
4.0
2.5
2.2
2.0
1.1
1.8
1.25
1.4
1.6

MICROCOPY RESOLUTION TEST CHART
NATIONAL BUREAU OF STANDARDS-1963-A

is dried, the thin lamina of water remains and provides a path for current flow. This effect is especially pronounced in clays. Another phenomenon which keeps soil from drying completely is surface tension. At low fluid content, water is held very tightly in between grains in what are known as meniscus contacts due to surface tension (see Fig.A.5). A certain minimum value exists for each soil where surface tension forces are greater than the water's natural tendancy to evaporate, and the water held in these meniscus contacts will remain unless the soil is subjected to abnormal conditions. The result of these two physical constraints on saturation is that each soil contains a minimum amount of water and, therefore, should have a minimum conductivity. This minimum value can be significant, as shown in Fig. A.6, where the minimum value of s for a 'clay soil' is around 10 per cent.

In summary, then, it has been shown that soil conductivity for frequencies below about 100,000 Hz is described by the relatively simple relationship, Archie's Law. The form of Archie's Law indicates that the solid components of soil are more or less electrically inert, and that the parameters which govern soil conductivity are porosity, amount of pore fluids, ionic content of pore fluids, and grain shape. The soil is such a complex system that the law must be modified by several empirically determined constants which allow for compositional and geometric variations between soils in order to describe each individual case. After experimentally determining these constants, an equation can be written which accurately expresses the conductivity of a given soil, and the meaning of such an equation has been the object of this investigation.

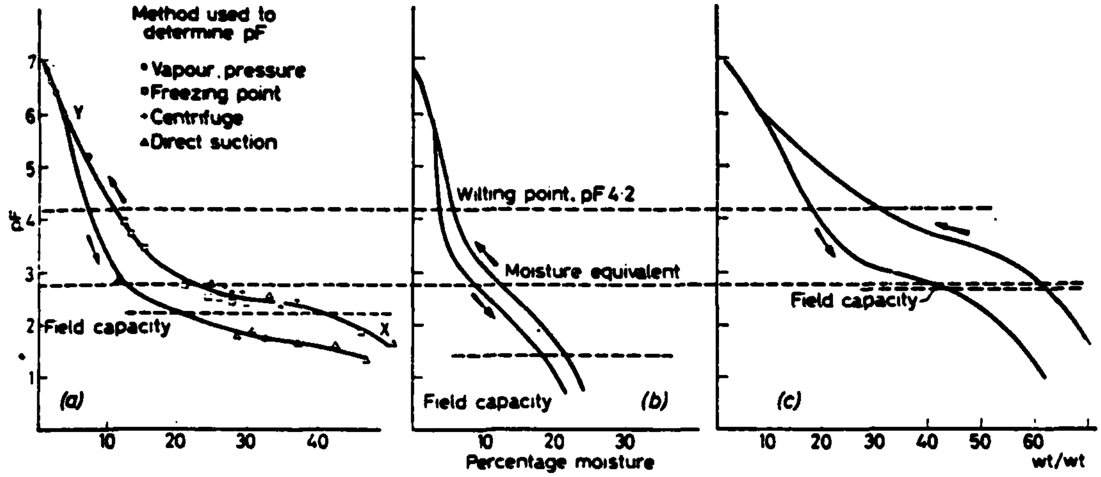

Fig. A.6 - Hysteresis curves showing per cent moisture vs. pF, a measure of the free energy of molecules of the water held in the soil, which is proportional to the amount of energy needed to get them out. Point Y represents 'air dryed' soil, and shows the associated minimum water content. a) Loam Soil; b) Sandy Soil; c) Heavy Clay Soil. (Fig. 4 from Ingram, [20]).

APPENDIX B
DATA BASE

Presented in this Appendix is the raw data from the experiments upon which many of the calculations in this report are based. The data are digitalizations of Polaroid photos and are presented as plots of voltage or current versus time.

In the figure captions, the first number is the shot number followed by a letter designating the group of experiments from which it was obtained. The second number is a, the radius of the center conductor; the third is b, the radius of the outer conductor. The fourth is L, the sample length, the fifth is ohmic resistivity in ohm-m. All distances are in meters. For example, 399A, 0.01, 0.5, 0.1, 350 sand mix means shot 399 of Exp. A, with $a = 0.01$ m, $b = 0.5$ m, $L = 0.1$ m, and $\rho_0 = 350$ Ω-m sand mix.

Also, V_0 indicates that the voltage on the center conductor in kilovolt is being plotted versus time in microsecond; I means that total sample current in amperes is being plotted. Finally, V indicates that a probe voltage is being plotted; and r is the radial position of a probe in meters; θ is azimuthal angle of probe in degrees; and bottom or top indicates that a probe was near the bottom on top of the soil sample.

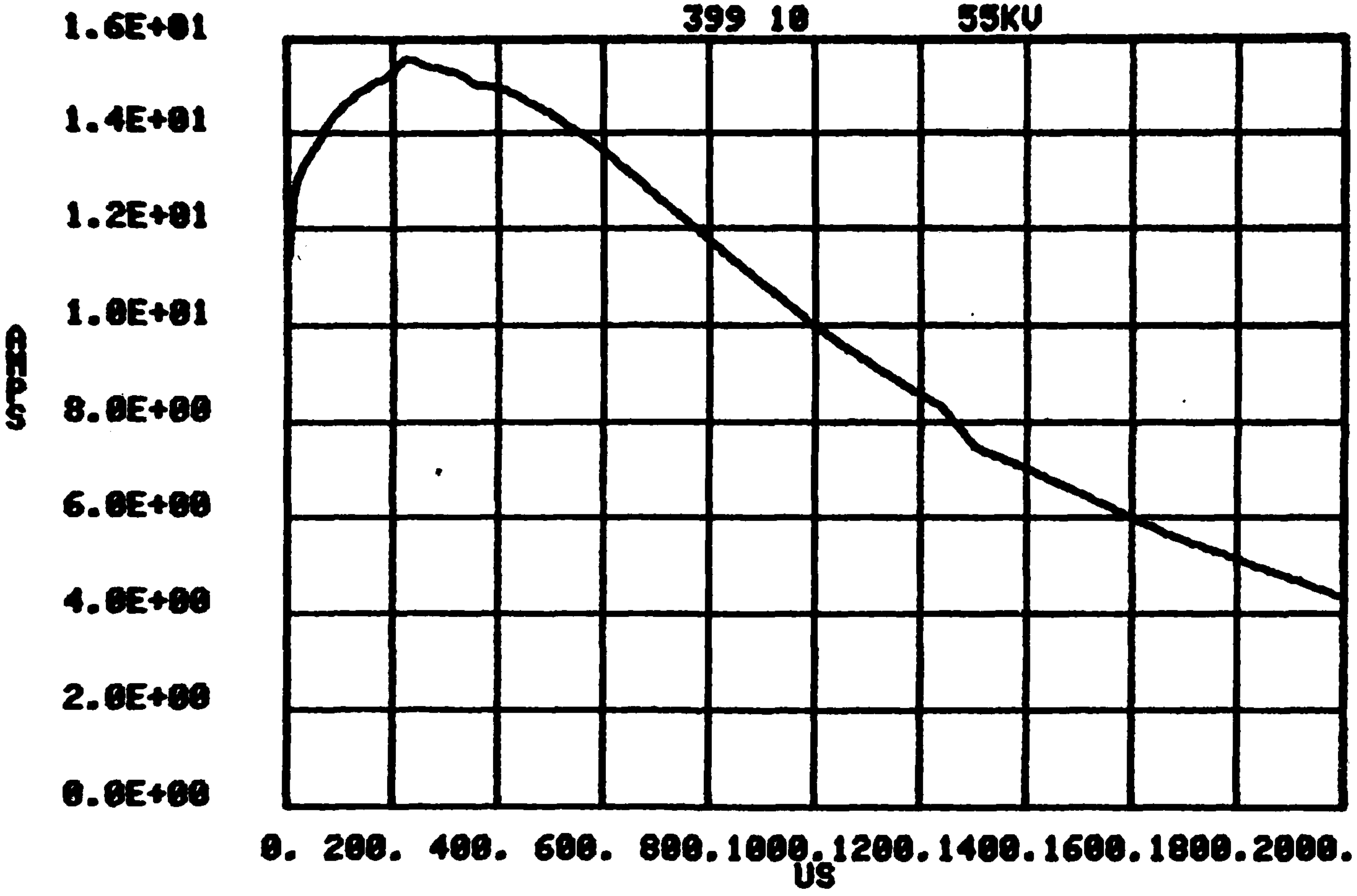

Figure B.1. 399A, .01, .1., .5, .1, 350 sand-mix; I.

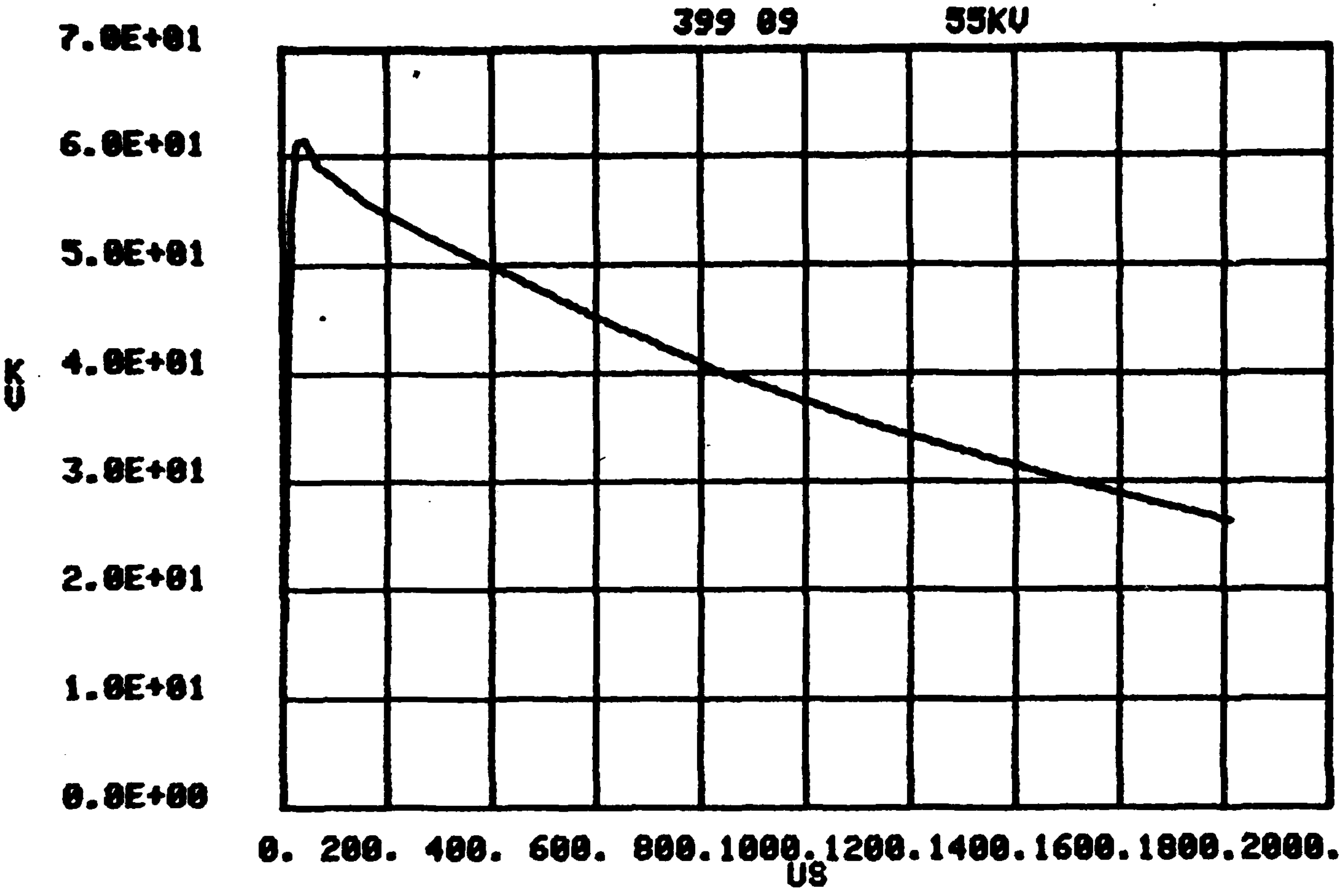

Figure B.2. 399A, .01, .1, .5, .1, 350 sand-mix; V_0; r = .01 m.

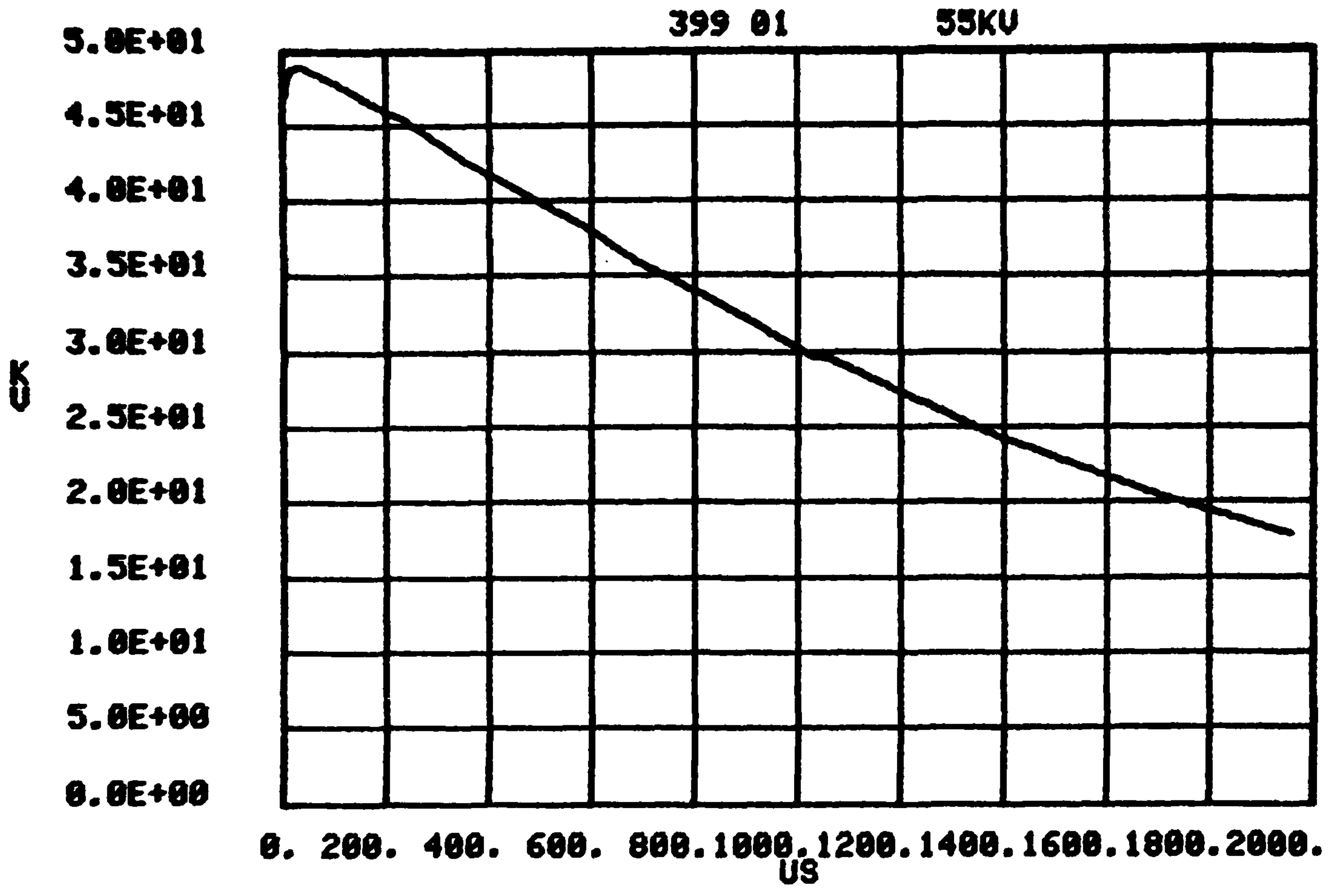

Figure B.3. 399A, .01, .1, .5, .1, 350 sand-mix; V at radial position 2; r = .059 m.

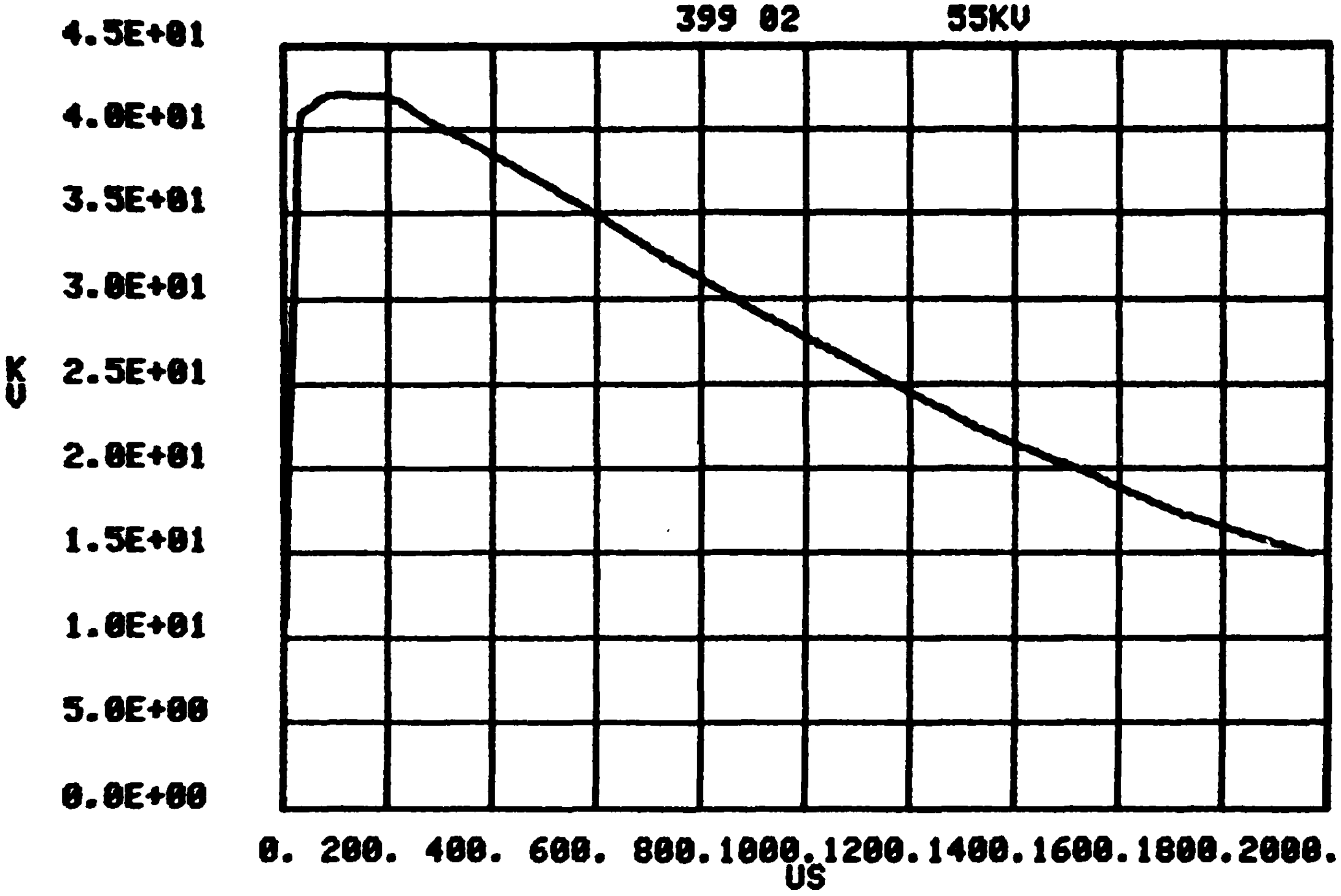

Figure B.4. 399A, .01, .1, .5, .1, 350 sand-mix; V at radial position 3; r = .109 m.

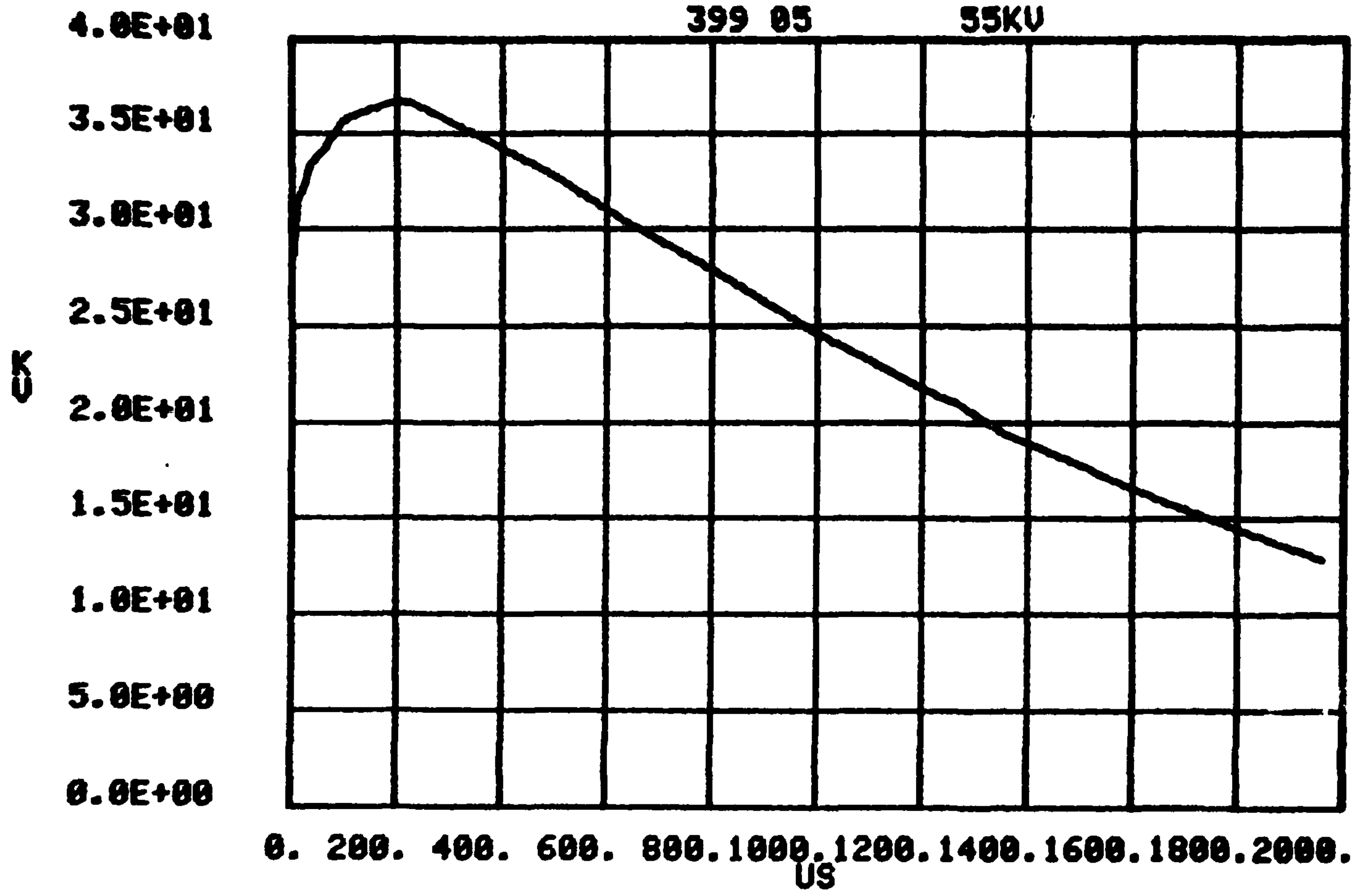

Figure B.5. 399A, .01, .1, .5, .1, 350 sand-mix; V at radial position 4; r = .159 m.

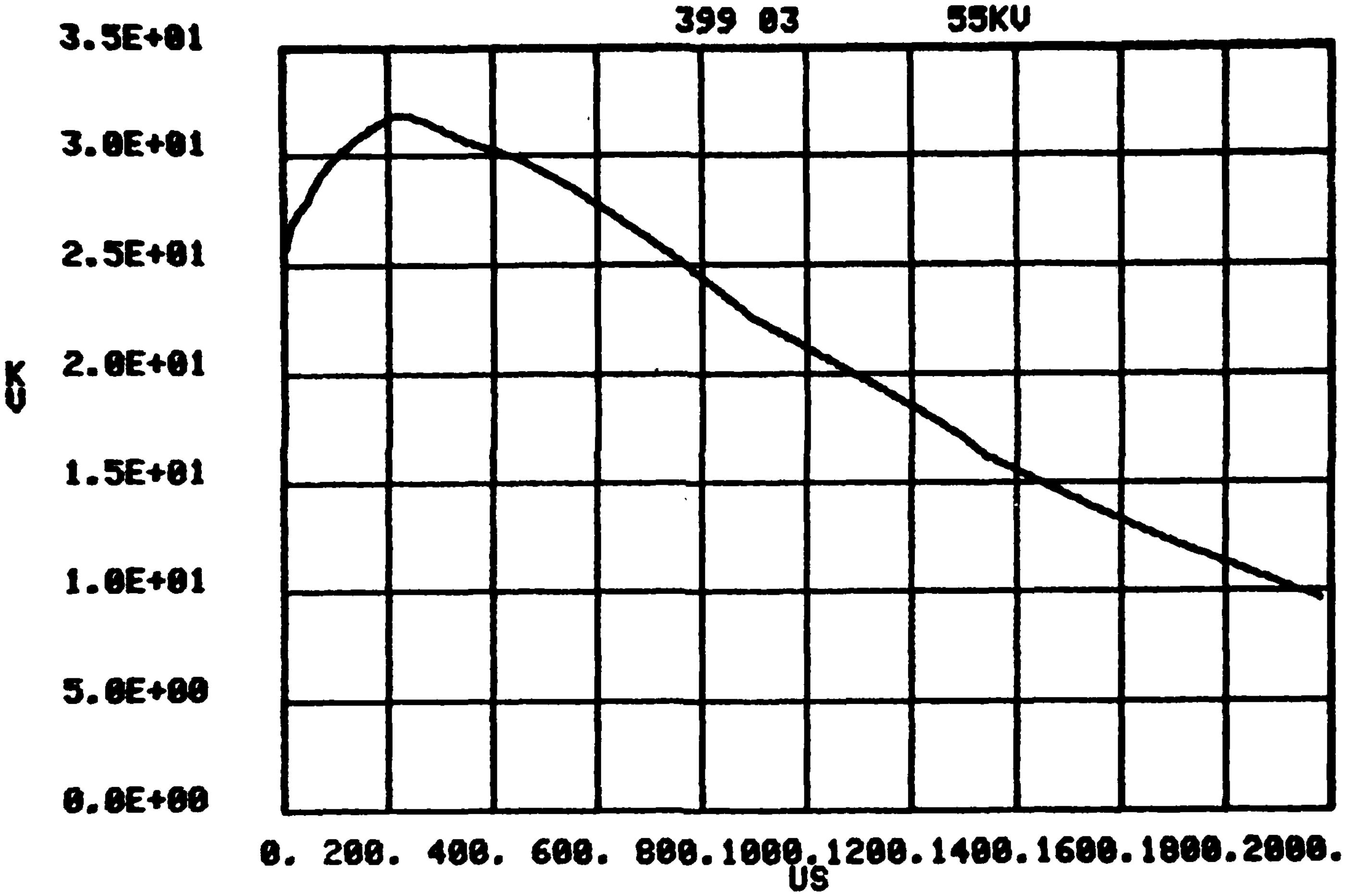

Figure B.6. 399A, .01, .1, .5, .1, 350 sand-mix; V at radial position 5; r = .209 m.

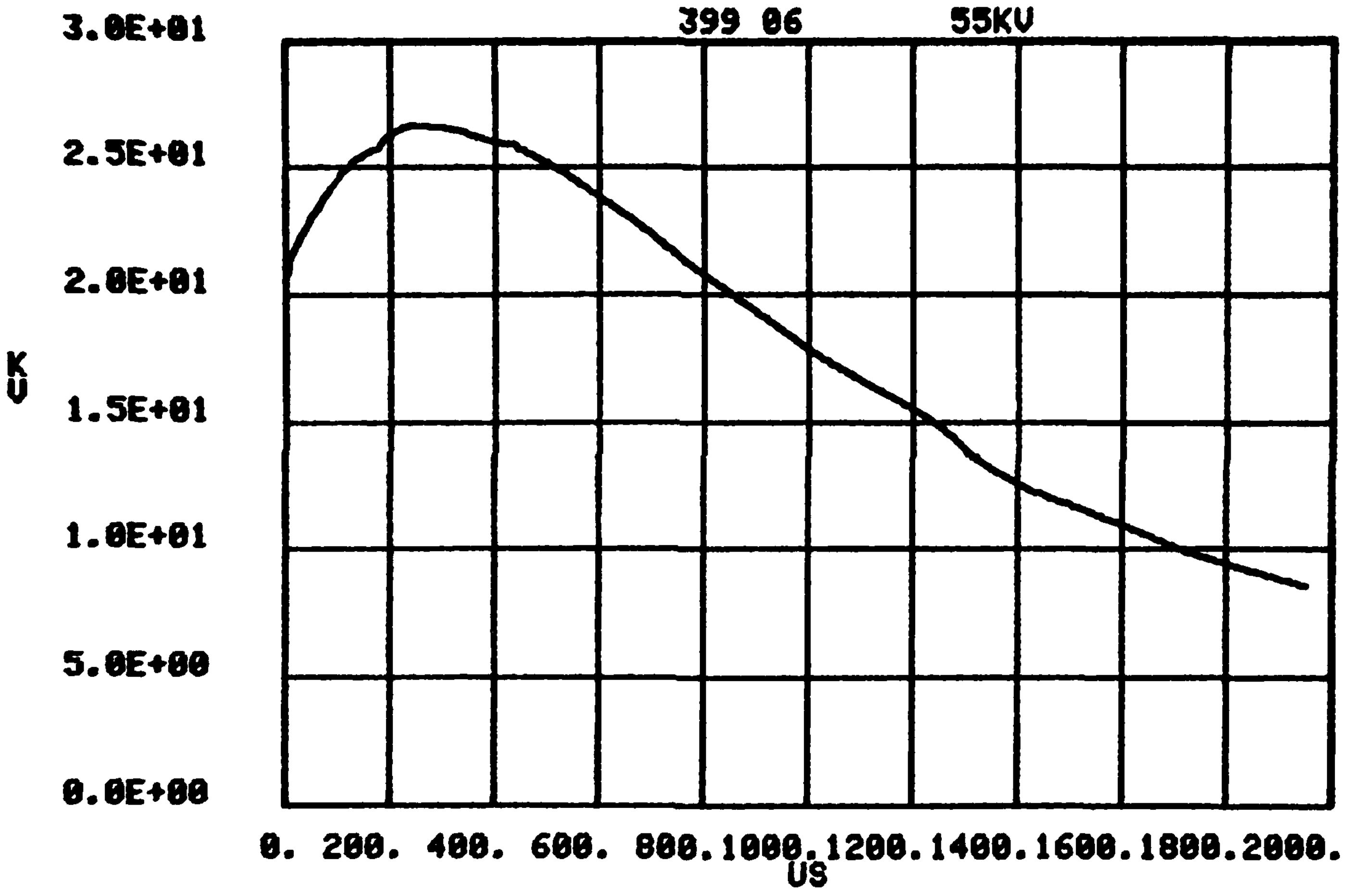

Figure B.7. 399A, .01, .1, .5, .1, 350 sand-mix; V at radial position 6; r = .259 m.

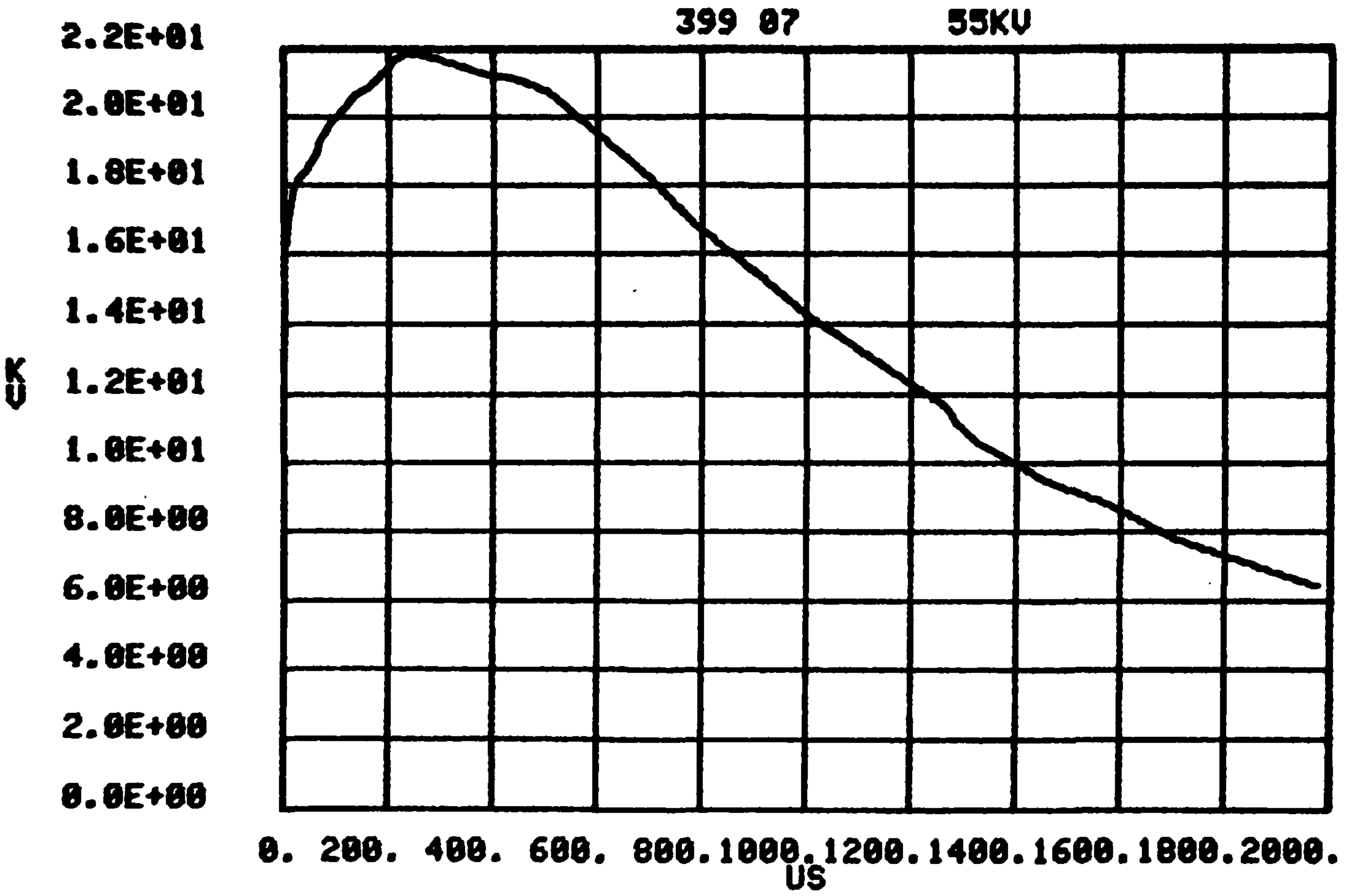

Figure B.8. 399A, .01, .1, .5, .1, 350 sand-mix; V at radial position 7; r = .309 m.

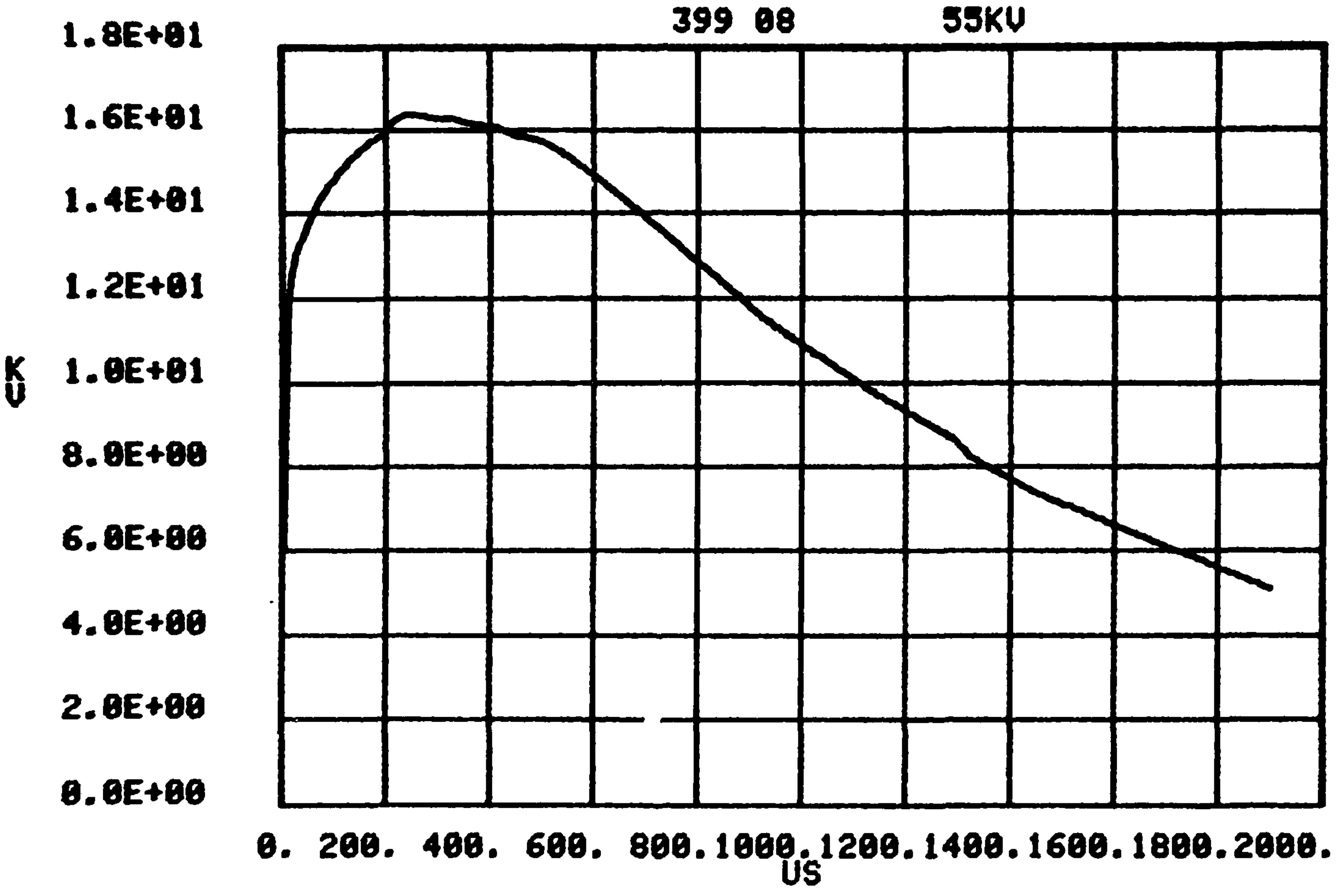

Figure B.9. 399A, .01, .1, .5, .1, 350 sand-mix; V at radial position 8; r = .359 m.

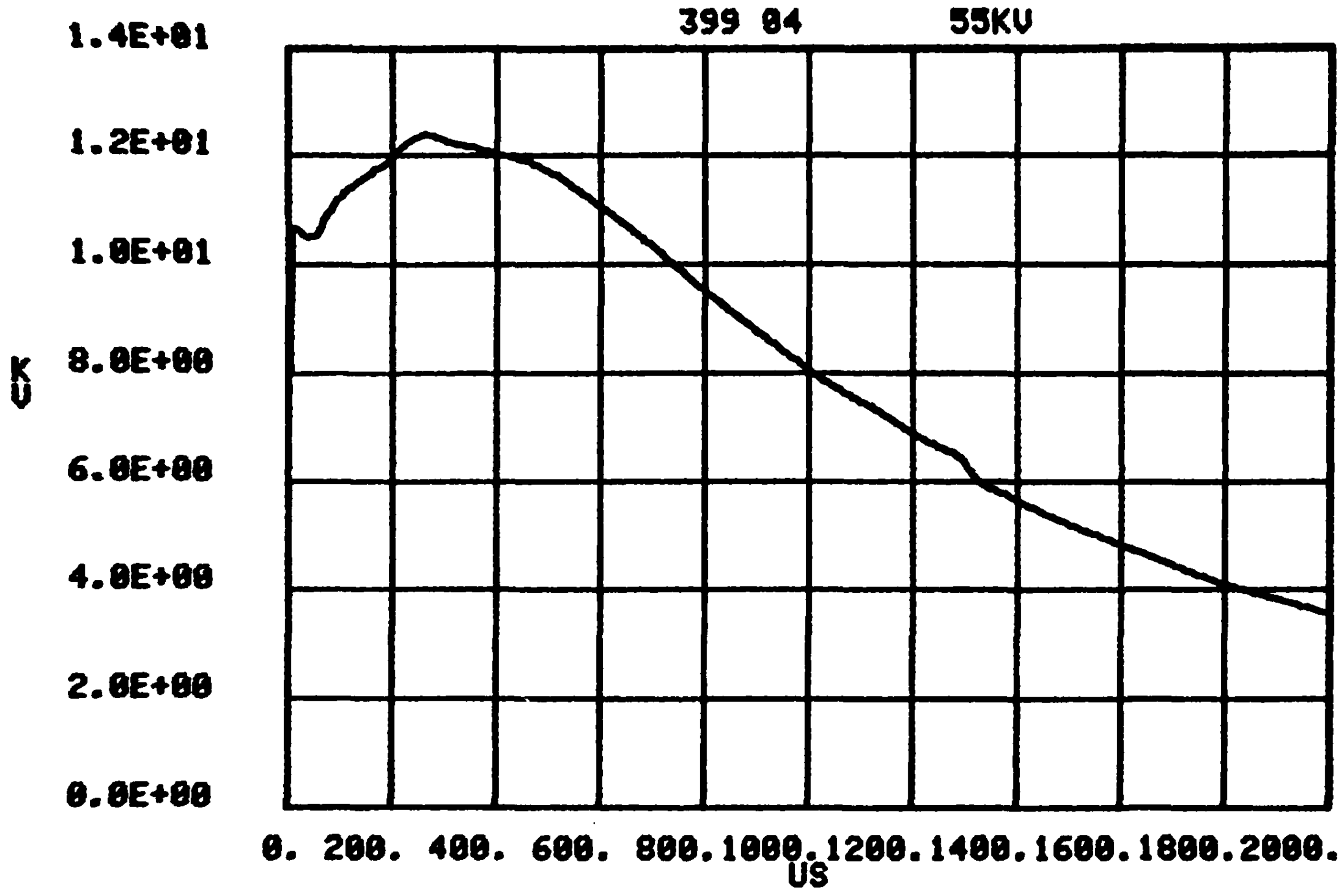

Figure B.10. 399A, .01, .1, .5, .1, 350 sand-mix; V at radial position 9; r = .409 m.

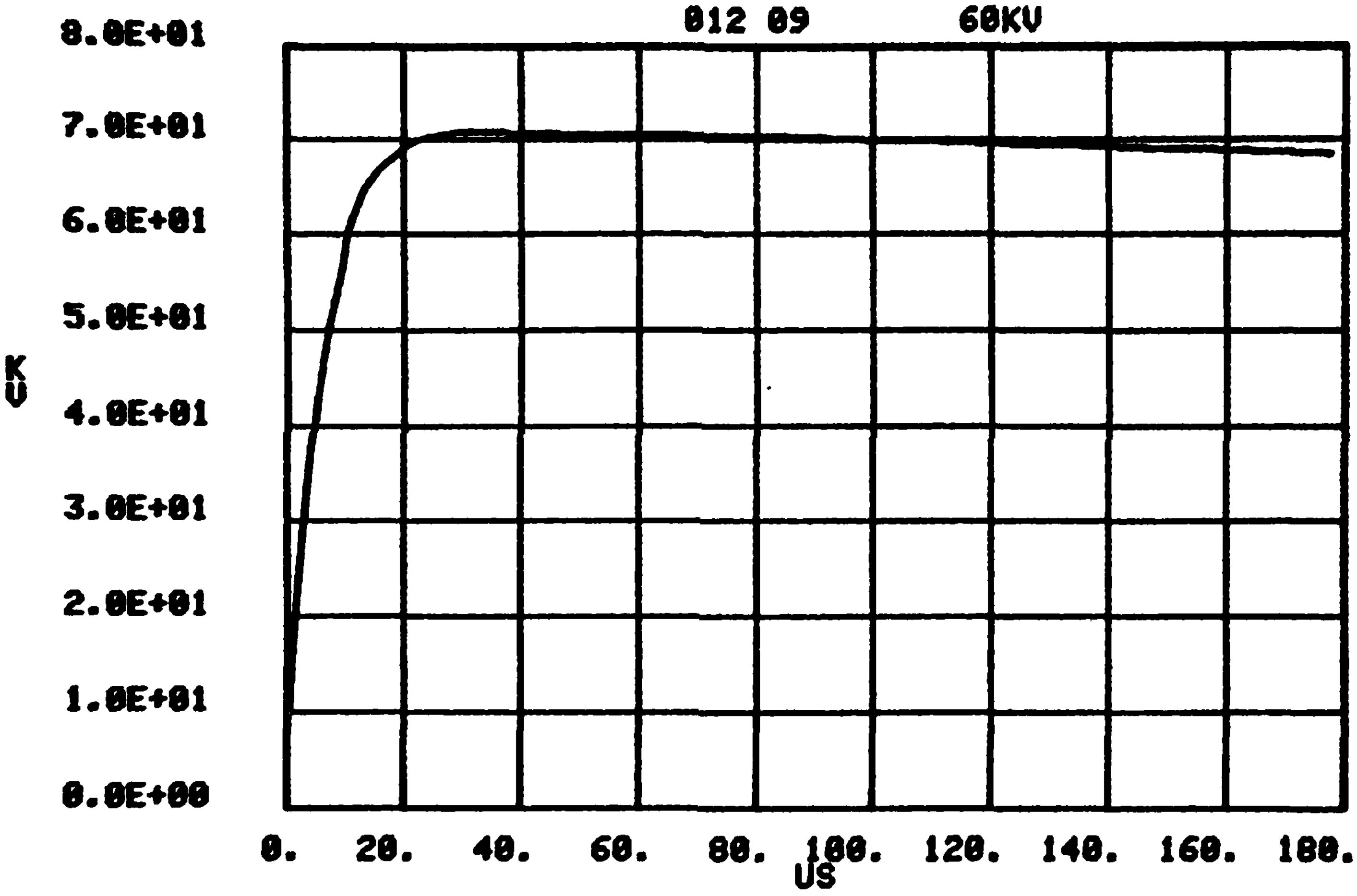

Figure B.11. 012A, .01, 1.0, .3, 1500 sand; V_o.

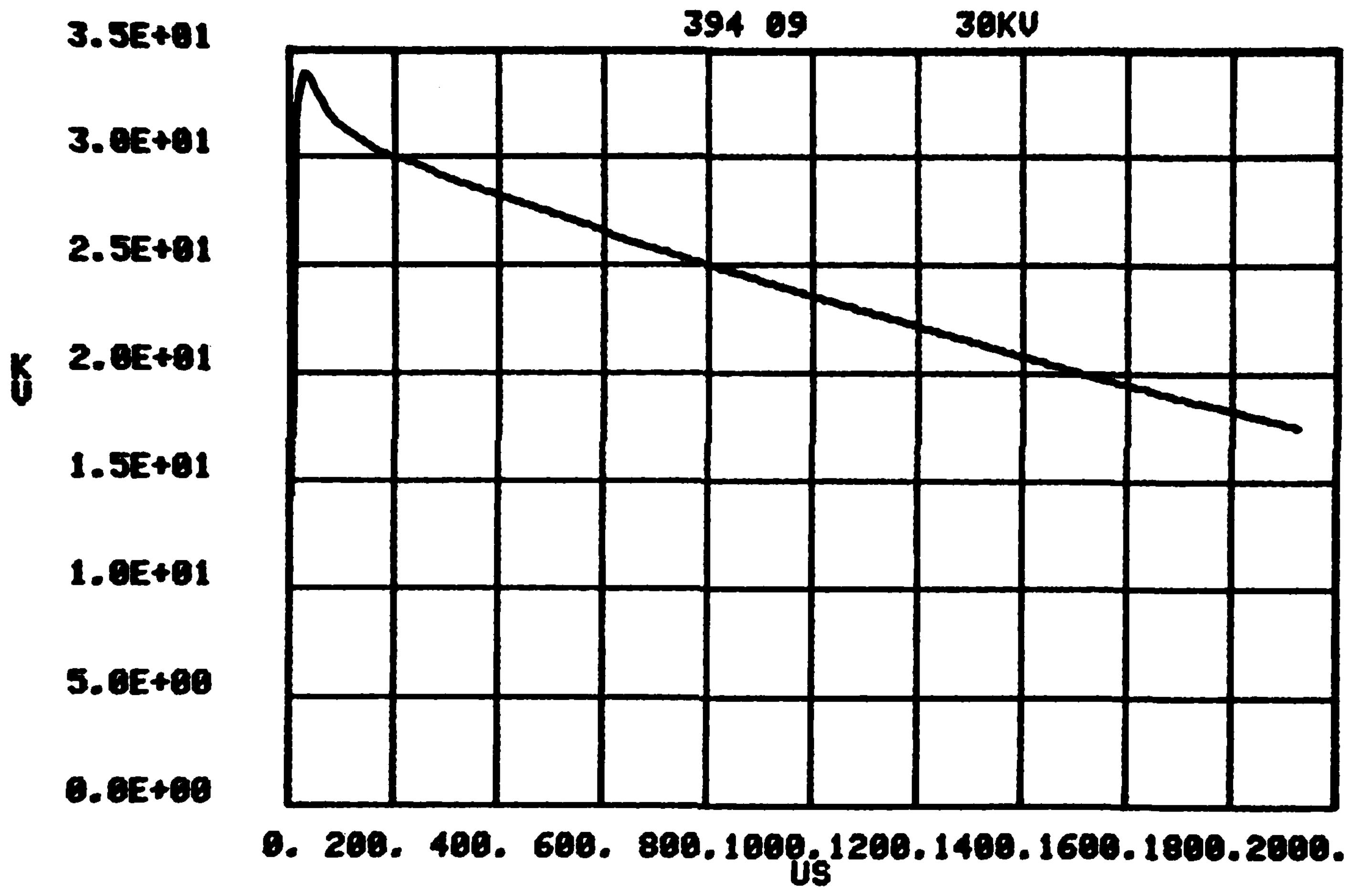

Figure B.12. 394A, .01, .5, .1, 350 sand mix; V_o.

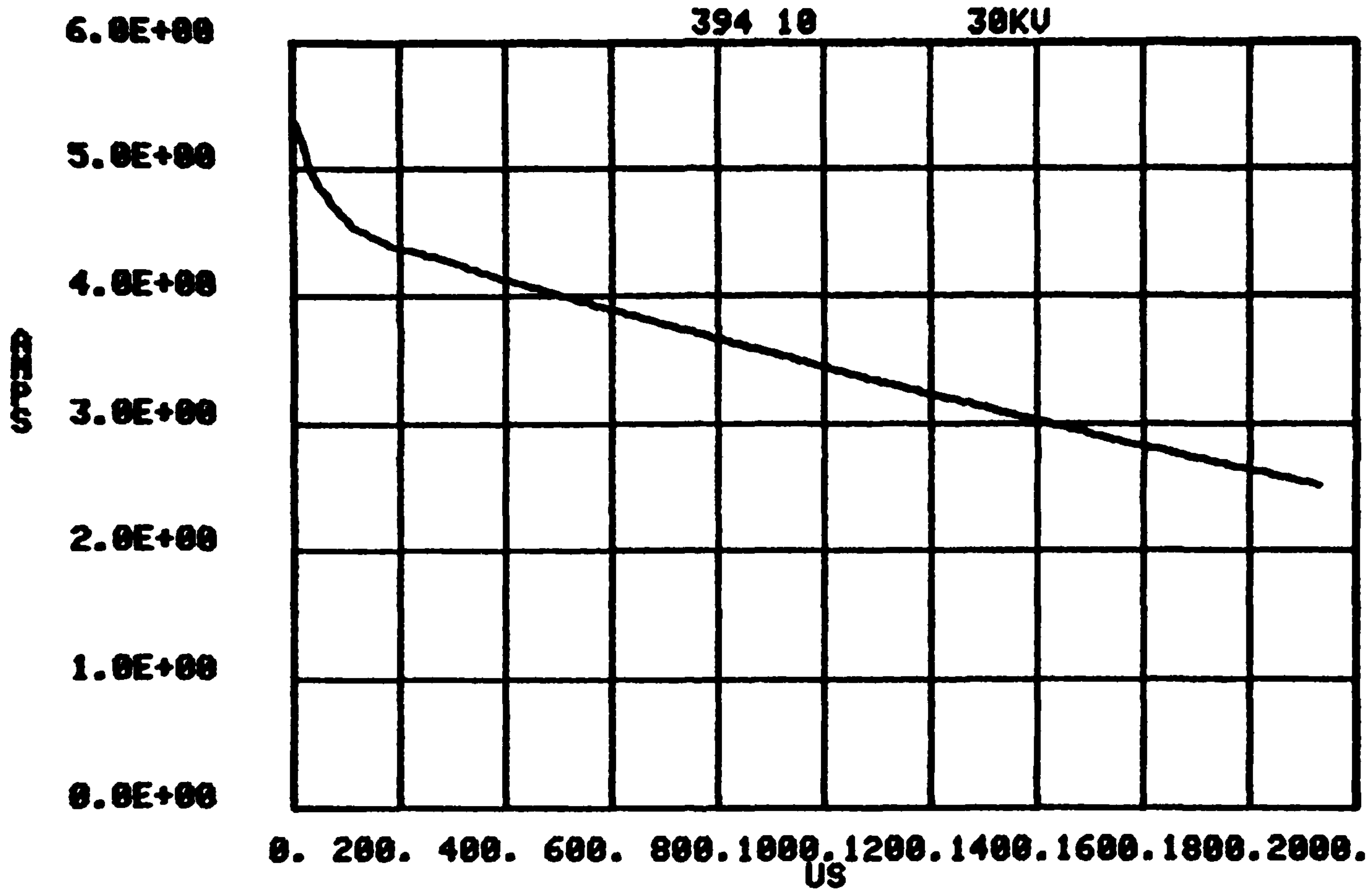

Figure B.13. 394A, .01, .5, .1, 350 sand mix; I.

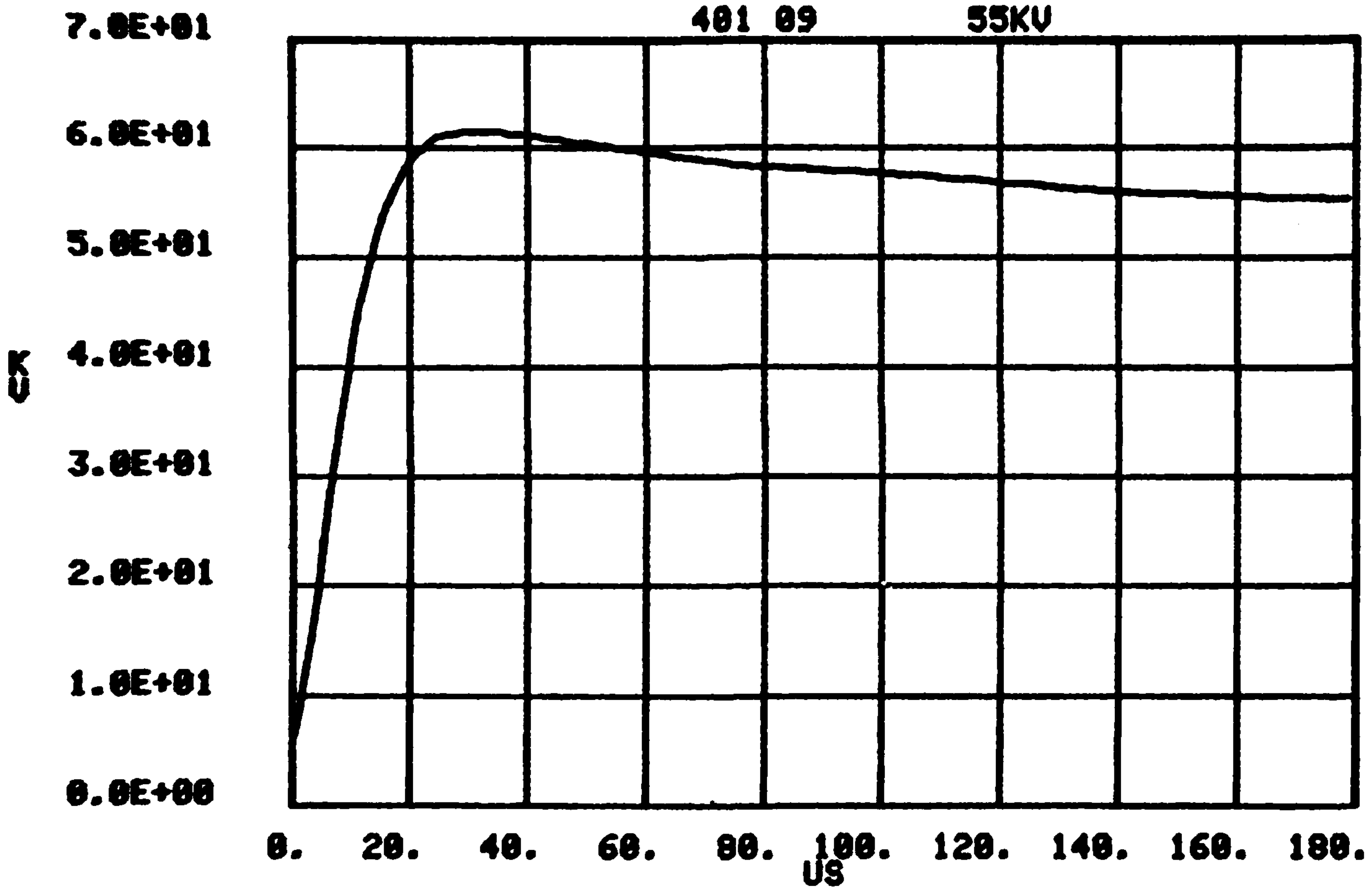

Figure B.14. 401A, .01, .5, .1, 350 sand mix; V_o.

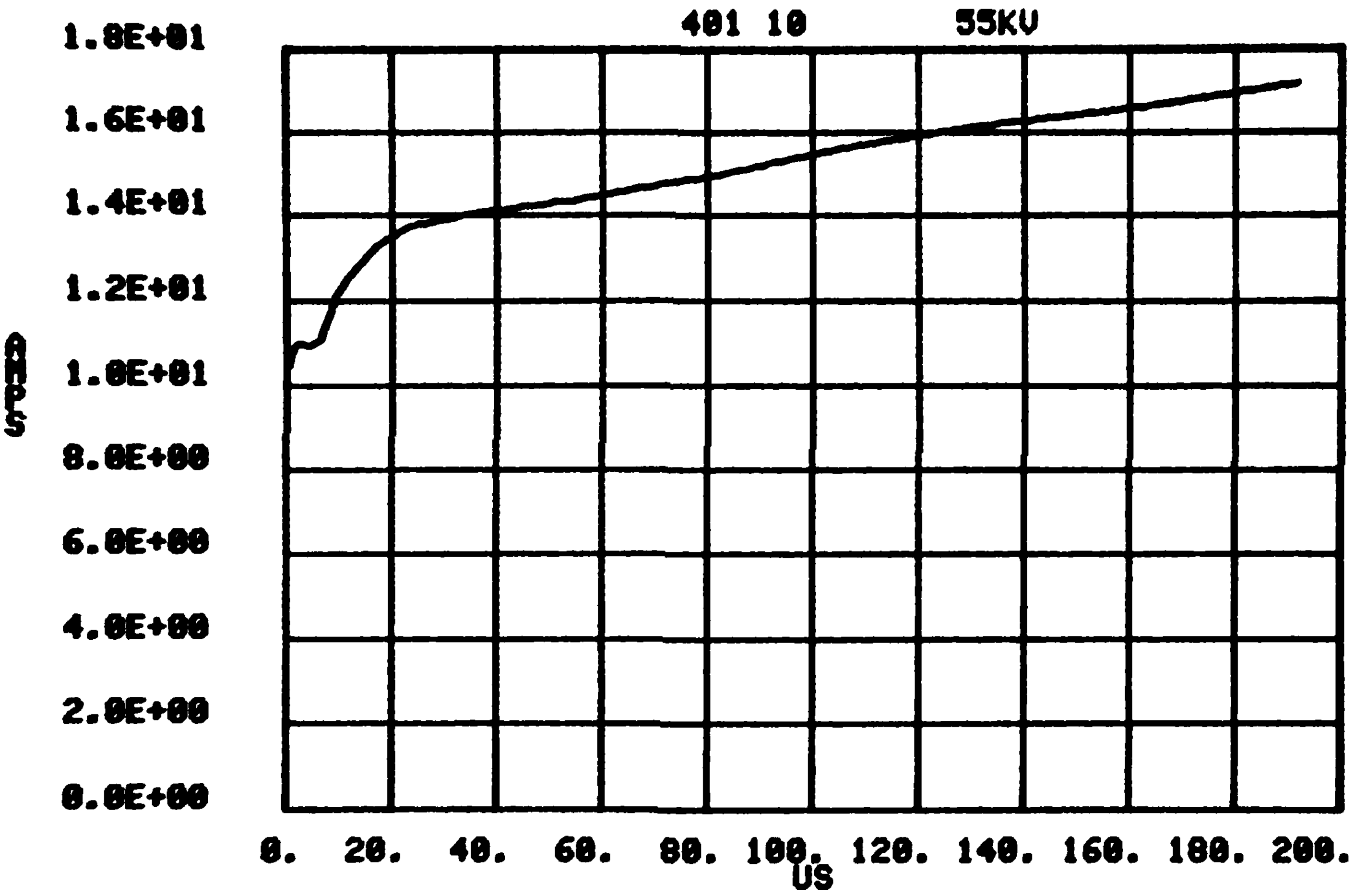

Figure B.15. 401A, .01, .5, .1, 350 sand mix; I.

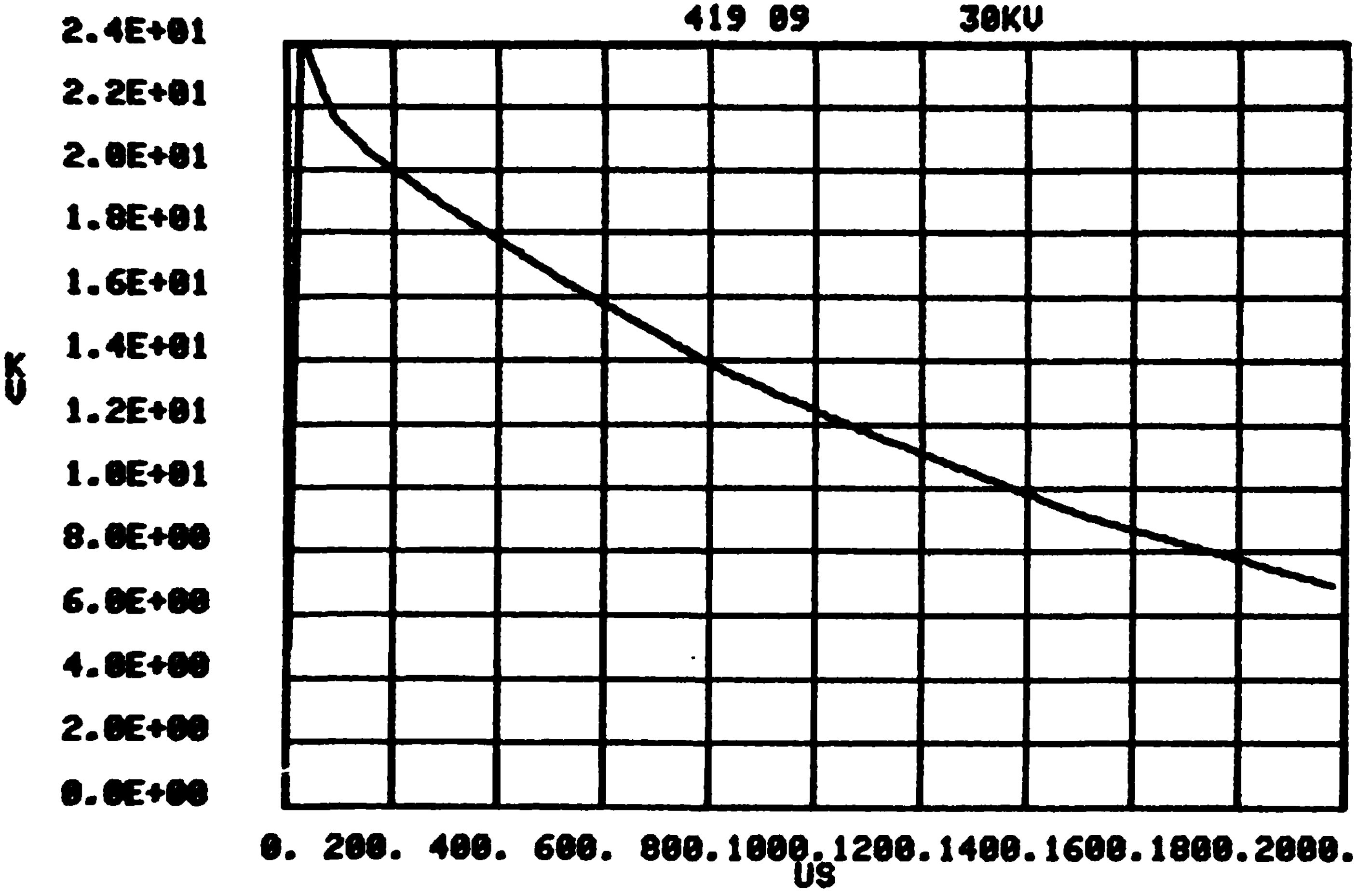

Figure B.16. 419A, .01, .5, .3, 350 sand mix; V_o.

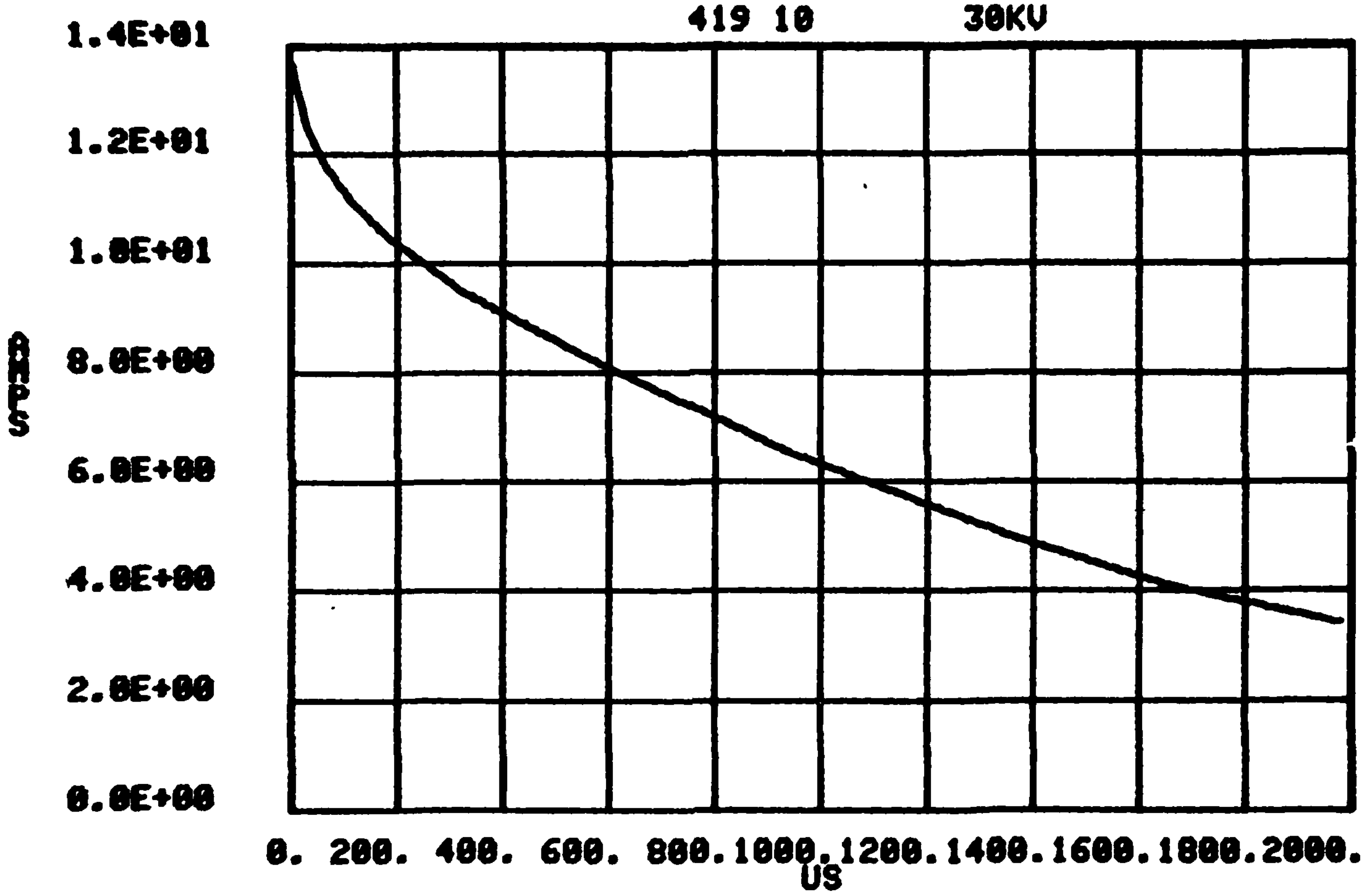

Figure B.17. 419A, .01, .5, .3, 350 sand mix; I.

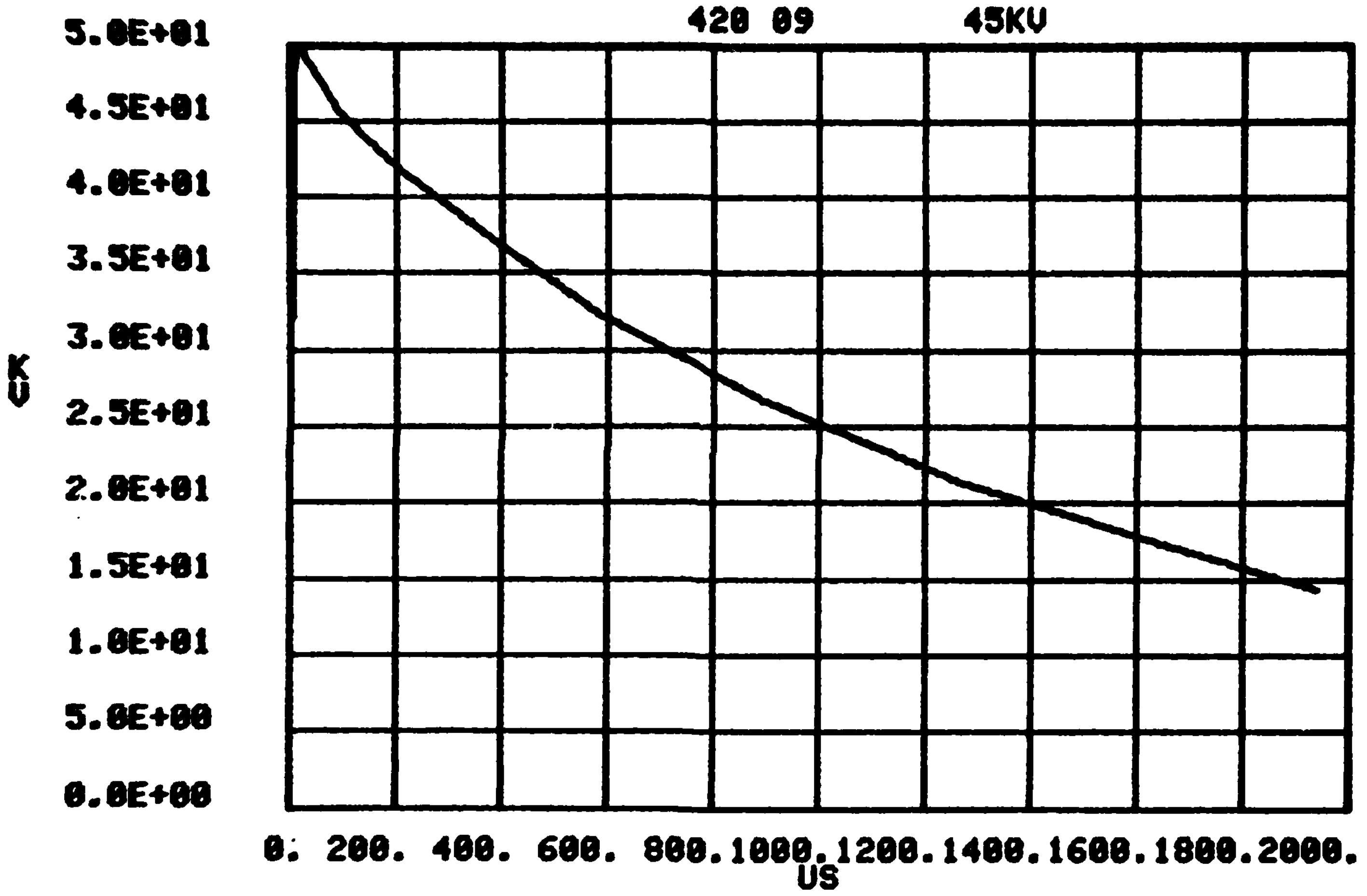

Figure B.18. 420A, .01, .5, .3, 350 sand mix; V_o.

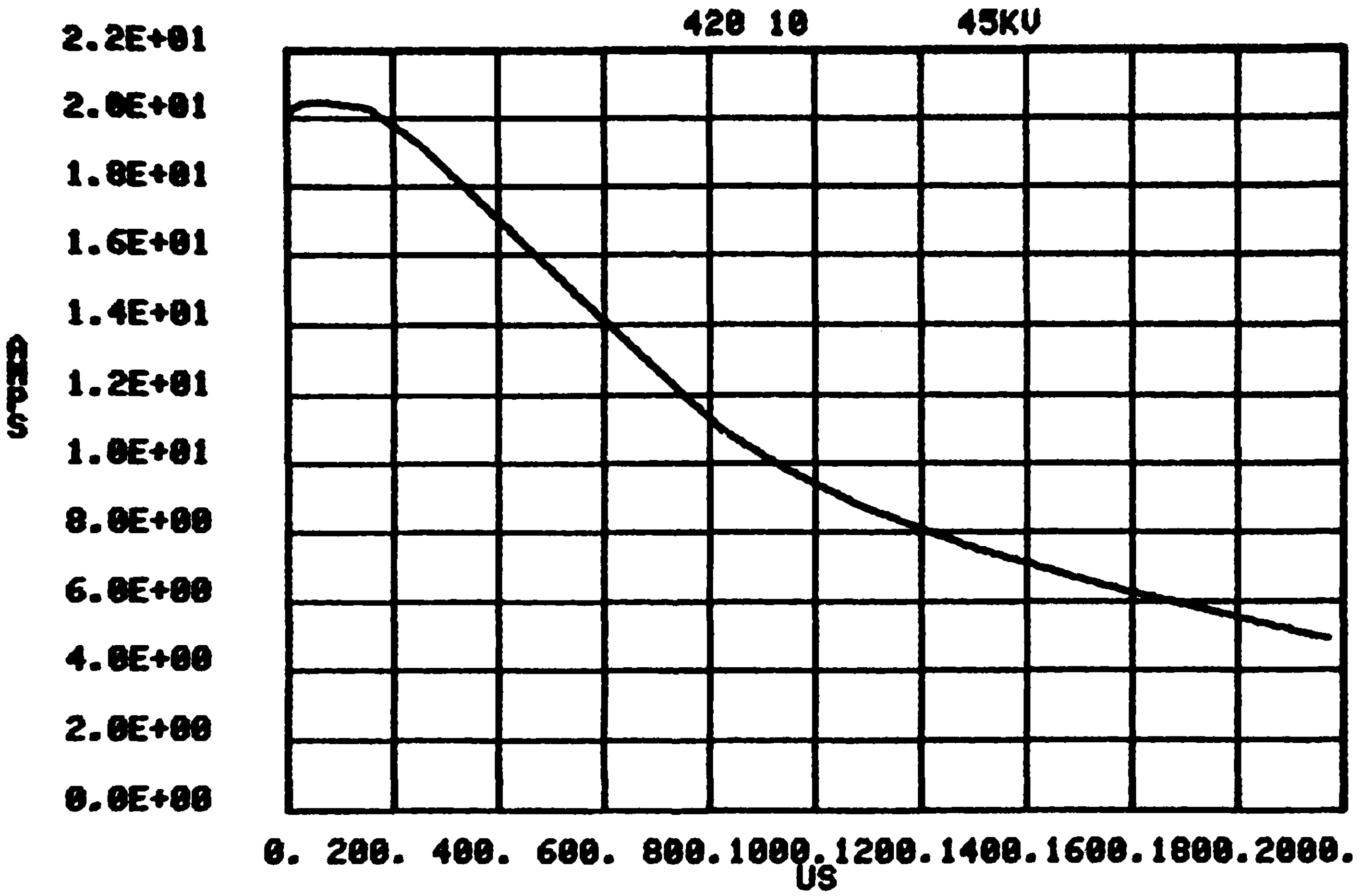

Figure B.19. 420A, .01, .5, .3, 350 sand mix; I.

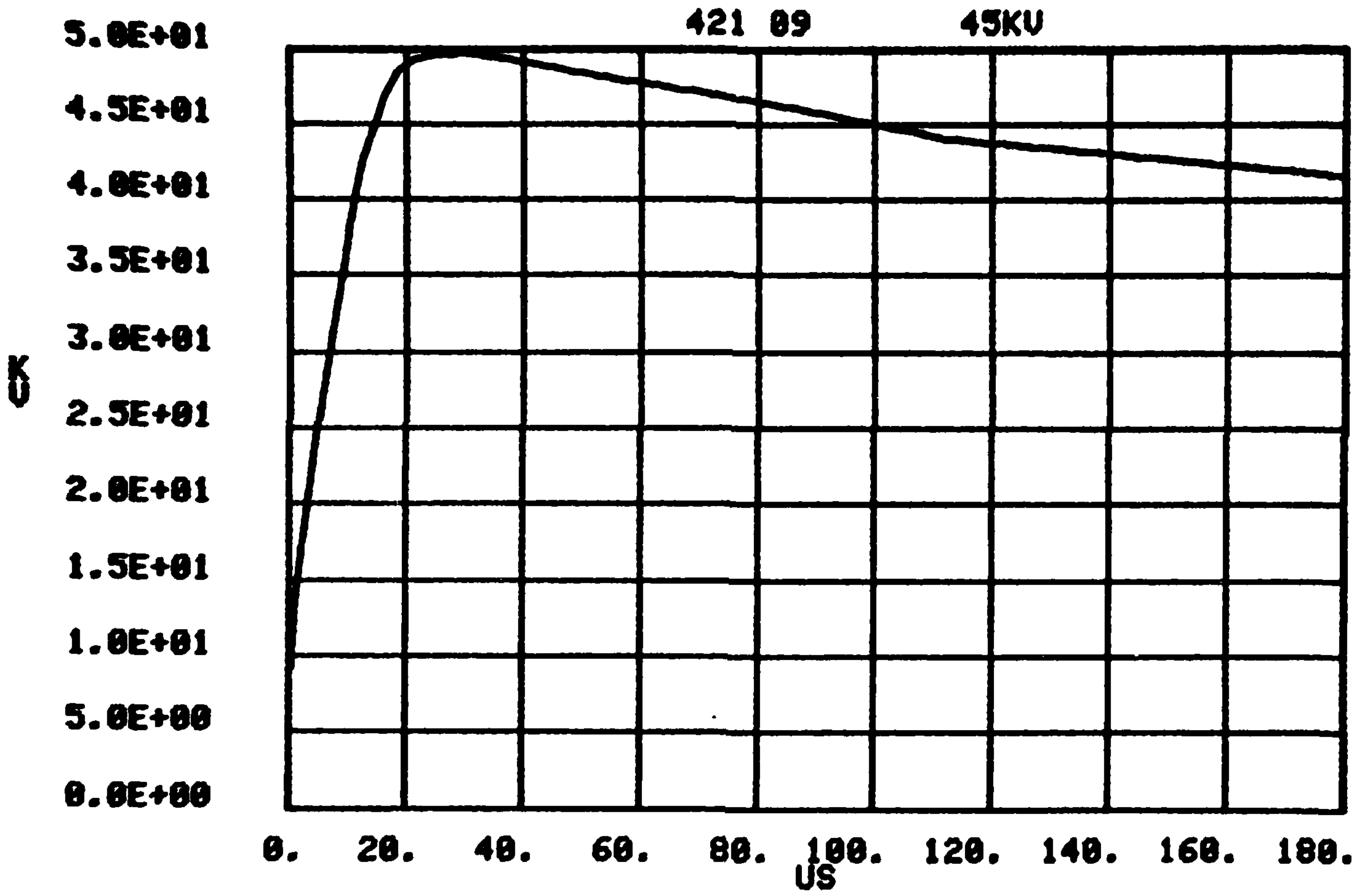

Figure B.20. 421A, .01, .5, .3, 350 sand mix; V_o.

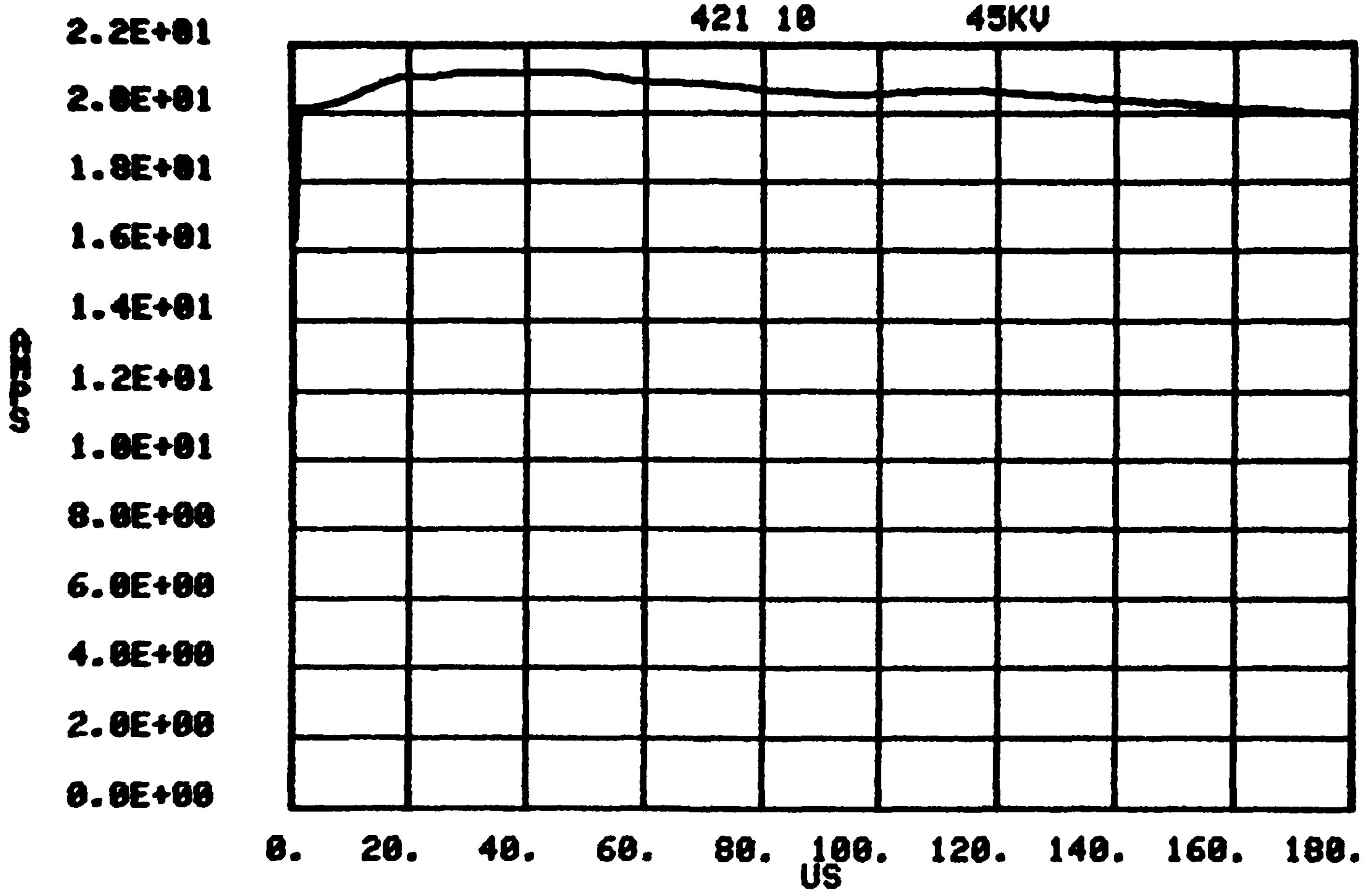

Figure B.21. 421A, .01, .5, .3, 350 sand mix; I.

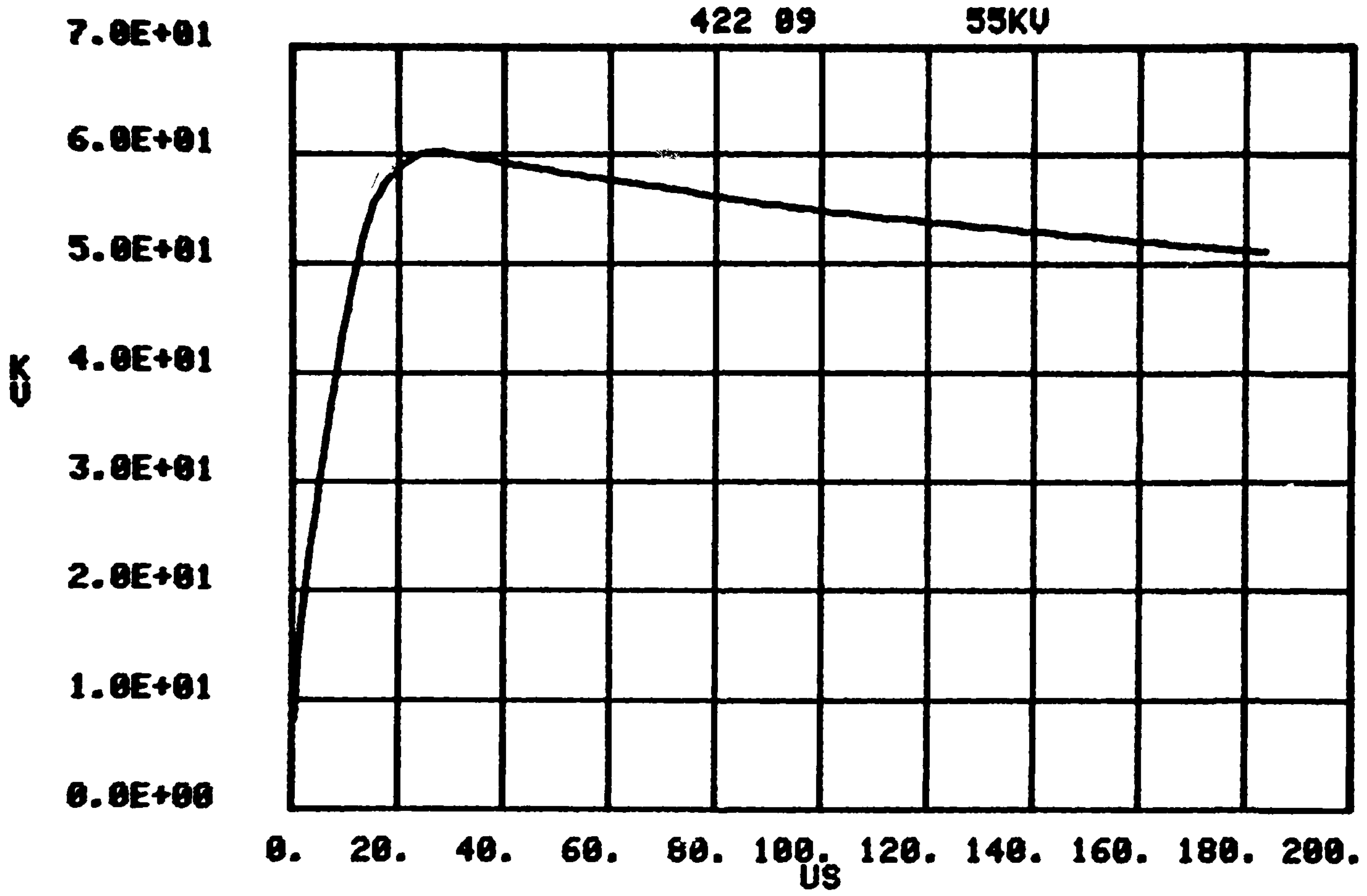

Figure B.22. 422A, .01, .5, .3, 350 sand mix; V_o.

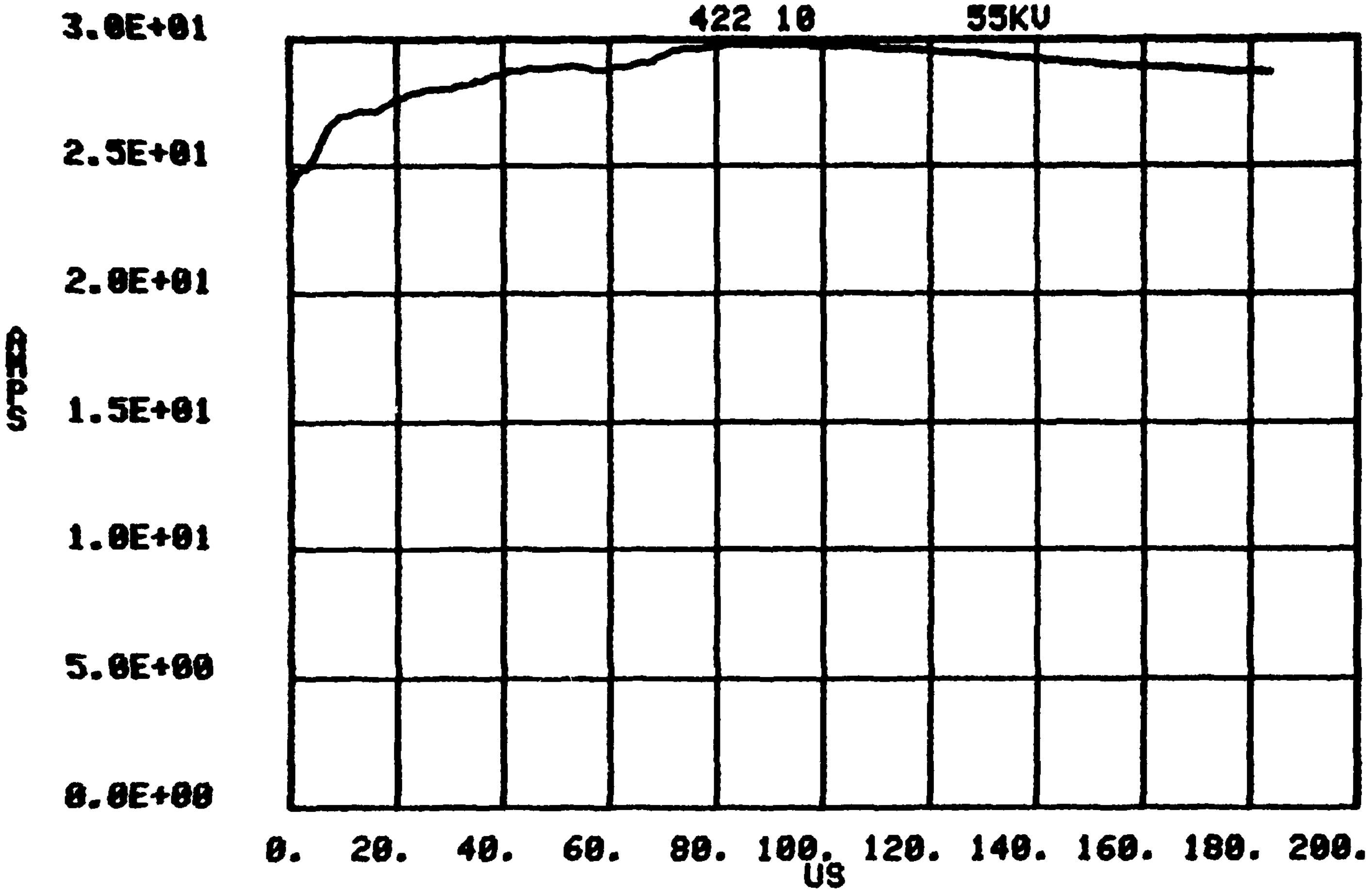

Figure B.23. 422, .01, .5, .3, 350 sand mix; I.

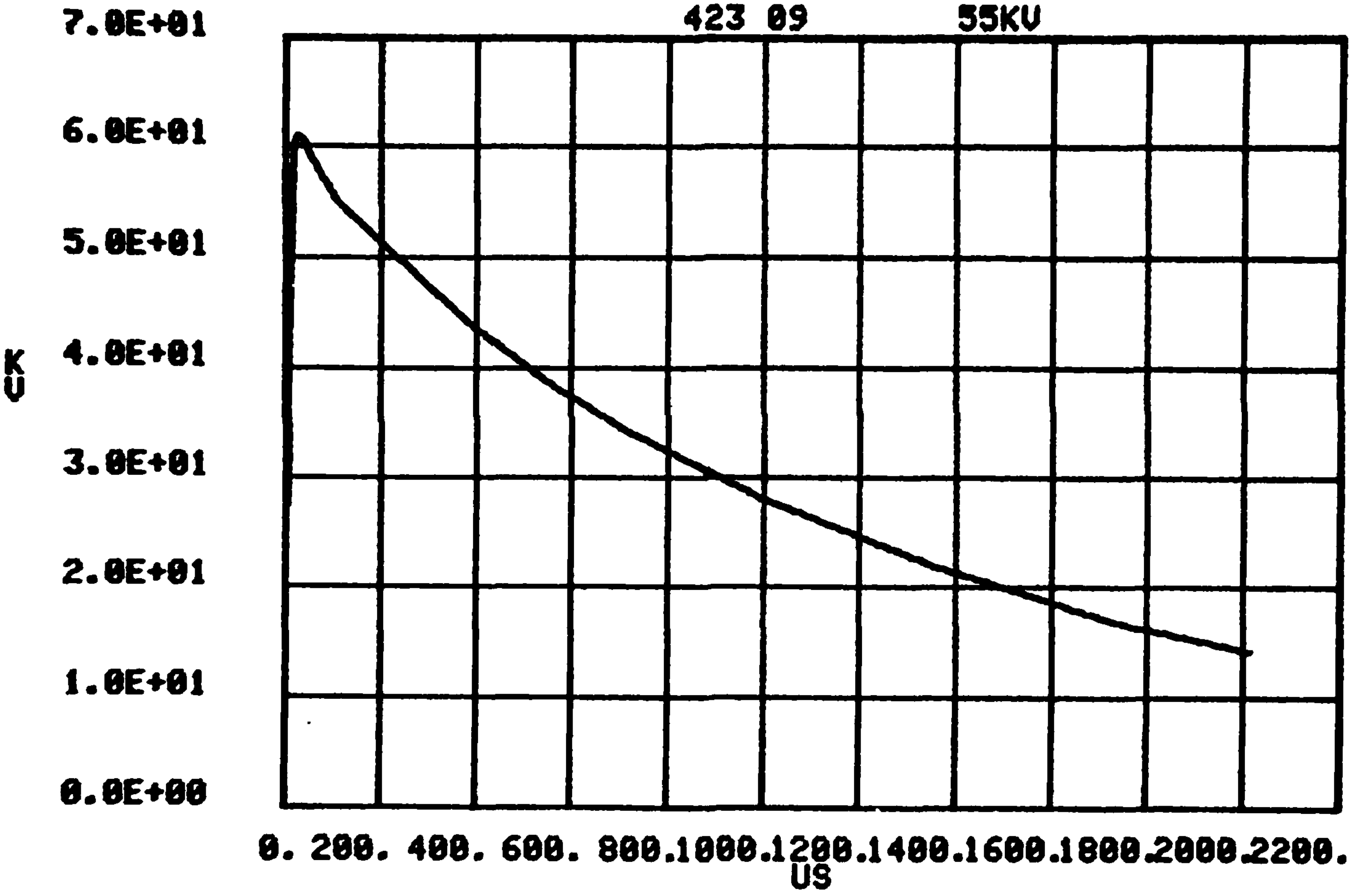

Figure B.24. 423A, .01, .5, .3, 350 sand mix; V_o.

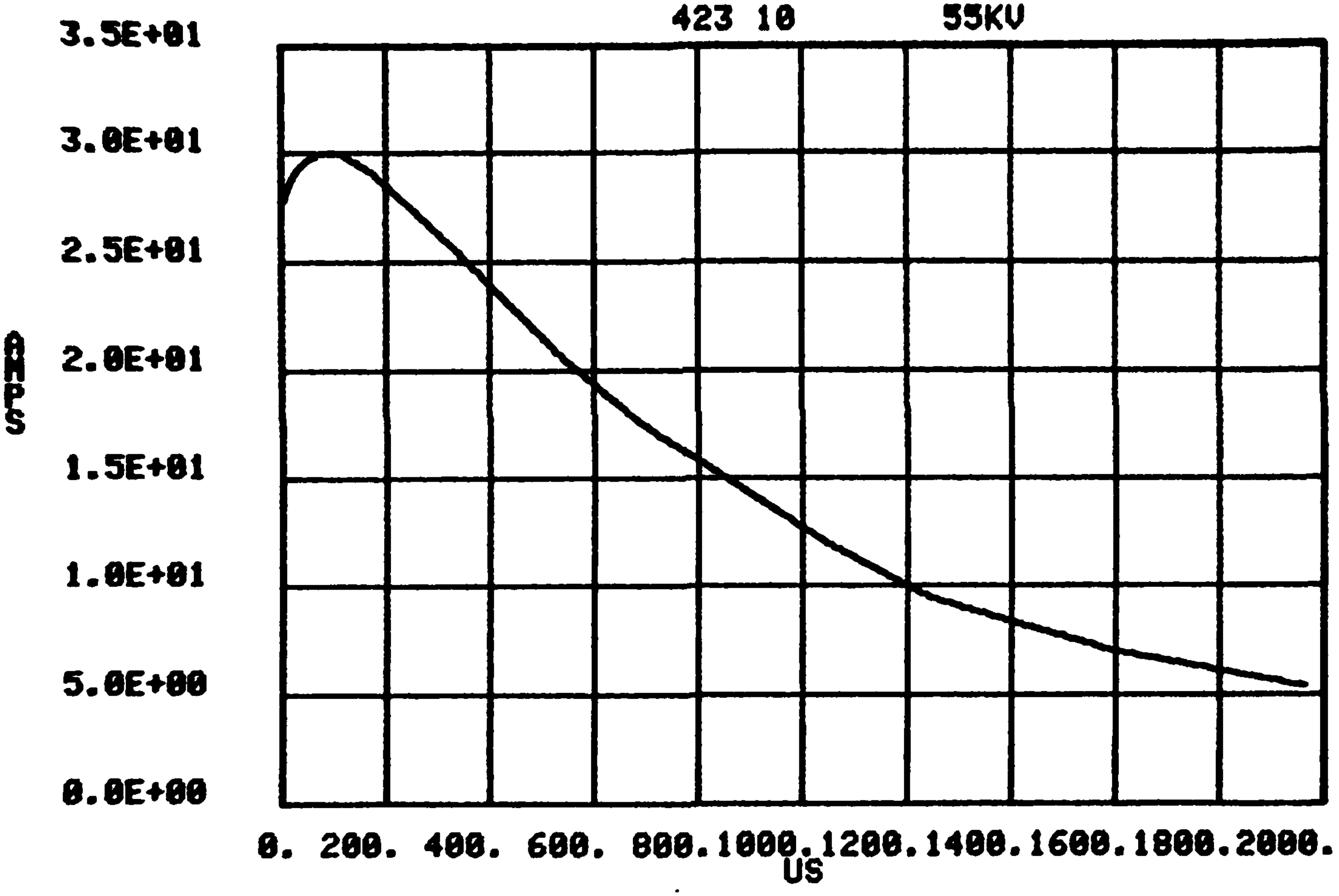

Figure B.25. 423A, .01, .5, .3, 350 sand mix; I.

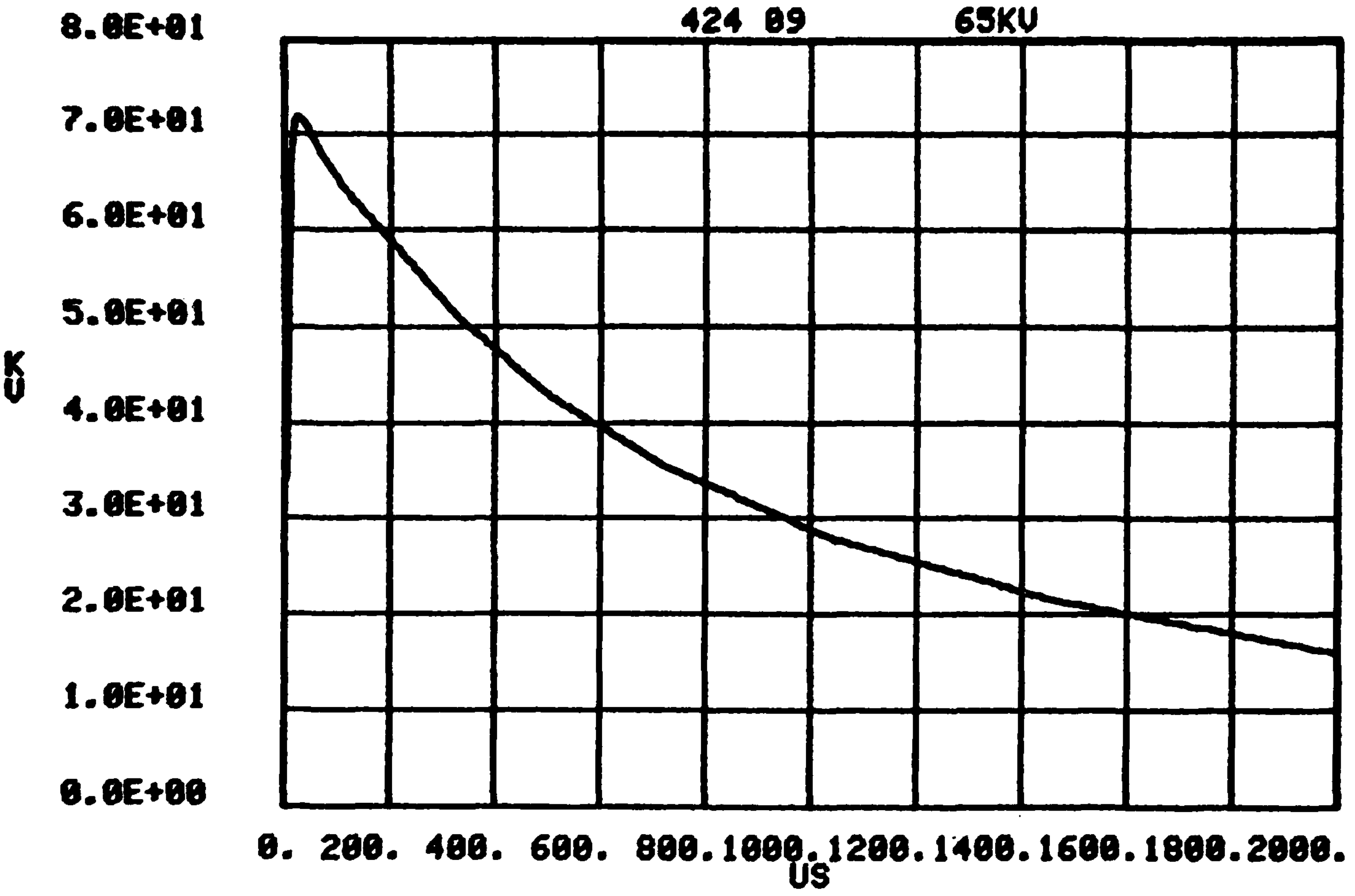

Figure B.26. 424A, .01, .5, .3, 350 sand mix; V_o.

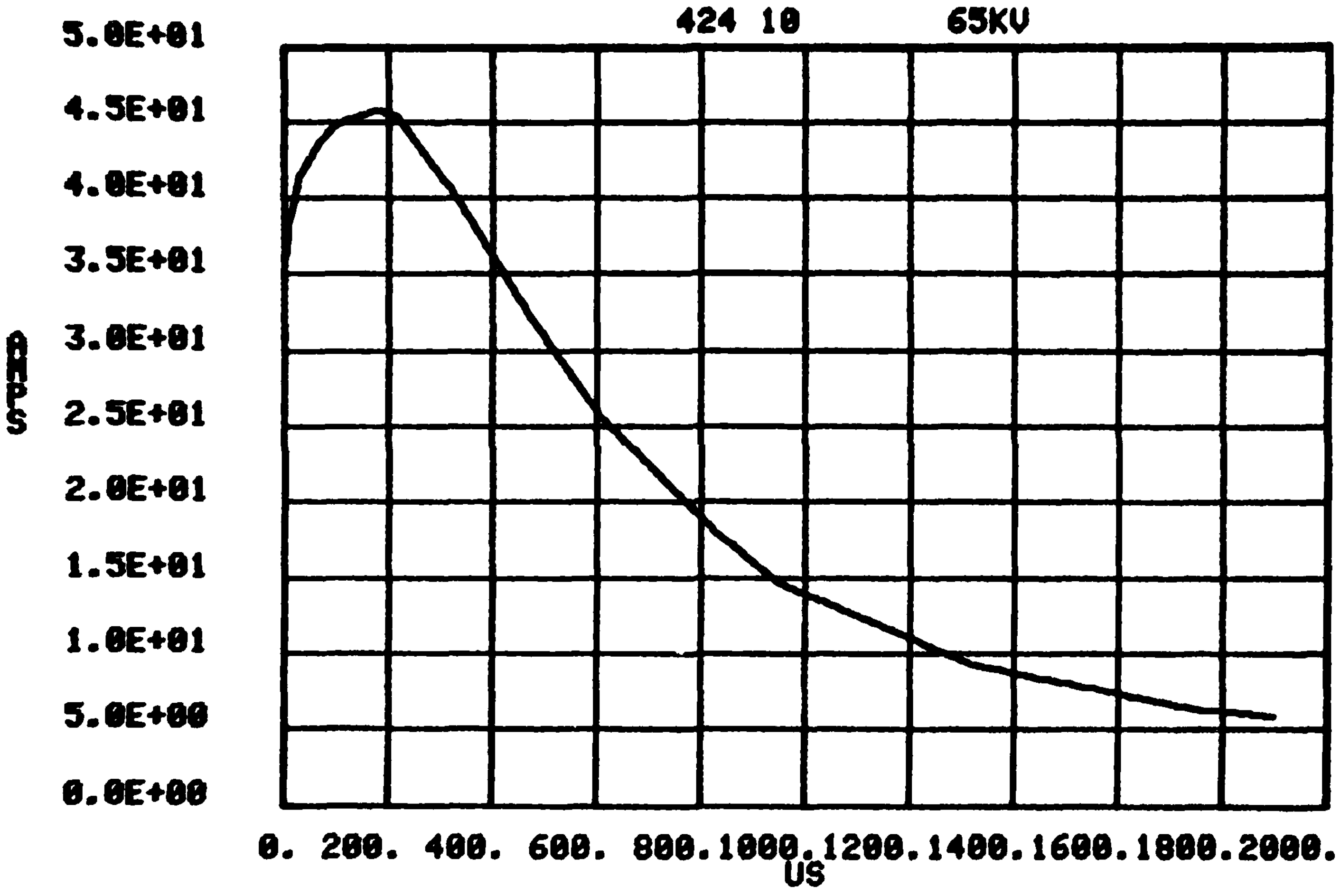

Figure B.27. 424A, .01, .5, .3, 350 sand mix; I.

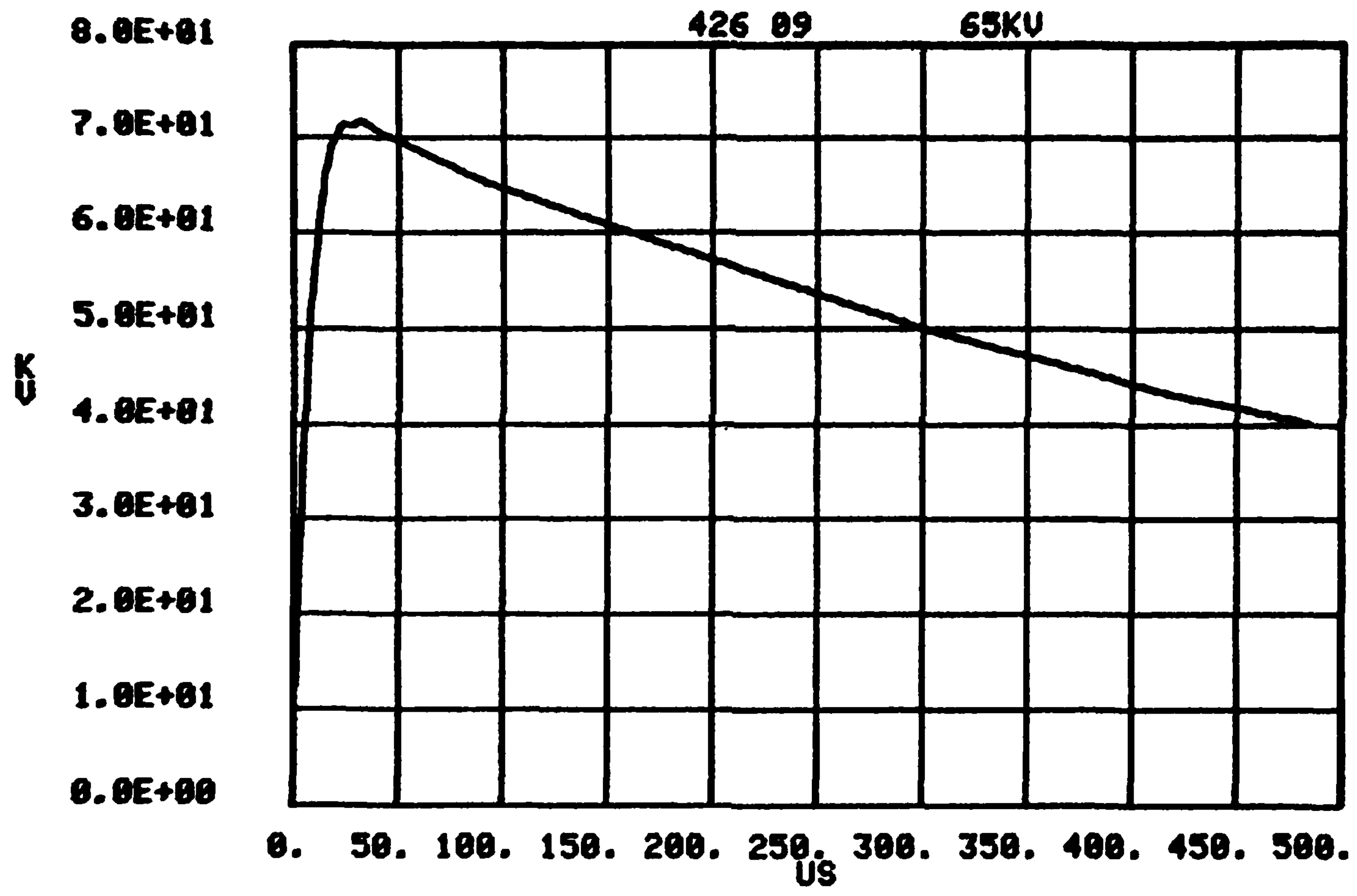

Figure B.28. 426A, .01, .5, .3, 350 sand mix; V_o.

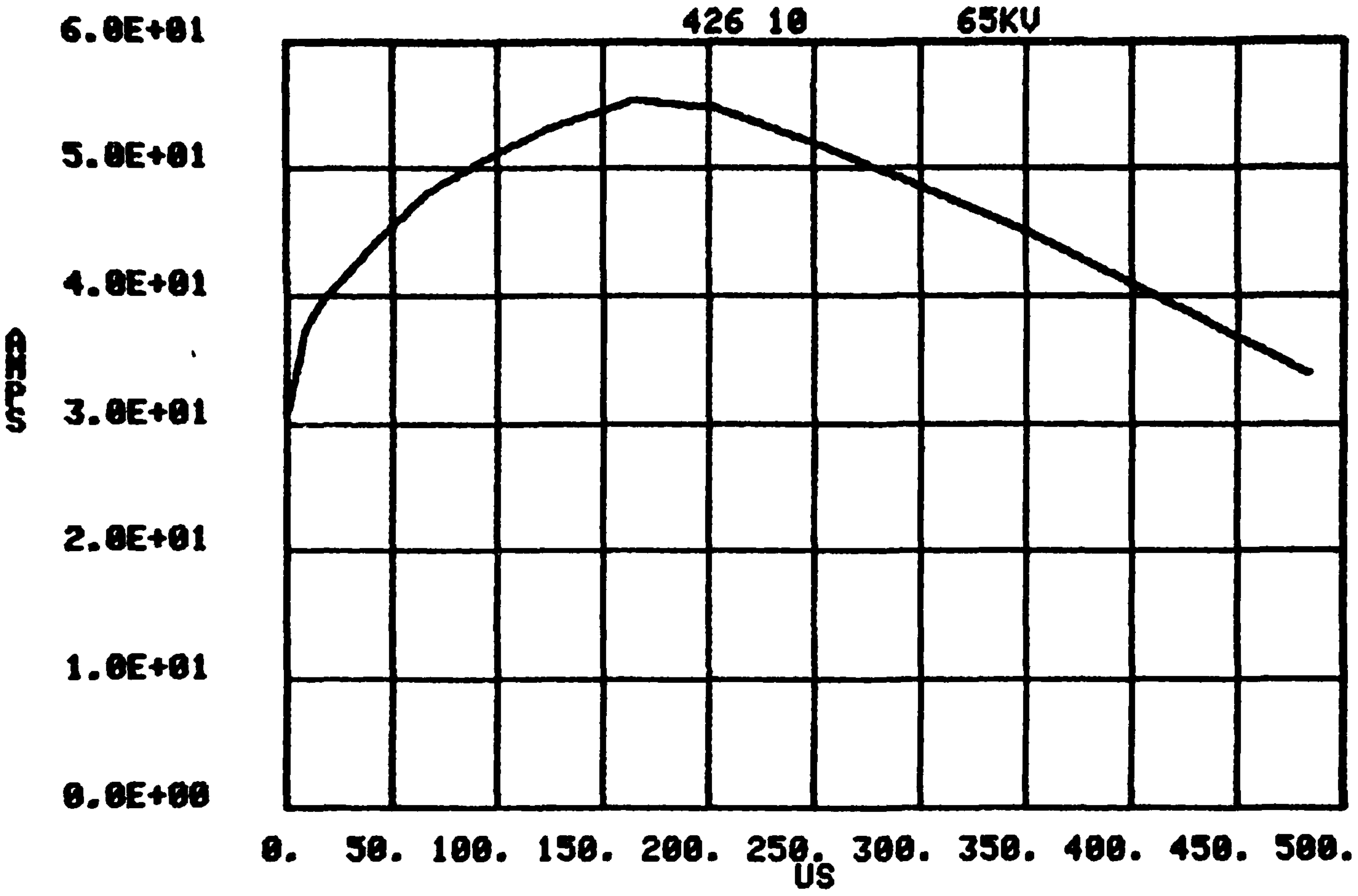

Figure B.29. 426A, .01, .5, .3, 350 sand mix; I.

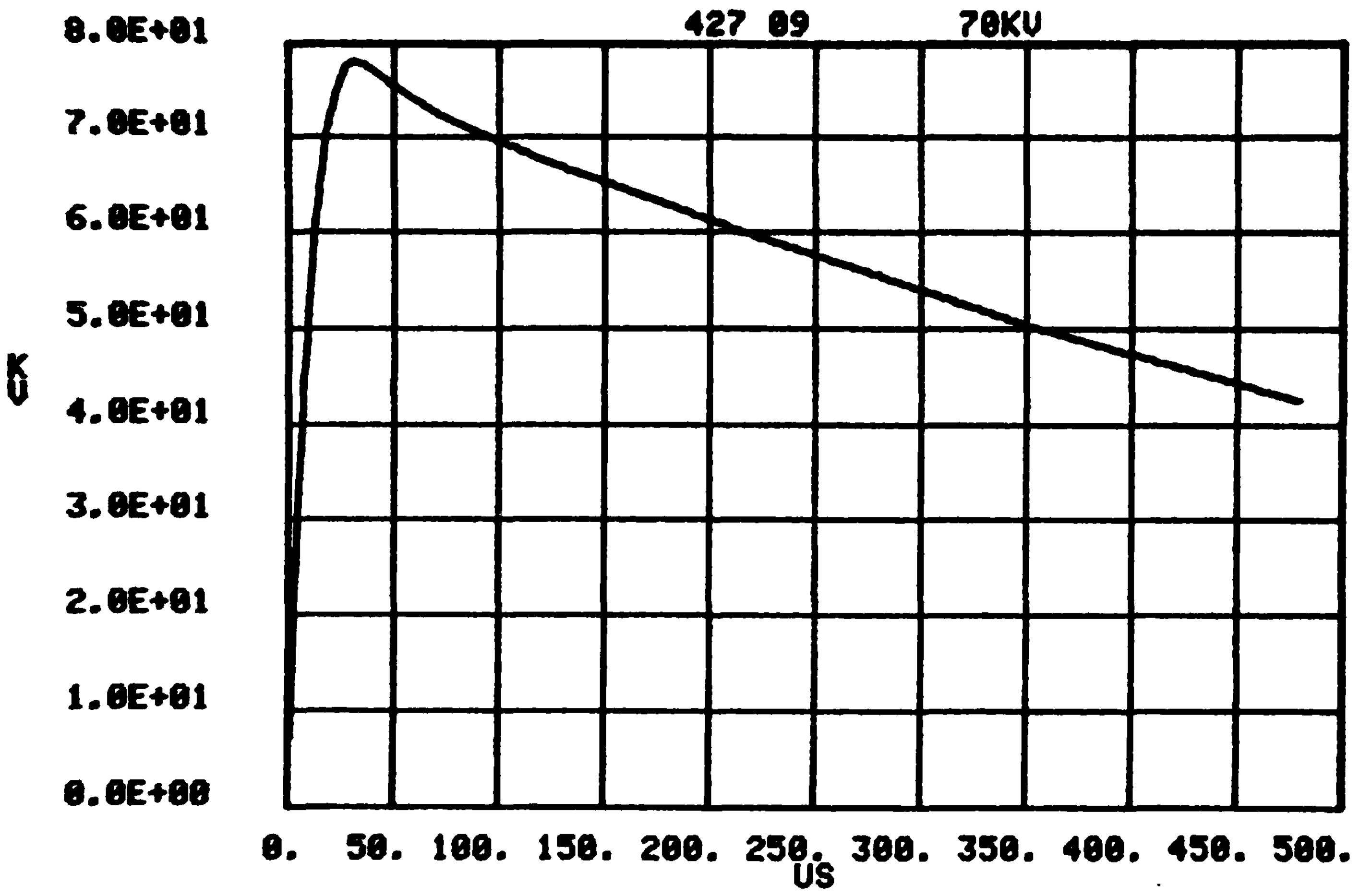

Figure B.30. 427A, .01, .5, .3, 350 sand mix; V_o.

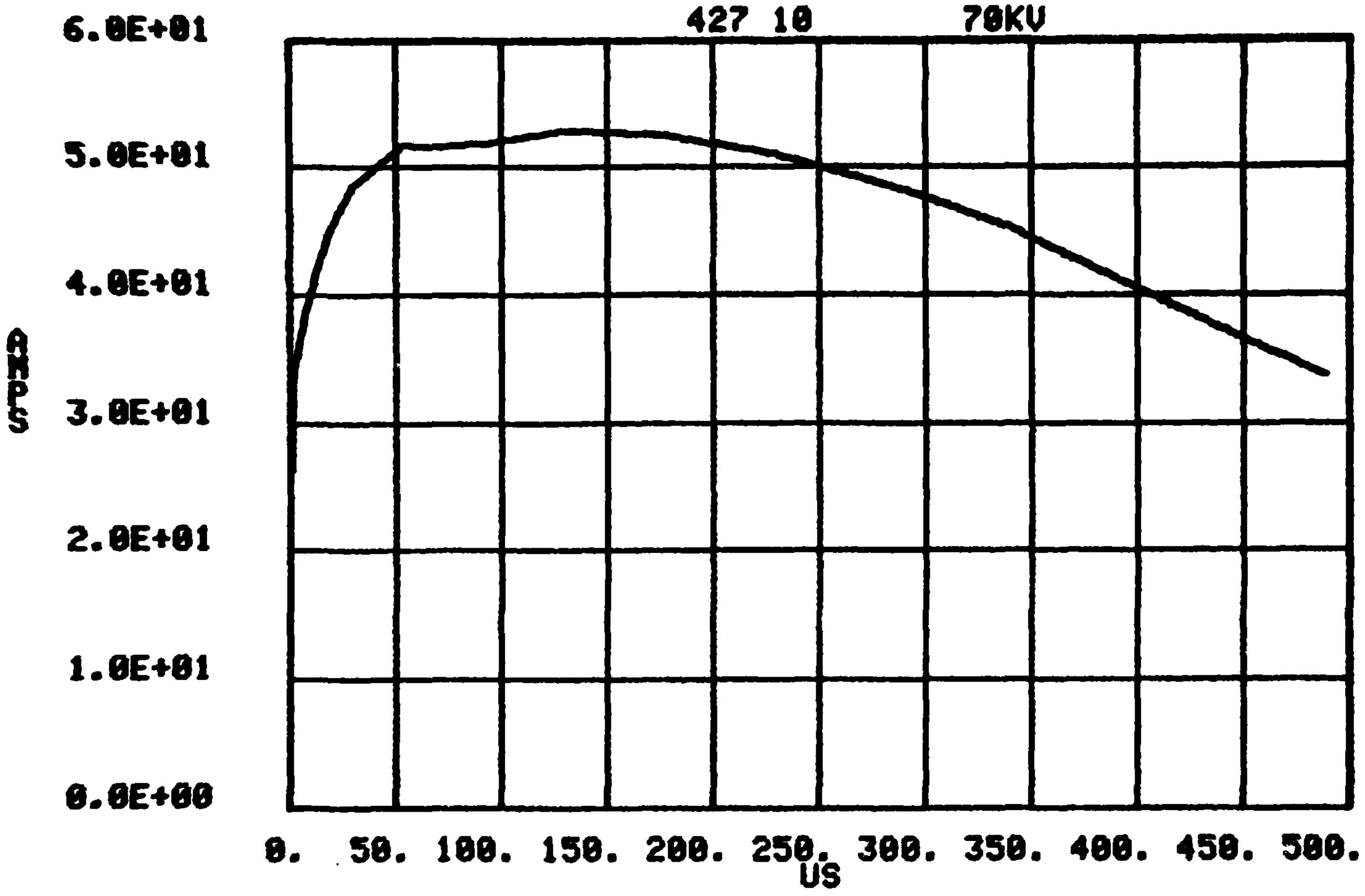

Figure B.31. 427A, .01, .5, .3, 350 sand mix; I.

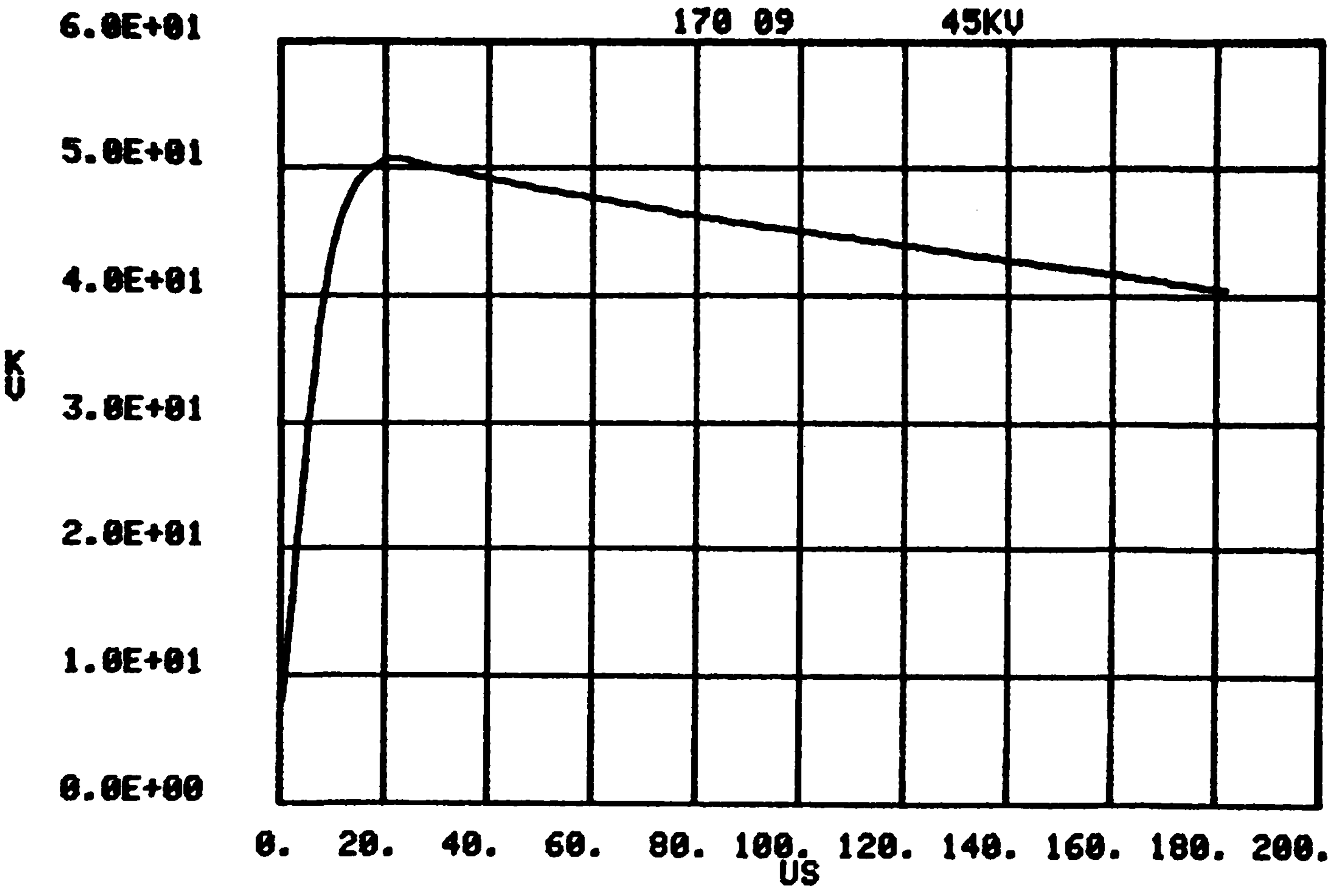

Figure B.32. 170A, .01, .5, .1, 200 sand; V_o.

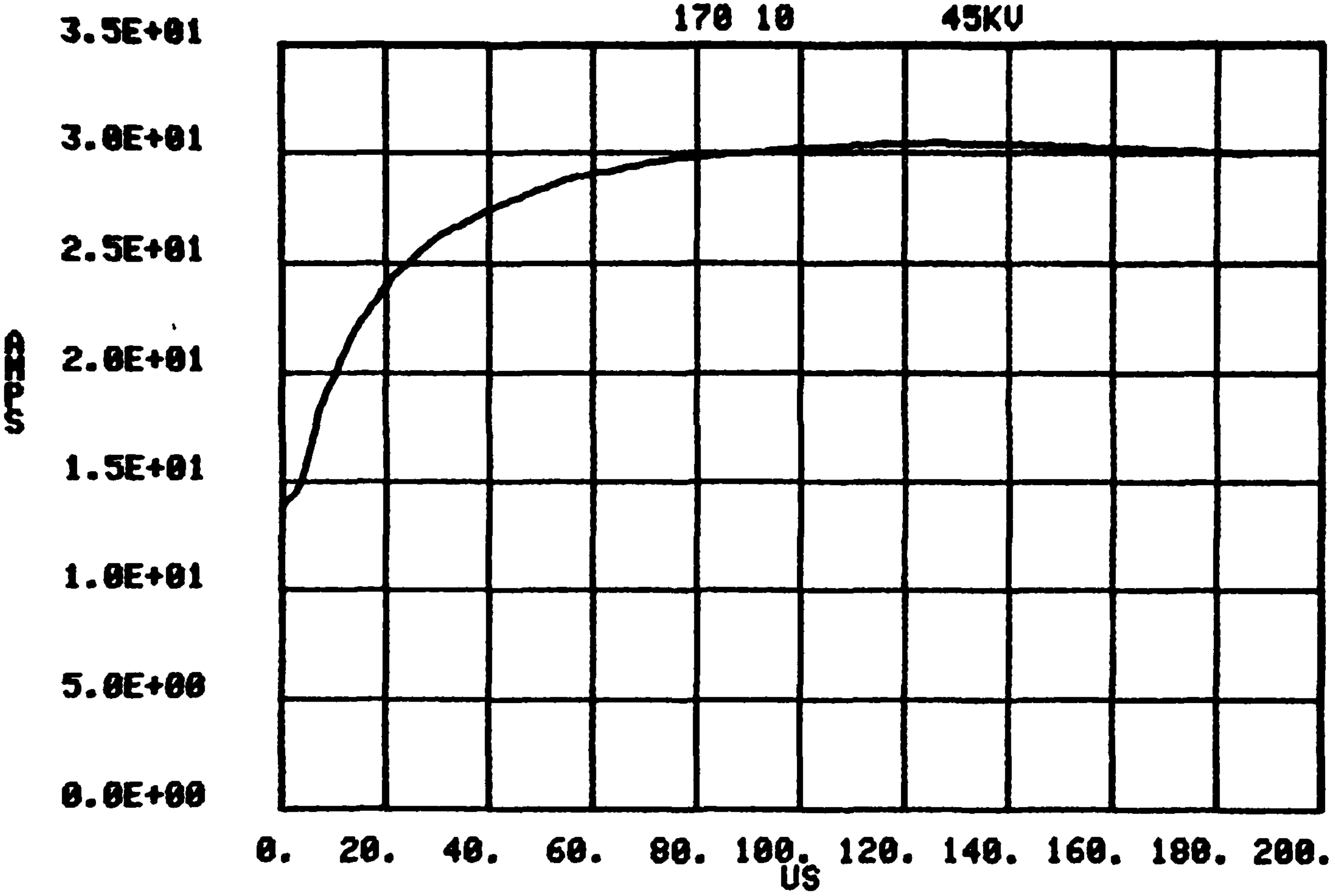

Figure B.33. 170A, .01, .5, .1, 200 sand; I.

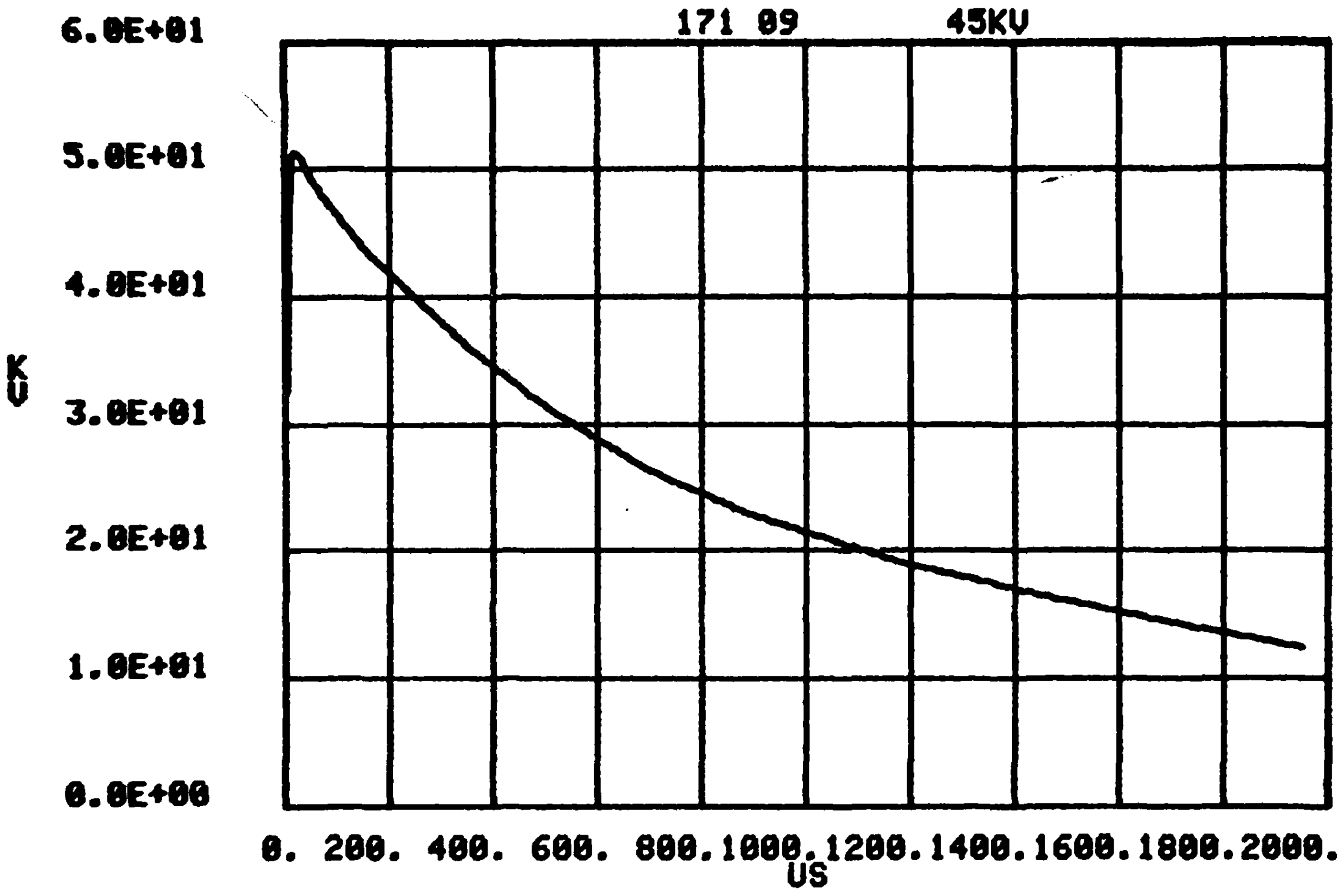

Figure B.34. 171A, .01, .5, .1, 200 sand; V_O.

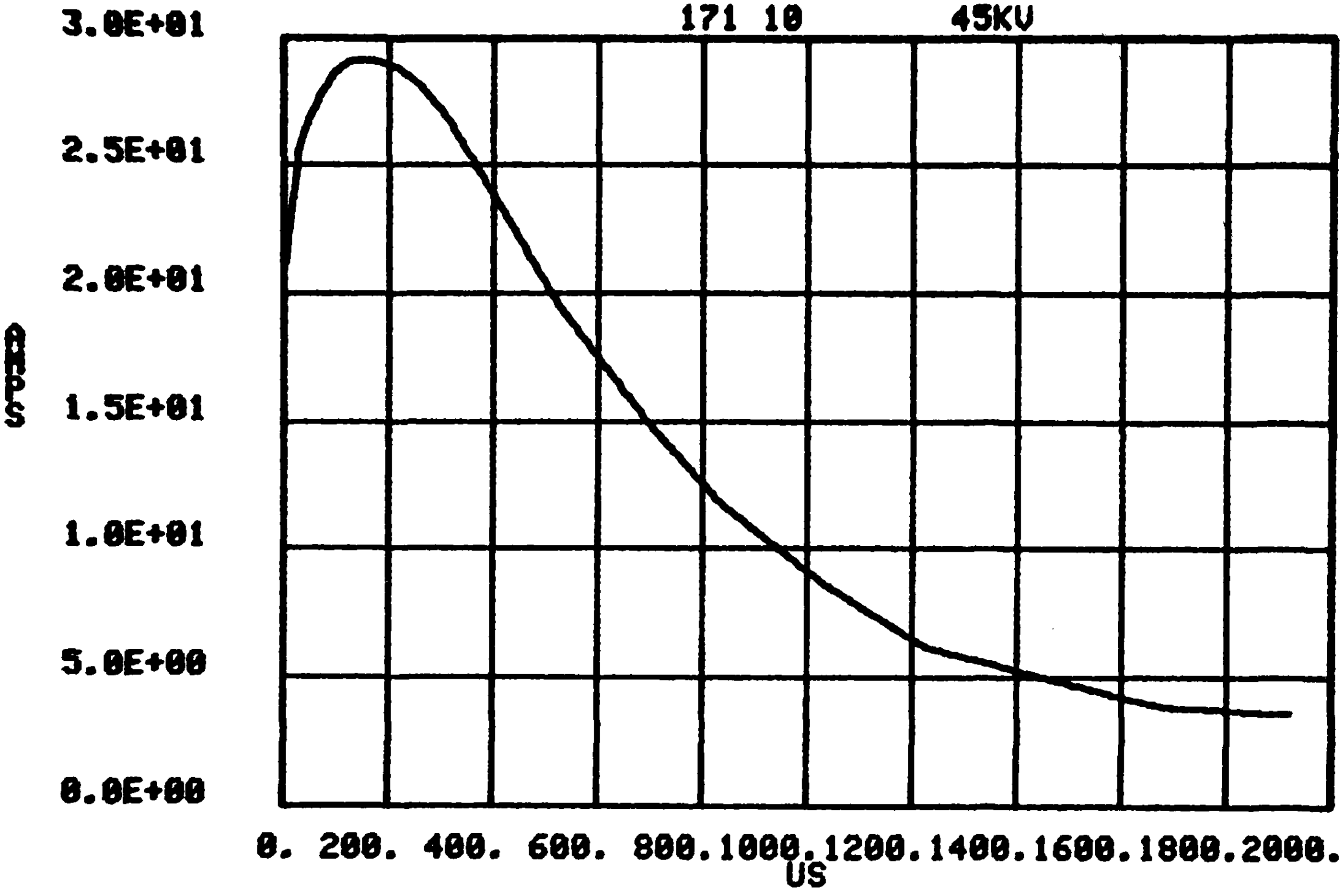

Figure B.35. 171A, .01, .5, .1, 200 sand; I.

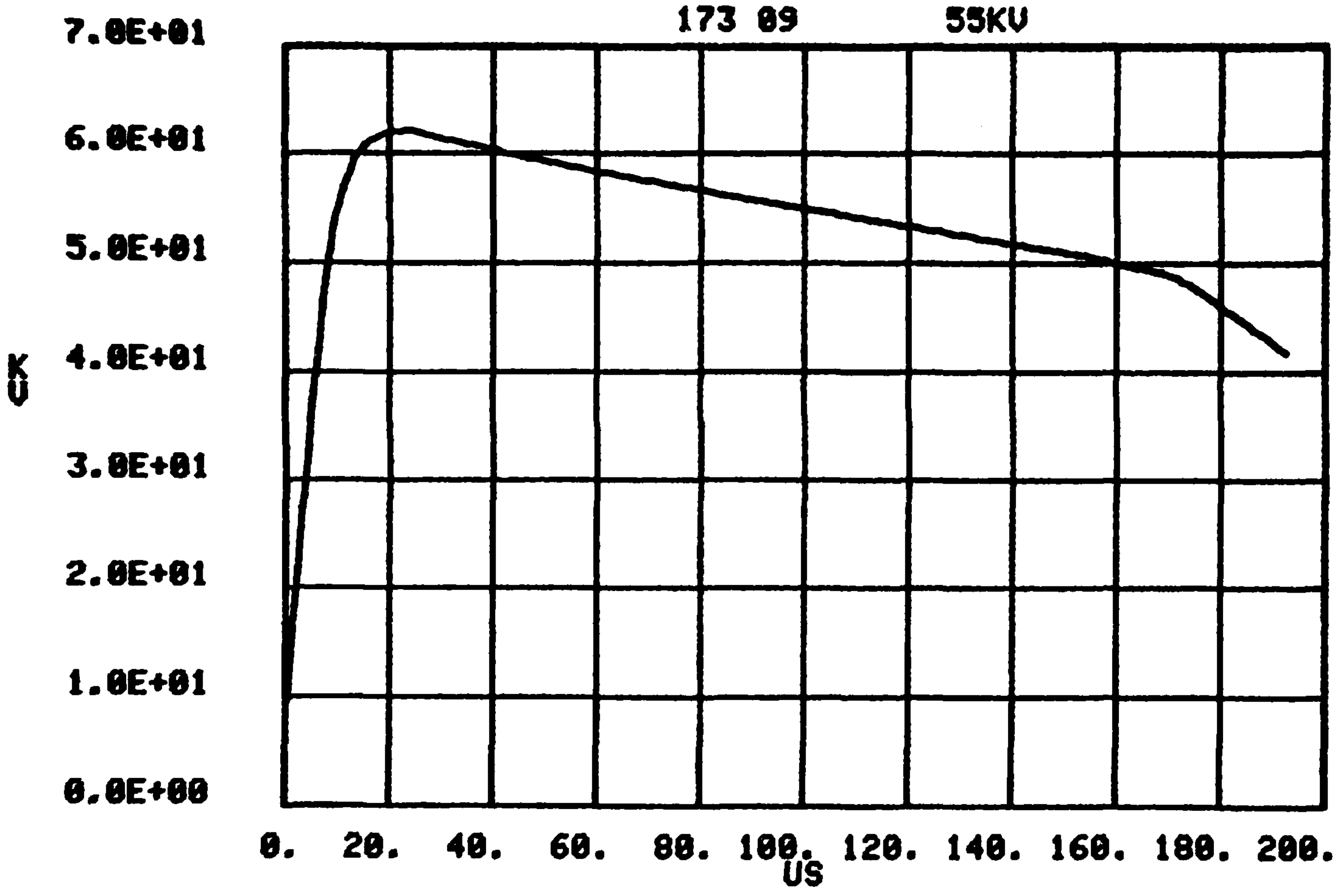

Figure B.36. 173A, .01, .5, .1, 200 sand; V_o.

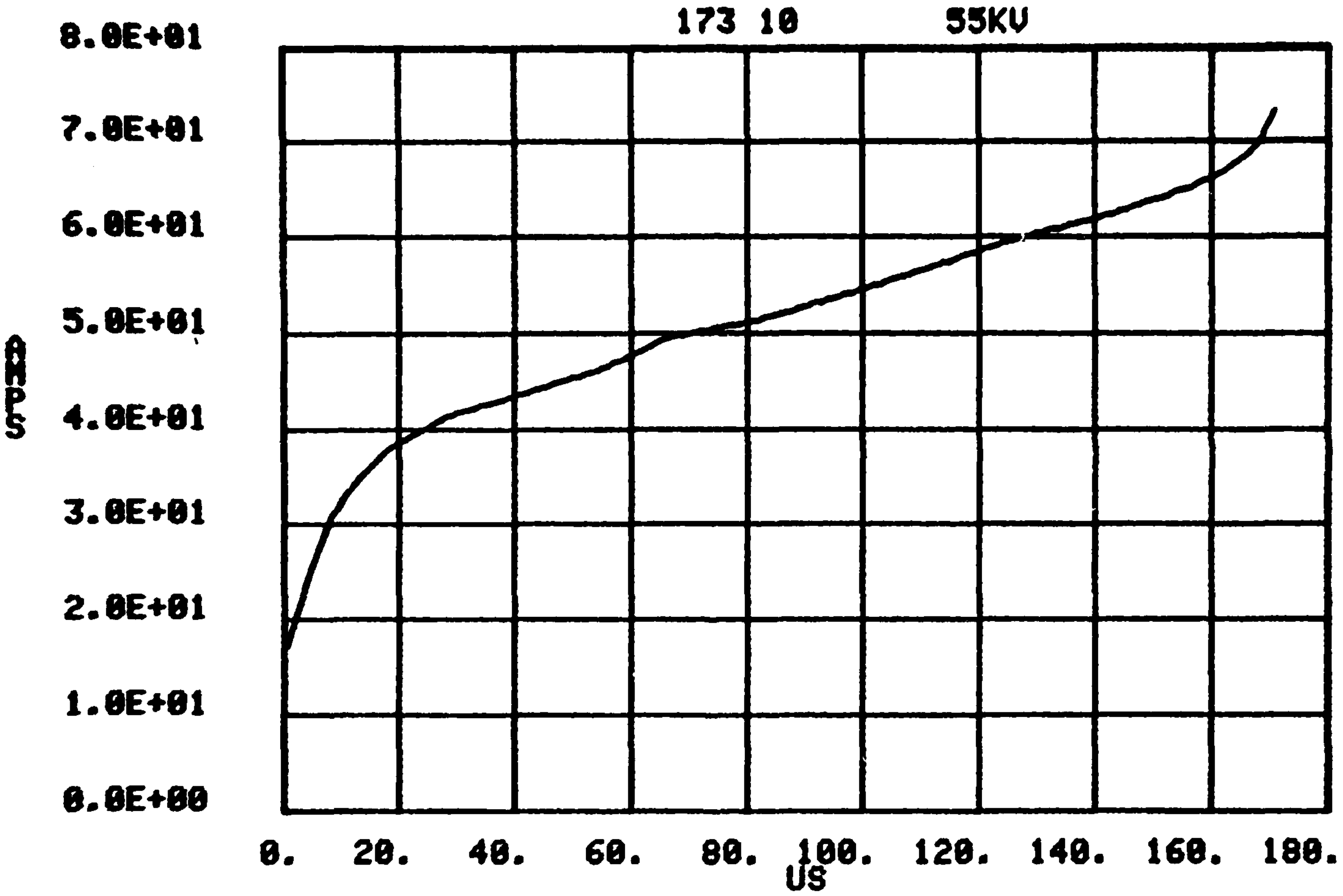

Figure B.37. 173A, .01, .5, .1, 200 sand; I.

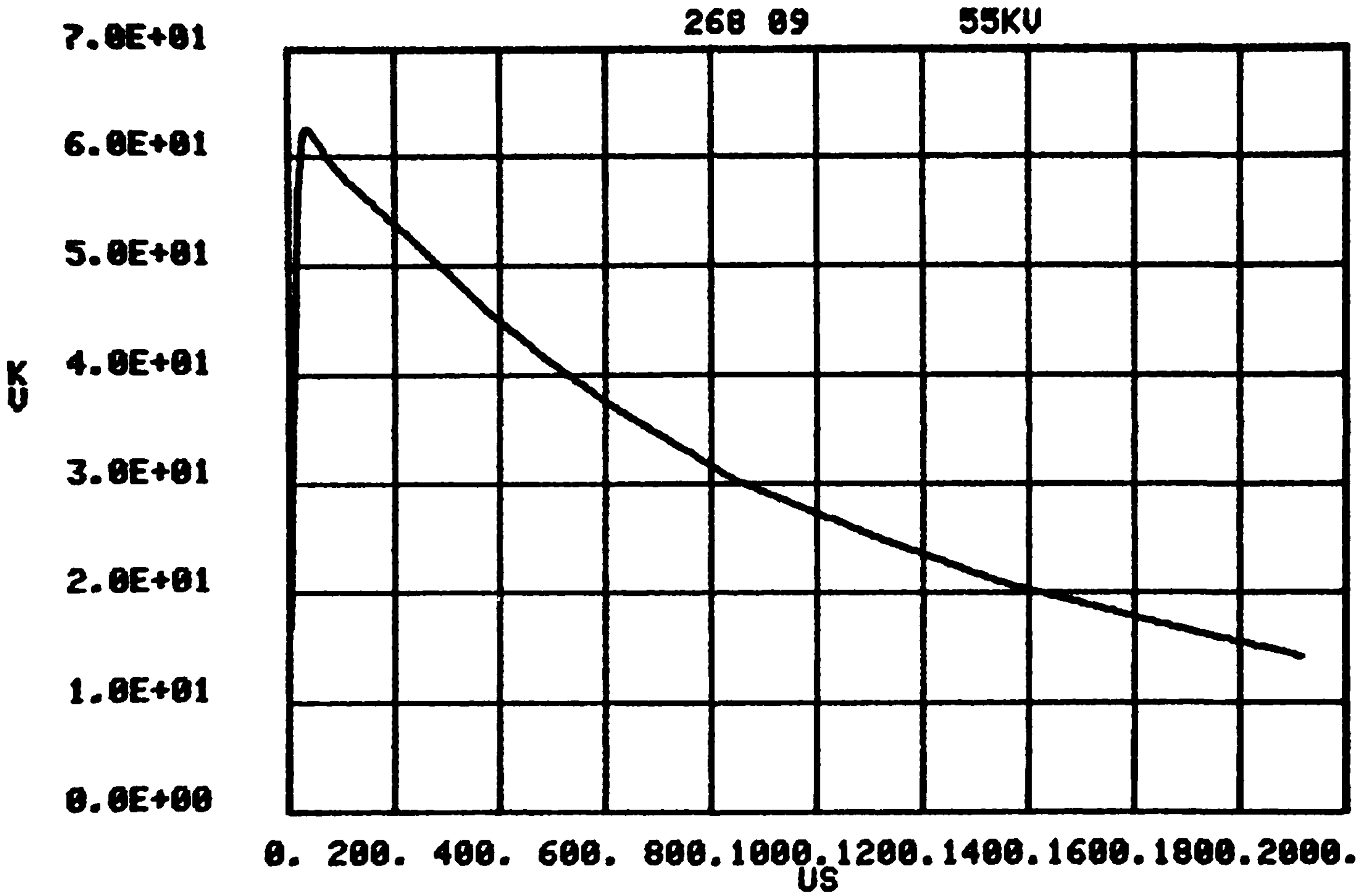

Figure B.38. 268A, .01, .5, .1, 170 Soil-B; V_o.

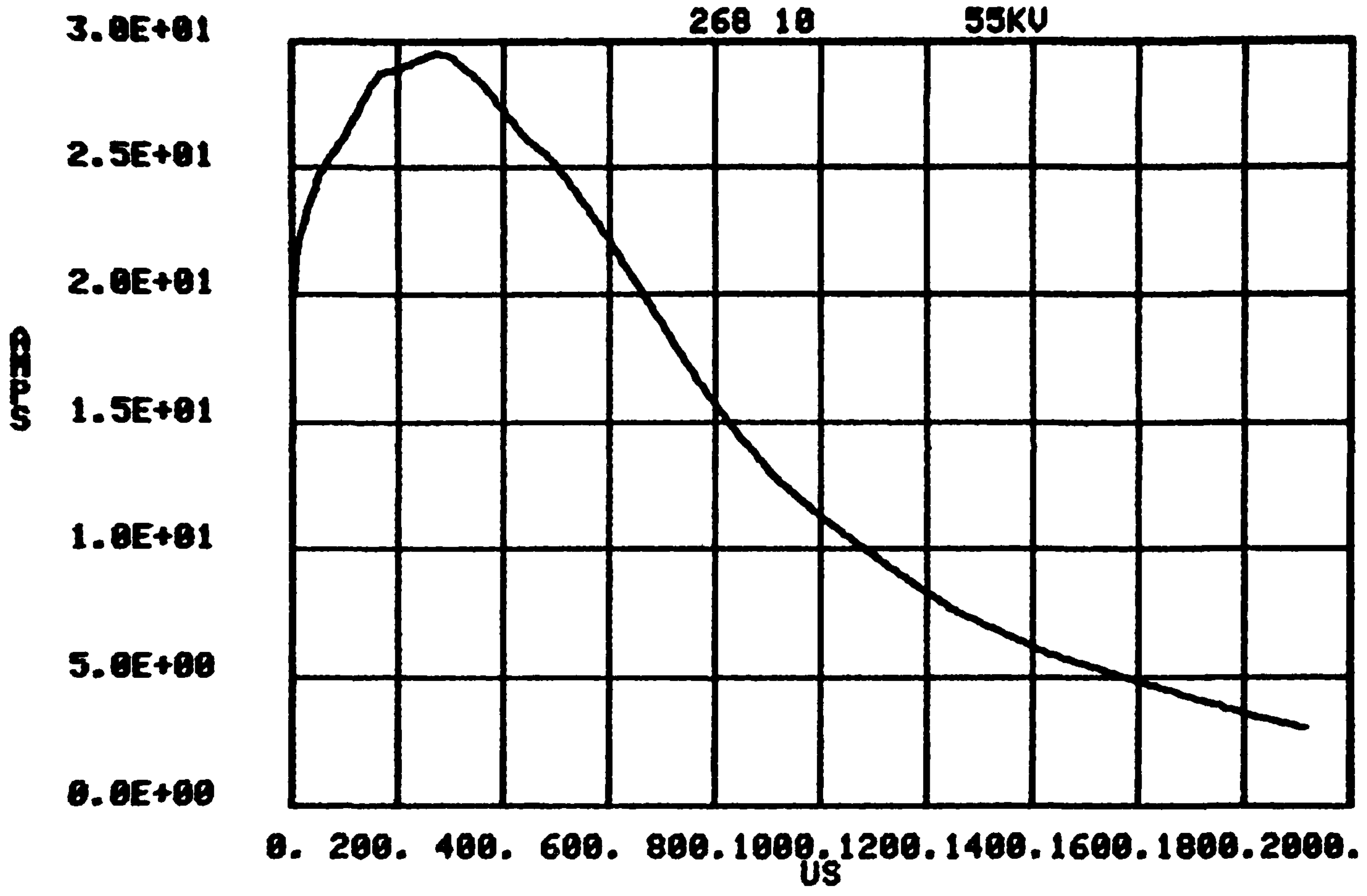

Figure B.39. 268A, .01, .5, .1, 170 Soil-B; I.

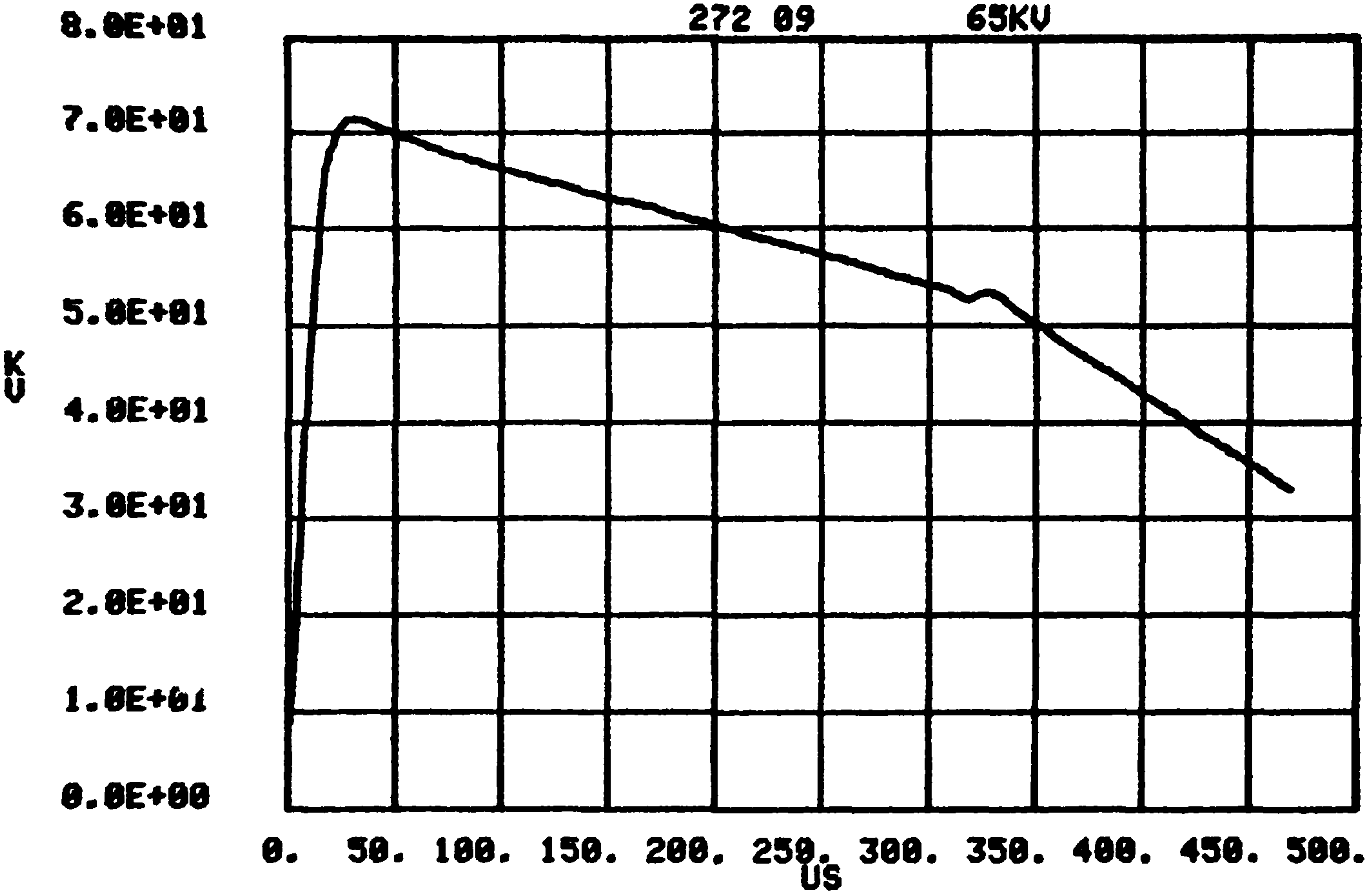

Figure B.40. 272A, .01, .5, .1, 170 Soil-B; V_o.

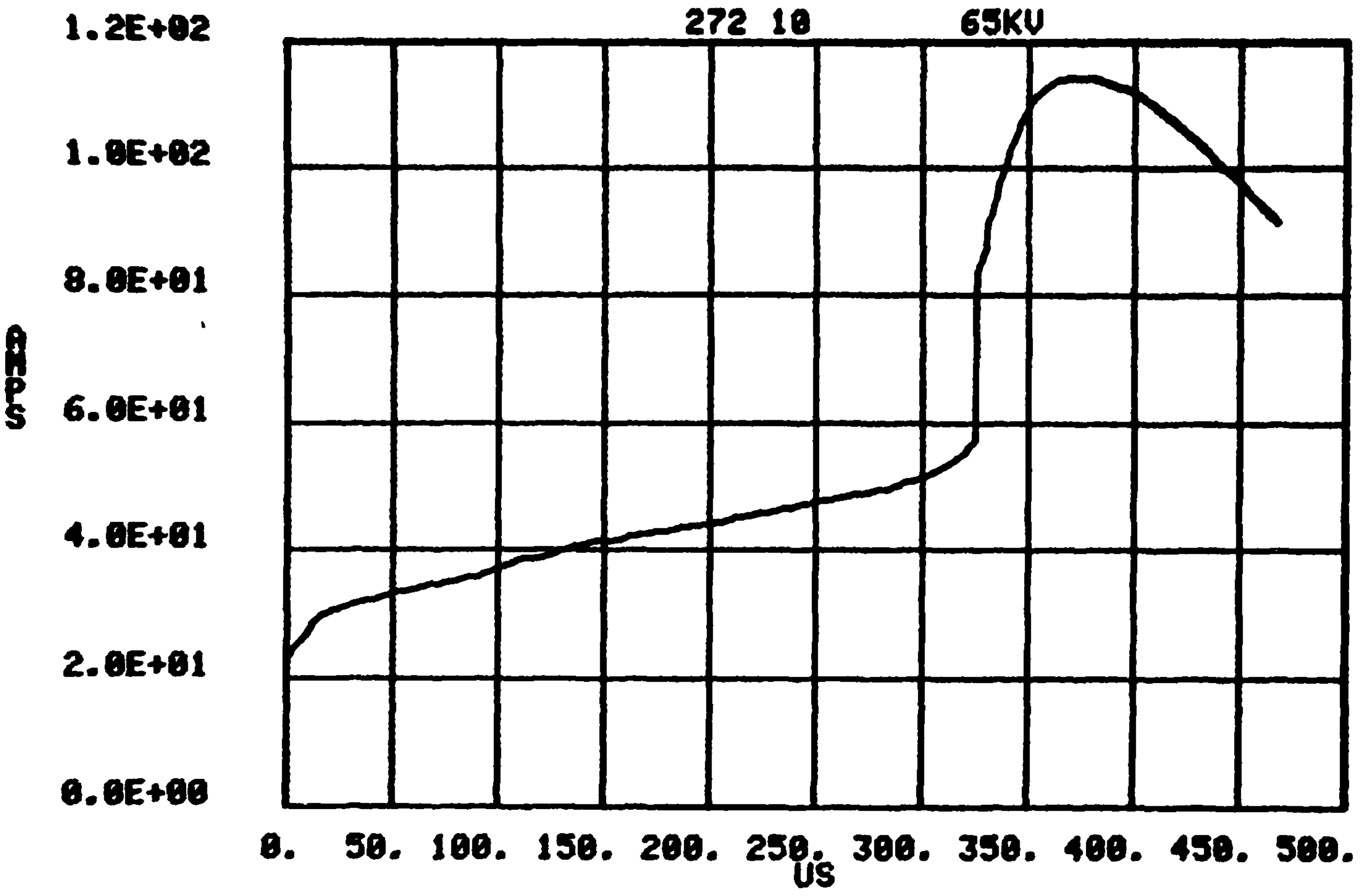

Figure B.41. 272A, .01, .5, .1, 170 Soil-B; I.

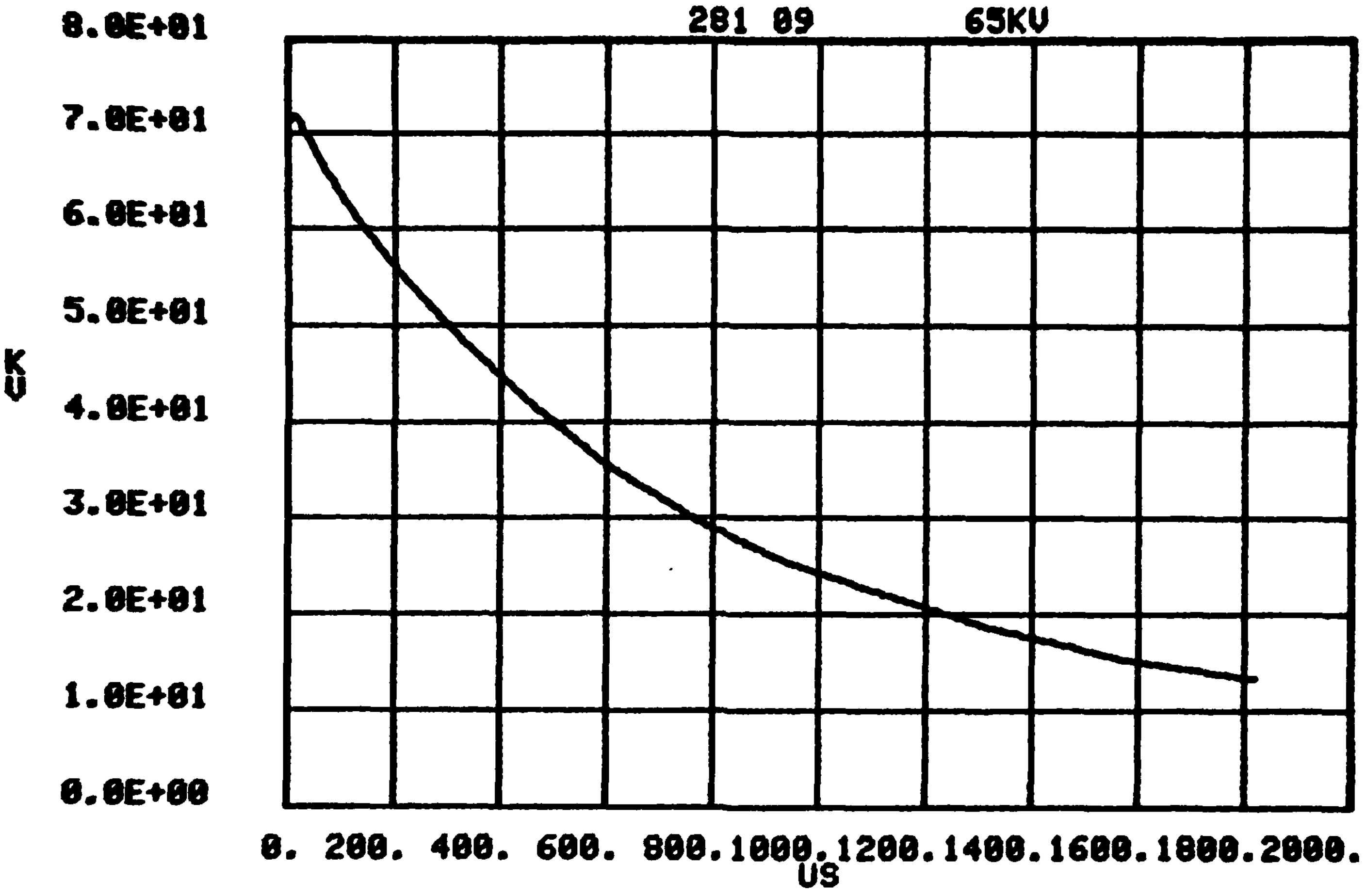

Figure B.42. 281A, .01, .5, .1, 130 Soil-B; V_o.

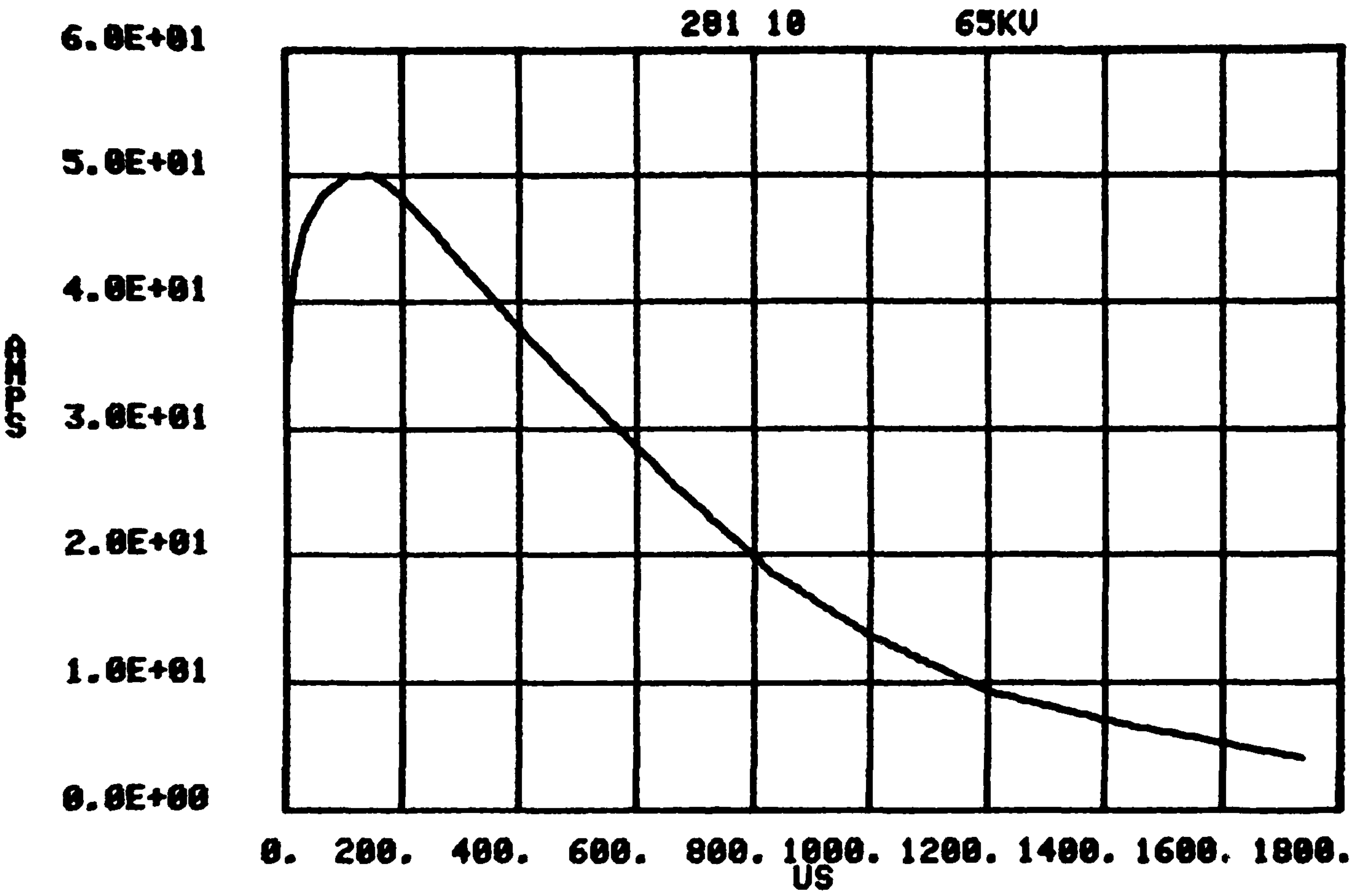

Figure B.43. 281A, .01, .5, .1, 130 Soil-B; I.

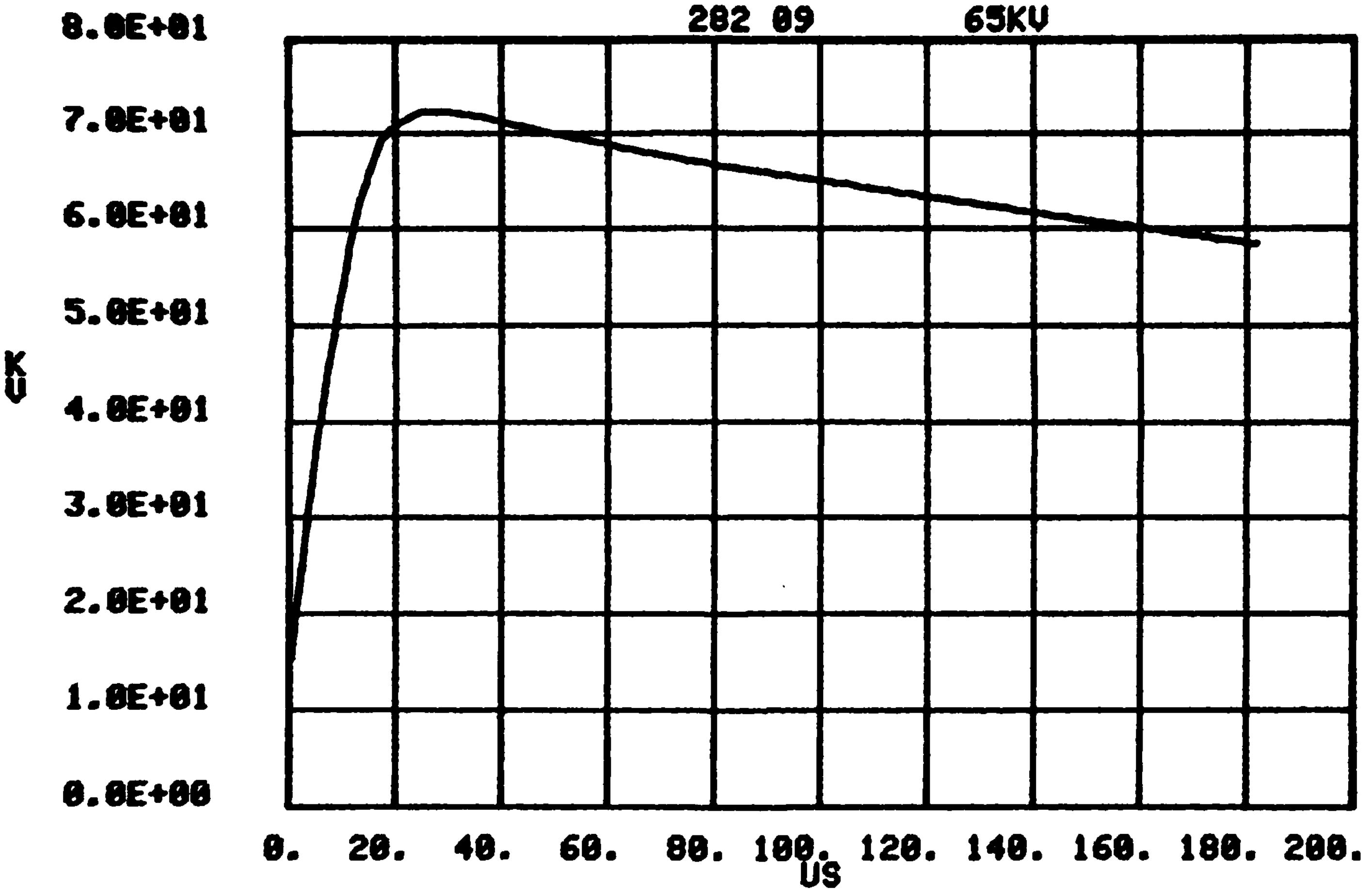

Figure B.44. 282A, .01, .5, .1, 130 Soil-B; V_o.

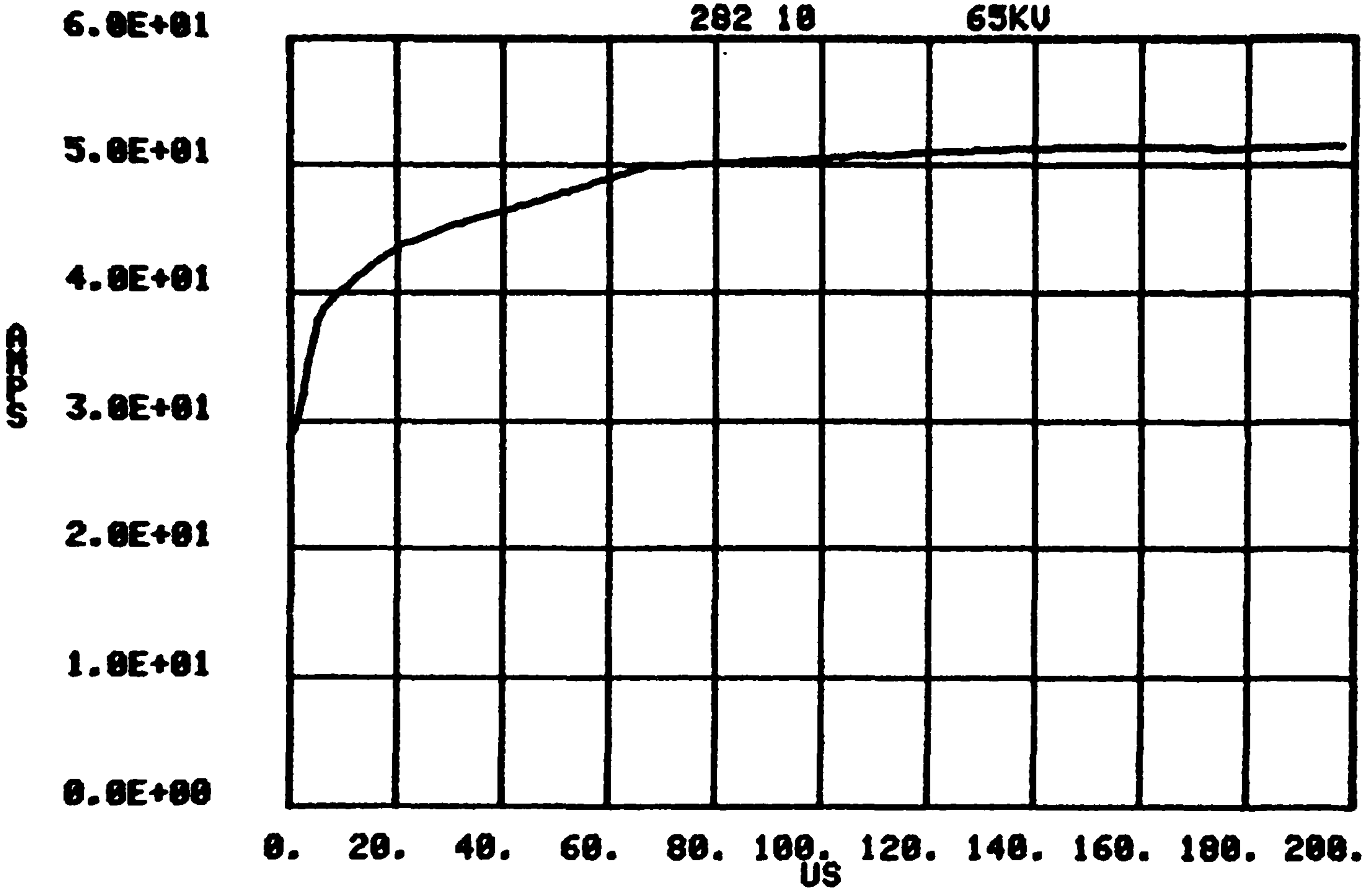

Figure B.45. 282A, .01, .5, .1, 130 Soil-B; I.

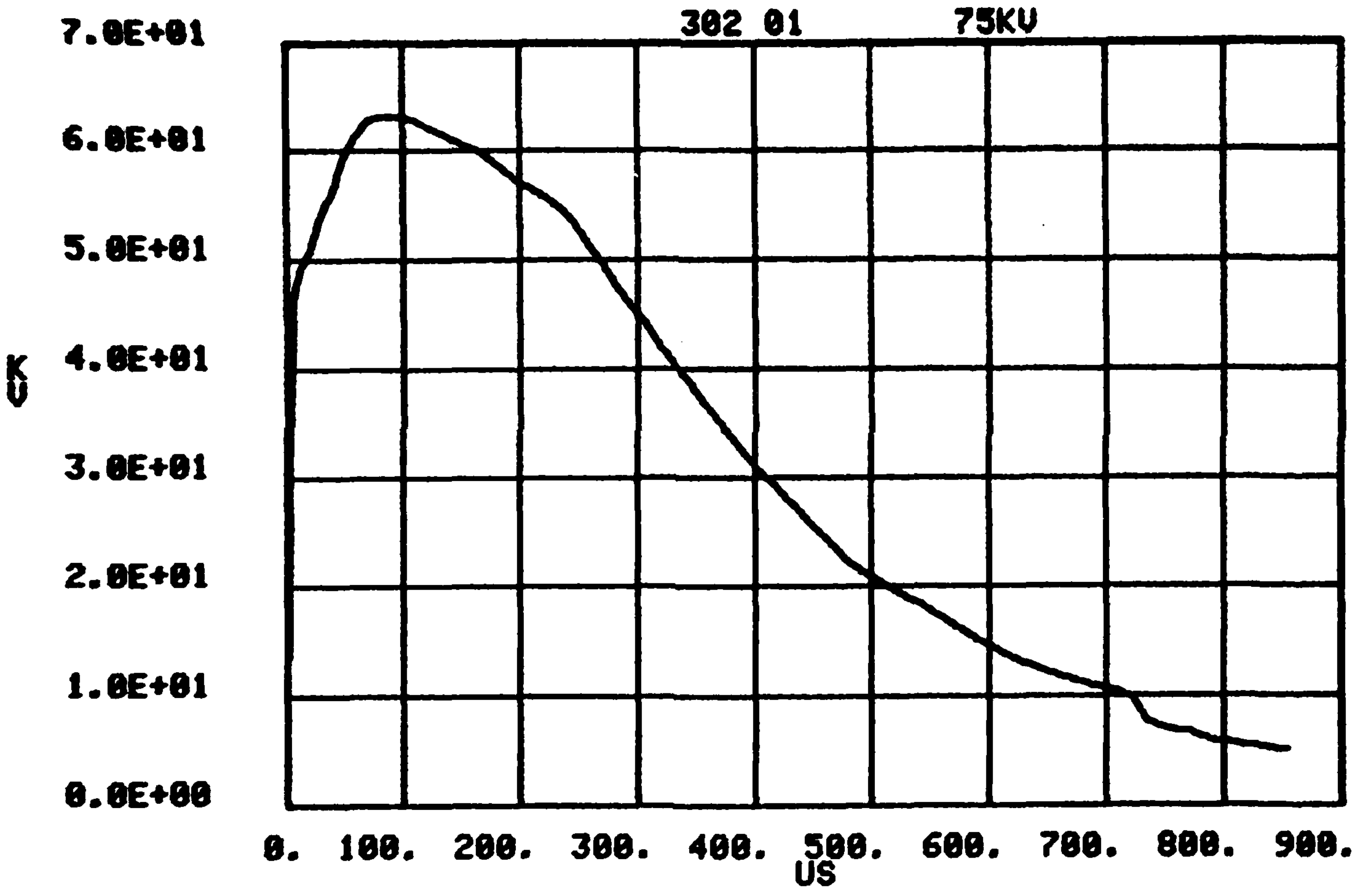

Figure B.46. 302A, .01, .5, .1, 130 Soil-B; V at azimuthal position 1.

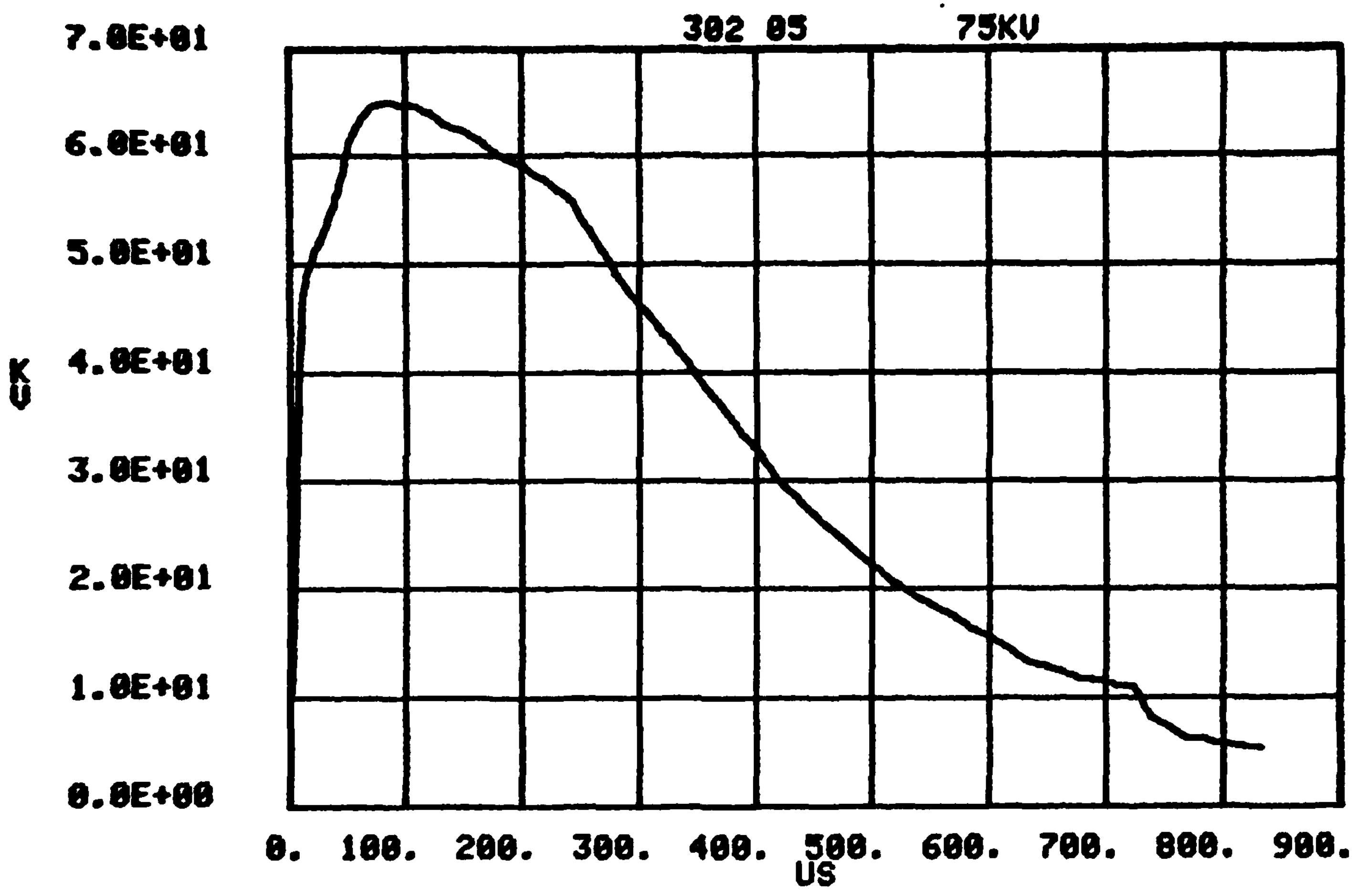

Figure B.47. 302A, .01, .5, .1, 130 Soil-B; V at azimuthal position 2.

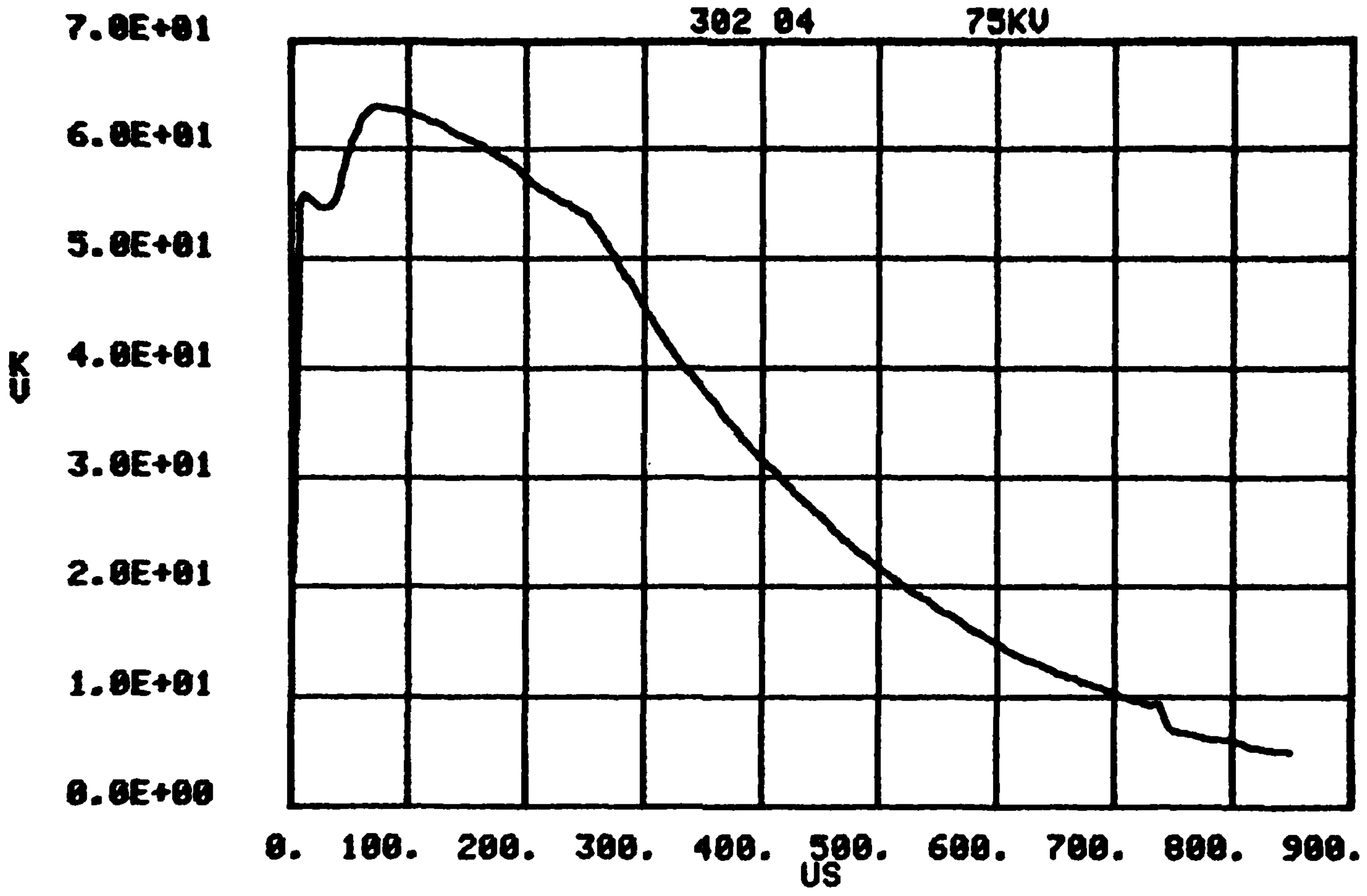

Figure B.48. 302A, .01, .5, .1, 130 Soil-B; V at azimuthal position 3.

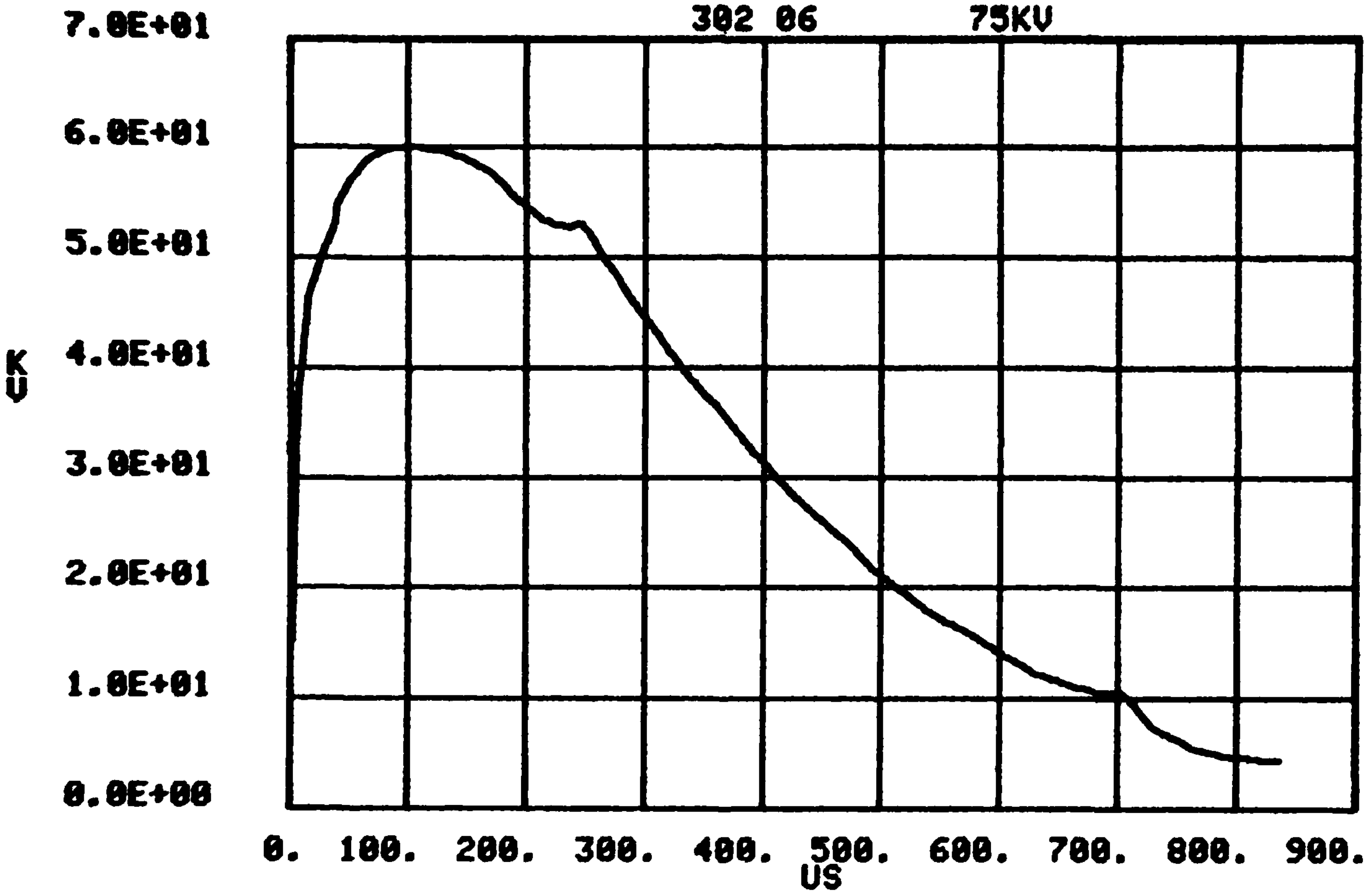

Figure B.49. 302A, .01, .5, .1, 130 Soil-B; V at azimuthal position 4.

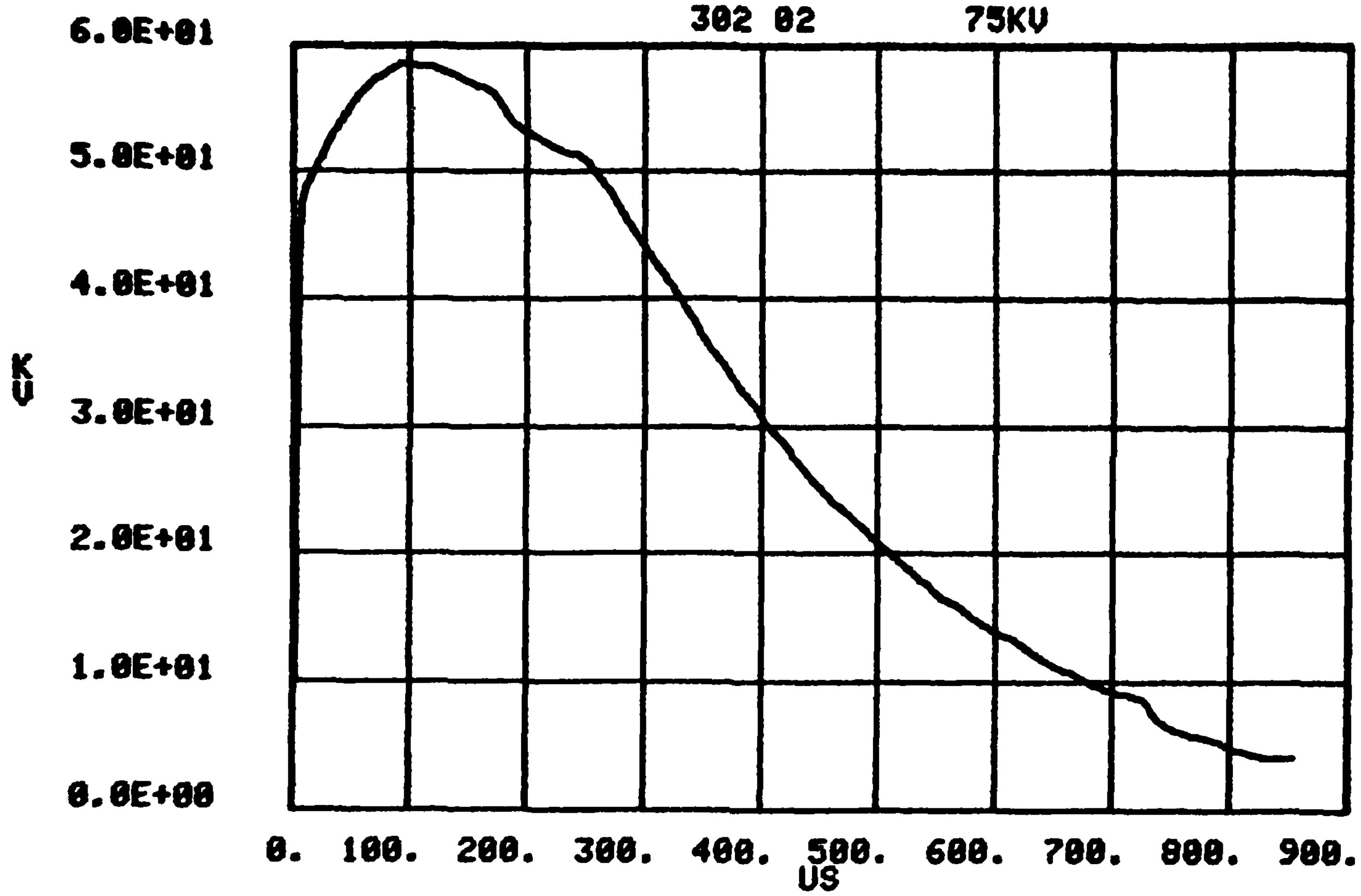

Figure B.50. 302A, .01, .5, .1, 130 Soil-B; V at azimuthal position 5.

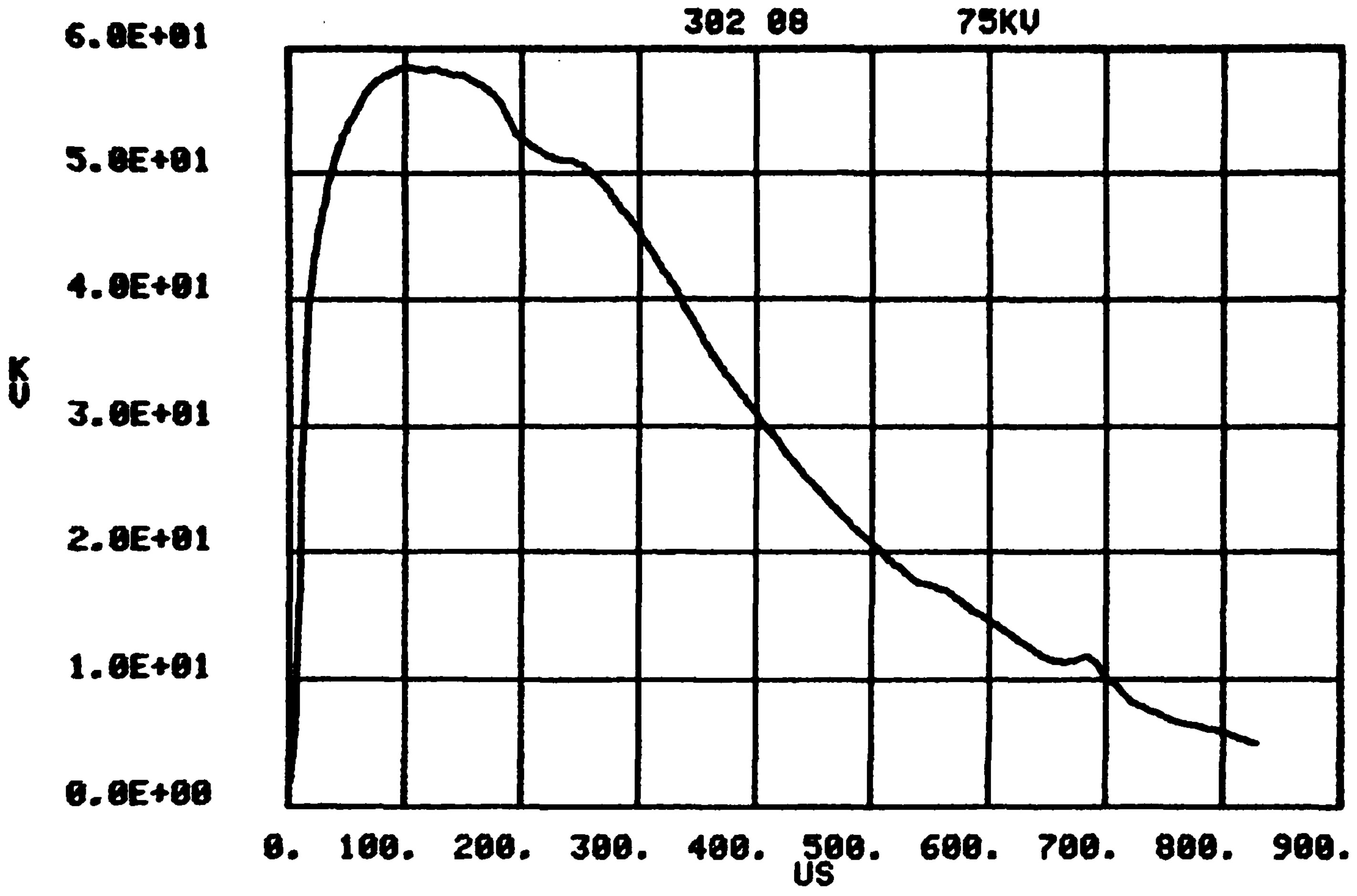

Figure B.51. 302A, .01, .5, .1, 130 Soil-B; V at azimuthal position 6.

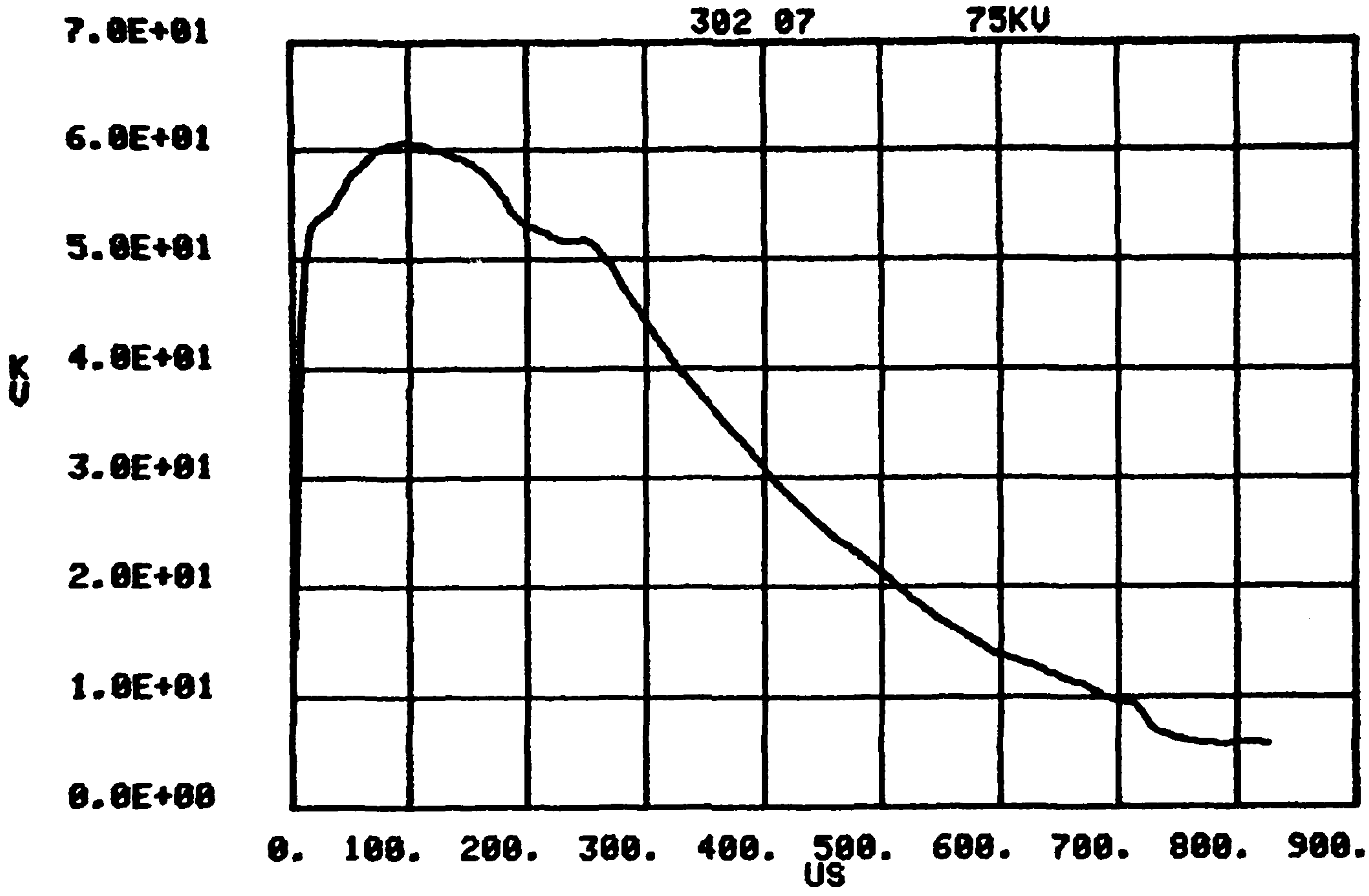

Figure B.52. 302A, .01, .5, .1, 130 Soil-B; V at azimuthal position 7.

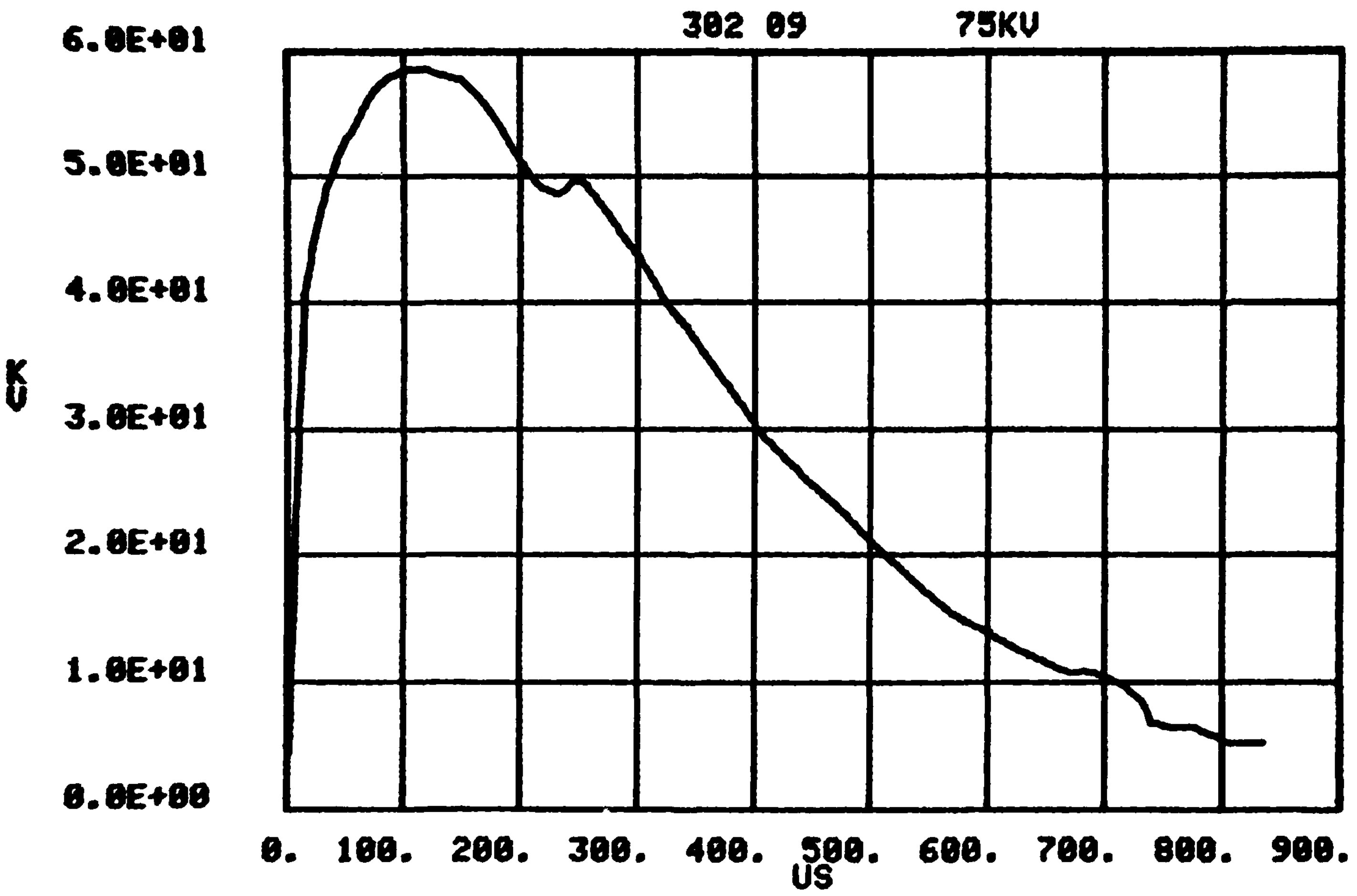

Figure B.53. 302A, .01, .5, .1, 130 Soil-B; V at azimuthal position 8.

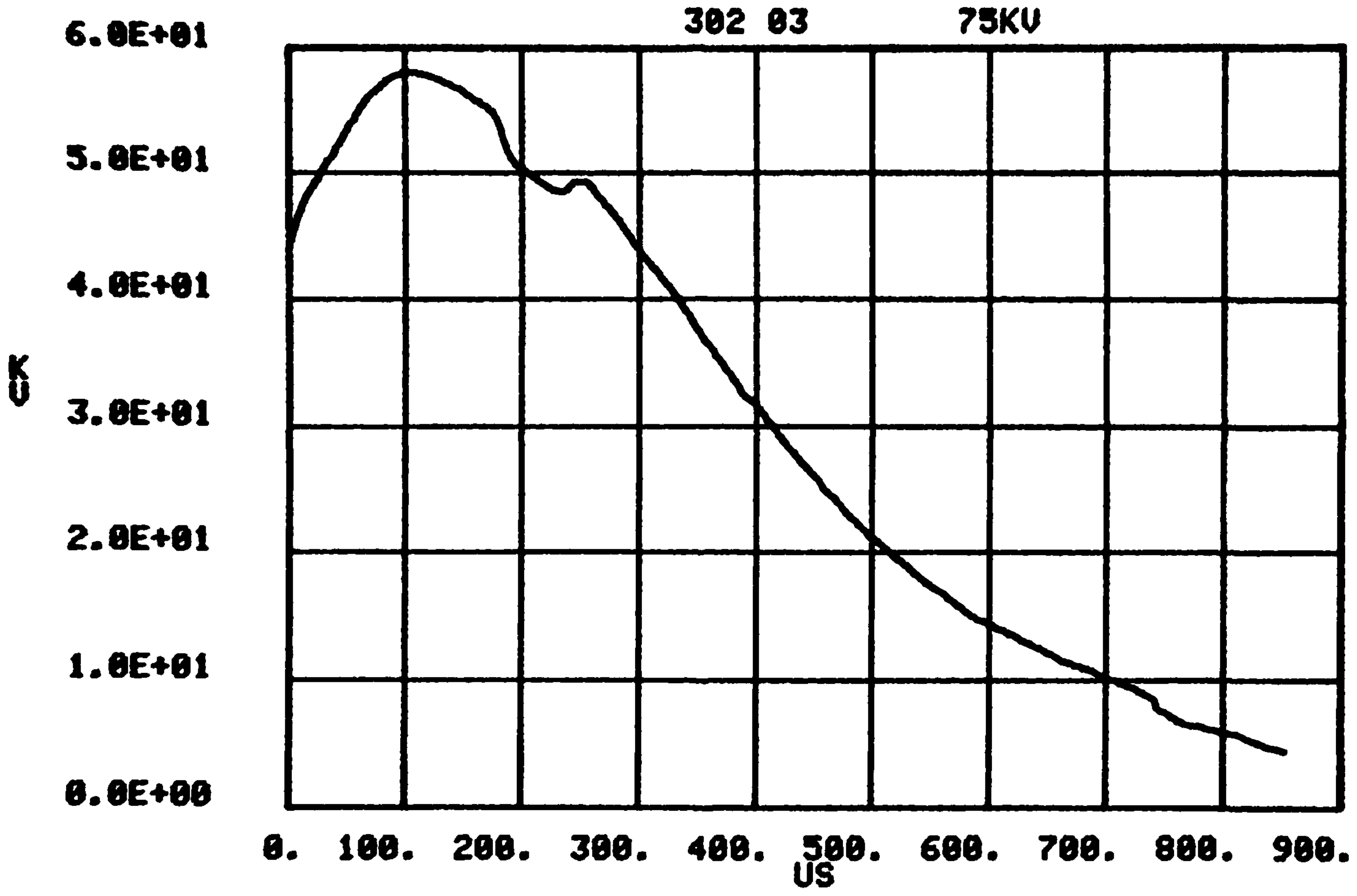

Figure B.54. 302A, .01, .5, .1, 130 Soil-B; V at azimuthal position 9.

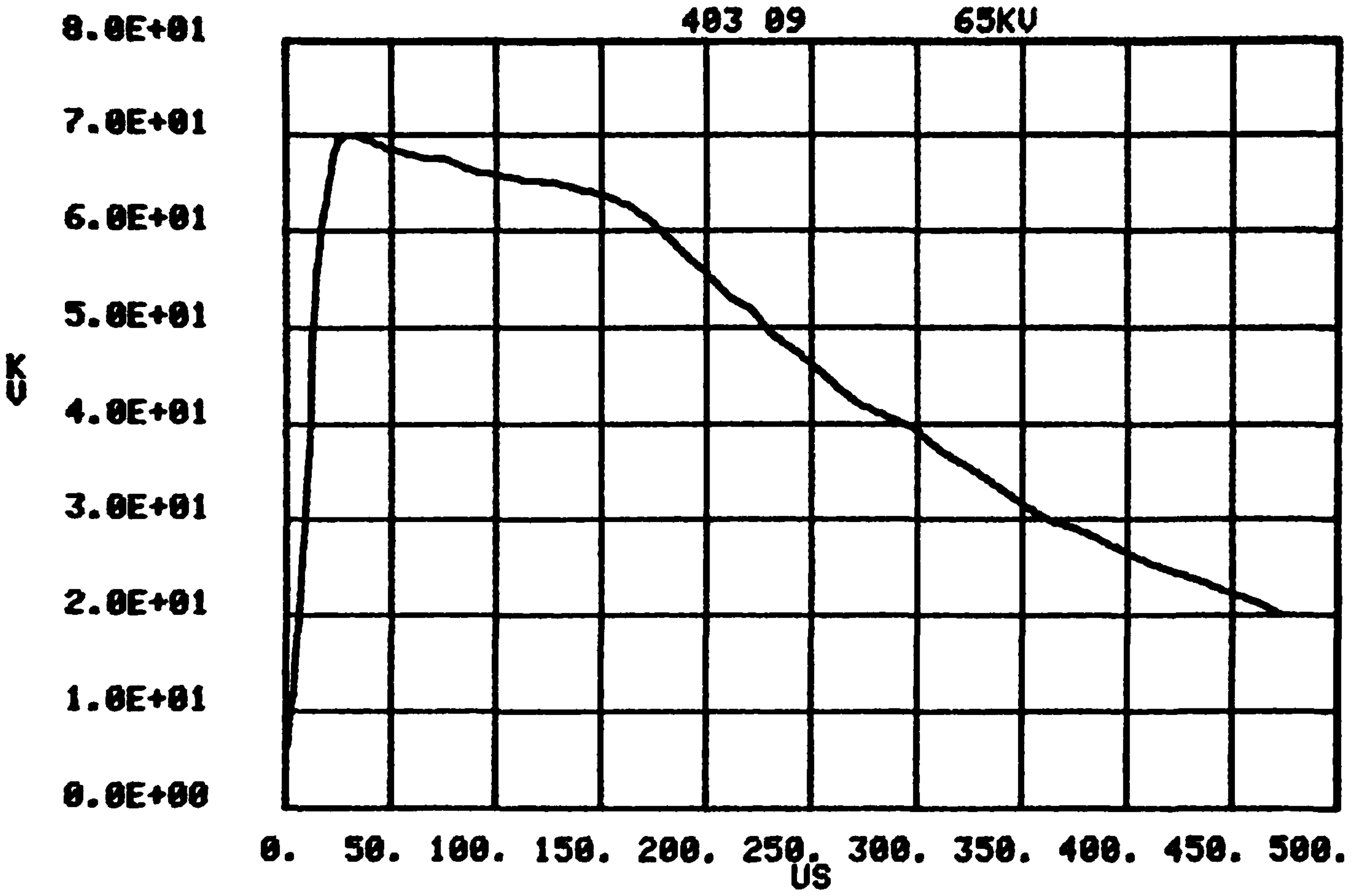

Figure B.55. 403A, .01, .5, .1, 350 sand-mix; V_o.

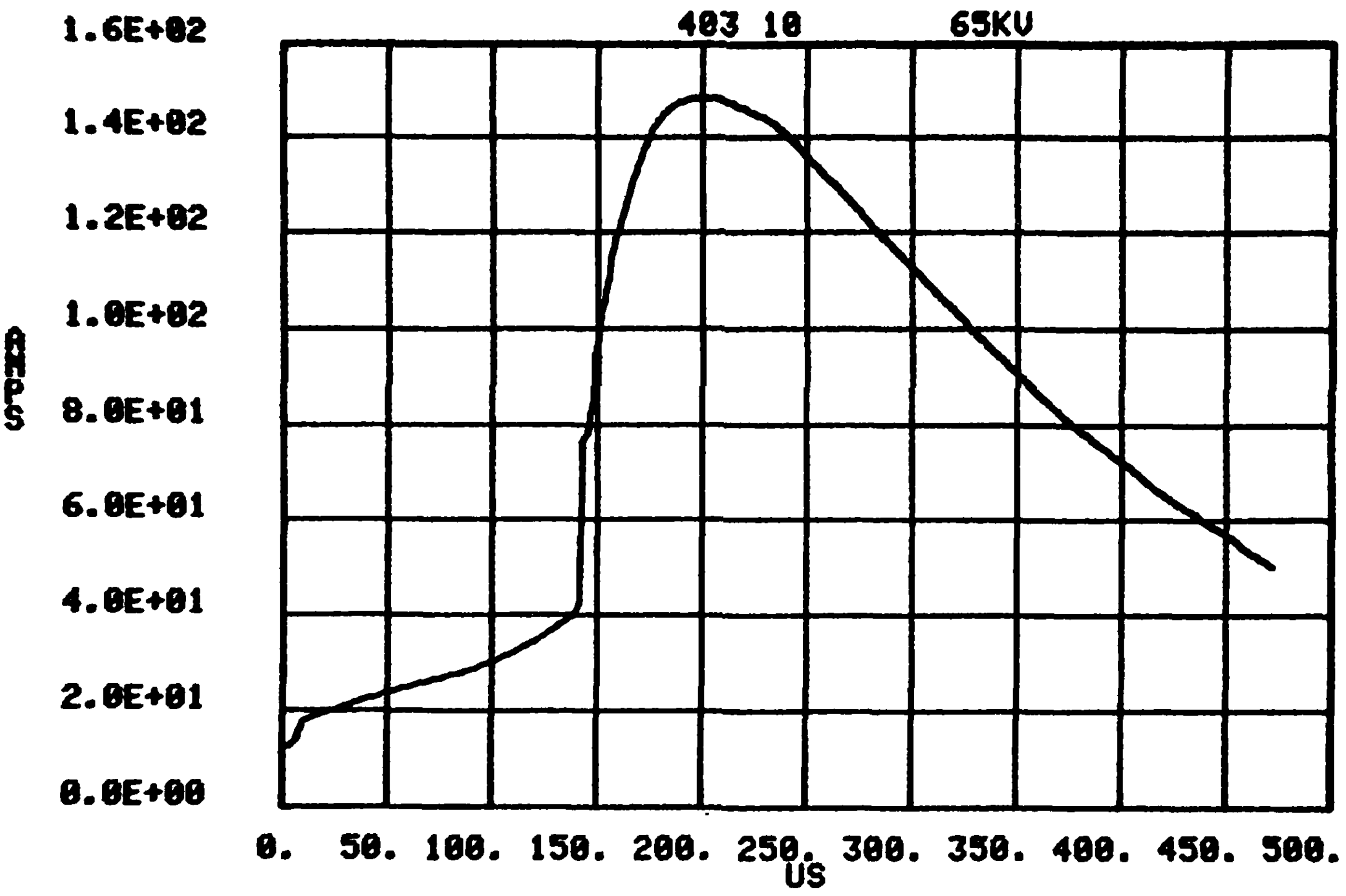

Figure B.56. 403A, .01, .5, .1, 350 sand-mix; I.

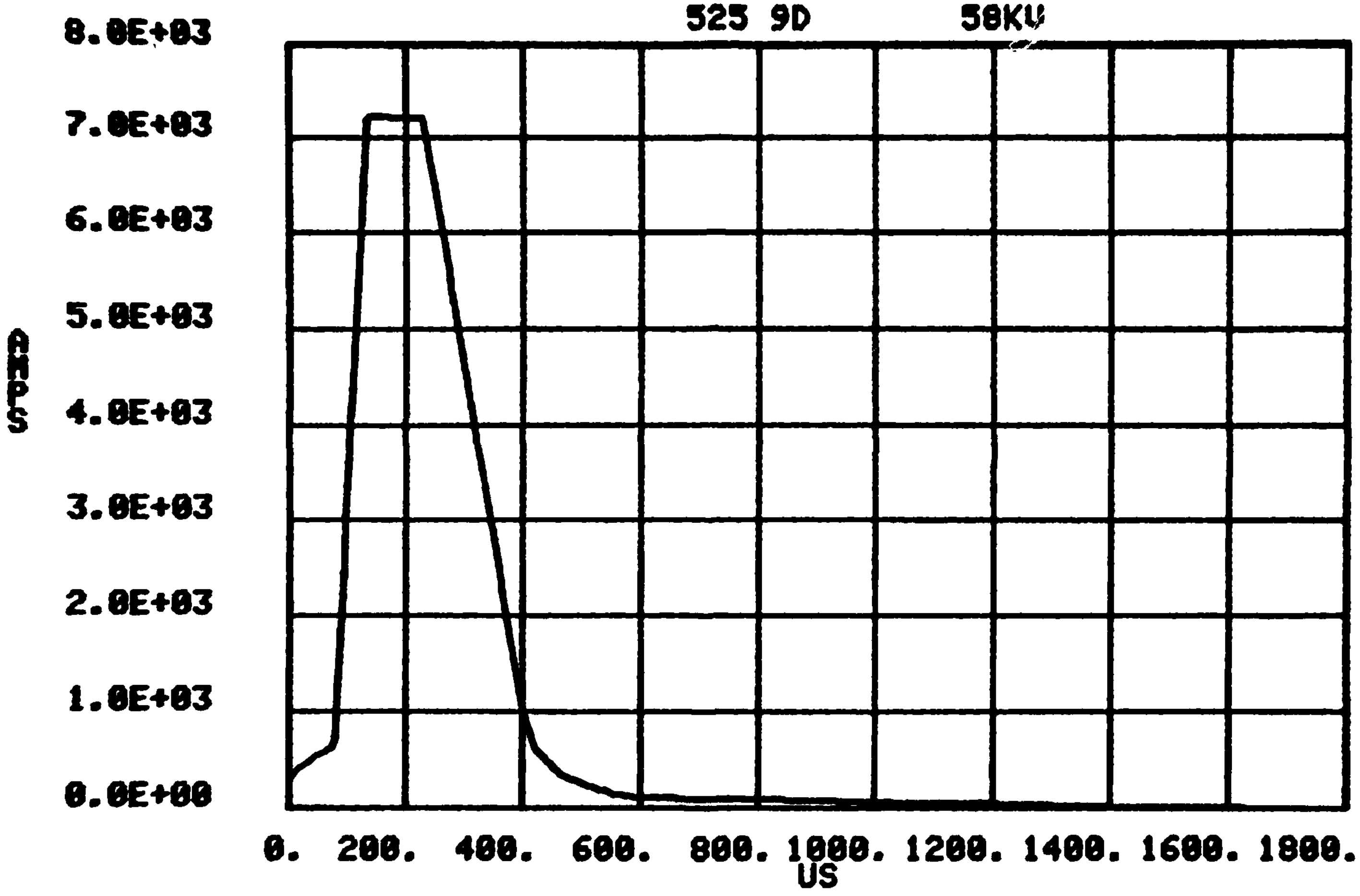

Figure B.57. 525B, .01, 1.0, 1.0, 300 sand-mix; I.

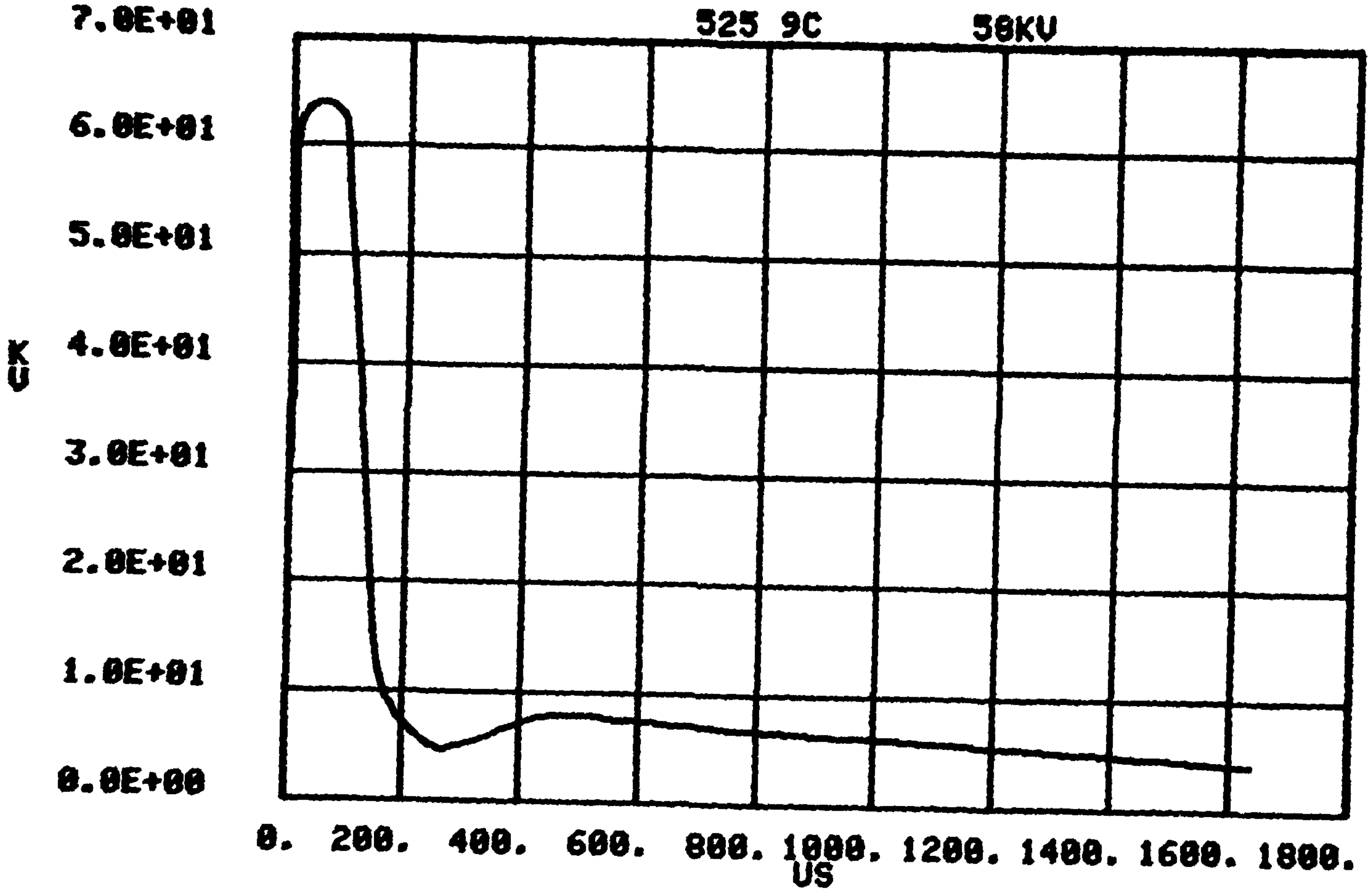

Figure B.58. 525B, .01, 1.0, 1.0, 300 sand-mix; V_o.

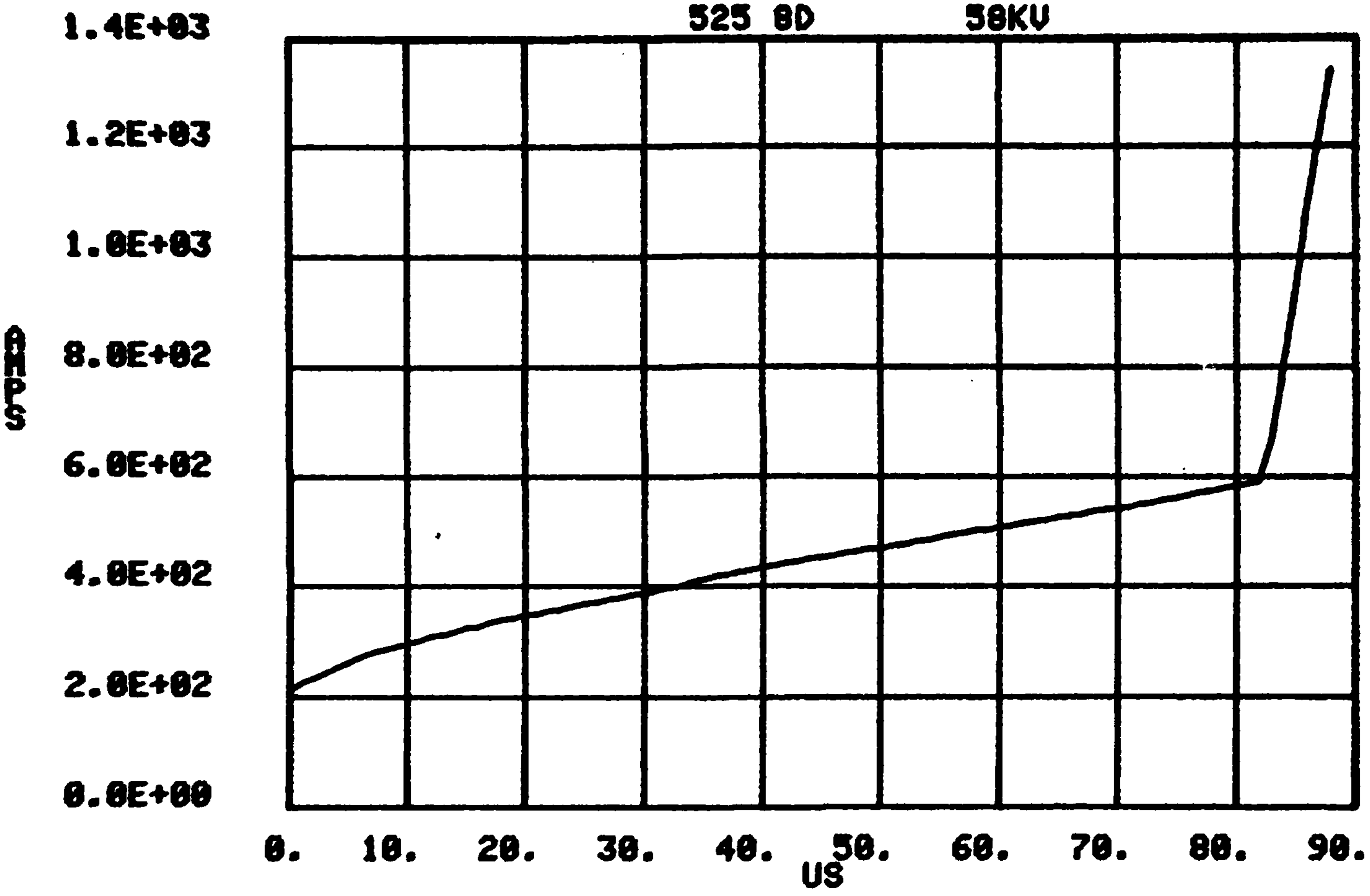

Figure B.59. 525B, .01, 1.0, 1.0, 300 sand-mix; I.

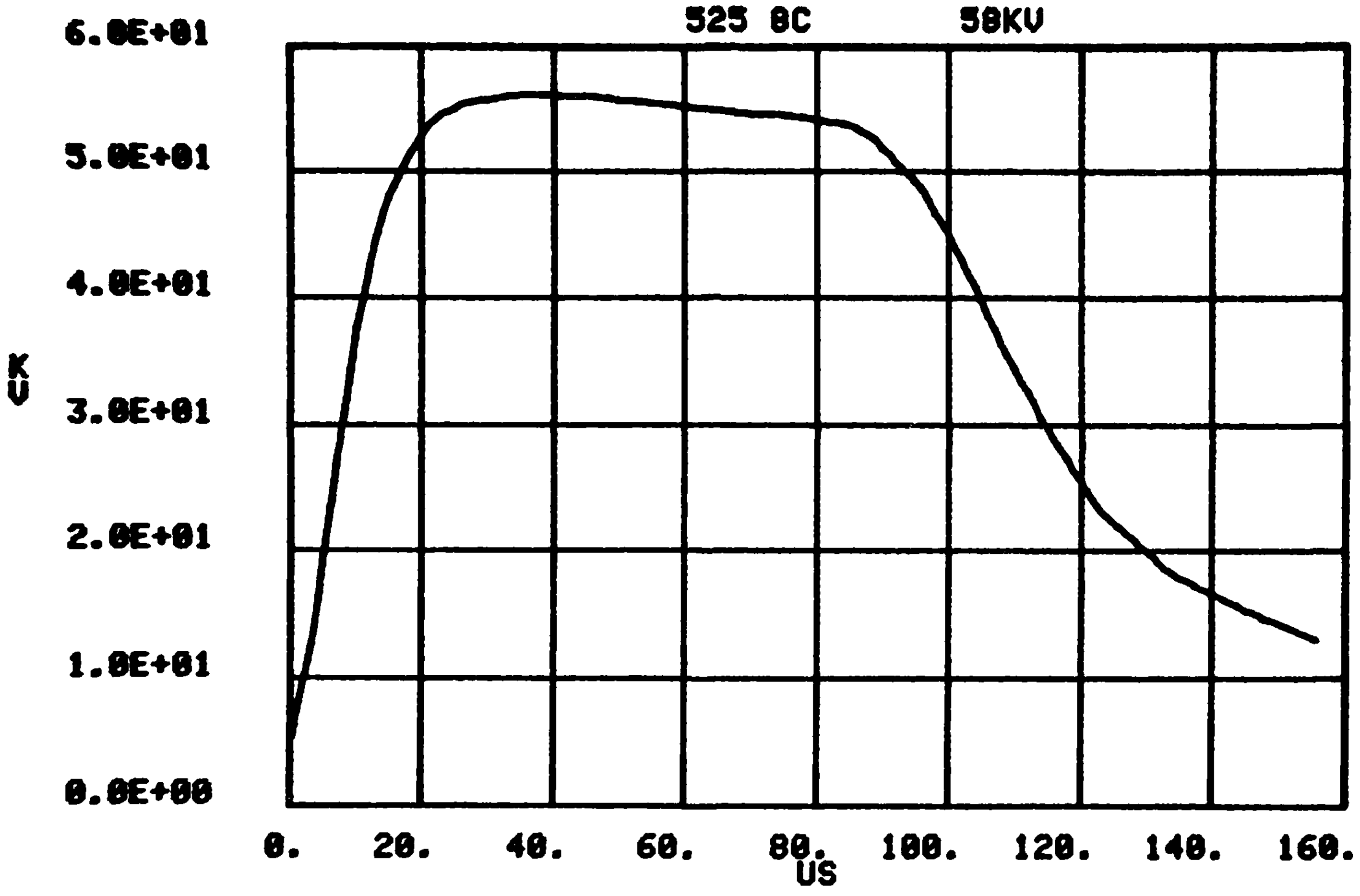

Figure B.60. 525B, .01, 1.0, 1.0, 300 sand-mix; I.

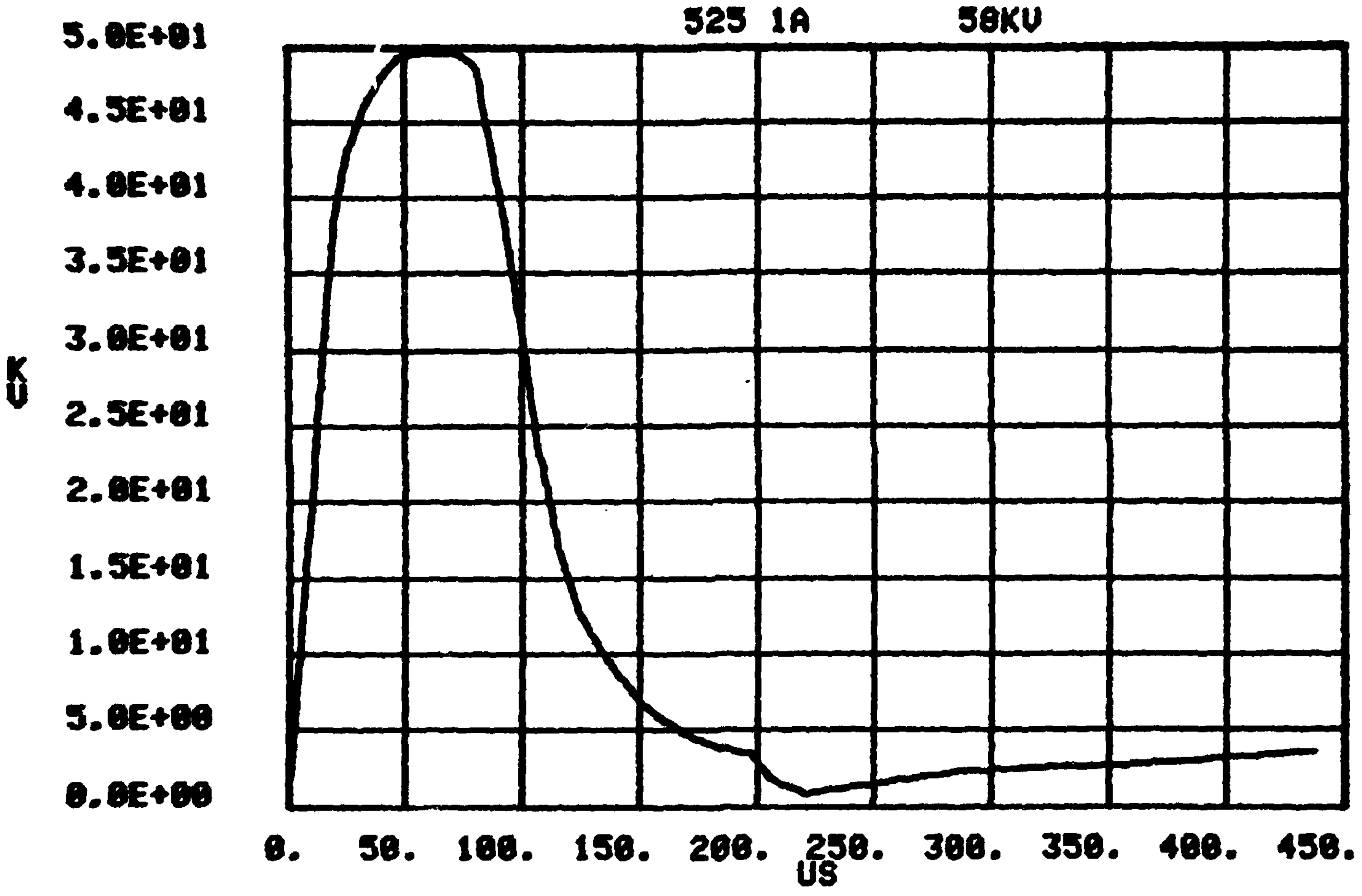

Figure B.61. 525B, .01, 1.0, 1.0, 300 sand-mix; V at r, θ = .51 m, 0° (bottom).

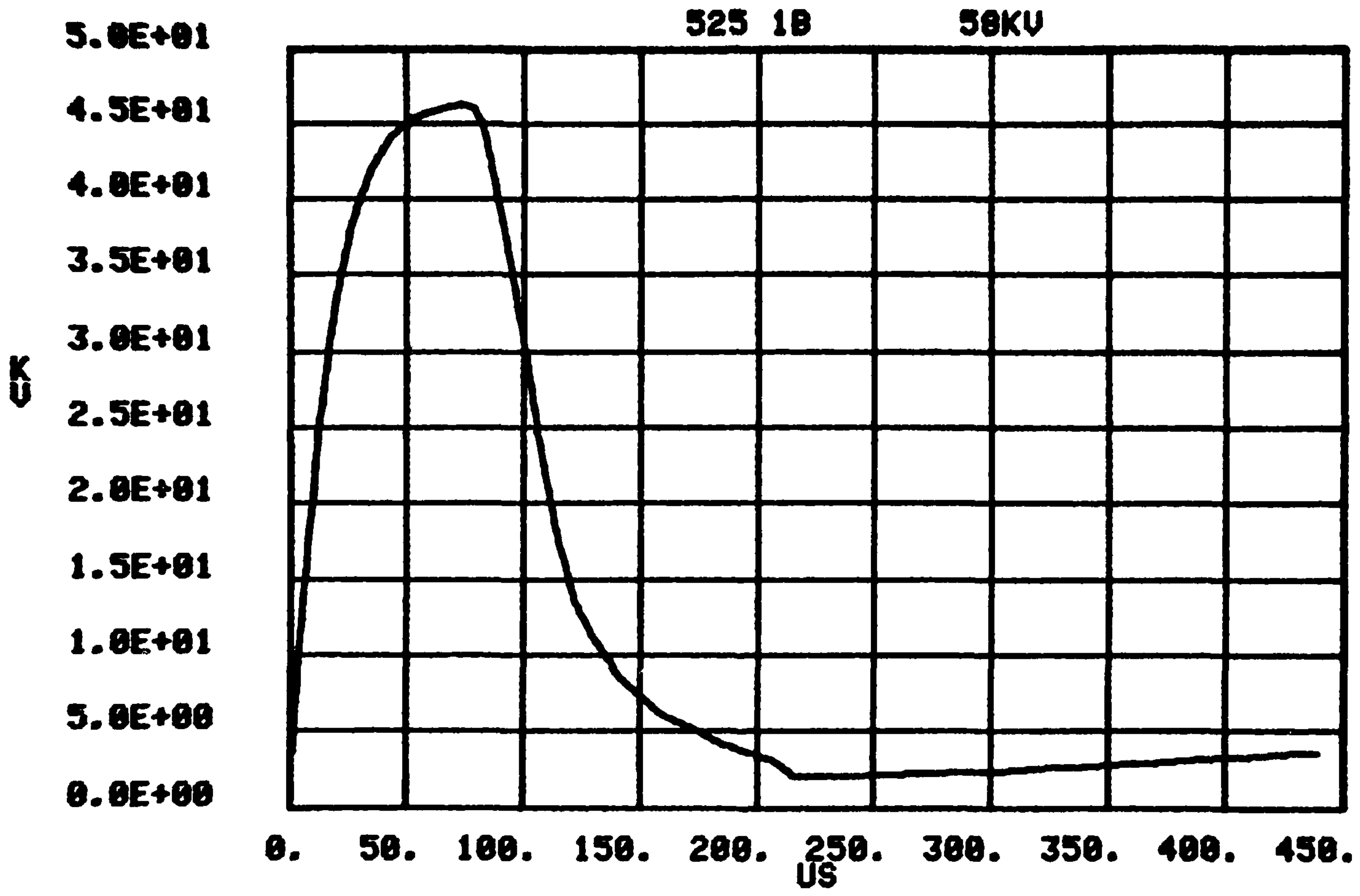

Figure B.62. 525B, .01, 1.0, 1.0, 300 sand-mix; V at r,θ = .10 m, 0° (bottom).

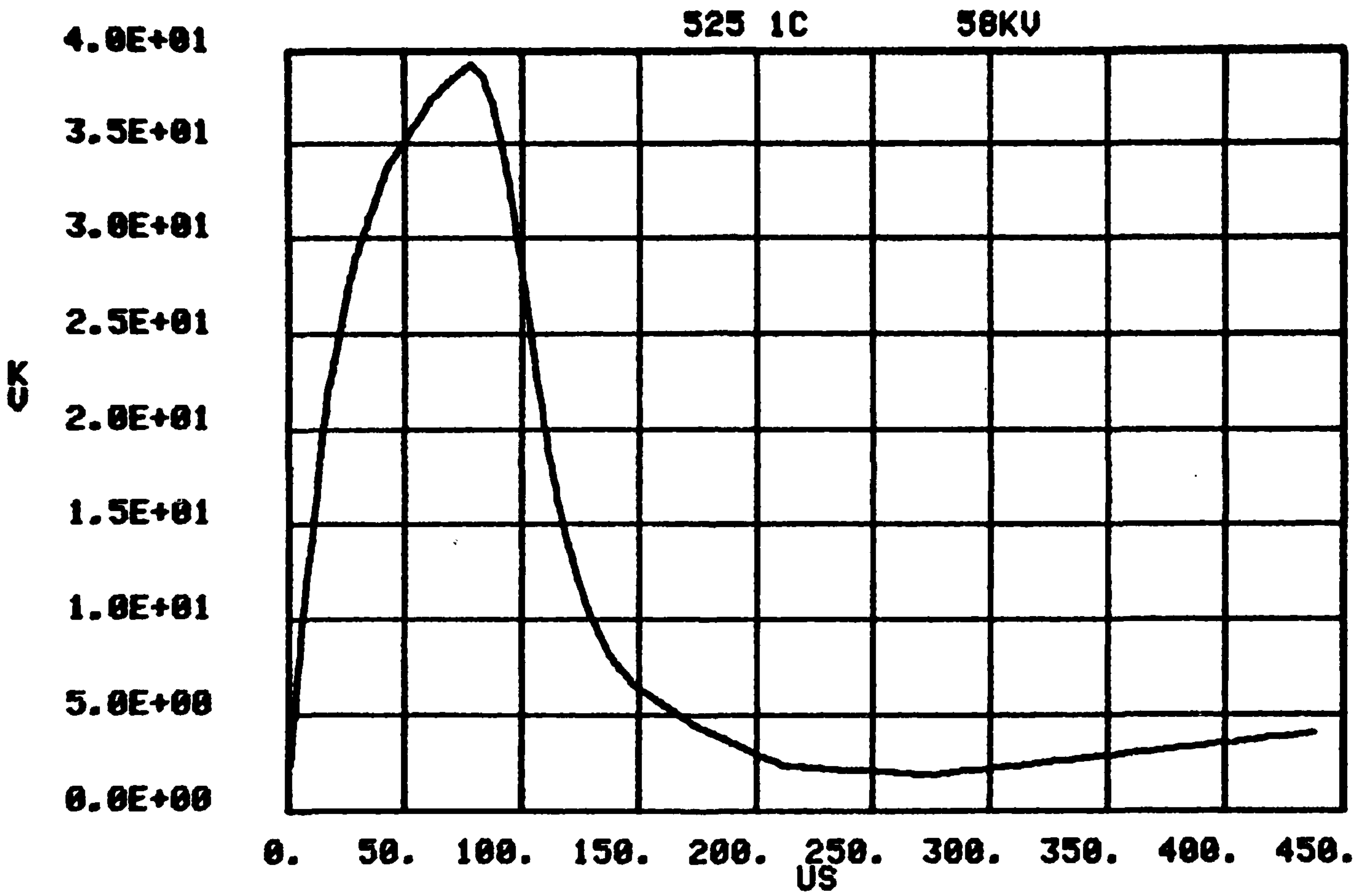

Figure B.63. 525B, .01, 1.0, 1.0, 300 sand-mix; V at r,θ = .18 m, 0° (bottom).

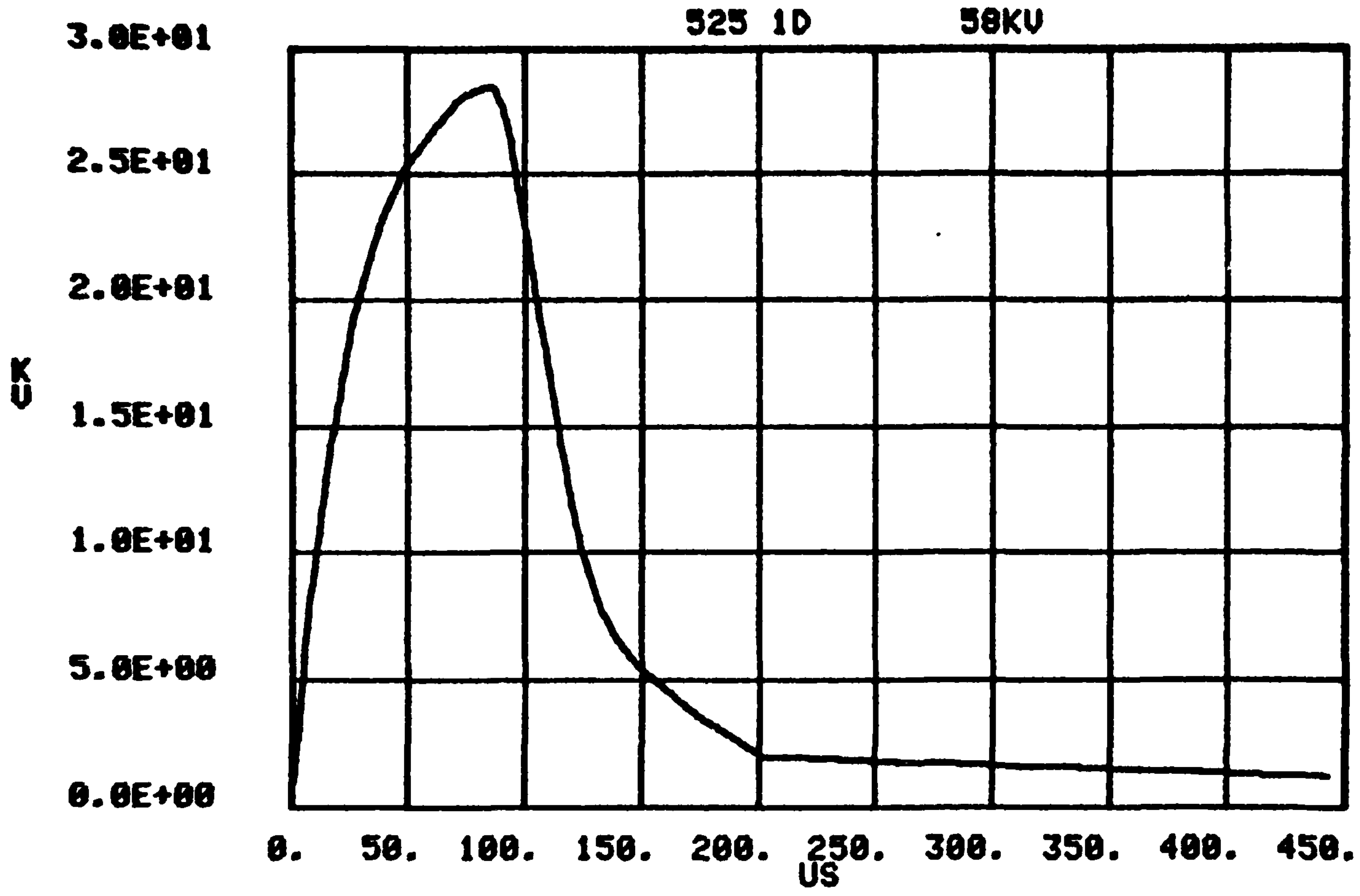

Figure B.64. 525B, .01, 1.0, 1.0, 300 sand-mix; V at r,θ = .30 m, 0° (bottom).

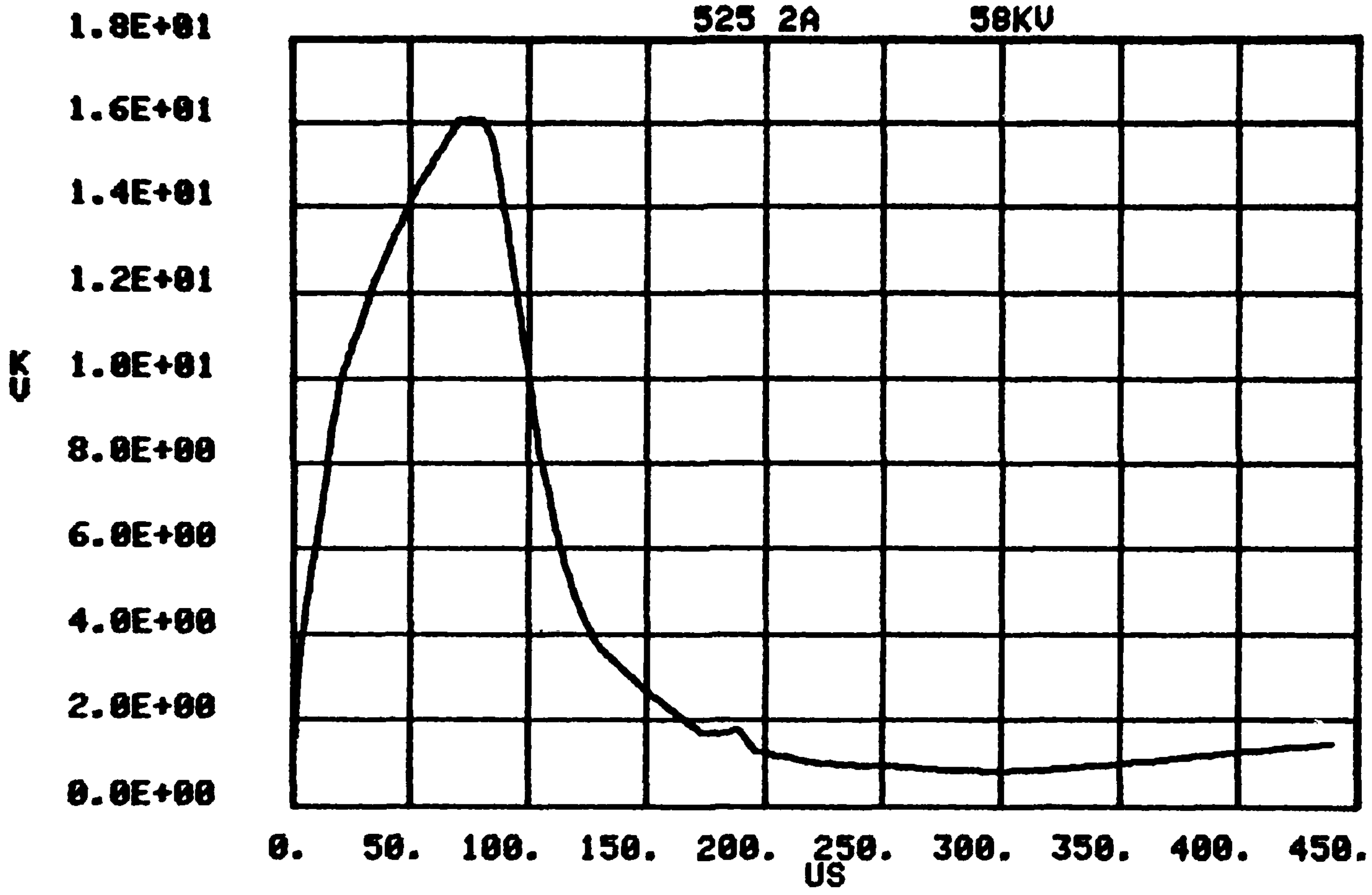

Figure B.65. 525B, .01, 1.0, 1.0, 300 sand-mix; V at r,θ = .51 m, 0° (bottom).

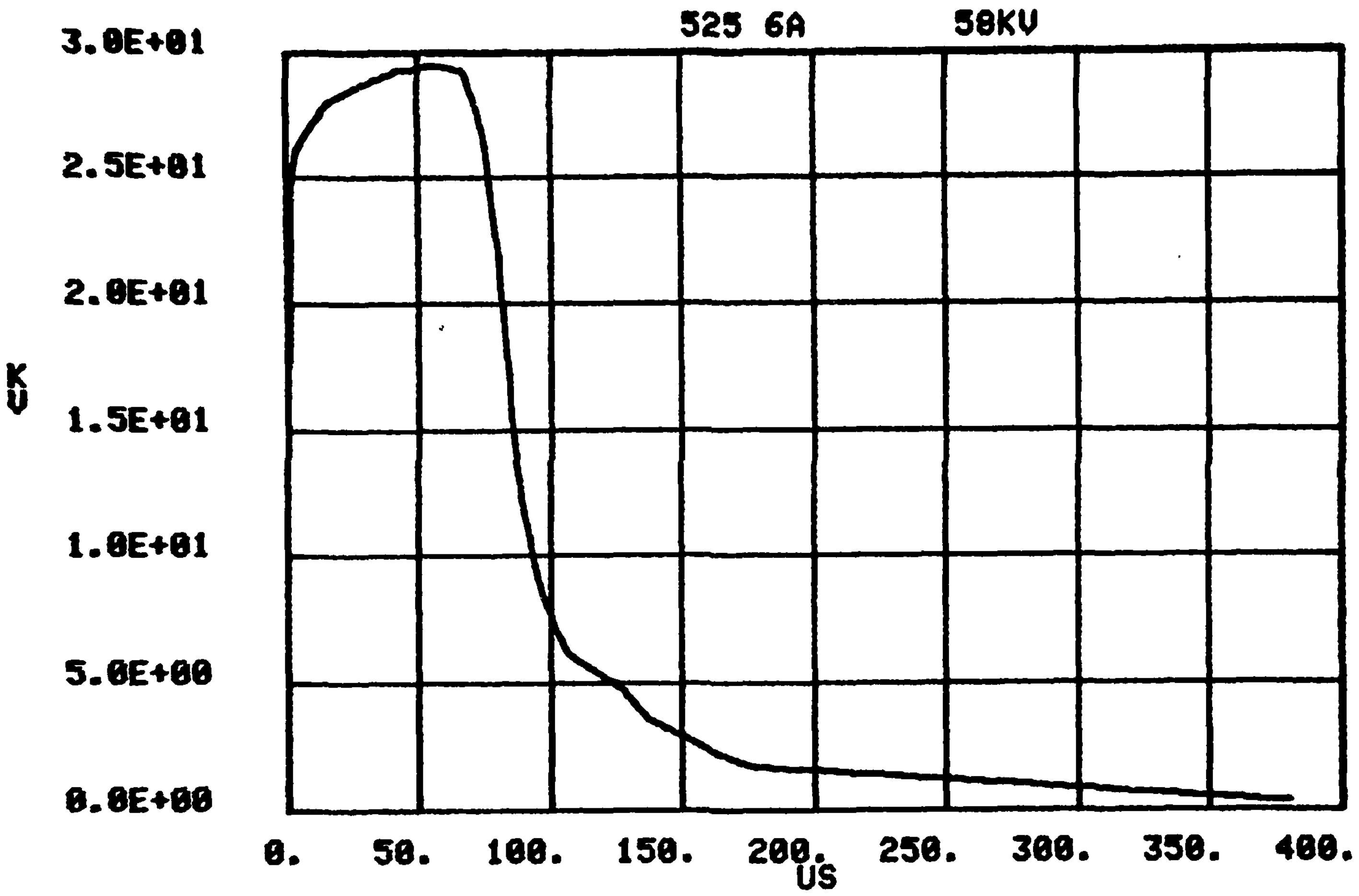

Figure B.66. 525B, .01, 1.0, 1.0, 300 sand-mix; V at r,θ = .15 m, 261 (top).

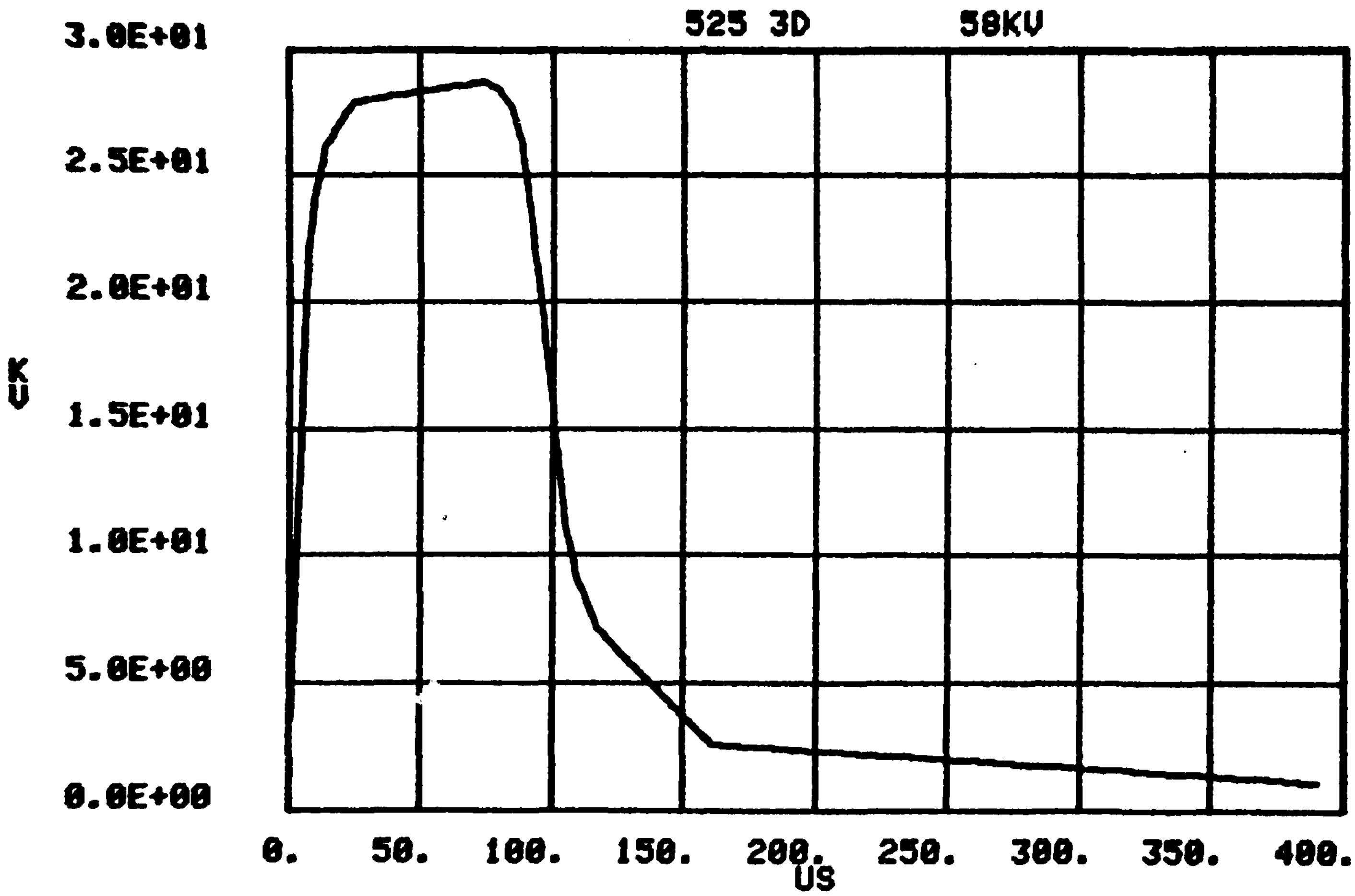

Figure B.67. 525B, .01, 1.0, 1.0, 300 sand-mix; V at r,θ = .15 m, 272 (top).

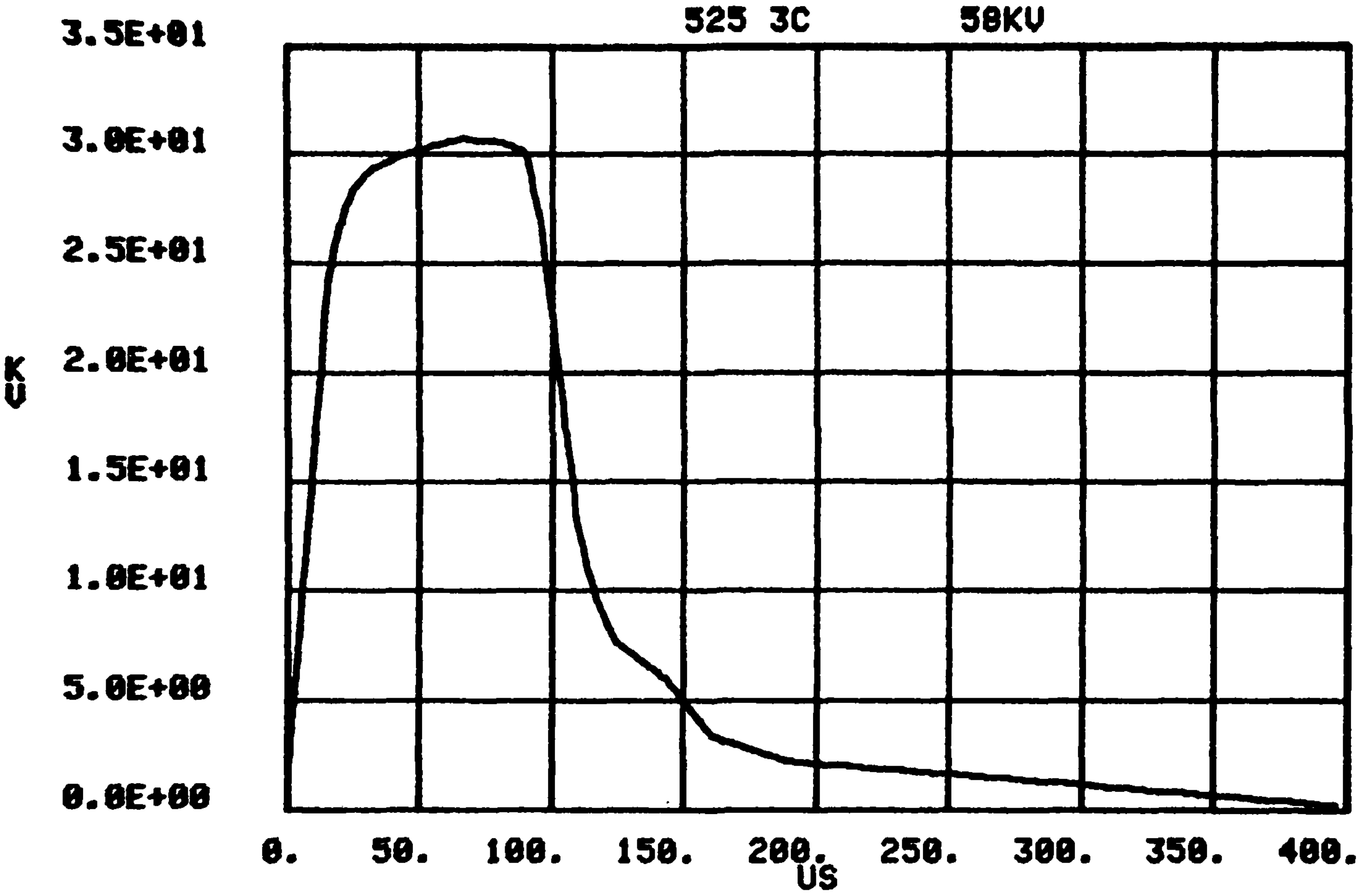

Figure B.68. 525B, .01, 1.0, 1.0, 300 sand-mix; V at r,θ = .15 m, 283 (top).

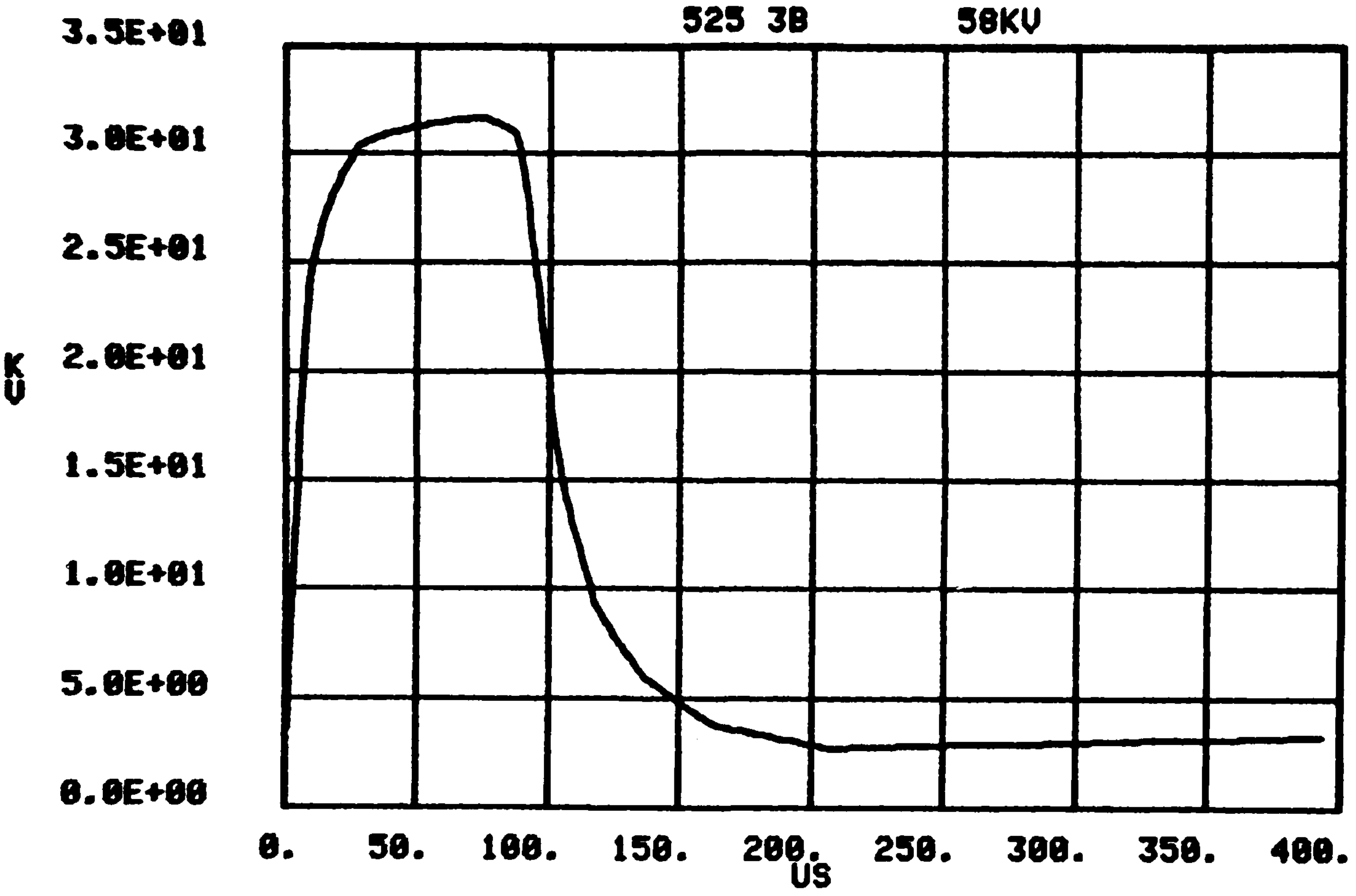

Figure B.69. 525B, .01, 1.0, 1.0, 300 sand-mix; V at r,θ = .15 m, 294 (top).

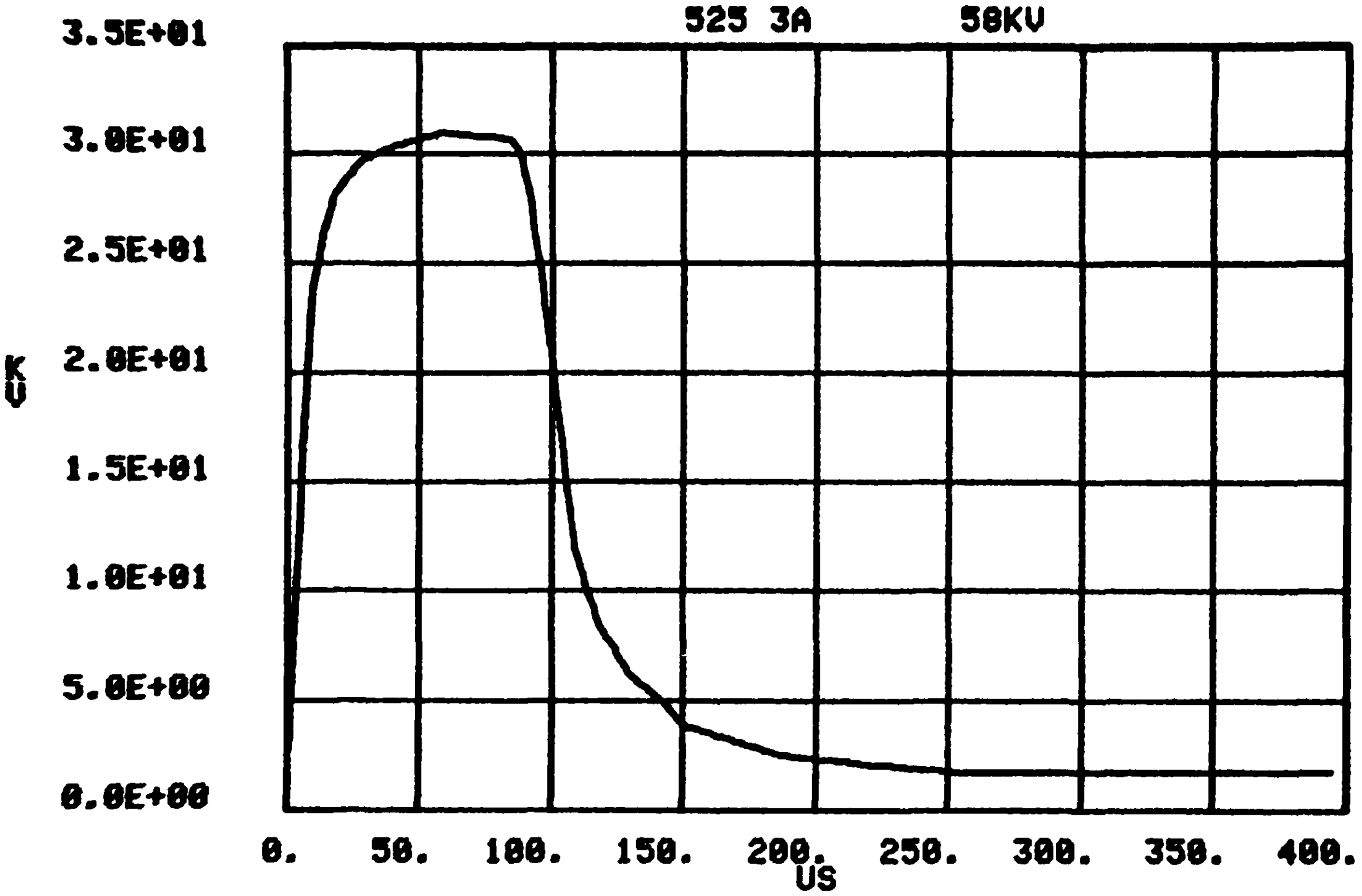

Figure B.70. 525B, .01, 1.0, 1.0, 300 sand-mix; V at r,θ = .15 m, 305 (top).

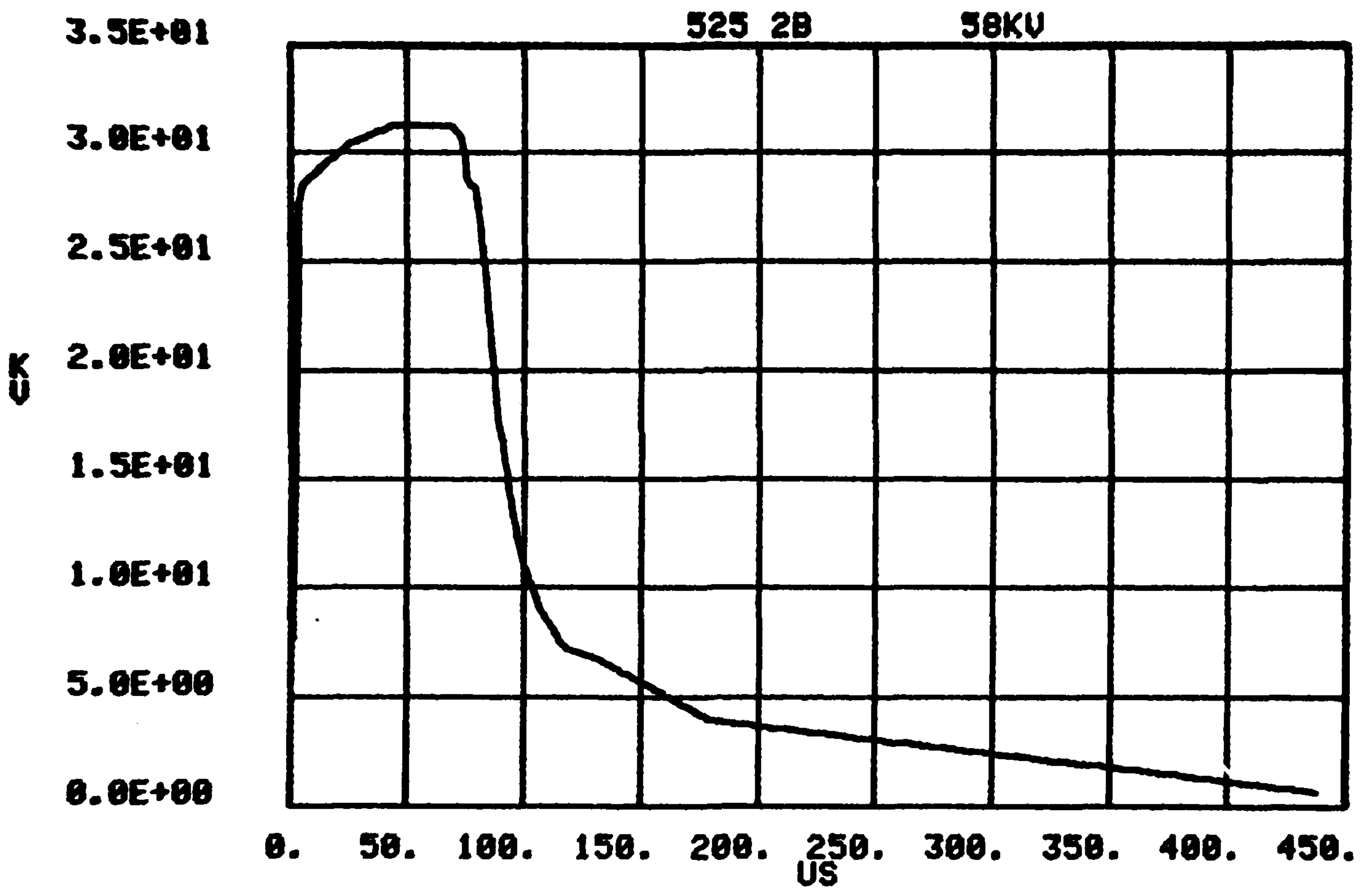

Figure B.71. 525B, .01, 1.0, 1.0, 300 sand-mix; V at r,θ = .15 m, 316 (top).

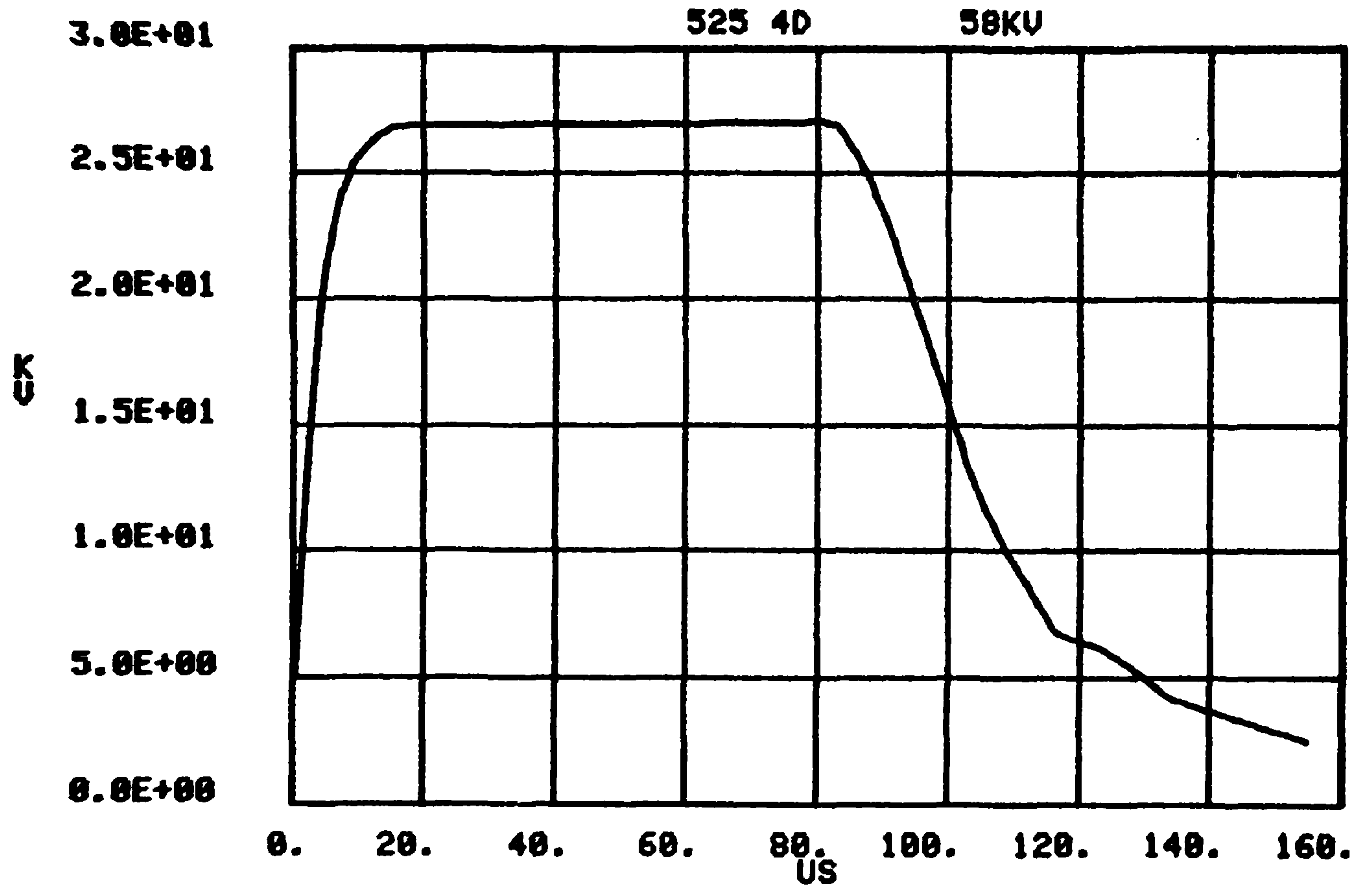

Figure B.72. 525B, .01, 1.0, 1.0, 300 sand-mix; V at r,θ = .15 m, 327 (top).

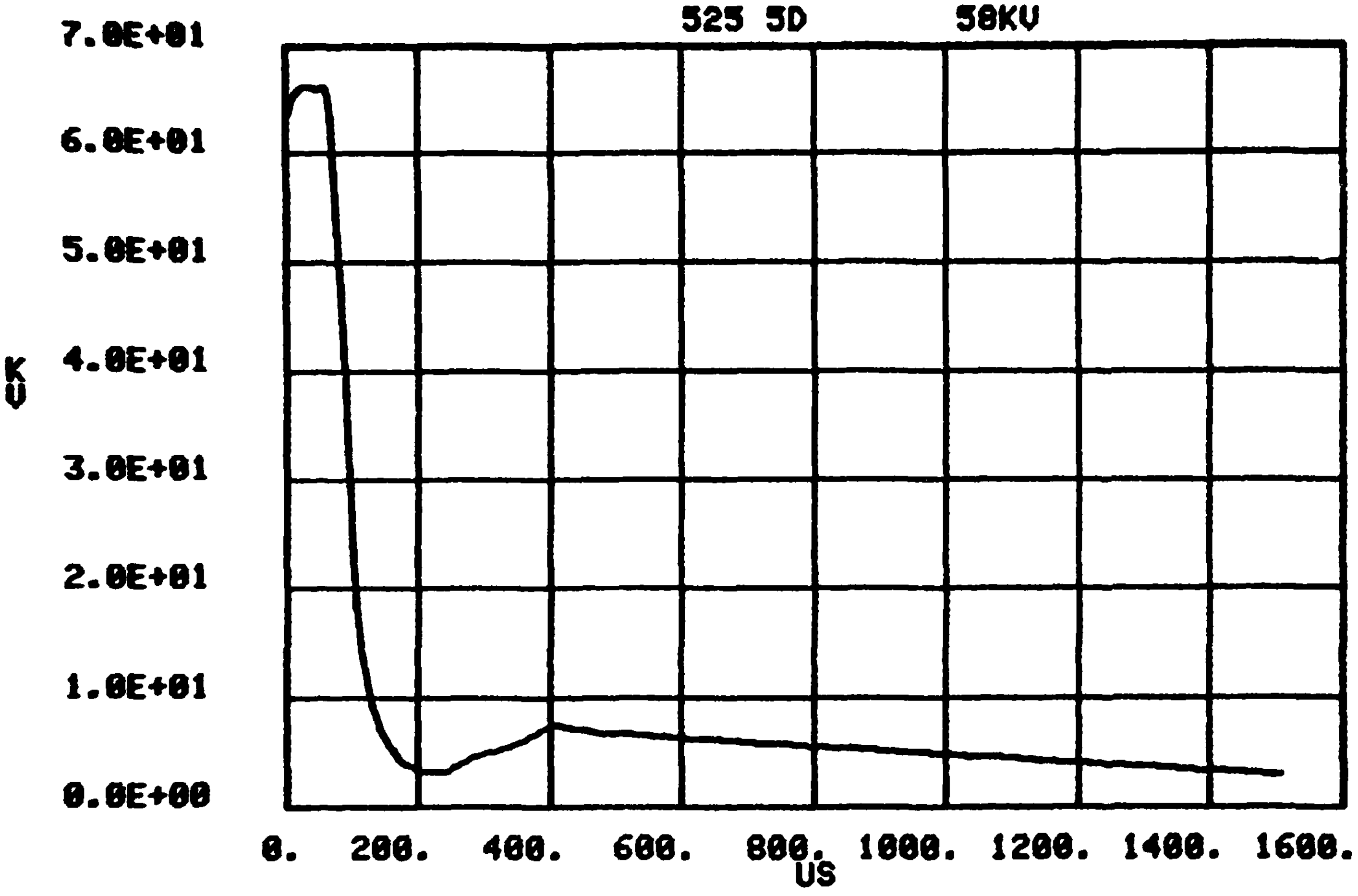

Figure B.73. 525B, .01, 1.0, 1.0, 300 sand-mix; V at r,θ = .15 m, 327 (top).

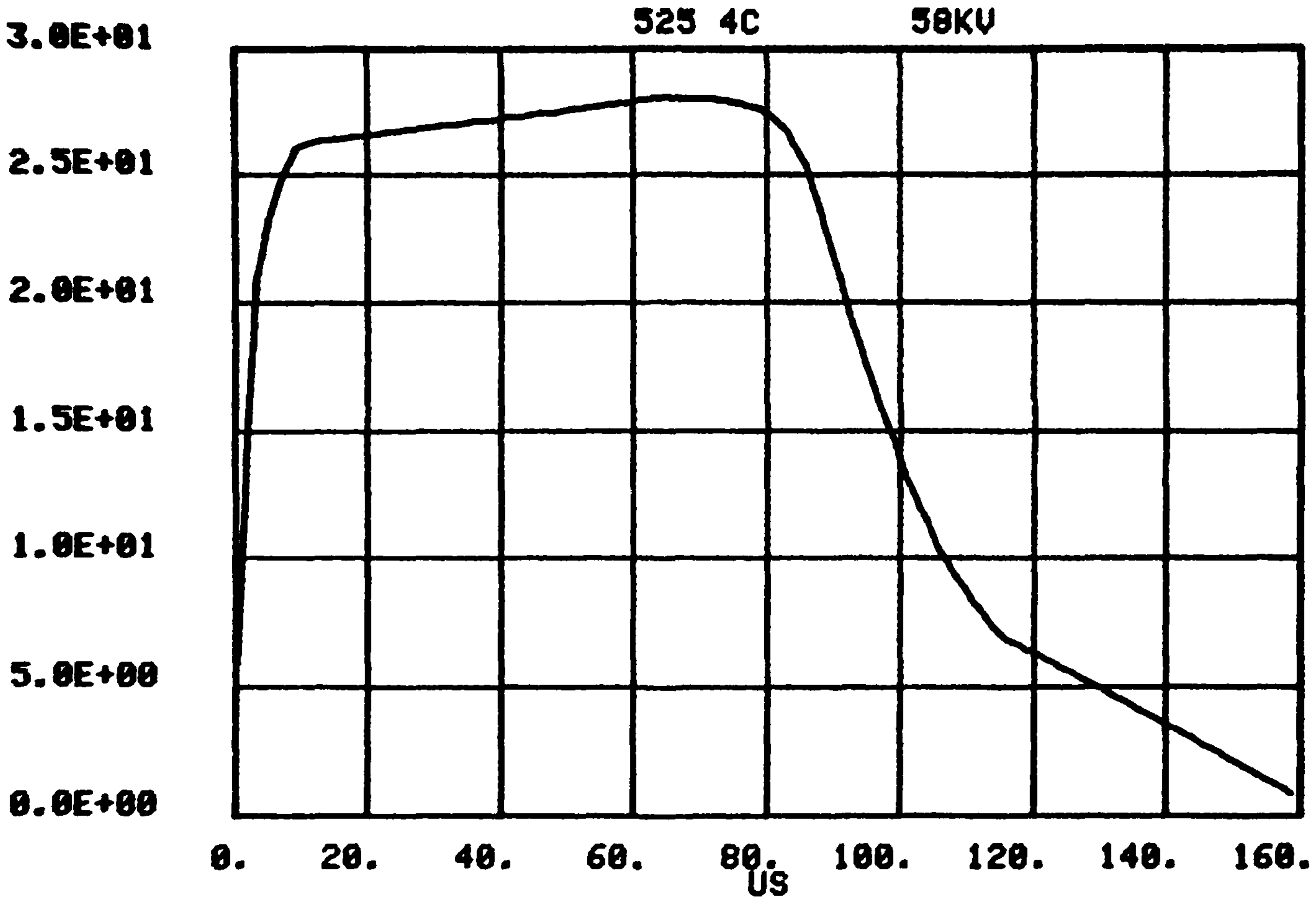

Figure B.74. 525B, .01, 1.0, 1.0, 300 sand-mix; V at r,θ = .15 m, 338 (top).

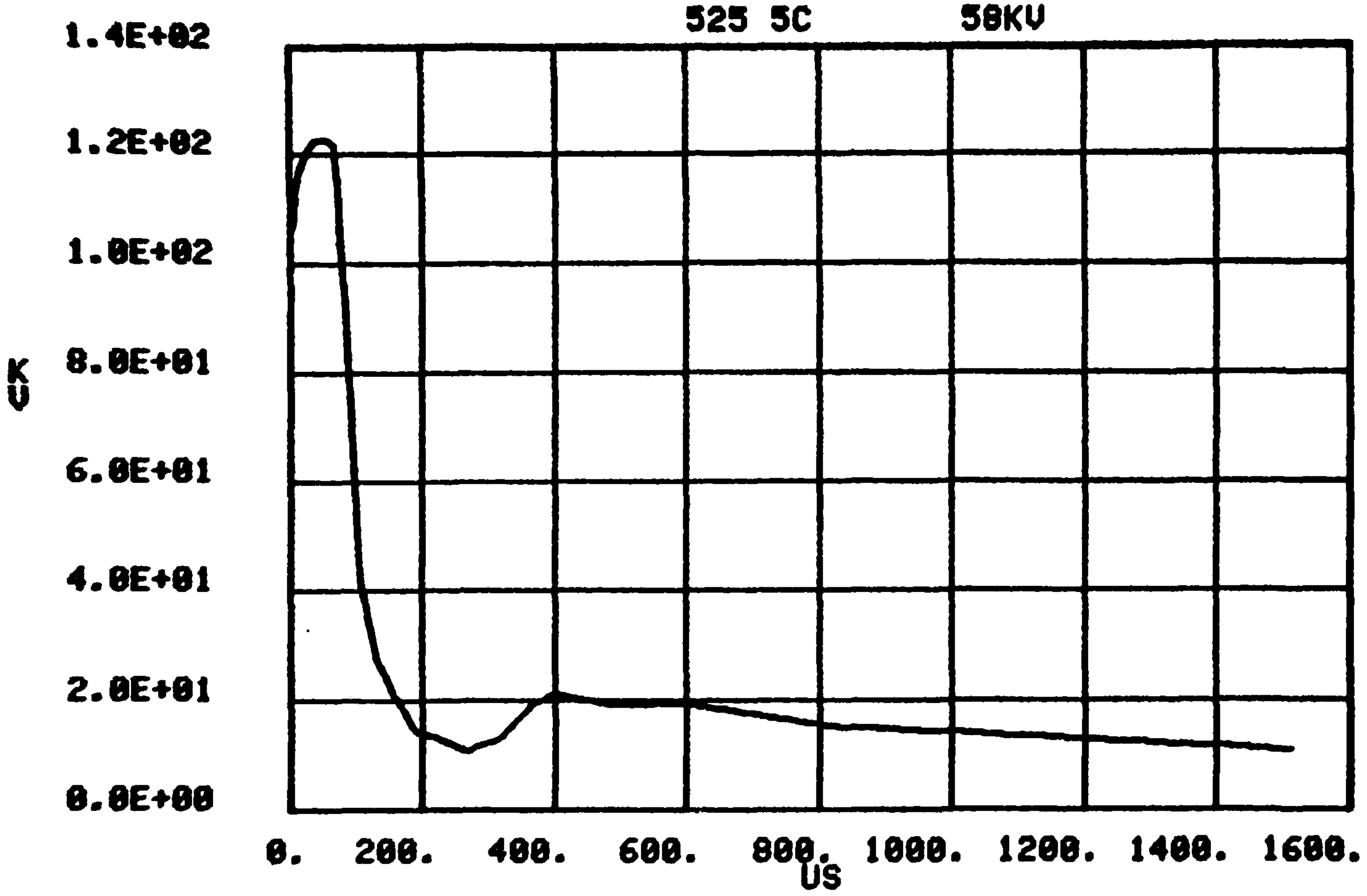

Figure B.75. 525B, .01, 1.0, 1.0, 300 sand-mix; V at r,θ = .15 m, 338 (top).

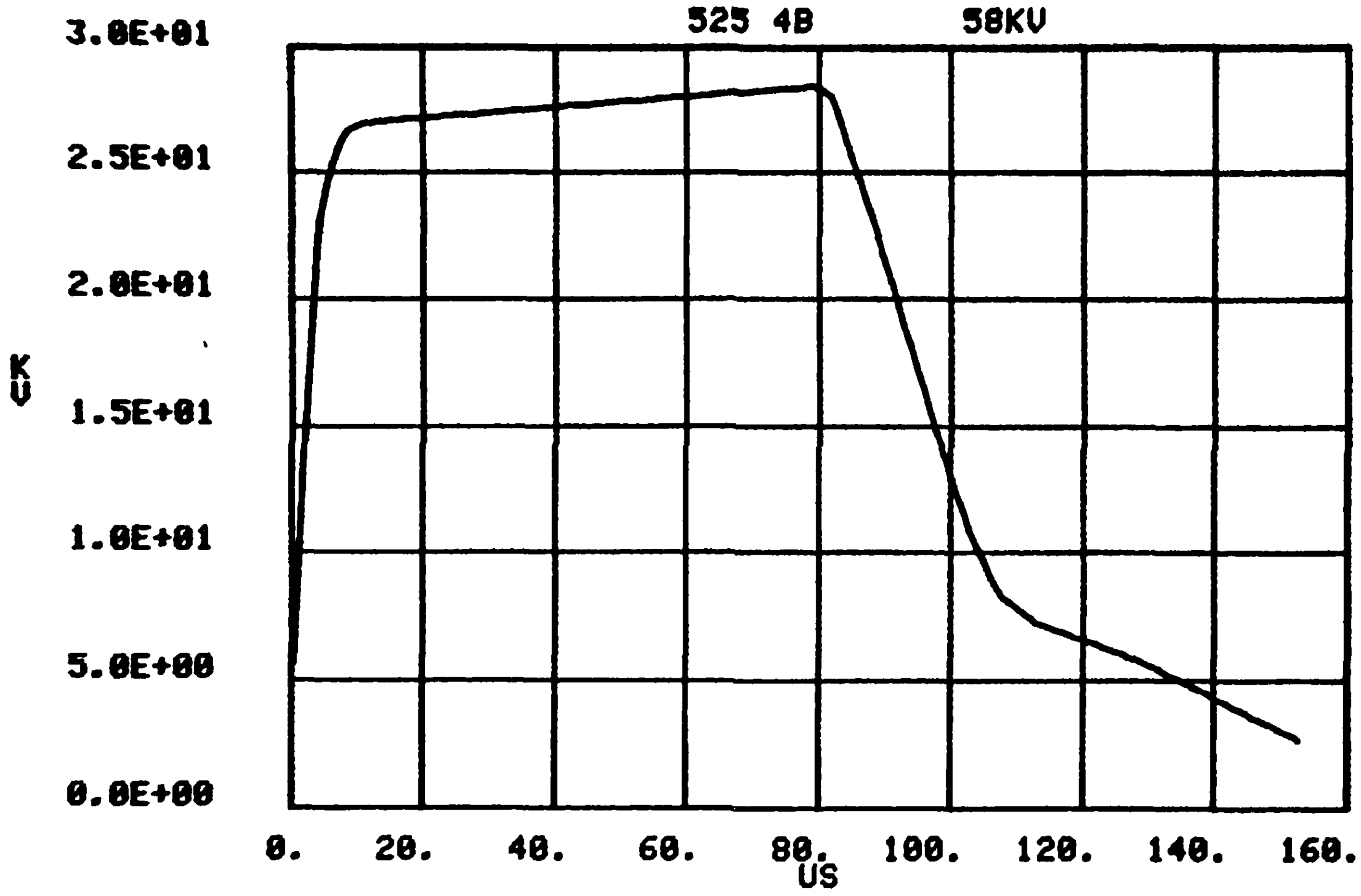

Figure B.76. 525B, .01, 1.0, 1.0, 300 sand-mix; V at r,θ = .15 m, 349 (top).

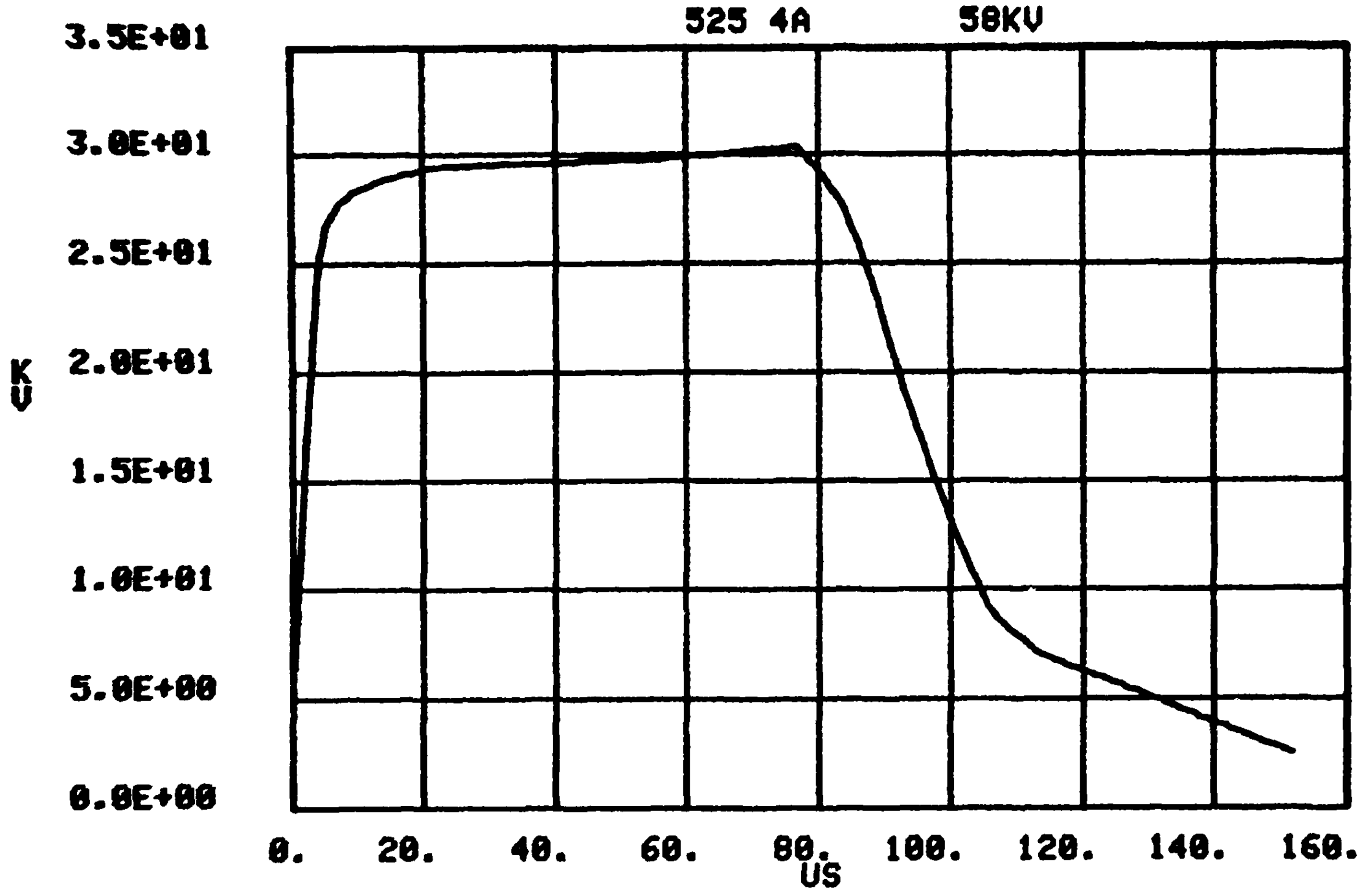

Figure B.77. 525B, .01, 1.0, 1.0, 300 sand-mix; V at r,θ = .15 m, 0 (top).

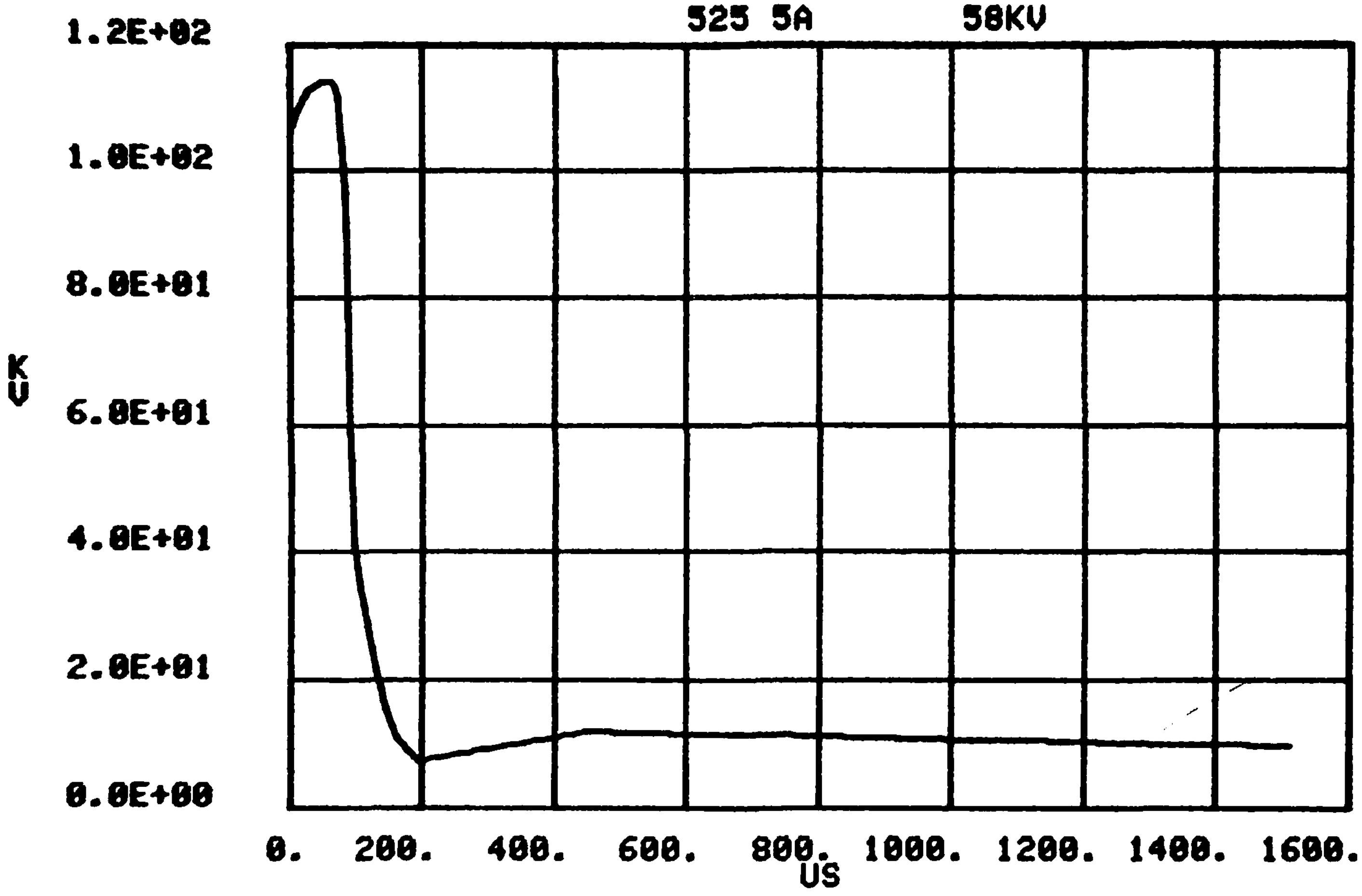

Figure B.78. 525B, .01, 1.0, 1.0, 300 sand-mix; V at r,θ = .15 m, 0 (top).

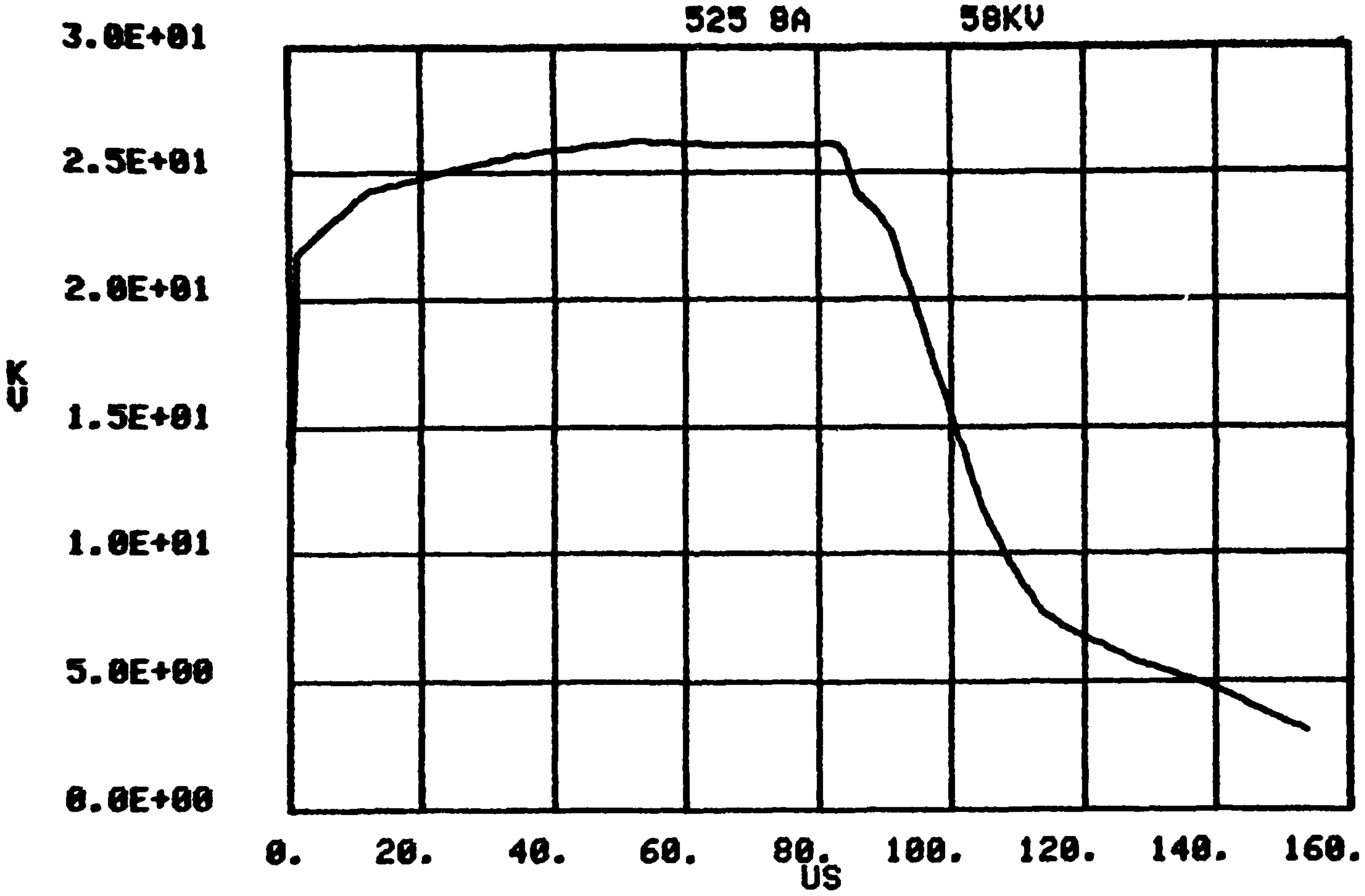

Figure B.79. 525B, .01, 1.0, 1.0, 300 sand-mix; V at r,θ = .15 m, 11 (top).

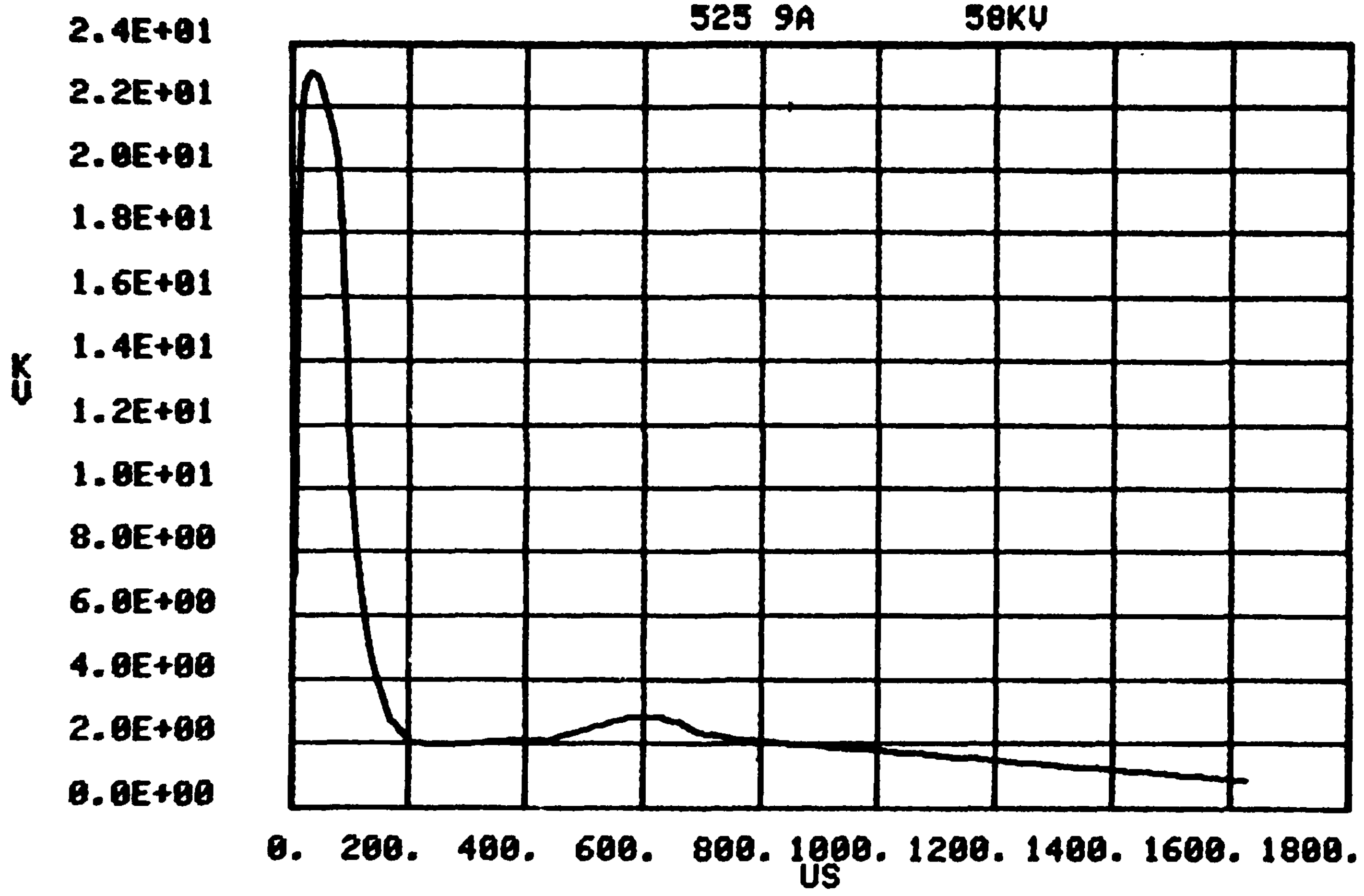

Figure B.80. 525B, .01, 1.0, 1.0, 300 sand-mix; V at r,θ = .15 m, 11 (top).

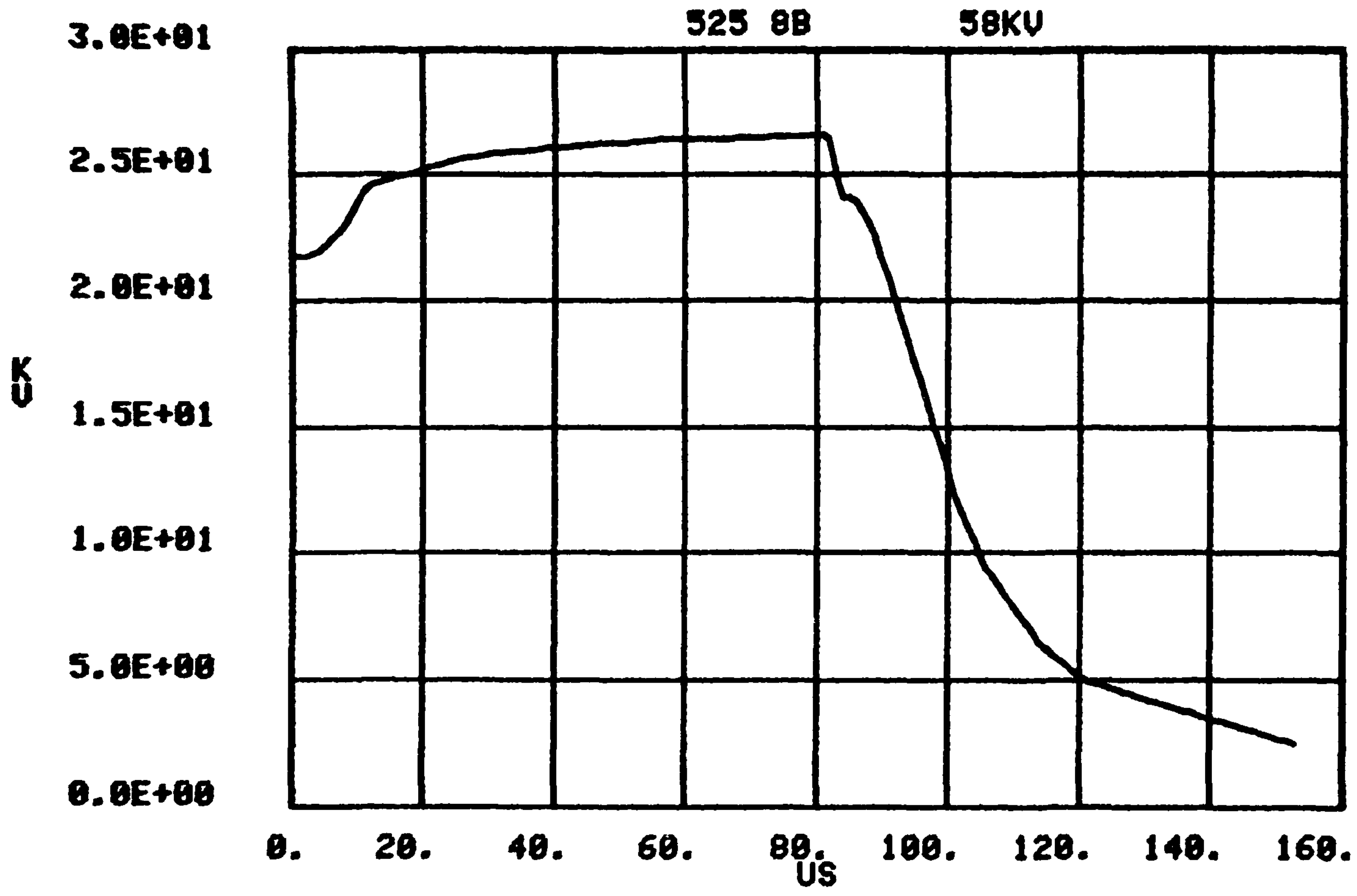

Figure B.81. 525B, .01, 1.0, 1.0, 300 sand-mix; V at r,θ = .15 m, 22 (top).

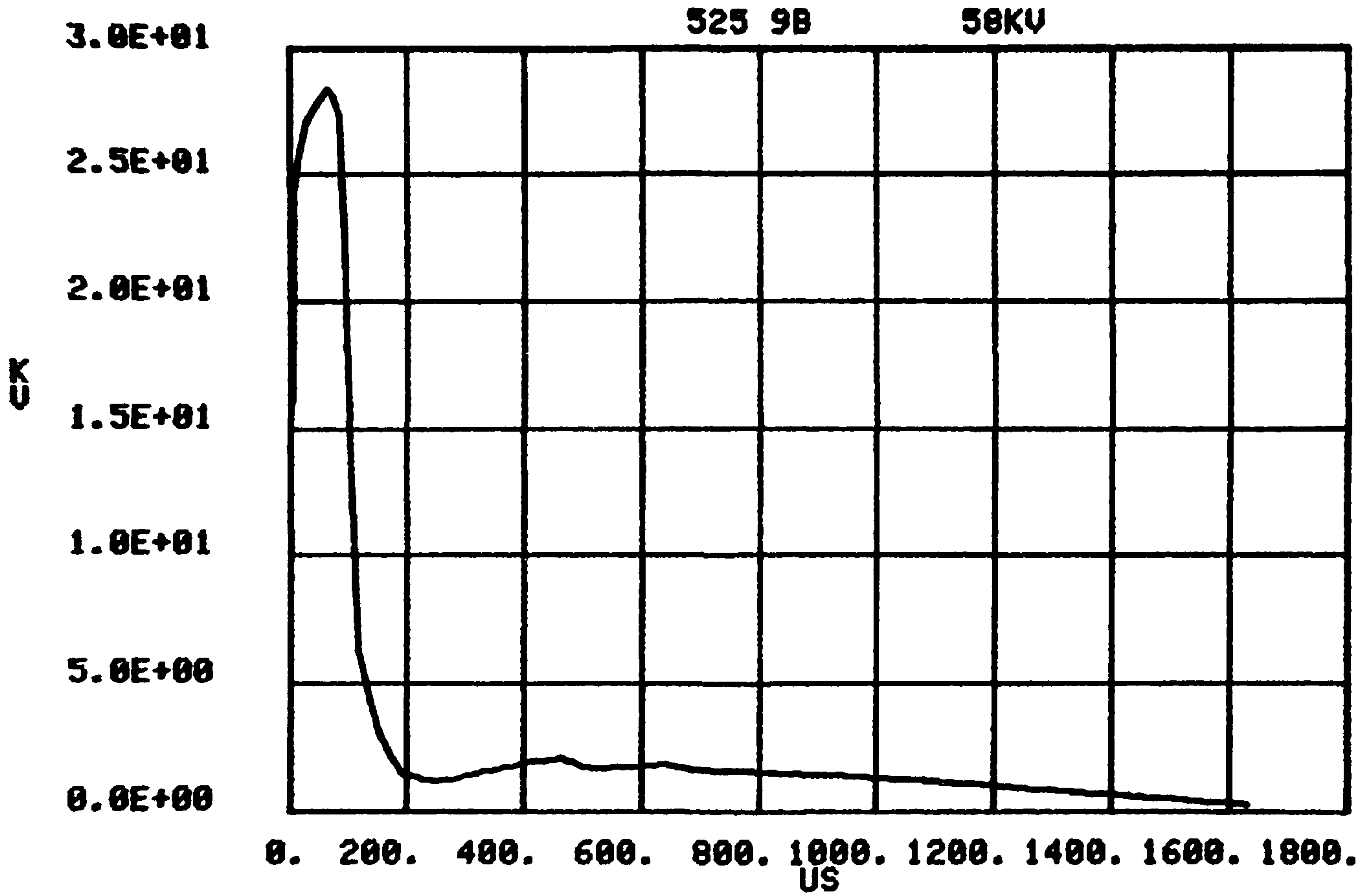

Figure B.82. 525B, .01, 1.0, 1.0, 300 sand-mix; V at r,θ = .15 m, 22 (top).

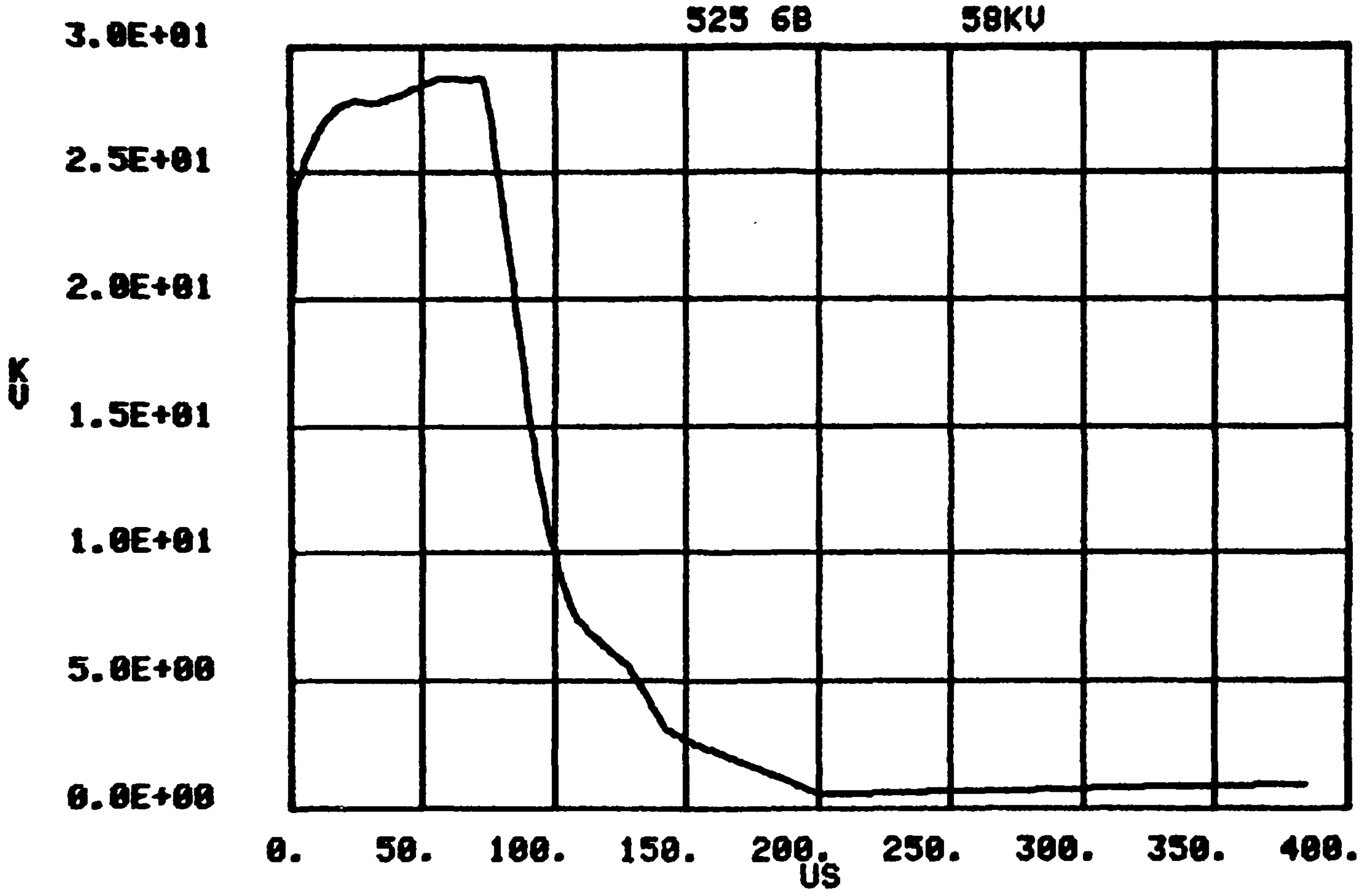

Figure B.83. 525B, .01, 1.0, 1.0, 300 sand-mix; V at r,θ = .15 m, 33 (top).

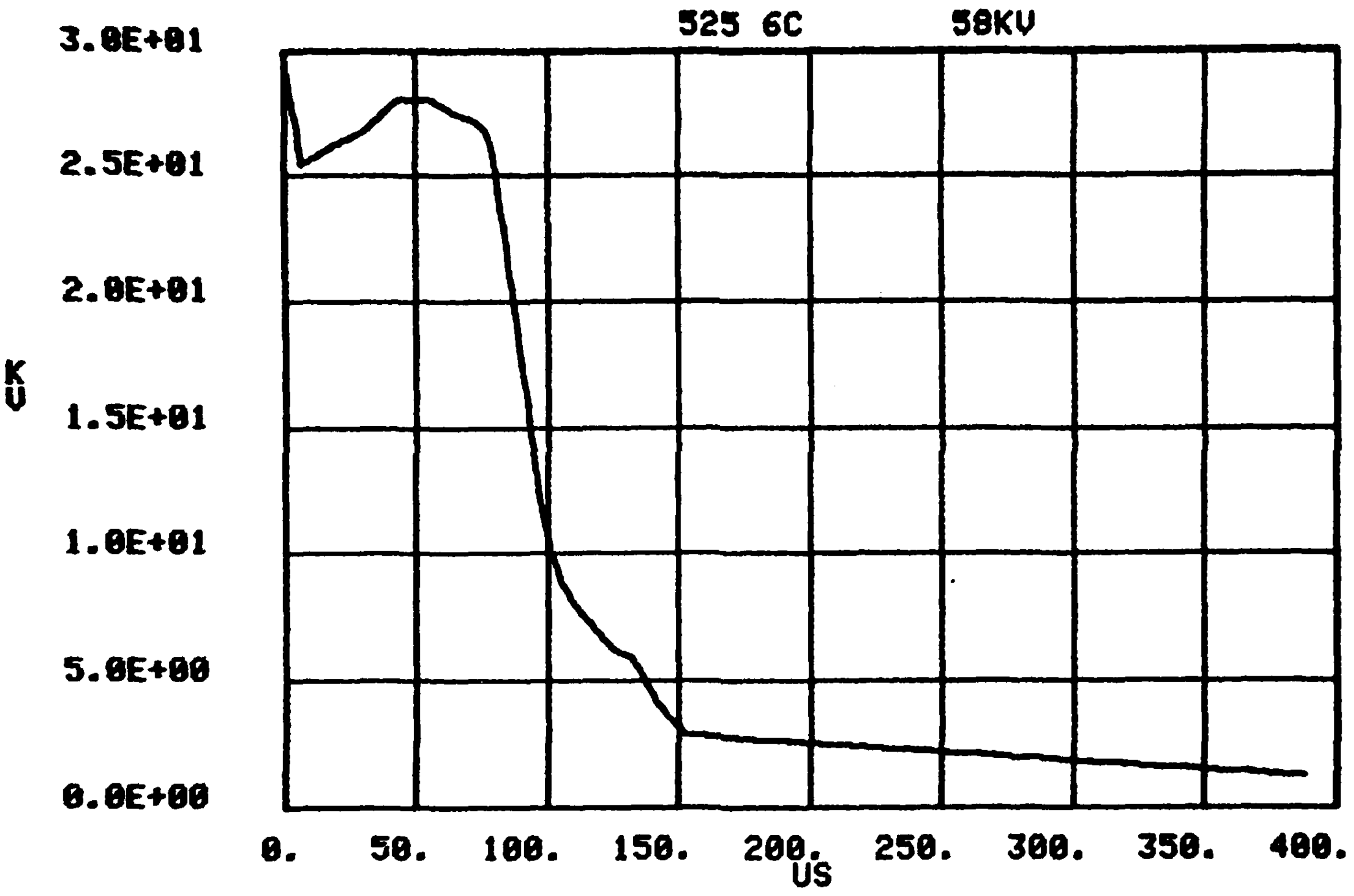

Figure B.84. 525B, .01, 1.0, 1.0, 300 sand-mix; V at r,θ = .15 m, 44 (top).

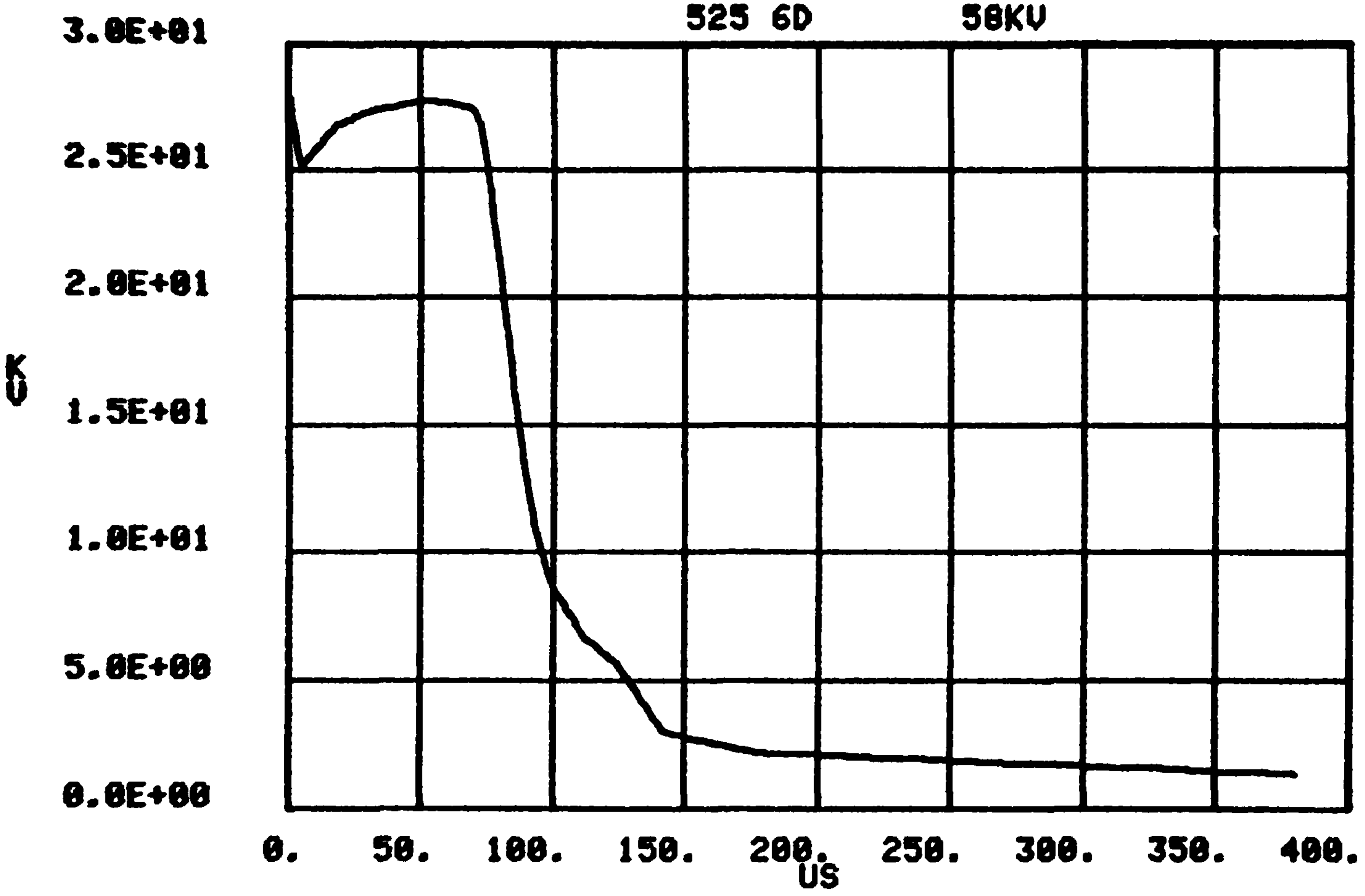

Figure B.85. 525B, .01, 1.0, 1.0, 300 sand-mix; V at r,θ = .15 m, 55 (top).

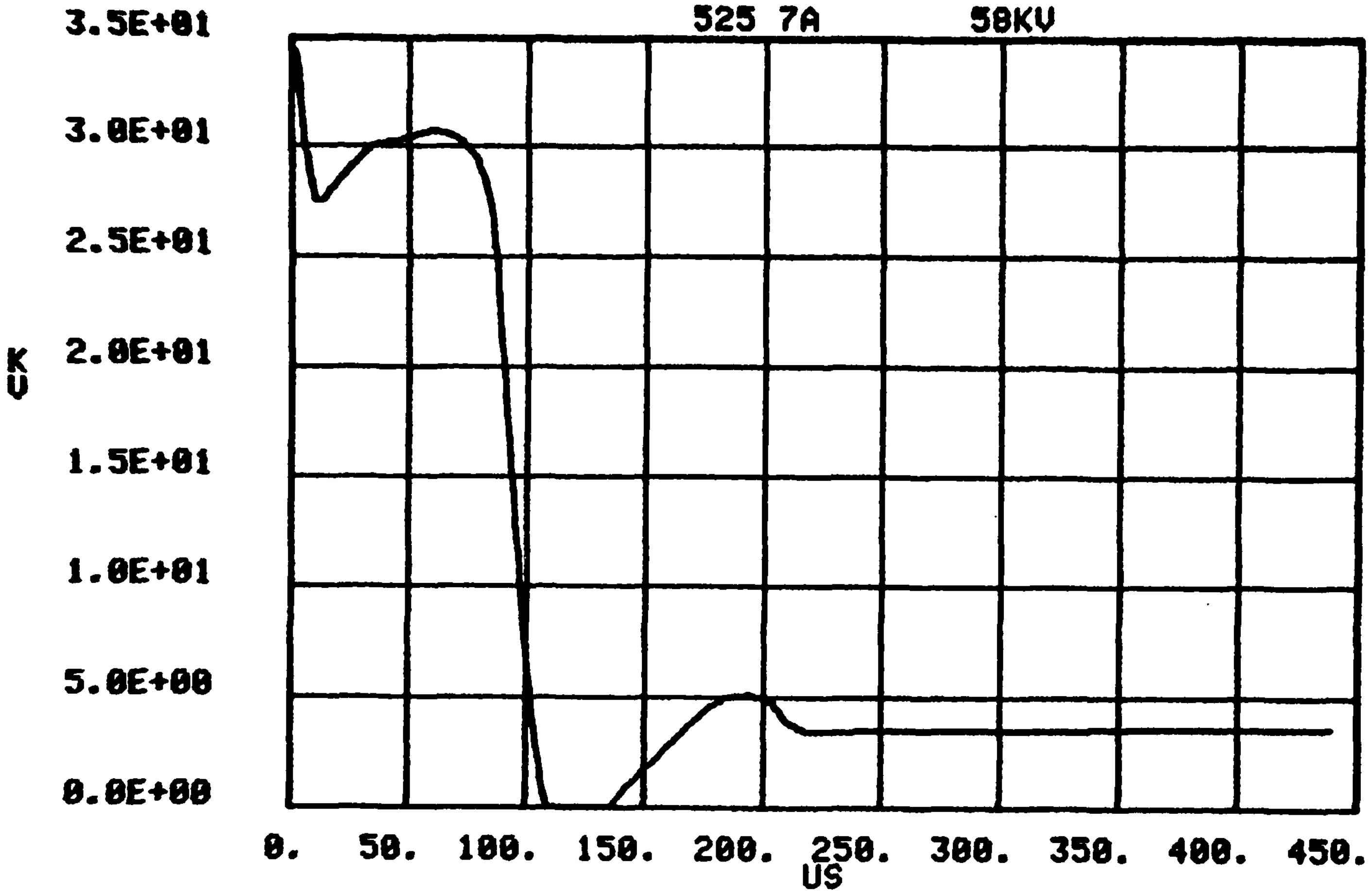

Figure B.86. 525B, .01, 1.0, 1.0, 300 sand-mix; V at r,θ = .15 m, 66 (top).

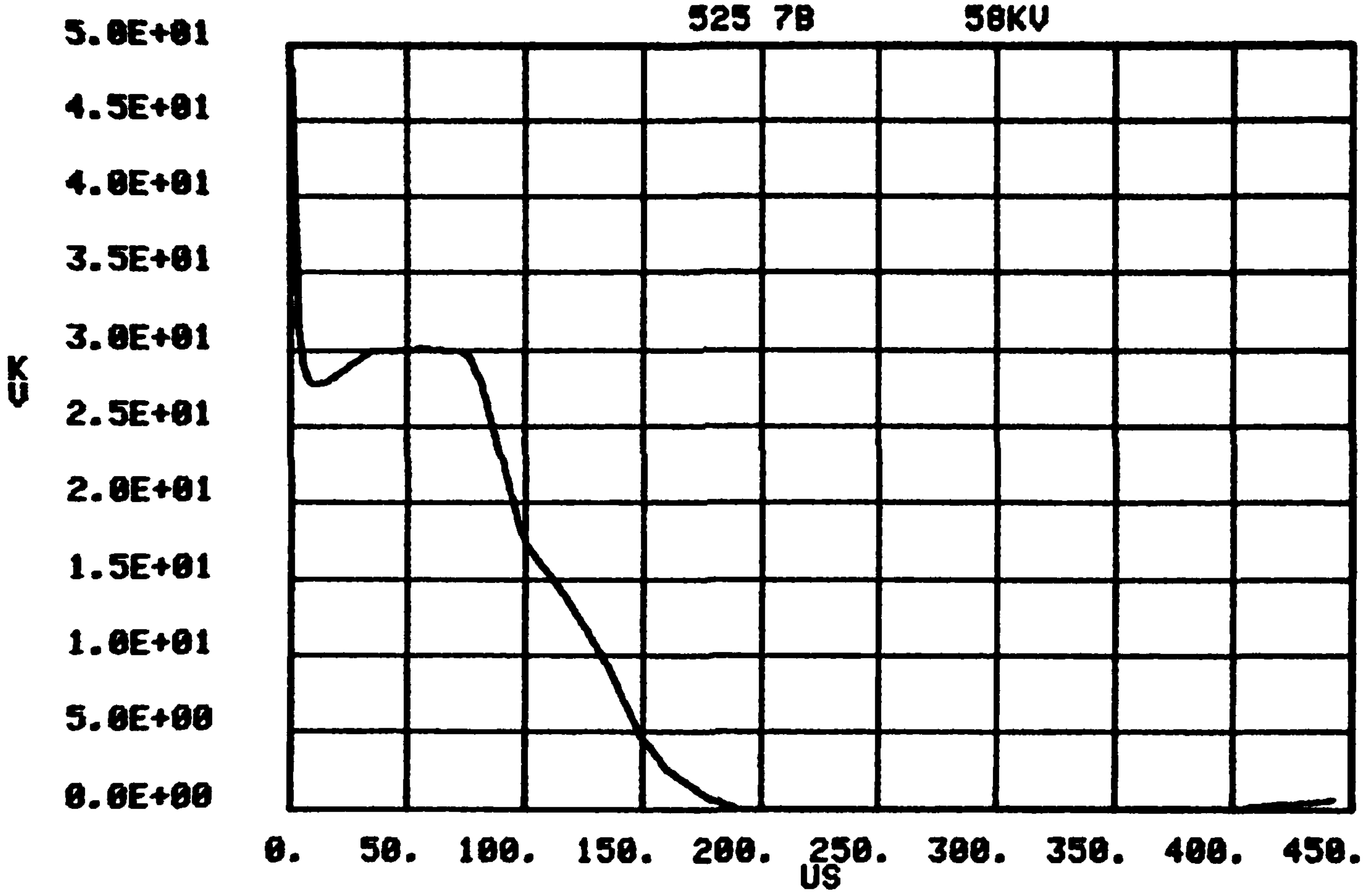

Figure B.87. 525B., .01, 1.0, 1.0, 300 sand-mix; V at r,θ = .15 m, 77 (top).

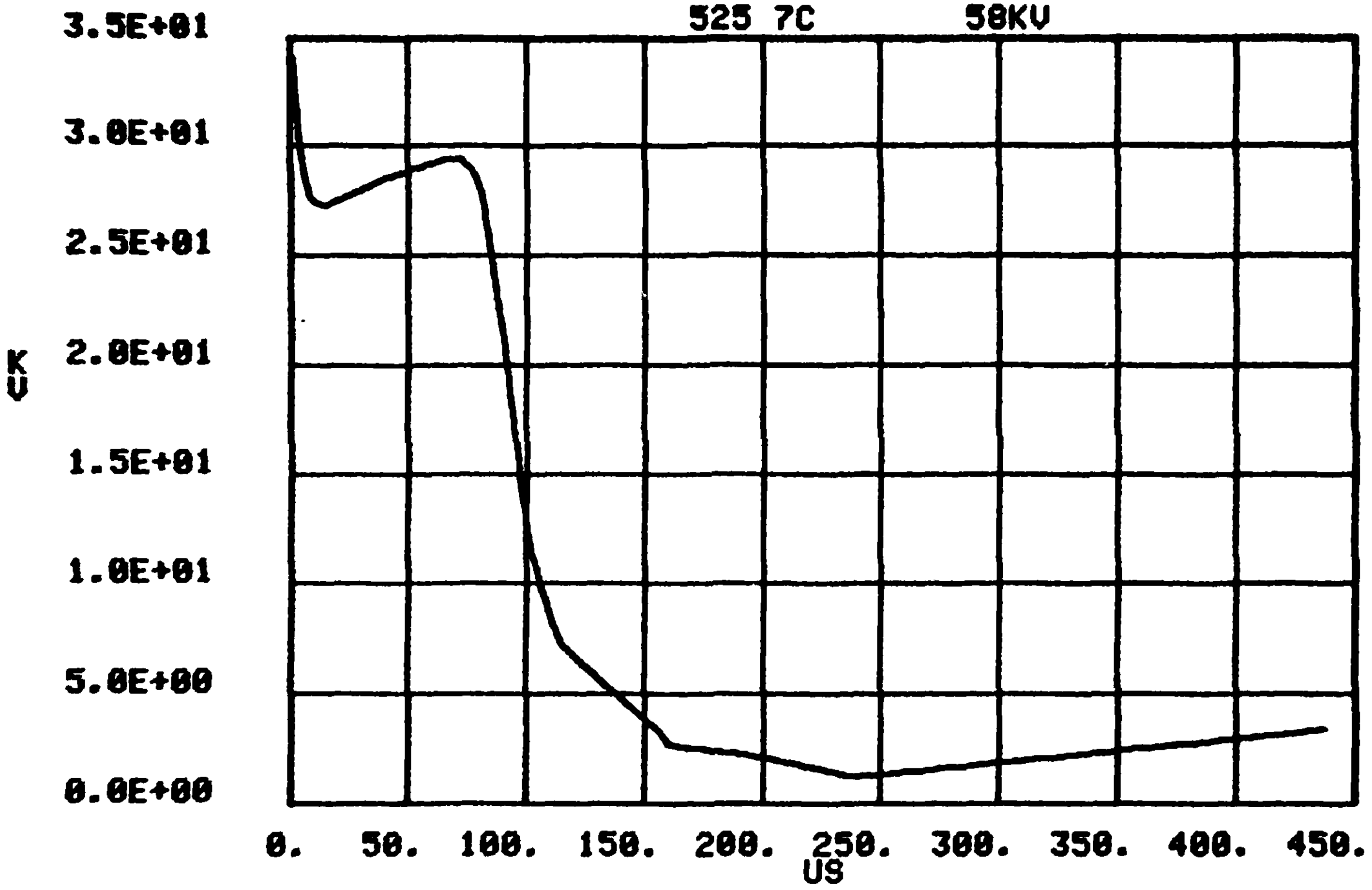

Figure B.88. 525B., .01, 1.0, 1.0, 300 sand-mix; V at r,θ = .15 m, 88 (top).

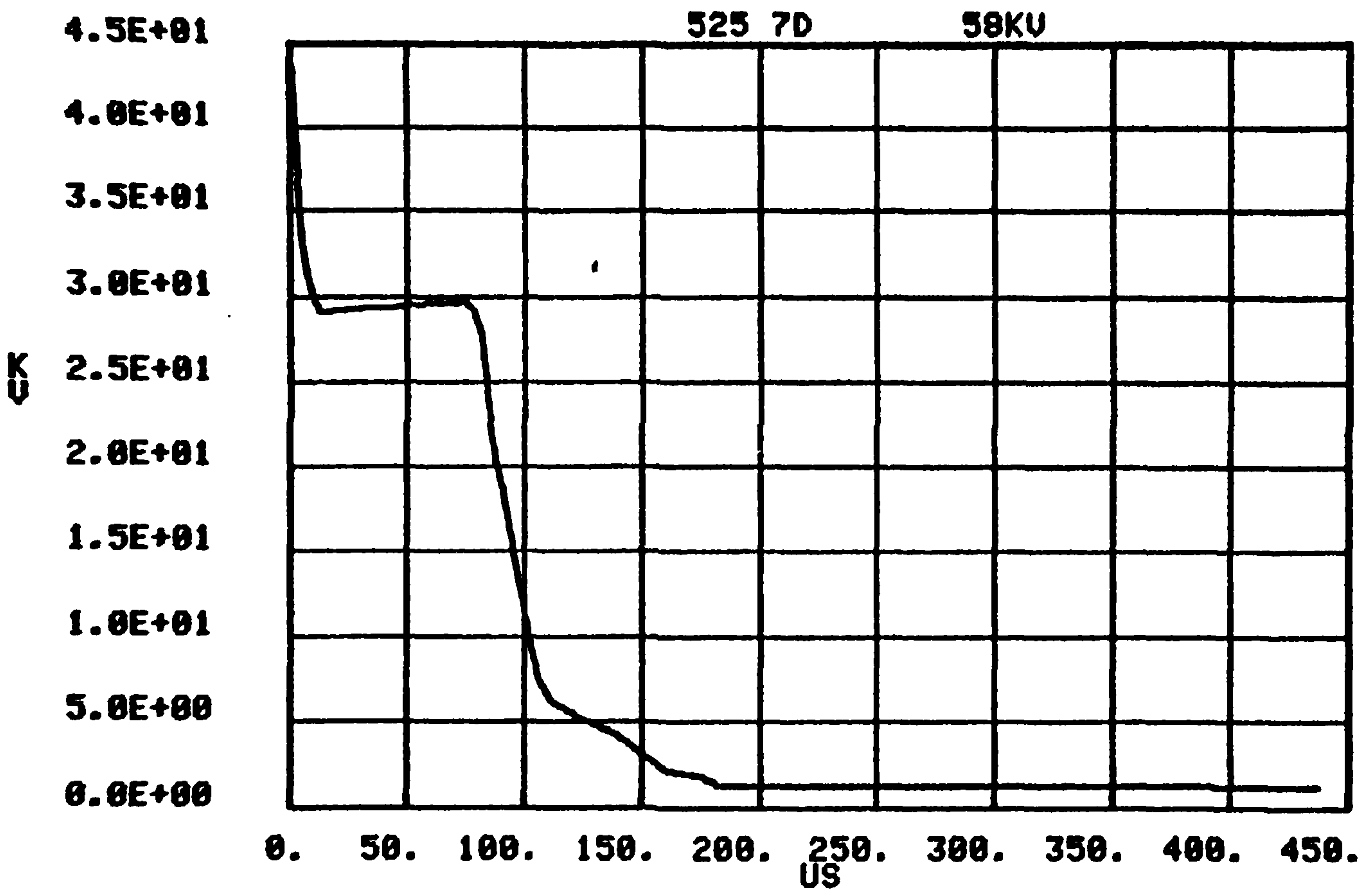

Figure B.89. 525B., .01, 1.0, 1.0, 300 sand-mix; V at r,θ = .15 m,99 (top).

FILME

4-84